

AD-A242 930



DTIC

EXACT

DEC 2 1981

S

C

D

ESL-TR-89-32



ENVIRONMENTAL FATE OF HYDRAZINES

N.B. MARTIN, D.D. DAVIS, J.E. KILDUFF, W.C. MAHONE

NATIONAL AERONAUTICS AND
SPACE ADMINISTRATION
WHITE SANDS TEST FACILITY
P.O. DRAWER MM
LAS CRUCES NM 88004

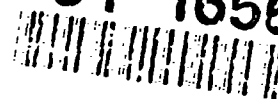
DECEMBER 1989

FINAL REPORT

MARCH 1985 — APRIL 1989

APPROVED FOR PUBLIC RELEASE: DISTRIBUTION UNLIMITED

91-16569



AIR FORCE ENGINEERING & SERVICES CENTER
ENGINEERING & SERVICES LABORATORY
TYNDALL AIR FORCE BASE, FLORIDA 32403

91 1126 057

NOTICE

PLEASE DO NOT REQUEST COPIES OF THIS REPORT FROM
HQ AFESC/RD (ENGINEERING AND SERVICES LABORATORY).

ADDITIONAL COPIES MAY BE PURCHASED FROM:

NATIONAL TECHNICAL INFORMATION SERVICE
5285 PORT ROYAL ROAD
SPRINGFIELD, VIRGINIA 22161

FEDERAL GOVERNMENT AGENCIES AND THEIR CONTRACTORS
REGISTERED WITH DEFENSE TECHNICAL INFORMATION CENTER
SHOULD DIRECT REQUESTS FOR COPIES OF THIS REPORT TO:

DEFENSE TECHNICAL INFORMATION CENTER
CAMERON STATION
ALEXANDRIA, VIRGINIA 22314

REPORT DOCUMENTATION PAGE				Form Approved OMB No. 0704-0188	
1a. REPORT SECURITY CLASSIFICATION UNCLASSIFIED			1b. RESTRICTIVE MARKINGS		
2a. SECURITY CLASSIFICATION AUTHORITY			3. DISTRIBUTION/AVAILABILITY OF REPORT Approved for Public Release Distribution Unlimited		
2b. DECLASSIFICATION/DOWNGRADING SCHEDULE					
4. PERFORMING ORGANIZATION REPORT NUMBER(S)			5. MONITORING ORGANIZATION REPORT NUMBER(S) ESL-TR-89-32		
6a. NAME OF PERFORMING ORGANIZATION National Aeronautics and Space Administration		6b. OFFICE SYMBOL (if applicable) WSTF	7a. NAME OF MONITORING ORGANIZATION HQ AFESC/RDVS Tyndall AFB FL 32403-6001		
6c. ADDRESS (City, State, and ZIP Code) White Sands Test Facility P.O. Drawer MM Las Cruces, New Mexico 88004			7b. ADDRESS (City, State, and ZIP Code) HQ AFESC/RDVS Tyndall AFB, FL 32403-6001		
8a. NAME OF FUNDING/SPONSORING ORGANIZATION AFESC		8b. OFFICE SYMBOL (if applicable) RDV	9. PROCUREMENT INSTRUMENT IDENTIFICATION NUMBER		
8c. ADDRESS (City, State, and ZIP Code) HQ AFESC/RDVS Tyndall AFB, FL 32403-6001			10. SOURCE OF FUNDING NUMBERS		
			PROGRAM ELEMENT NO. 6.2	PROJECT NO. 1900	TASK NO. 2073
			WORK UNIT ACCESSION NO.		
11. TITLE (Include Security Classification) Environmental Fate of Hydrazines (UNCLASSIFIED)					
12. PERSONAL AUTHOR(S) Nathalie B. Martin, Dennis D. Davis, Jan E. Kilduff, and William C. Mahone					
13a. TYPE OF REPORT Final		13b. TIME COVERED FROM Mar 85 to Apr 89		14. DATE OF REPORT (Year, Month, Day) December 1989	
15. PAGE COUNT					
16. SUPPLEMENTARY NOTATION Availability of this report is specified on reverse of front cover.					
17. COSATI CODES			18. SUBJECT TERMS (Continue on reverse if necessary and identify by block number)		
FIELD	GROUP	SUB-GROUP			
07	04		Hydrazine, Monomethylhydrazine, Unsymmetrical Dimethylhydrazine, Environmental Chamber, Surface Reactions, Surface Adsorption, Air Oxidation, Oxone Oxidation (continued)		
21	09	01			
19. ABSTRACT (Continue on reverse if necessary and identify by block number) Kinetic and mechanistic studies of the oxidative reactions of hydrazine, monomethylhydrazine (MMH), and unsymmetrical dimethylhydrazine (UDMH) have been studied to assess the impact of these propellants on the atmosphere. Studies were conducted using an environmental chamber, a packed flow-reactor, and a new type of laminar-flow reactor designed to minimize wall effects. Air-oxidation rates in a 6515-liter fluorocarbon-film environmental chamber were found to be much slower than the loss due to adsorption and permeation through the walls. Half-lives of 40, 19, and 60 hours were found for hydrazine, MMH, and UDMH, respectively. Metal surfaces were found to increase the rates of oxidation, and bayerite-coated aluminum (corroded aluminum) was found to be a particularly effective oxidation catalyst for hydrazine. (continued)					
20. DISTRIBUTION/AVAILABILITY OF ABSTRACT <input checked="" type="checkbox"/> UNCLASSIFIED/UNLIMITED <input type="checkbox"/> SAME AS RPT <input type="checkbox"/> DTIC USERS			21. ABSTRACT SECURITY CLASSIFICATION UNCLASSIFIED		
22a. NAME OF RESPONSIBLE INDIVIDUAL Dr Daniel A. Stone			22b. TELEPHONE (Include Area Code) (904) 283-4298		22c. OFFICE SYMBOL HQ AFESC/RDVS

Block 18 (cont.):

Metal-Surface Catalyzed Oxidation, Flow Microreactor, Laminar-Flow Reactor, Diffuse Reflectance, Diffusion Coefficients, Delayed-Branching Kinetics, Atmospheric Oxidation, Liquid Propellants, Amine Fuels

Block 19 (cont.)

A packed microreactor containing metal powders was used to determine rate constants and products for the surface-catalyzed air oxidation of MMH. The metal surfaces decreased in reactivity (per m^2 , at 328 K) in the following order: iron, Al_2O_3 , zinc, 316 stainless steel, titanium, chromium, aluminum, 304-L stainless steel, and nickel. Products were mainly methanol, methyldiazene, and methane.

A new laminar-flow reactor was constructed that used microporous permeation tubes to introduce low concentrations of hydrazine or MMH into a laminar flow of air containing 25 - 100 ppm of ozone. The diffusionally confined reaction zone was monitored by FTIR, and the products and rate constants for the reaction of hydrazine ($15.4 \pm 0.8 \times 10^{-17} \text{ cm}^3 \text{ molecule}^{-1} \text{ sec}^{-1}$) and MMH with ozone ($8.7 \pm 0.4 \times 10^{-17} \text{ cm}^3 \text{ molecule}^{-1} \text{ sec}^{-1}$) were measured at 299 K and 85 kPa total pressure.

Thermodynamic, kinetic, and DRIFT spectroscopic studies of the adsorption, permeation, and diffusional properties of the propellants, along with the kinetic data, were used to develop mechanisms for the surface-catalyzed and ozone oxidation reactions.

EXECUTIVE SUMMARY

Hydrazine and its alkyl-substituted derivatives, monomethylhydrazine (MMH) and unsymmetrical dimethylhydrazine (UDMH) are widely used as propellants or fuels in military and aerospace applications. Because the hydrazines are both toxic and carcinogenic, their environmental fate is of considerable interest.

The goal of this project was to investigate the kinetics, mechanisms, and products of the homogeneous and heterogeneous atmospheric-oxidation reactions of hydrazine, MMH, and UDMH.

An understanding of the kinetics and mechanisms of the gas-phase and surface-catalyzed oxidation reactions allows the identification of those factors that control the environmental lifetimes, decomposition pathways, and degradation products of these compounds. This mechanistic insight is a vital component in the total assessment of the environmental impact of hydrazine use.

The project had five specific objectives:

- To investigate the chemistry of the auto-oxidation reactions of the hydrazines in pure air using a large environmental reaction chamber constructed of inert wall-materials
- To ascertain the relative importance of surface reactions in the oxidation scheme by adding metal surfaces to the environmental chamber
- To focus on the surface-catalyzed component of the air-oxidation reactions using microreactor techniques
- To determine the rates and mechanisms of the reactions of hydrazines with ozone using an apparatus that minimizes or eliminates wall effects
- To examine the nature of the hydrazine/surface interaction using a surface spectroscopic technique

As a result of unwanted surface reactions, accurate gas-phase kinetic data on the rate of air-oxidation of the hydrazines have not been previously available. Although noted, the details of these surface-catalyzed reactions have not been previously investigated in detail. Atmospheric particulates, as well as the surfaces of man-made enclosures, are likely to affect the rates and

product distributions for the decomposition reactions of the hydrazines. The effects of enclosures are especially interesting from the standpoint of occupational health and safety. Personnel are most likely to come in contact with high concentrations of gas-phase hydrazines in or around man-made enclosures.

In order to minimize wall-effects, a 6515-liter fluorocarbon-film environmental chamber was employed to study possible air-oxidation reactions of the hydrazines. With a surface-to-volume ratio of 3.39 m^{-1} and an almost totally fluorocarbon surface, catalytic effects were expected to be minimal. The hydrazines disappeared slowly from the environmental chamber with half-lives of 19 - 60 hours; however, the loss was due to the physical interactions of adsorption onto and permeation through the fluorocarbon walls rather than by chemical oxidation. In pure nitrogen, the rate of disappearance of the hydrazines was the same as in air. If any oxidation occurred in pure air, the rate of oxidation was too slow to measure by this technique. Detailed kinetic models for the adsorption and permeation of hydrazines in the fluorocarbon-film chamber were developed.

Adding metallic wall-materials, such as aluminum, galvanized steel, stainless steel, titanium, or corroded aluminum, to the chamber increased the rate of disappearance of the hydrazines. With corroded aluminum surfaces, a rapid surface-catalyzed air-oxidation reaction of hydrazine occurred, which produced the reactive intermediates diazene and hydrogen peroxide. MMH was less reactive, and no evidence of reactivity was noted for UDMH on the corroded aluminum surface. The rates of reaction of hydrazine and MMH increased with the square of the surface area of the added corroded aluminum. Kinetic and mechanistic models for these reactions have been proposed.

The surface-catalyzed air oxidation reactions were further characterized by studies using a packed microreactor. At slightly elevated temperatures in air, hydrazine was completely oxidized on all powdered metallic and environmental surfaces studied (sand, concrete, and cinder block). MMH was less reactive, and the rates and products of the surface-catalyzed oxidation could be determined.

The relative activities of oxide-coated metal surfaces for the oxidation of MMH in air is:



In the absence of oxygen, the passivation and thermodynamics of adsorption of hydrazines on metallic surfaces were studied by gas chromatographic techniques.

The nature of the surface-hydrazine interaction with silica, silica-alumina, and alumina was investigated spectroscopically by an infrared reflectance technique. Diffuse reflectance infrared Fourier transform (DRIFT) spectroscopy confirmed that surface adsorption was primarily physical and that the adsorbed hydrazines do not undergo major structural changes when adsorbed.

A new type of reactor that made use of the properties of laminar flow to minimize wall reactions was used to investigate the reactions of ozone with the hydrazines. The laminar flow reactor (LFR) allowed the determination of the overall kinetic scheme and individual rate constants for the reactions of hydrazine and MMH with ozone. The ozonation of MMH occurred by a delayed branching-chain mechanism. The LFR proved to be an important new tool for the study of the chemical kinetics of atmospheric reactions.

The current understanding of the environmental fates of the propellant hydrazines in the atmosphere is based on an evaluation of the relative importance of the heterogeneous and homogeneous reactions with atmospheric constituents. Although oxygen is the major reactive component of air, its homogeneous rate of reaction with the hydrazines is so slow that the ultimate fate of the hydrazines is dictated by reaction with ozone, particulate matter, and other minor atmospheric constituents.

Using the rate constants determined by the LFR technique, the half-lives of hydrazine and MMH in a moderately polluted daytime atmosphere containing ozone, hydrocarbons, and nitrogen oxides is less than two hours, due to their reactions with ozone and hydroxyl radicals. Although their environmental persistence is quite short, the mechanistic studies suggest that the environmen-

tal impact of the hydrazines may be manifested primarily by their effect of increasing the hydroxyl/hydroperoxyl radical concentrations in the atmosphere.

A balancing factor is the efficiency of the adsorption process, surface-catalyzed air-oxidation process, or both, that may take place on hydrophilic airborne particulate matter. These surface interactions generally do not result in the desorption of reactive intermediates and represent an relatively innocuous pathway for the removal of atmospheric hydrazine or MMH.

It was concluded that the factors that substantially contribute to the environmental fate of hydrazines in the atmosphere are:

- their reactions with reactive constituents of the atmosphere such as ozone, and
- catalyzed reactions with oxygen on the surfaces of particulates or enclosure walls

The characteristics of the individual reaction sequences that control the gas phase concentrations of hydrazine and MMH are now fairly well understood; however, our understanding of the interdependence of these sequences with the complex suite of reactions already present in our polluted atmosphere is only minimal. The results of these mechanistic and kinetic studies provide much of the necessary input for atmospheric modeling programs to estimate the consequences of hydrazine release into the atmosphere.

PREFACE

This report was prepared by the National Aeronautics and Space Administration (NASA) White Sands Test Facility (WSTF), Las Cruces, N. Mex., for the Air Force Engineering and Services Center (AFESC), Tyndall Air Force Base, Florida 32403-6001. The contract was performed by Lockheed-ESC, P.O. Drawer MM, Las Cruces, N. Mex., 88004, under Program Element USAF R&D 62206F. Dr. Daniel A. Stone (AFESC) was the project officer. This report summarizes work performed between March 1985 and April 1989.

This report has been reviewed by the Public Affairs Office and is releasable to the National Technical Information Service (NTIS). At NTIS, it will be available to the general public, including foreign nationals.

This technical report has been reviewed and is approved for publication.

Daniel A. Stone
DANIEL A. STONE, GS-13
Project Officer

F. Thomas Lubozynski
F. THOMAS LUBOZYNSKI, Maj, USAF, BSC
Chief, Environics Division

Wayne P. Chepren
WAYNE P. CHEPREN, Capt, USAF
Chief, Environmental Sciences
Branch

Frank P. Gallagher
FRANK P. GALLAGHER III, Colonel, USAF
Director, Engineering and Services
Laboratory

Accession For	
NTIS UNCLASS	<input checked="checked" type="checkbox"/>
DTIC TAB	<input type="checkbox"/>
Unannounced	<input type="checkbox"/>
Justification	
By	
Distribution/	
Availability Codes	
Avail and/or	
Dist	Special
A-1	



TABLE OF CONTENTS

Section	Title	Page
I	INTRODUCTION	1
	A. OBJECTIVES	1
	B. BACKGROUND	2
	C. SCOPE	2
II	ENVIRONMENTAL CHAMBER STUDIES	4
	A. INTRODUCTION	4
	1. Objective	4
	2. Background	4
	3. Scope	4
	B. EXPERIMENTAL	5
	1. Materials	5
	2. Instrumentation	8
	3. Apparatus	9
	4. Procedures	11
	C. RESULTS	13
	1. Characterization of Chamber with Inert Gases	13
	2. Hydrazine Loss Processes in the Chamber	13
	3. MMH Loss Processes in the Chamber	30
	4. UDMH Loss Processes in the Chamber	33
	5. Aerozine-50 Loss Processes in the Chamber	33
D.	DISCUSSION	34
	1. Fluorocarbon-Film Interaction	34
	2. Metallic Surface Interactions	43
	E. CONCLUSIONS	55
III	FLOW REACTOR STUDIES: PACKED MICROREACTOR	56
	A. INTRODUCTION	56
	B. EXPERIMENTAL	57
	1. Materials	57
	2. Instrumentation	58

TABLE OF CONTENTS (CONTINUED)

Section	Title	Page
	3. Apparatus	59
	4. Procedures	59
C.	RESULTS	62
	1. Reactivity Screening	62
	2. Adsorption Studies	65
D.	DISCUSSION	69
	1. Hydrazine	70
	2. MMH	70
E.	CONCLUSIONS	78
IV	FLOW REACTOR STUDIES: LAMINAR FLOW REACTOR	79
A.	INTRODUCTION	79
	1. Overview of the Laminar Flow Reactor Concept	80
	2. General Flow Reactor Theory	80
B.	EXPERIMENTAL	85
	1. Materials	85
	2. Instrumentation	85
	3. Apparatus	87
	4. Procedures	89
C.	RESULTS	91
	1. Flow and Diffusion Characteristics of the Laminar Flow Reactor	91
	2. Kinetic Behavior of the Ozonization Reaction	98
	3. Products of the Ozonization Reaction	114
D.	DISCUSSION	119
	1. The Laminar Flow Reactor	119
	2. Kinetics and Mechanism of the Ozonization Reaction	124
E.	CONCLUSIONS	139

TABLE OF CONTENTS
(CONCLUDED)

Section	Title	Page
V	SURFACE SPECTROSCOPIC STUDIES	140
A.	INTRODUCTION	140
1.	Objective	140
2.	Background	140
B.	EXPERIMENTAL	141
1.	Materials	141
2.	Instrumentation	141
3.	Procedures	142
C.	RESULTS	142
1.	Silica Surfaces	142
2.	Other Surfaces	151
D.	DISCUSSION	157
E.	CONCLUSIONS	161
VI	CONCLUSIONS	162
	REFERENCES	163
APPENDIX		
A	TEST DATA FOR SECTION II	175
B	TEST DATA FOR SECTION IV	193

LIST OF FIGURES

Figure	Title	Page
1	SEM Photograph of AlO_x Surface at 150X Showing Normal Aluminum Surface and Aluminum Hydroxide Encrustations	6
2	SEM Photograph of AlO_x Surface at 2500X Showing Aluminum Hydroxide Encrustations	7
3	Schematic of the 6515-Liter Environmental Reaction Chamber (Without Polyethylene Liner)	10
4	Loss of Hydrazine Vapor From Chamber in Dry Air	14
5	Loss of Hydrazine Vapor From Chamber in Dry Nitrogen	15
6	Variations of Hydrazine Vapor Loss in Interrupted Run When Additional Hydrazine Vapor Was Added	17
7	Hydrazine Loss Rate Curves in Dry and Humid Air	19
8	Hydrazine Loss Rate Constants for Early Kinetic Runs Showing Conditioning Effects	21
9	Effects of Conditioning and Humidity (14,600 ppm, v/v) on Hydrazine Loss Rate Constants (24 m ² of Additional FEP Surface)	23
10	Effects of 23.8 m ² of AlO_x on the Hydrazine Loss Rate in Air	26
11	Gas-Phase IR Spectrum of Hydrogen Peroxide, Diazene, and Hydrazine	27

LIST OF FIGURES
(CONTINUED)

Figure	Title	Page
12	Gas-Phase IR Spectrum of Hydrogen Peroxide, Diazene, and Hydrazine	28
13	Formation - Decay Curve for Hydrogen Peroxide Plus Diazene, from the Reaction of Hydrazine in Air on 23.8 m ² of AlO _x . . .	29
14	MMH Loss Rate in the Presence and Absence of 23.8 m ² of AlO _x .	32
15	UDMH Loss Rate in the Presence and Absence of 23.8 m ² of AlO _x	35
16	Theoretical Versus Actual Hydrazine Concentration as Integrated Area in Initial Nonlinear Portion of Hydrazine Loss Rate Curve	42
17	Log(k _m) Versus Log(area) for Hydrazine and MMH; Lines Shown Have a Slope of 2	45
18	Laminar Flow Reactor	81
19	Head-on View of the Laminar Flow Reaction Cell	81
20	Vaporizer (Fritted-Glass Gas Dispersion Bubbler)	88
21	Ln(absorbance) Versus Time for Methane Diffusion Characterization	94
22	Hydrazine Loss Rate in the Presence and Absence of Ozone . . .	100
23	Effect of Temperature on the Hydrazine Loss Rate in Ozone . . .	104

LIST OF FIGURES
(CONTINUED)

Figure	Title	Page
24	Arrhenius Plot for the Reaction of Hydrazine and Ozone	105
25	Hydrazine Loss Rate in Ozone Using the Alternate Kinetic Procedure	106
26	MMH Loss Rate in the Presence and Absence of Ozone	107
27	Effect of Temperature on the MMH Loss Rate Profile in Ozone	109
28	Arrhenius Plot for the Initiation Reaction of MMH and Ozone	110
29	Arrhenius Plot for the Branching Reaction of MMH and Ozone . .	112
30	MMH Rate Loss Profile in Ozone Using the Alternate Kinetic Procedure	113
31	Gas-Phase IR Spectra of (a) Ozone and (b) Hydrazine Showing Comparative Band Positions	115
32	Gas-Phase IR Spectra of Hydrazine/Ozone: (a) Reaction Mixture; (b) Products, Including Hydrogen Peroxide and Diazene	116
33	Gas-Phase IR Spectra of (a) Ozone and (b) MMH Showing Comparative Band Positions	117

LIST OF FIGURES (CONTINUED)

Figure	Title	Page
34	Gas-Phase IR Spectra of MMH/Ozone: (a) Reaction Mixture; (b) Products, Including Methyldiazene, Methanol, Hydrogen Peroxide, Formaldehyde, and Diazomethane	118
35	Gas-Phase IR Spectra of (a) TME and (b) TME/Ozone Reaction Mixture	120
36	Gas-Phase IR Spectra of (a) TME/Ozone Reaction Product, and (b) Acetone Reference Spectrum	121
37	Initial Reactant Profile Under Typical LFR Conditions	123
38	Superimposed Experimental and Theoretical Data for the Reaction of MMH and Ozone Based on Equation (94)	132
39	Superimposed Experimental Data and Monte Carlo Simulation Results	136
40	Diffuse Reflectance Spectrum of Deuterated Cab-O-Sil® (Nondeuterated Reference Spectrum)	144
41	Diffuse Reflectance Spectrum of Hydrazine Absorbed onto Deuterated Cab-O-Sil®	145
42	Diffuse Reflectance Spectrum of Hydrazine Adsorbed on Deuterated Cab-O-Sil® After Evacuation (Deuterated Cab-O- Sil® Reference)	147

LIST OF FIGURES
(CONCLUDED)

Figure	Title	Page
43	Diffuse Reflectance Spectrum of MMH Adsorbed on Deuterated Cab-O-Sil® (Deuterated Cab-O-Sil® Reference)	148
44	Carbon-Hydrogen Stretching Region of MMH (Thick Film)	149
45	Diffuse Reflectance Spectrum of MMH Adsorbed on Copper(I) Oxide After 2-Minute Exposure (Copper(I) Oxide Reference) . . .	154
46	Diffuse Reflectance Spectrum of MMH Adsorbed on Copper(I) Oxide, 2 Minutes After Evacuation (Copper(I) Oxide Reference) .	155
47	Diffuse Reflectance Spectrum of Copper(I) Oxide Surface After Exposure to MMH and Heating to 343 K for 30 Minutes (Copper(I) Oxide Reference)	156
48	Illustration Showing MMH Adsorbed to Silica Surface	158
49	Correlation of Sanderson Electronegativities with Methyl Deformation Frequencies	160

LIST OF TABLES

Table	Title	Page
1	BACKGROUND HYDRAZINE LOSS RATE CONSTANTS IN AIR AND NITROGEN	18
2	OBSERVED HYDRAZINE LOSS RATE CONSTANTS WITH AlO_x SURFACES IN AIR AND NITROGEN	24
3	OBSERVED HYDRAZINE LOSS RATE CONSTANTS WITH METAL SURFACES IN AIR	25
4	OBSERVED MMH LOSS RATE CONSTANTS WITH METAL SURFACES IN AIR	31
5	OBSERVED UDMH AND AEROZINE-50 LOSS RATE CONSTANT IN THE PRESENCE AND ABSENCE OF AlO_x SURFACES IN AIR	34
6	FIRST-ORDER LOSS RATE CONSTANTS FROM FEP CHAMBERS	37
7	VAPOR TRANSMISSION RATES THROUGH FEP	38
8	DERIVED RATE CONSTANTS FOR ADSORPTION/PERMEATION OF FUEL HYDRAZINES ON FEP	41
9	RATE CONSTANTS FOR FUEL HYDRAZINES WITH METAL SURFACES IN AIR	46
10	INFRARED ANALYTICAL FREQUENCIES AND EXTINCTION COEFFICIENTS . .	60
11	RECOVERY OF HYDRAZINE IN NITROGEN CARRIER	64
12	MICROREACTOR PRODUCTS: MMH IN AIR	65

LIST OF TABLES
(CONTINUED)

Table	Title	Page
13	COMPARISON OF MMH REACTIONS IN NITROGEN, AIR, AND HUMIDIFIED AIR	66
14	STRONG ADSORPTION OF HYDRAZINES ON METAL AND OXIDE SURFACES IN AIR	67
15	STRONG ADSORPTION OF METHYLAMINES ON METAL AND OXIDE SURFACES IN AIR	68
16	REVERSIBLE GAS-SOLID EQUILIBRIUM CONSTANTS IN AIR	68
17	RETENTION VOLUMES OF METHANE, METHANOL, AND UDMH ON 316 SS IN AIR	69
18	SURFACE REACTIVITIES FOR MMH OXIDATION IN AIR	74
19	METHANOL PRODUCT SELECTIVITY	75
20	MICROPOROUS TUBING FLOW LOSS RATES	93
21	BACKGROUND HYDRAZINE LOSS RATE CONSTANTS IN NITROGEN	96
22	BACKGROUND MMH LOSS RATE CONSTANTS IN NITROGEN	97
23	DIFFUSION COEFFICIENTS IN AIR	98
24	TEMPERATURE DEPENDENCE OF DIFFUSION COEFFICIENTS	99
25	HYDRAZINE LOSS RATE CONSTANTS WITH OZONE IN NITROGEN	102

LIST OF TABLES
(CONCLUDED)

Table	Title	Page
26	MMH LOSS-RATE CONSTANTS WITH OZONE IN NITROGEN	108
27	METHYL GROUP FREQUENCIES OF MMH ADSORBED ON DEUTERATED CAB-O-SIL®	150
28	METHYL GROUP FREQUENCIES OF UDMH ADSORBED ON DEUTERATED CAB-O-SIL®	152
29	SUMMARY OF OBSERVED FREQUENCY SHIFTS FOR METHYL ADSORBATES . .	152
30	METHYL GROUP FREQUENCIES OF MMH AND UDMH ADSORBED ON IRON(III) OXIDES	153

SECTION 1

INTRODUCTION

Hydrazine and its alkyl-substituted derivatives, monomethylhydrazine (MMH) and unsymmetrical dimethylhydrazine (UDMH), are used as propellants or fuels in a number of military and aerospace applications. Because the hydrazines are both toxic and carcinogenic (References 1 and 2), their environmental fate is of considerable interest and has been the subject of a number of studies (References 3 - 7).

A. OBJECTIVES

The overall goal of this project was to provide further insight into the mechanisms of the homogeneous and heterogeneous reactions by which propellant hydrazines decompose in the atmosphere. This insight is critical for understanding the relative importance of each kinetic pathway for the decomposition of these compounds, which is, in turn, essential for input into models of the environmental impact of hydrazine use.

The overall goal involved five specific objectives:

- To investigate the chemistry of the auto-oxidation reactions of the hydrazines in an environmental reaction chamber constructed of inert wall-materials
- To ascertain the relative importance of surface reactions in the auto-oxidation scheme by adding metal surfaces to the environmental chamber
- To focus on the surface-catalyzed component of the air-oxidation reactions using catalytic microreactor techniques
- To determine the rates and mechanisms of the reactions of hydrazines with ozone using an apparatus that minimizes or eliminates wall effects
- To examine the nature of the hydrazine/surface interaction by using a surface spectroscopic technique

B. BACKGROUND

The pioneering work of Stone (References 3 - 5) and Tuazon et al. (Reference 6) led to the identification of the major products and intermediates formed by air-oxidation of the hydrazines. These products and intermediates include diazenes, nitrosamines, nitramines, diazoalkanes, and peroxides. Because the hydrazines are comparable to water in volatility, any spill or intentional release of the hydrazines can result in local gas-phase concentrations well in excess of the established threshold limit values (TLV's) of 0.1 to 0.5 ppm.

Surface chemical reactions have plagued the gas-phase kinetics studies of Pitts, Stone, and others (References 3 - 7). The surface-to-volume ratio and the type of surface treatment of the reaction vessel have dramatic effects on the decomposition kinetics of the hydrazines (References 3 - 5). As a result, accurate gas-phase kinetic data are not available. In addition, the effects of surface chemical reactions on the environmental fates of the hydrazines have not been evaluated. Atmospheric particulates, both man-made and natural, as well as the surfaces of man-made enclosures, are likely to affect the rate and product distribution of the decomposition of the hydrazines. The effects of enclosures are especially interesting from the standpoint of occupational health and safety. Personnel are most likely to come in contact with high concentrations of gas-phase hydrazines in or around man-made enclosures.

As a result of similar USAF and NASA interests in the environmental fate of the hydrazines, NASA White Sands Test Facility (WSTF) personnel and representatives of the Air Force Engineering and Services Center (AFESC) initiated a test project to investigate the influence of surface and atmospheric chemical reactions on the environmental fates of the hydrazines.

C. SCOPE

This report presents the results of kinetic and mechanistic studies of the atmospheric oxidation reactions of the fuel hydrazines. The approach was: (1) to evaluate the importance that surface-catalyzed reactions might have on the standard environmental (smog) chamber experiment, (2) to study the kinetics of

the air-oxidation under conditions designed to allow the surface-catalyzed component to predominate, and, (3) to study the kinetics of the air-oxidation under conditions where the surface-catalyzed components were designed to be absent.

Current environmental impact computer models require accurate kinetic data and reaction schemes for both the homogeneous and heterogeneous reactions of possible pollutants. The rate constants and reaction schemes presented in this report can be used as inputs into these models and as aids in predicting the potential environmental impact of hydrazine fuel use.

SECTION II

ENVIRONMENTAL CHAMBER STUDIES

A. INTRODUCTION

1. Objective

The objective of the environmental chamber studies was to study the kinetics and mechanisms of the homogeneous and heterogeneous atmospheric oxidation reactions of hydrazine, MMH, and UDMH in a fluorinated-ethylene propylene (FEP) polymer film chamber. Wall effects due to FEP or added metal surfaces were also to be determined.

2. Background

Surface reactions on the walls of the containers interfere with gas-phase studies by dramatically affecting the decomposition kinetics (References 3 - 7). To minimize these effects, studies of the atmospheric reactions in low surface-to-volume ratio (s/v) chambers constructed of inert materials are required. Characterization of the nature of the hydrazine/wall reaction with both supposedly inert and presumably catalytic materials is also essential to the development of a reasonably complete understanding of the hydrazine/environment interaction.

3. Scope

This work involved the design and construction of a 6515-liter fluorocarbon-film reaction chamber with a low surface-to-volume ratio. The loss rates of both unreactive gases and fuel hydrazine vapors from the chamber were studied. The effects of humidity, oxygen, and fluorocarbon surface-area on these rates were determined. The kinetics and products of metal-surface promoted reactions were also investigated when metal plates were added to the chamber to simulate enclosure walls.

B. EXPERIMENTAL

1. Materials

Hydrazine, MMH, and Aerozine-50 were propellant grades (Olin) analyzed according to MIL-P-26536-C, MIL-P-27404B, and MIL-P-27402B, respectively. UDMH (Aldrich) was reagent grade and used as received. Methane (Airco), methylamine (Airco), CO₂ (Big Three) and ammonia (Scott) were used as supplied. All other solvents were ACS reagent grade and used as supplied. Sheets of 0.16-cm (20-gauge) 304-L Stainless Steel (SS), hot-dipped galvanized steel (zinc), titanium 6Al-4V, and aluminum 6061-T6 were cut into 0.46 × 0.46-m plates. Before use, the plates were scrubbed with a nylon bristle brush in a solution of 1:128 (1 oz./gal) Liqui-Det 2 (Oakite Products), which is a mildly alkaline liquid detergent. Each plate was then rinsed with isopropyl alcohol and dried in a stream of gaseous nitrogen. The dried plates were packaged in a polyethylene bag until required.

During testing, it was found that aluminum plates adventitiously encrusted with a crystalline substance were significantly reactive. The grayish-white crystalline substance, which covered approximately 15 to 25 percent of the geometric surface area of the aluminum plates, was examined by scanning electron microscopy (SEM) at 150X and 2500X (Figures 1 and 2). The SEM photographs revealed cones and somatoids of a hexagonal crystalline structure characteristic of aluminum surfaces exposed to oxygen and moisture, which is indicative of an aluminum-hydroxide (Reference 9). The crystalline material was mechanically removed using a razor blade, and a BET surface-area determination yielded 60 m² per gram of material. The mechanical scraping of the aluminum surfaces fractured the crystalline material, which increased the surface area by an estimated two or three times greater than its native value on the aluminum substrate. Differential scanning calorimetry (DSC) was performed on a portion of this material. A single endotherm at 544 K was observed. The material underwent a 25 percent weight loss, which corresponds to the dehydration loss of one H₂O from a compound of the molecular formula Al(OH)₃. Based on these observations, the material was tentatively identified as bayerite (Reference 10). Bayerite forms on clean aluminum surfaces from ambient temperatures up to

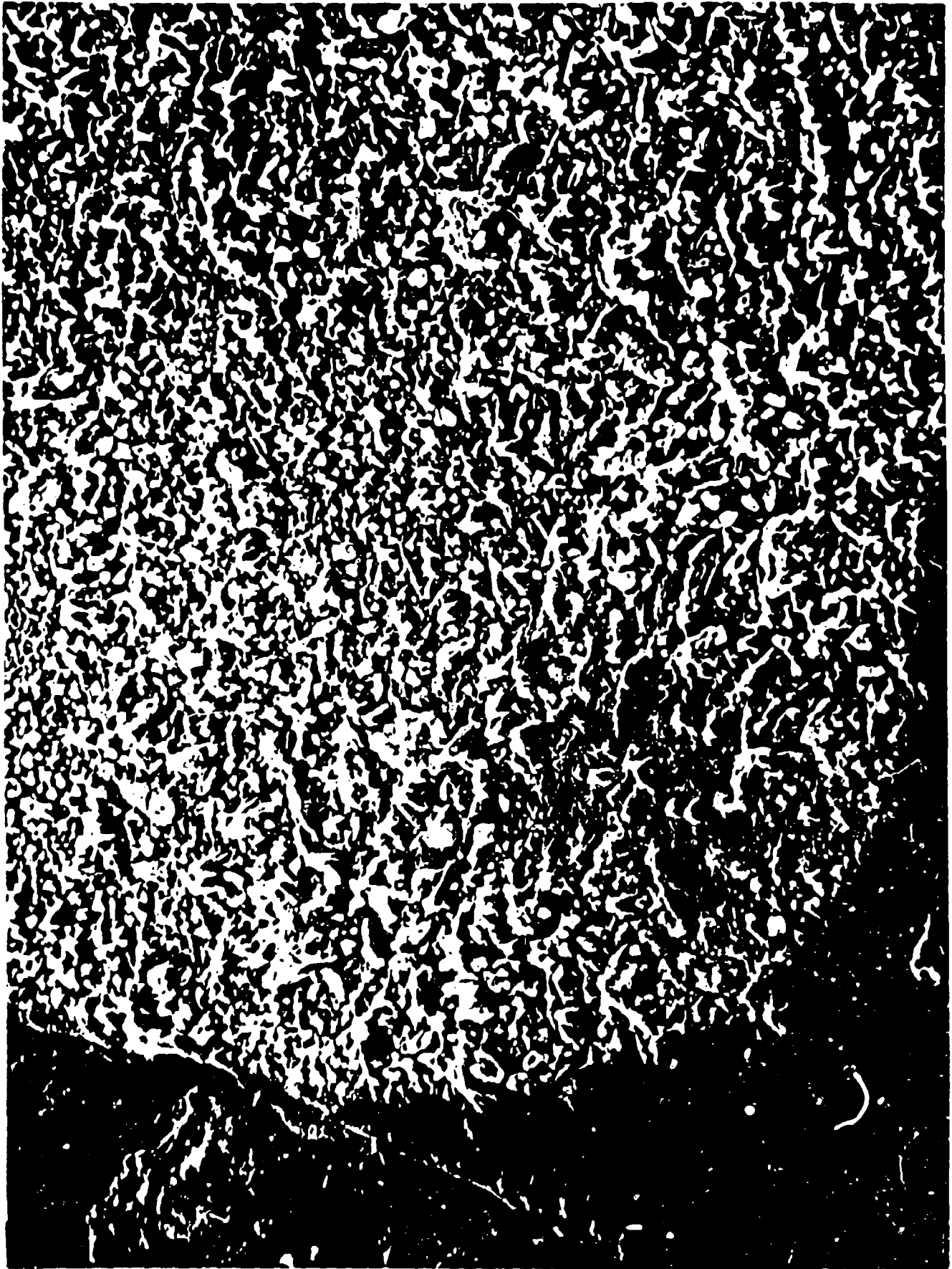


Figure 1. SEM Photograph of AlO_x Surface at 150X
Showing Normal Aluminum Surface and
Aluminum Hydroxide Encrustations



Figure 2. SEM Photograph of AlO_x Surface at 2500X
Showing Aluminum Hydroxide Encrustations

NASA-USF
0988-3125

313 K, forms mechanically removable crystals, and yields a single peak in thermal analysis. For the remainder of this report, the combination of aluminum substrate metal and bayerite coating will be referred to as AlO_x , representative of an aluminum hydroxide on an aluminum surface. The origin of the AlO_x crust is unknown.

2. Instrumentation

Changes in reactant and product concentrations within the chamber were monitored by absorbance changes with a Fourier transform infrared (FTIR) spectrometer in conjunction with a White Cell optical system.

a. FTIR Spectrometer

A Mattson Sirius 100 FTIR spectrometer equipped with a remote mercury-cadmium-telluride (HgCdTe) detector operated at 77 K was used. The HgCdTe detector was mounted on an adjustable aluminum base plate external to the FTIR, but within a purgeable air space. The entire optical path outside the chamber was purged by dry nitrogen. Data collection and processing were performed using a Pixel 80 supermicrocomputer with the UNIX operating system and Mattson-supplied programs. Data was recorded over the mid-infrared region (4000 to 700 cm^{-1}) at 1 cm^{-1} resolution. Background or sample spectra were obtained by co-adding 100 instrument scans and storing the results. Spectral acquisition and processing were user-controlled via a C-Shell program.

b. Multiple-Path Optics

A White cell optical system of 74.9-m pathlength was used (Reference 8). The multiple-path optical system consisted of two 20.3-cm field mirrors and an in-focus mirror with 2.45-cm zinc selenide (ZnSe) windows. The mirrors were gold-coated and held in polytetrafluoroethylene (PTFE)-coated frames. The overall pathlength of the optical system was determined to be a multiple of the base length (2.34 m) by counting the number of dots on the nesting mirror made by a coincidental helium-neon (HeNe) laser beam. The beam

could be made coincident by interposing a removable mirror into the spectrometer's internal optics.

c. Analytical Frequencies and Extinction Coefficients

The FTIR absorption spectra of molecular species of interest were recorded in calibration experiments, and regions showing the least interference from CO_2 and water vapor were integrated for concentration determinations. Included were hydrazine (1000 to 880 cm^{-1}), MMH (800 to 700 cm^{-1}), UDMH (955 to 865 cm^{-1}), 1,1,2-trichloro-1,2,2-trifluoroethane (TF Freon, 831 to 790 cm^{-1}), water (3900 to 3500 cm^{-1}) and CO_2 (2400 to 2200 cm^{-1}). Due to a slight overlap of methanol and water bands, methanol was integrated over four different wavenumber regions; 3100 to 2800 cm^{-1} , 2900 to 2800 cm^{-1} , 1100 to 950 cm^{-1} , and 1085 to 975 cm^{-1} . In some experiments, single absorption peaks were used when suitable nonoverlapped spectral regions could not be found. Included were hydrazine (958 cm^{-1}), MMH (888 cm^{-1}), UDMH (909 cm^{-1}), methane (3017 and 1306 cm^{-1}), and CO_2 (2360 and 2362 cm^{-1}).

A comparison was made to the extinction coefficients used by other workers for single absorption peaks to verify the accuracy of the experimental system. The values (at 1- cm^{-1} resolution) determined for hydrazine $\epsilon_{(e)} = 6.7 \text{ atm}^{-1}\text{cm}^{-1}$ at 958 cm^{-1} , MMH $\epsilon_{(e)} = 7.6 \text{ atm}^{-1}\text{cm}^{-1}$ at 888 cm^{-1} , and UDMH $\epsilon_{(e)} = 6.6 \text{ atm}^{-1}\text{cm}^{-1}$ at 909 cm^{-1} compared favorably to the values for hydrazine $\epsilon_{(e)} = 6.6 \text{ atm}^{-1}\text{cm}^{-1}$, MMH $\epsilon_{(e)} = 7.2 \text{ atm}^{-1}\text{cm}^{-1}$, and UDMH $\epsilon_{(e)} = 7.5 \text{ atm}^{-1}\text{cm}^{-1}$ listed by Tuazon et al. (Reference 6).

3. Apparatus

a. Environmental Reaction Chamber

An environmental reaction chamber, $2.34 \times 2.34 \times 1.19 \text{ m}$, was constructed from 0.013-cm (5-mil) sheets of FEP (Figure 3). The sheets were joined by heat-sealing and the seams were reinforced with polytetrafluoroethylene (PTFE) pressure-sensitive tape. The chamber was supported by an outside metal framework, and the framework was covered by a 0.025-cm (10-mil) polyethyl-

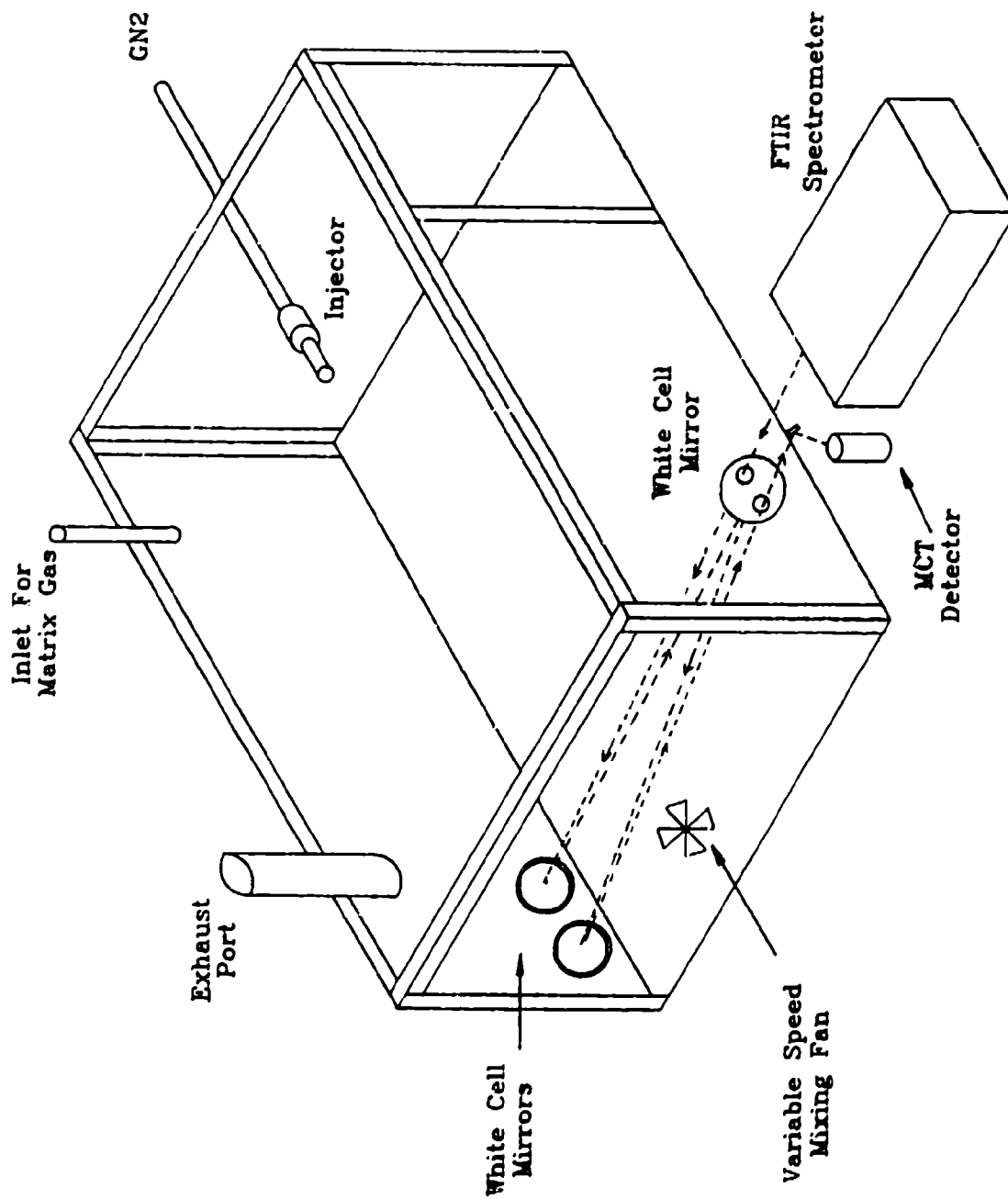


Figure 3. Schematic of the 6515-L Environmental Reaction Chamber (Without Polyethylene Liner)

ene liner. A 5-cm purgeable air space between the inner FEP and outer polyethylene liner provided thermal and mechanical protection. The internal volume of the chamber was 6515 liters. A 250-mL glass bulb, wrapped in heating tape, acted as an injector system in which fuel hydrazine, water (for humidity adjustments), or inert materials could be vaporized and transferred into the chamber by gaseous nitrogen flow. The chamber could be vented through a 5-cm PTFE pipe-exhaust stack. A 1.19 × 0.91-meter FEP door, sealed with PTFE tape, provided access to the chamber interior. The chamber was also fitted with a 30.5-cm PTFE-coated variable-speed fan to mix the chamber contents. Except for the ZnSe windows and the gold mirror surfaces, the entire interior surface of the chamber was FEP or PTFE.

b. Gas Purification System

The interior of the chamber and the space between the FEP wall and the outer jacket were purged with purified air provided by a Balston Model 75-20 air filter (360 L/min maximum flow), or a Model 75-50 air purifier (30 L/min maximum flow, low CO₂ content), and a sequence of disposable absorbent cartridges containing activated carbon, type 13X molecular sieves, and sodium/calcium hydroxides. The air filter removed all suspended impurities and dried the air to a dew point of 233 K (127 ppm, v/v). The air purifier removed CO₂ to 1 ppm v/v. The absorbent cartridges removed trace gas contaminants, including remaining water and CO₂. Gas outlet-valves after each unit provided for air with various CO₂ and water contents. Alternatively, nitrogen that was further purified by the Balston unit could be substituted for air.

4. Procedures

a. General Procedure

A typical experiment consisted of placing a known area of test surface into the chamber (if required), attaining the required atmosphere, adding fuel hydrazine vapor, and determining the time/vapor-concentration relationship over 12 to 48 hours, using FTIR spectroscopy.

b. Test Method

The requisite number of metal plates (none, in the case of a background run) were placed vertically in PTFE racks in the chamber, which was then purged with matrix gas for at least 6 hours at 300 L/min to provide at least 17 turnovers of the atmosphere of the 6515-liter chamber. The inner purge was then halted, and the space between the polyethylene liner and the chamber was purged at 150 L/min. A reference spectrum was collected by the FTIR system, stored, and subsequently used to compute absorbance spectra for concentration measurements. Liquid or vapor samples were injected by syringe into the glass injector system, which was heated to approximately 325 K. The vapors were then swept into the chamber with nitrogen. Typically, 0.5 to 1.75-mL samples of the fuel hydrazines were used to create an atmosphere containing 60 to 100-ppm v/v fuel hydrazine in the chamber. High-speed stirring with the mixing fan was carried out during sample introduction, followed by low-speed stirring during the remainder of the run. Immediately after introduction of the fuel hydrazine, data acquisition was started via the C-Shell program, which acquired and processed sample spectra at specified time intervals. The temperature of the room containing the environmental chamber varied from 294 - 300 K.

c. Kinetics

The rate of fuel hydrazine disappearance from the chamber was determined by measuring changes in the vapor concentration over a 12- to 48-hour period. Using either area integration or peak height, 30 to 100 spectra were analyzed and a graph of time versus the natural log of the percent remaining was constructed. The decay curve was usually biphasic with a short nonexponential initial phase (15 to 25 percent of the total change) followed by a purely exponential decay. The exponential decay portion was treated by least squares analysis to yield an apparent first-order rate constant.

A more detailed analysis of the observed decay kinetics based on a set of consecutive reactions was carried out. The analytical solutions to the differential equations for this kinetic scheme are available (References 11, 12) and were used to determine rate constants for processes occurring during

both stages of the decay process. When multiple runs under identical test conditions were made, the average and standard error were calculated for those rate constants.

C. RESULTS

1. Characterization of Chamber with Inert Gases

The chamber integrity was verified by observing the loss rates of nonreactive vapors in dry air or nitrogen. The slow disappearance of either methane or TF-Freon was treated as an exponential decay and was found to have apparent first-order rate constants of $4.3 \pm 1.0 \times 10^{-3} \text{ hr}^{-1}$ (half-life $[t_{1/2}] = 161$ hours) and $5.0 \times 10^{-3} \text{ hr}^{-1}$ ($t_{1/2} = 139$ hours), respectively. A similar treatment of four methanol experiments yielded an apparent first-order rate constant of $1.6 \pm 0.2 \times 10^{-2} \text{ hr}^{-1}$ ($t_{1/2} = 43$ hours). No significant differences were observed between kinetic runs for methane and methanol conducted in air or nitrogen.

2. Hydrazine Loss Processes in the Chamber

Extensive testing regarding atmospheric constituents, conditioning effects, and increased FEP surface area was performed with hydrazine, which was considered to be representative of the other fuel hydrazines.

a. Background Rates

Rates for kinetic runs conducted with only air or nitrogen and hydrazine present in the chamber are referred to as background loss rates and are characterized by the first-order rate constant (k_{bkg}) determined from the exponential portion of the decay.

The average hydrazine k_{bkg} was $1.72 \pm 0.10 \times 10^{-2} \text{ hr}^{-1}$ ($t_{1/2} = 40.3$ hours) in dry air and $1.65 \pm 0.13 \times 10^{-2} \text{ hr}^{-1}$ ($t_{1/2} = 41.9$ hours) in dry nitrogen (Figures 4 and 5). There is no significant difference, therefore, in average hydrazine k_{bkg} in dry nitrogen or dry air.

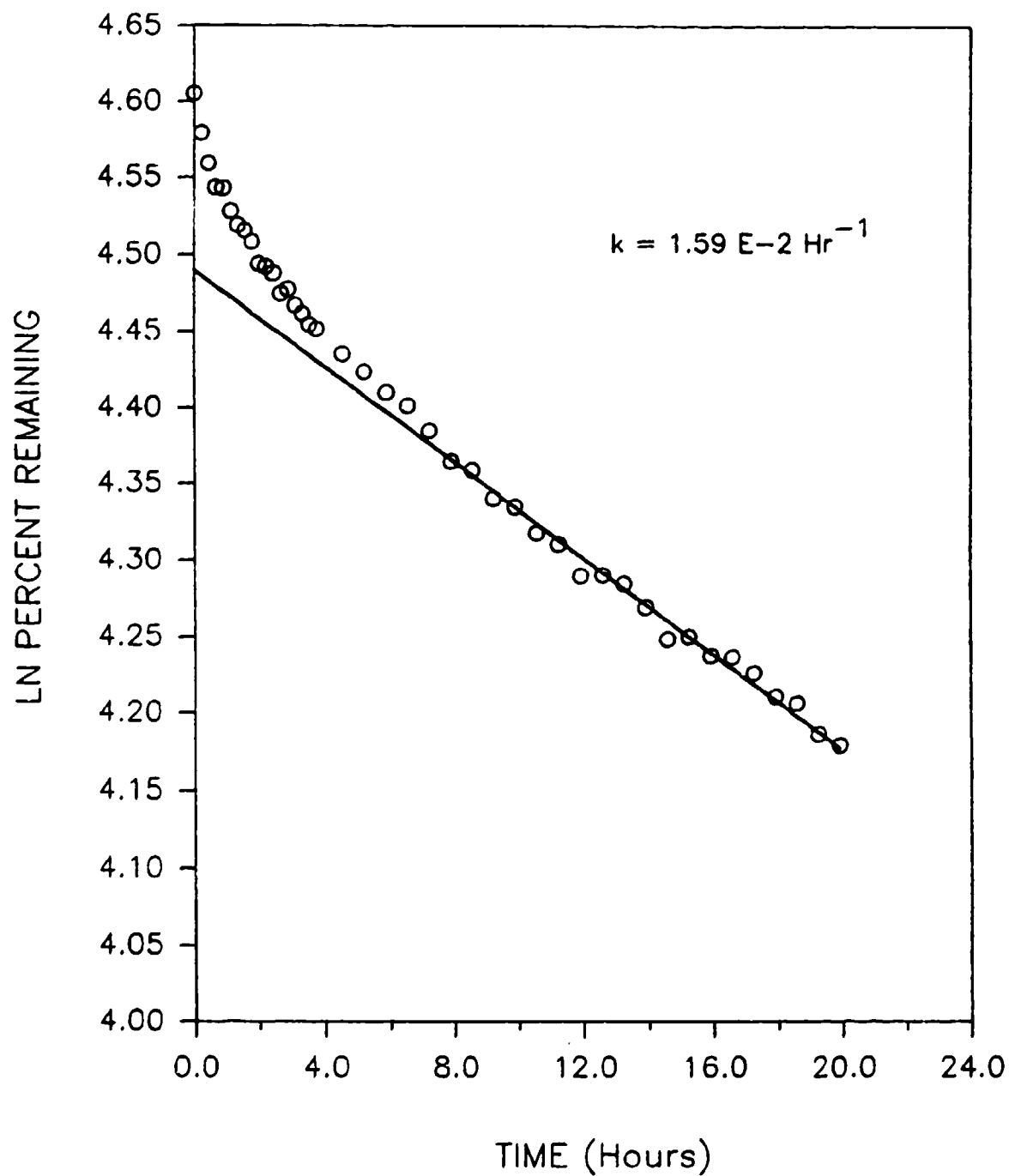


Figure 4. Loss of Hydrazine Vapor From Chamber in Dry Air

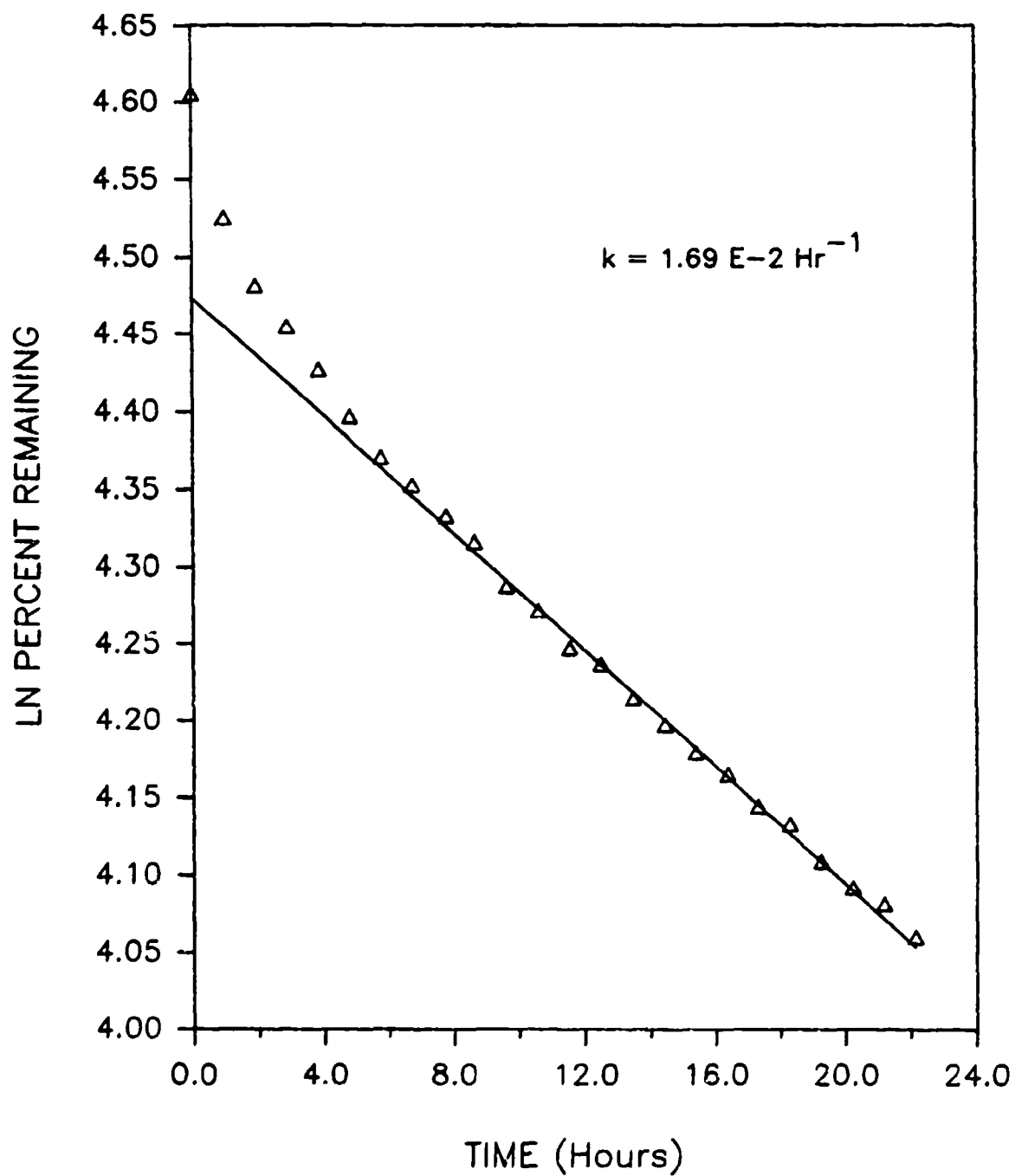


Figure 5. Loss of Hydrazine Vapor From Chamber in Dry Nitrogen

Graphical and numerical analyses show that after the first 15 to 25 percent of hydrazine disappearance, the data are well represented as an exponential decay. The deviation from simple exponential decay, as shown by curvature in the log plot, was evident in each new run. When a run was interrupted after about 25-percent loss and sufficient hydrazine vapor added to raise the concentration of hydrazine to the original value, the initial curvature was not evident and the subsequent loss rate was purely exponential (Figure 6). This suggests that the process responsible for the initial, more rapid disappearance of hydrazine becomes inoperative or has reached a steady state during the later phase of the decay.

b. Products

Examination of the spectra generated during background kinetic runs showed no evidence of IR-detectable intermediates or products such as hydrogen peroxide, diazene or ammonia. Although water vapor concentration generally increased during a run, this could have been due to permeation from outside the chamber.

c. Effects of Atmospheric Constituents

(1) Oxygen. The k_{bkg} for hydrazine loss is the same in both dry air and dry nitrogen (Table 1). To measure the extent of oxygen permeation into the chamber, the chamber was purged with nitrogen for 16 hours, sealed, and changes in oxygen concentration were monitored by gas chromatography (GC). Over the 4-hour test period, the oxygen concentration was found to increase at 0.13 percent per hour. Although rigorous oxygen-free conditions could not be maintained in the chamber, the slow permeation rate and equality of loss rates in air or nitrogen suggests no kinetic dependence on oxygen.

(2) Water Vapor. The average k_{bkg} for hydrazine decay in wet air (relative humidity [RH] initially at 50 percent) was $3.47 \pm 0.13 \times 10^{-2} \text{ hr}^{-1}$ ($t_{\frac{1}{2}} = 20.0$ hours). The water content of the matrix gas, therefore, appears to be a major factor in determining hydrazine loss rates (Figure 7). Such effects have been noted by earlier workers (References 6, 13, 14).

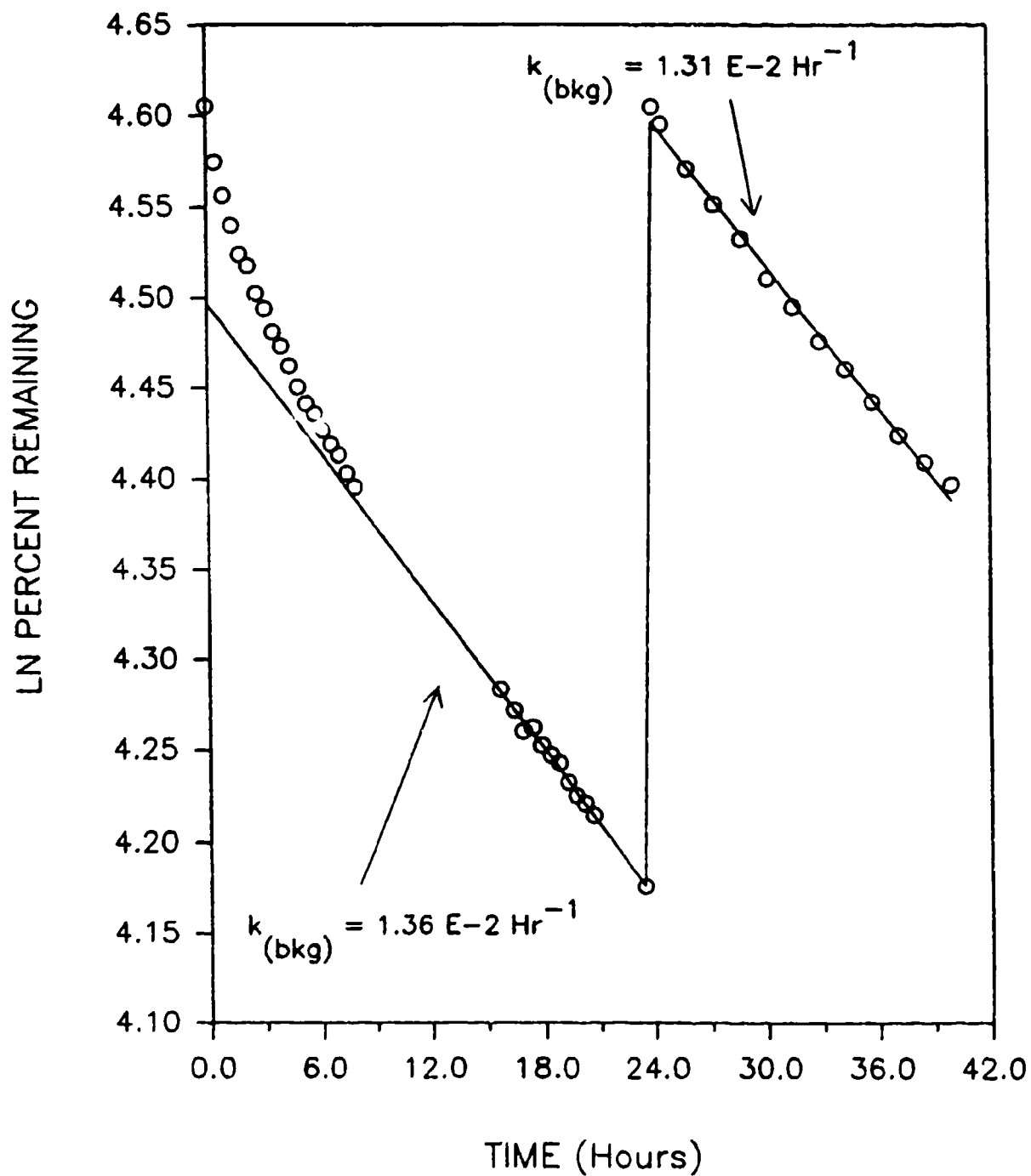


Figure 6. Variations of Hydrazine Vapor Loss in Interrupted Run When Additional Hydrazine Vapor Was Added

TABLE 1. BACKGROUND HYDRAZINE^a LOSS RATE CONSTANTS IN AIR AND NITROGEN

Run (#)	$k_{bkg} \times 10^2$ (hr ⁻¹)	Gas	Average ^b $\times 10^2$ (hr ⁻¹)
31	1.67	Air ^c	
44	1.59	"	
48	1.95	"	1.72 \pm 0.10
49	1.44	"	
86	1.95	"	
94	1.69	Nitrogen ^d	
95	1.62	"	
96	1.48	"	1.66 \pm 0.13
97	1.36	"	
100	2.13	"	

^a Initial hydrazine concentration 69 ppm v/v

^b Errors are standard errors

^c Average air temperature 298 \pm 2 K

^d Average nitrogen temperature 295 \pm 1 K

In experiments with dry air or dry nitrogen, water vapor increased over the duration of the experiment. This was presumably due to the fact that the chamber atmosphere was always drier than the ambient atmosphere. Both fluorocarbon and polyethylene films are permeable to water vapor, and the half-life for water vapor equilibration to the level of the chamber exterior was between 12 and 24 hours.

The water vapor content of the nitrogen used in these experiments was typically less than 10 ppm v/v, while the "dry air" produced by the Balston unit had an ultimate lower limit of 130 ppm v/v water vapor.

In several experiments, large amounts of water vapor were introduced into a well-purged chamber, and hydrazine vapor appeared in the chamber atmosphere. The hydrazine apparently had been displaced from the chamber surface by the water vapor. The concentration of the desorbed hydrazine was estimated at approximately 3 ppm v/v (about 3 to 5 percent of the amount

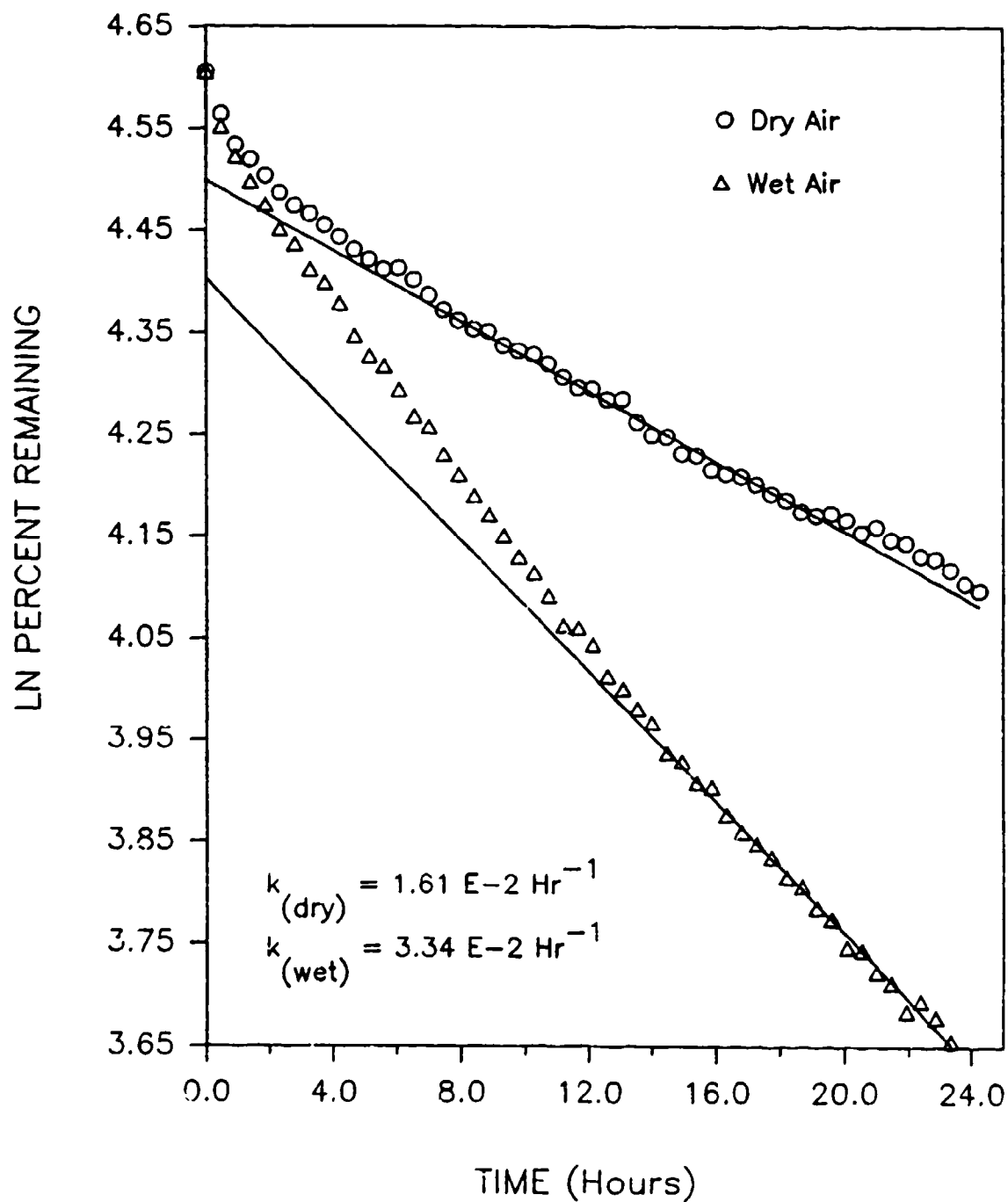


Figure 7. Hydrazine Loss Rate Curves in Dry and Humid Air

initially used), which strongly suggests that reversible absorption or surface adsorption effects are involved in the hydrazine loss processes.

(3) Carbon Dioxide. The chamber is permeable to CO_2 , as shown by its appearance during experiments with CO_2 -free air and nitrogen. To examine the effects of CO_2 permeation on hydrazine loss, an experiment was performed by adding 1000 ppm v/v CO_2 to dry air that contained the normal 300 ppm v/v CO_2 ($k_{\text{bkg}} = 3.43 \times 10^{-2} \text{ hr}^{-1}$). A second similar kinetic run with 1000 ppm v/v CO_2 added and 14,600 ppm v/v added H_2O vapor ($k_{\text{bkg}} = 2.90 \times 10^{-2} \text{ hr}^{-1}$) showed no significant differences between them. The k_{bkg} obtained for both runs, however, was approximately twice the normal k_{bkg} . The presence of either water or CO_2 , therefore, doubles the k_{bkg} , but they apparently do not have a cumulative effect on the k_{bkg} when combined.

d. Effects of Conditioning and Mixing

The first kinetic runs yielded k_{bkg} that gradually decreased as more kinetic runs were conducted (Figure 8). These first sequential kinetic runs, made over a three week period, are not considered representative of typical hydrazine k_{bkg} (Appendix). The largest k_{bkg} was observed in Run A, presumably due to the interaction of hydrazine vapor with contamination on the chamber walls accumulated during its construction. The k_{bkg} obtained from Run B was less than half that observed in the initial run. Kinetic Runs C, D, and E were performed in dry nitrogen, and the k_{bkg} obtained were quite similar to the average k_{bkg} obtained in a conditioned chamber with air or nitrogen.

Sequential kinetic Runs F through K were conducted in air, and each run produced a decreasing k_{bkg} until the conditioned chamber value of Run K was obtained.

Initial experiments performed in the chamber used a high-speed mixing fan during introduction of hydrazine vapor into the chamber, after which stirring was halted and hydrazine decay measured. During metal substrate testing, it was anticipated that the close spacing of the metal plates might

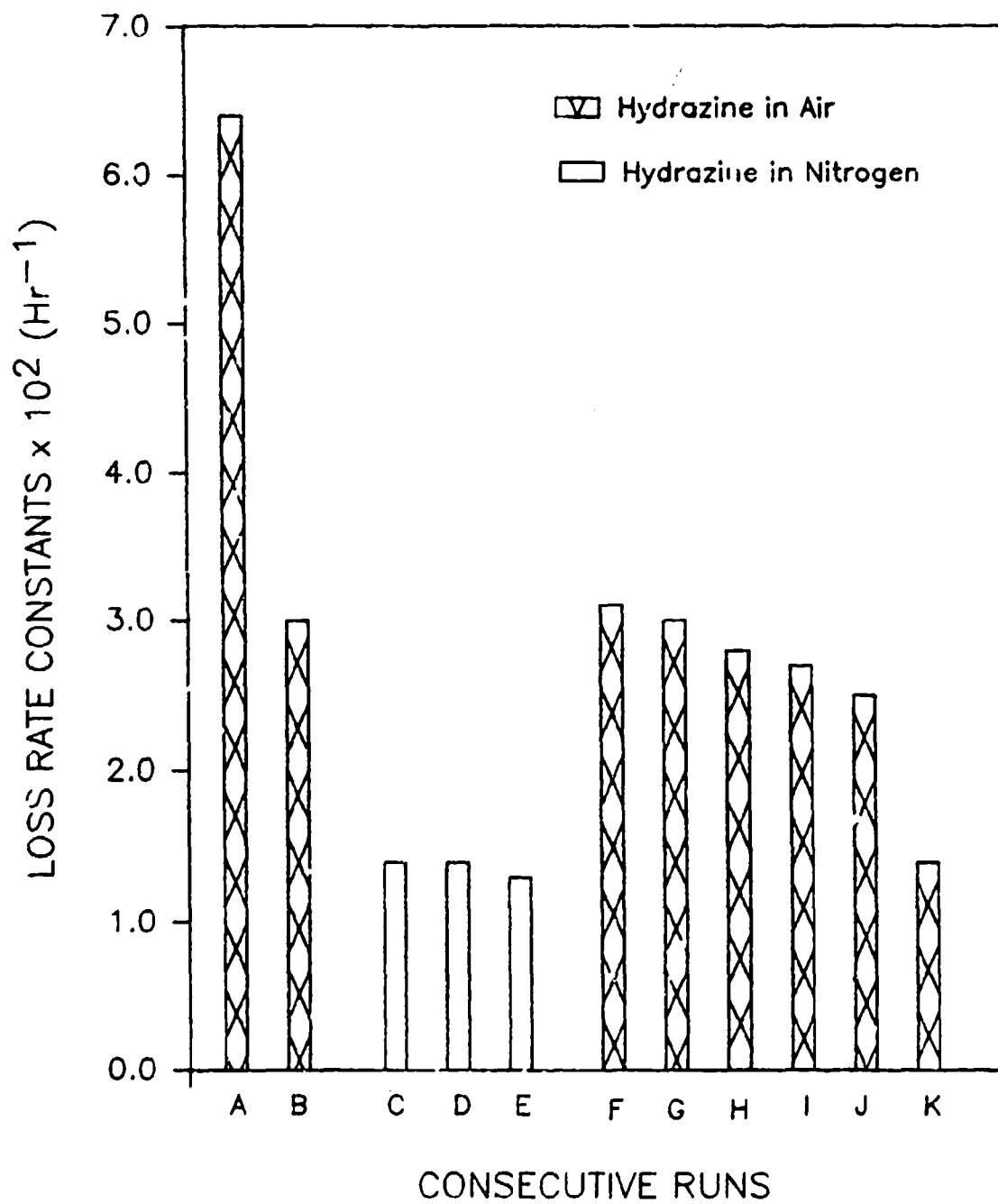


Figure 8. Hydrazine Loss Rate Constants for Early Kinetic Runs Showing Conditioning Effects

require the high-speed fan to be on at all times. The high speed fan caused significant vibration to the optical system, so it was turned off during data collection. To determine the effects of stirring rate and sequencing, a kinetic run with 49 closely spaced 304-L SS plates (20.5 m^2) was conducted. The fan was run continuously at high speed during the first 7 hours (except during two 4-minute data collection intervals each hour) and was turned off for the last 10 - 12 hours. The k_{bkg} during the stirred portion was $6.2 \times 10^{-2} \text{ hr}^{-1}$ while during the unstirred portion it was $2.83 \times 10^{-2} \text{ hr}^{-1}$. High-speed stirring thus increased the hydrazine k_{bkg} by a factor of two.

A variable speed DC motor was then installed that was operated at high speed during sample introduction and at low speed during a kinetic run. To determine the effects of this stirring sequence on hydrazine loss rate constants, several experiments were performed in which the fan was shut off during the last 25 percent of a kinetic run. Linear regression and graphical analysis of the hydrazine concentration data did not show any difference between the stirred and unstirred portions of the kinetic run. This stirring sequence, therefore, was used for all further experiments, and all data and k_{bkg} were acquired under these conditions.

e. Effects of Added FEP Surface

To test whether a surface-dependent reaction was occurring on the chamber FEP, an additional 24 m^2 of FEP were added to the chamber interior. The additional FEP increased the overall s/v to 7.07 m^{-1} while it maintained the exterior s/v at 3.39 m^{-1} . Under these conditions, the k_{bkg} was $1.7 \times 10^{-2} \text{ hr}^{-1}$, which is the same as the k_{bkg} without the added surface area of FEP. Also doubling the surface area did not appear to affect the nonlinear portion of the hydrazine decay curve. In dry nitrogen, a k_{bkg} of $2.33 \times 10^{-2} \text{ hr}^{-1}$ was obtained, a value slightly higher than normal.

When 14,600 ppm v/v of water vapor was added to the chamber with the added FEP, the average value for k_{bkg} increased to $3.47 \pm 0.13 \times 10^{-2} \text{ hr}^{-1}$. A conditioning effect was also observed, as shown by the decrease in the hydrazine k_{bkg} as this series of experiments progressed (Figure 9).

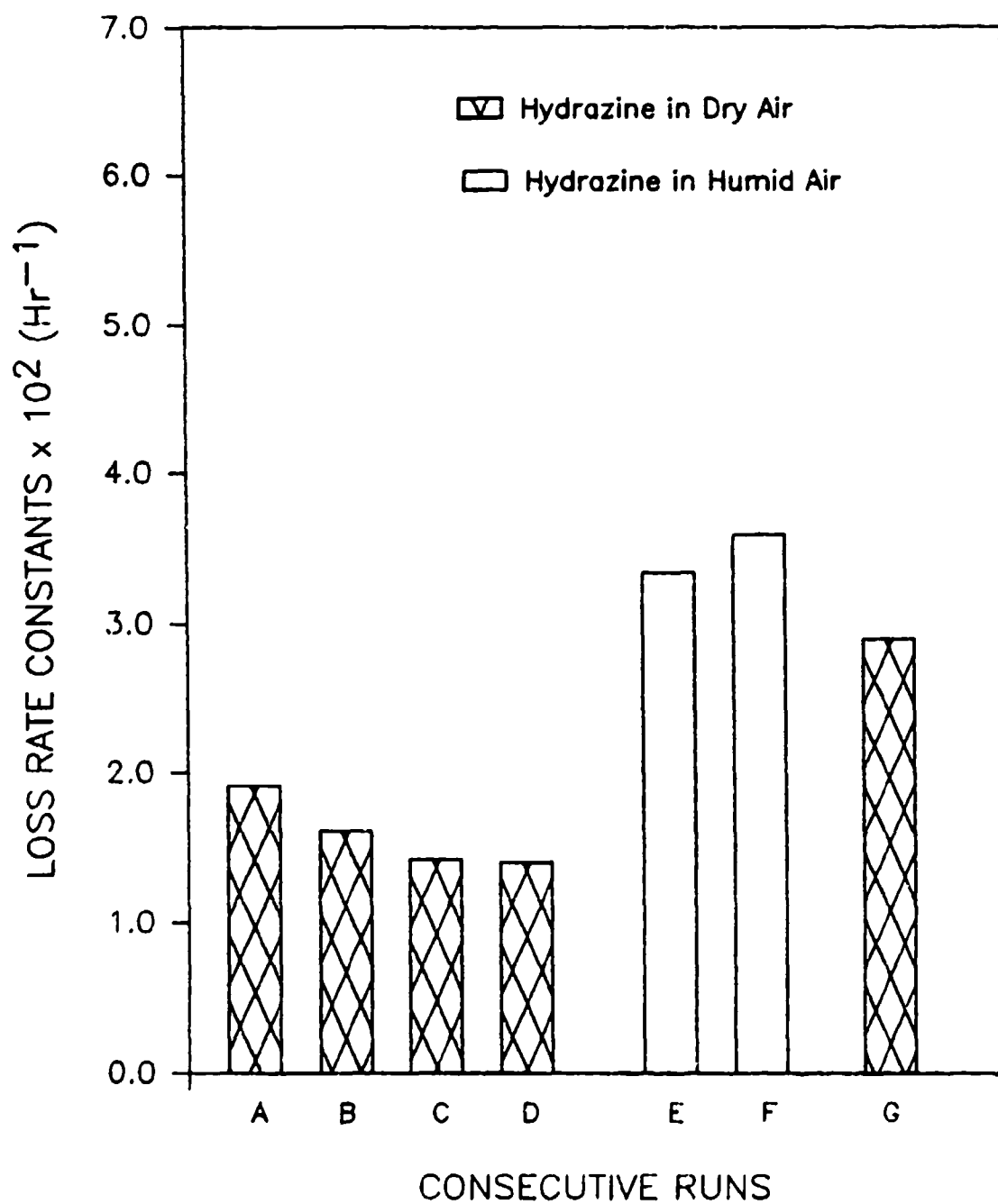


Figure 9. Effects of Conditioning and Humidity (14,600 ppm, y/v) on Hydrazine Loss Rate Constants (24 m² of Additional FEP Surface)

f. Effects of Metal Surfaces

Observed first-order rate constants (k_{obs}) for hydrazine in the presence of AlO_x , titanium, 304-L SS, zinc, and aluminum plates were 2 to 100 times higher than the k_{bkg} in the empty chamber. The most reactive surface proved to be AlO_x and the least reactive surface was aluminum. The k_{obs} in the presence of metal are shown in Tables 2 and 3.

TABLE 2. OBSERVED HYDRAZINE^a LOSS RATE CONSTANTS WITH AlO_x SURFACES IN AIR AND NITROGEN

Run (#)	Gas ^b	Surface Area (m ²)	$k_{obs} \times 10^2$ (hr ⁻¹)
33	Air	23.8	183
34	"	23.8	230
35	"	23.8	224
45	"	23.8	194
Average ^c =			208 ± 11
39	Air	3.3	4.8
40	"	6.7	13.4
41	" (H ₂ O) ^d	11.7	60.0
60	"	13.4	30.0
43	"	13.4	37.7
36	Nitrogen	23.8	74.5
37	"	23.8	99.2
46	"	23.8	41.6
Average ^c =			71.8 ± 16.7
e ₈₉	Nitrogen	23.8	76.3
e ₉₁	"	23.8	46.6
e ₉₂	"	23.8	17.3

^a Initial hydrazine concentration 68 ppm v/v

^b 298 ± 2 K

^c Errors are standard errors

^d Water 14,600 ppm v/v added to air

^e Surface previously exposed to 80 ppm v/v UDMH

TABLE 3. OBSERVED HYDRAZINE^a LOSS RATE CONSTANTS WITH METAL SURFACES IN AIR^b

Run (#)	Metal	Surface Area (m ²)	k _{obs} × 10 ² (hr ⁻¹)
62	Aluminum	20.9	3.60
63	"	20.9	3.15
Average ^c =			3.38 ± 0.23
38	304-L SS	20.9	3.58
61	Titanium	2.1	2.5
42	Zinc	19.2	4.77
87	"	21.3	4.98

^a Initial concentration approximately 69 ppm v/v

^b 298 ± 2 K

^c Error is standard error

(1) AlO_x . Kinetic runs were performed in both air and nitrogen with variable surface areas of AlO_x (Table 2). At the largest available surface area of AlO_x plates (23.8 m²), the average value of k_{obs} for hydrazine in air was 2.08 ± 0.11 hr⁻¹ (t_½ = 0.33 hours). Figure 10 shows a typical run with AlO_x present. The average rate constant obtained in nitrogen with the same surface area was 0.72 ± 0.17 hr⁻¹ (t_½ = 0.96 hours).

Under these conditions, the presence of reactive intermediates with IR bands at 3180 to 3050 cm⁻¹ and 1380 to 1275 cm⁻¹ were detected (Figures 11 and 12). The IR bands at 1380 to 1275 cm⁻¹ are identified as those due to superimposed hydrogen peroxide and diazene (Reference 15). The hydrogen peroxide/diazene concentration reached a maximum after approximately 1.5 hours; after 16 hours, no hydrazine, hydrogen peroxide, or diazene remained (Figure 13). Ammonia, at 3 to 5-percent of the initial hydrazine concentration, was present as a final product. Ammonia was never seen in the background runs. With smaller surface areas of AlO_x , or with other metals, the buildup of detectable concentrations of hydrogen peroxide or diazene was not observed.

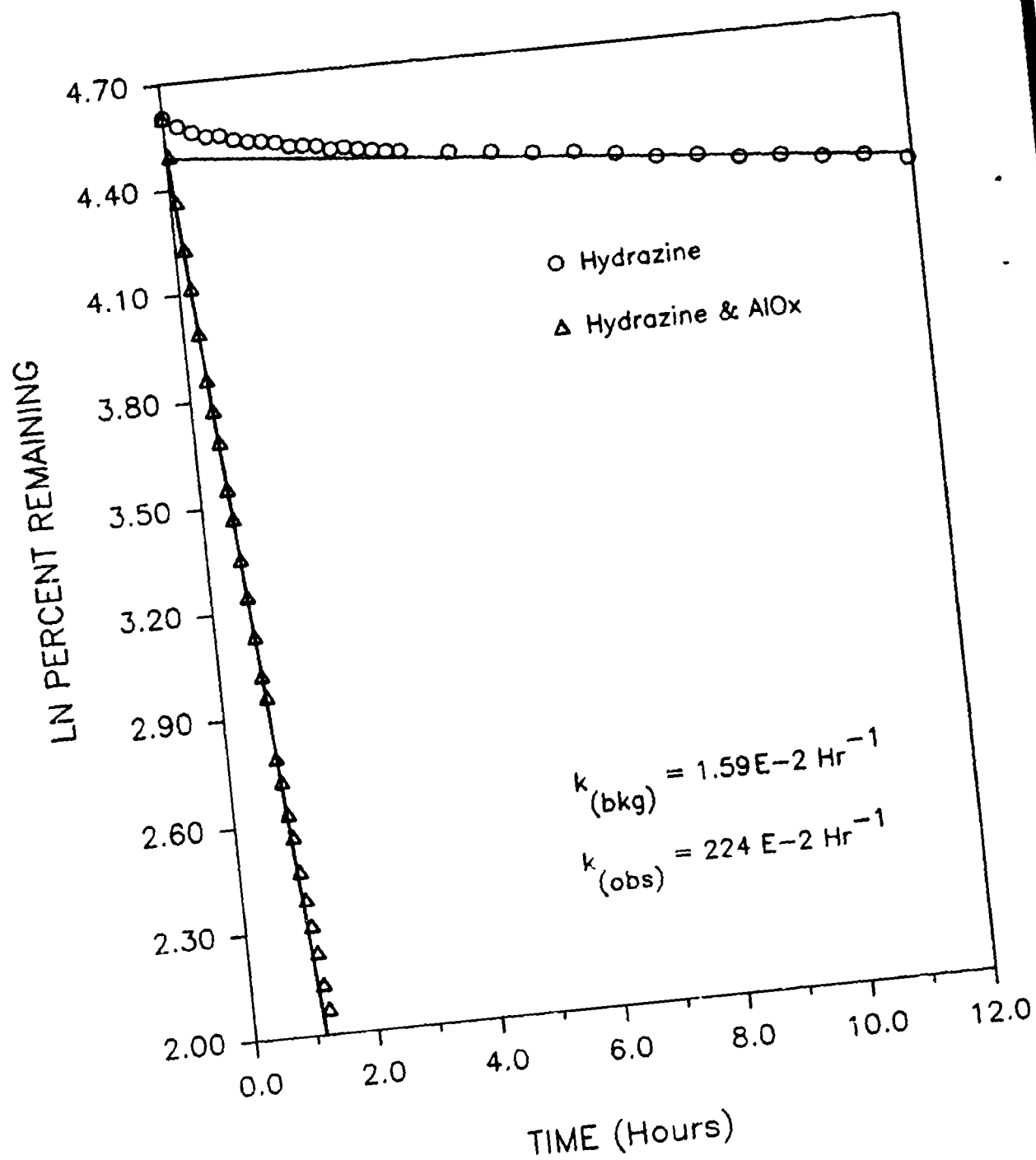


Figure 10. Effects of 23.8 m² of AlOx on the Hydrazine Loss Rate in Air

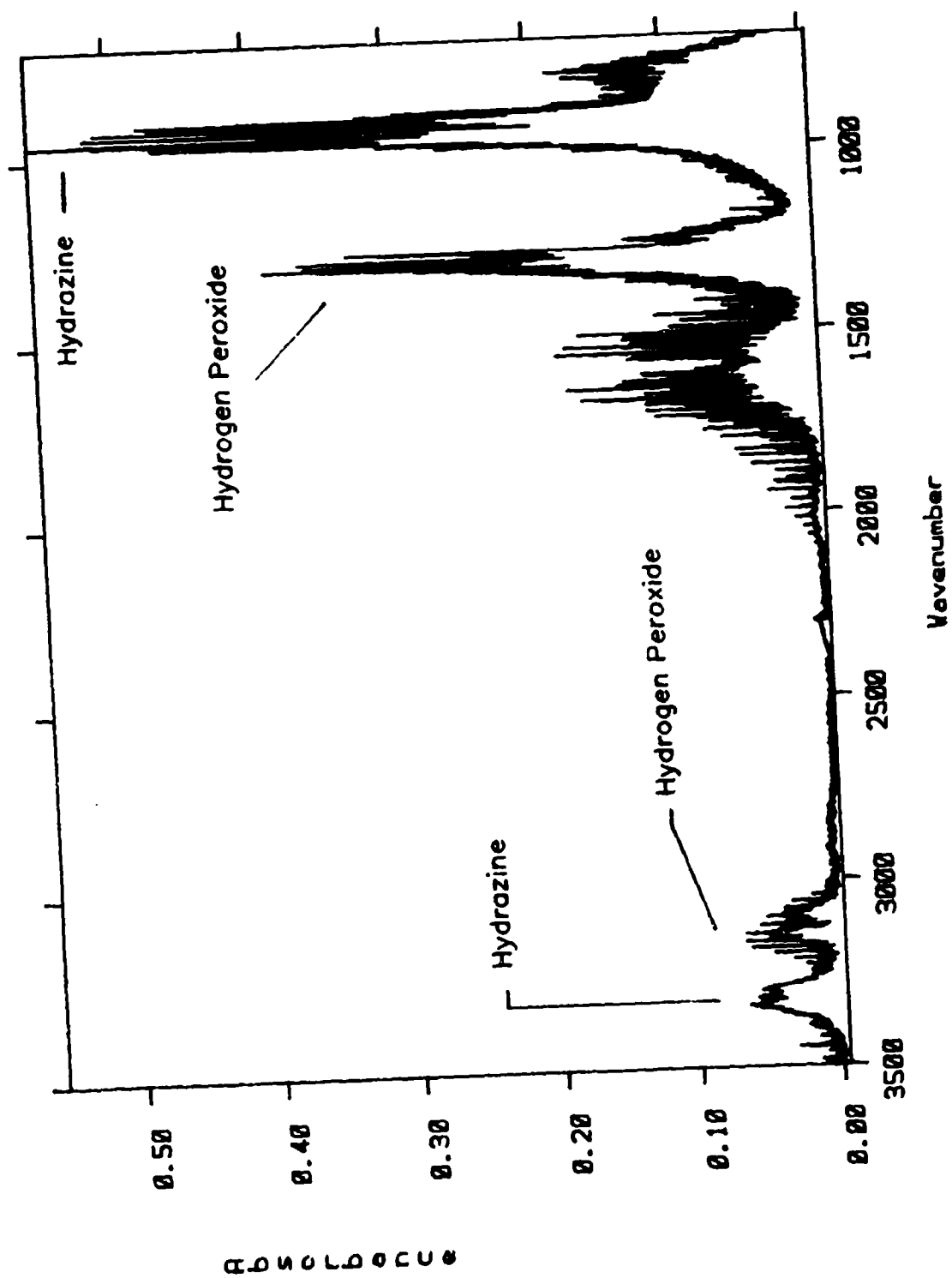


Figure 11. Gas-Phase IR Spectrum of Hydrogen Peroxide, Diazene, and Hydrazine

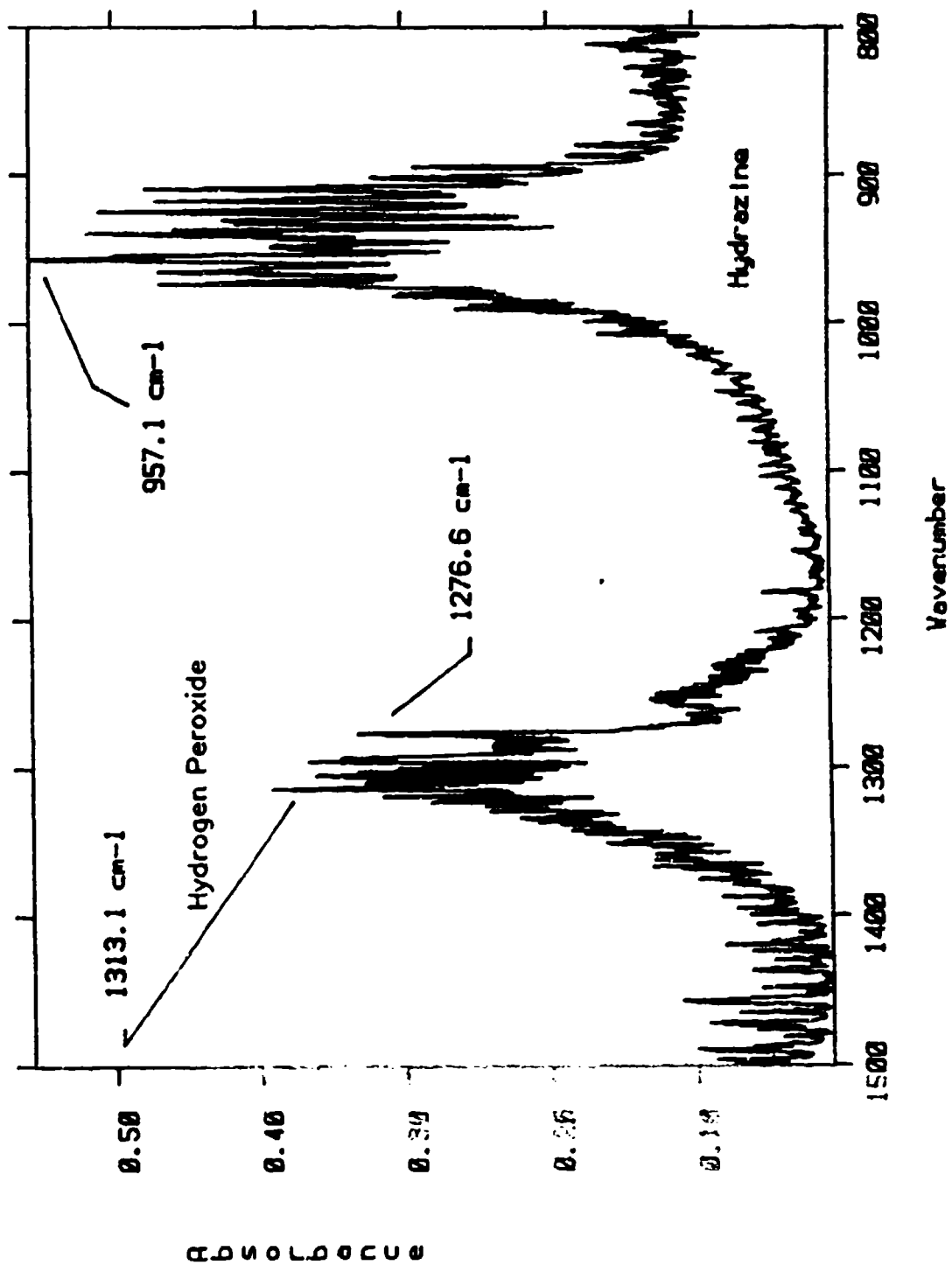


Figure 12. Gas-Phase IR Spectrum of Hydrogen Peroxide, Diazene, and Hydrazine

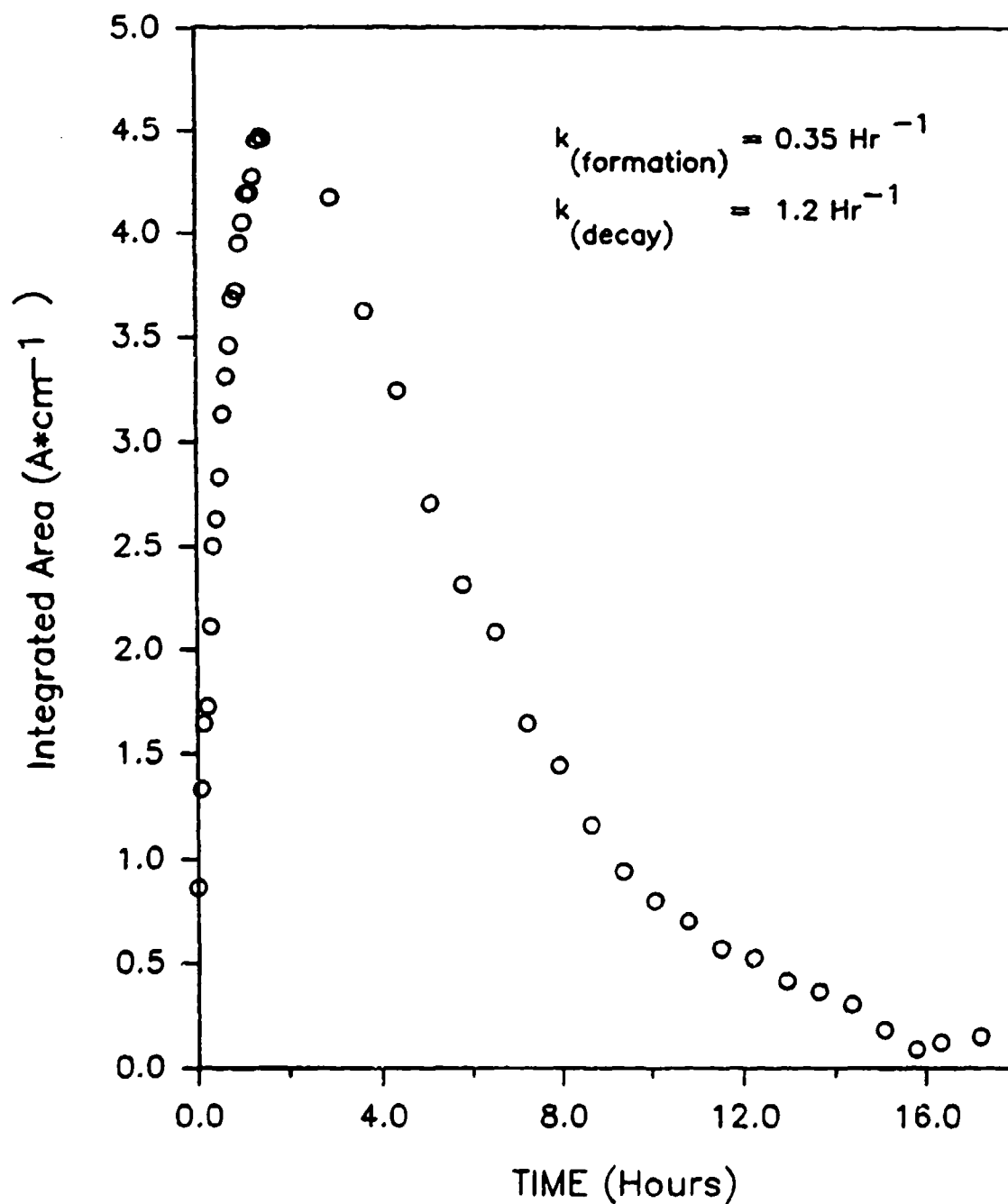


Figure 13. Formation - Decay Curve for Hydrogen Peroxide Plus Diazene, from the Reaction of Hydrazine in Air on 23.8 m^2 of AlO_x

Numerical analysis of the appearance/disappearance curve for the hydrogen peroxide/diazene mixture, treated as two consecutive first-order reactions, gives 0.35 hr^{-1} and 1.2 hr^{-1} as the overall formation and decay rate constants. The maximum concentration of diazene and hydrogen peroxide is estimated to be 18 percent of the initial hydrazine concentration of 69 ppm v/v.

(2) Aluminum. Aluminum was exposed to hydrazine under the same conditions as AlO_x (air, slow stirring, ambient temperature). At the maximum surface area (20.9 m^2), the k_{obs} for hydrazine loss was $3.38 \pm 0.23 \times 10^{-2} \text{ hr}^{-1}$, which is only twice the k_{bkg} . Hydrogen peroxide, diazene, or other reaction products were not detected.

(3) Other Metals. Titanium, 304-L SS, and zinc had values for k_{obs} of 3.58×10^{-2} , 2.5×10^{-2} , and $5.98 \times 10^{-2} \text{ hr}^{-1}$ for 20.9, 2.1, and 21.3 m^2 , respectively, when tested in the same conditions as AlO_x . The maximum surface area of titanium was an order of magnitude lower than the other metals. Hydrazine exposure with each metal was conducted at the largest available surface area, and no detectable concentrations of hydrogen peroxide, diazene, or other reaction products were observed.

3. MMH Loss Processes in the Chamber

a. Background Rates

The k_{bkg} for MMH in air was $3.66 \pm 0.17 \times 10^{-2} \text{ hr}^{-1}$ ($t_{\frac{1}{2}} = 19$ hours). This was higher than either hydrazine or UDMH, and MMH was the only fuel hydrazine studied that yielded reaction products in the absence of metal surfaces. Both methanol (at 2 percent of the initial MMH concentration) and traces of methyldiazene ($\text{HN}=\text{NCH}_3$, Reference 16) were detected in the background runs. The plots of the natural log of the percent remaining were linear throughout the entire range of concentration.

b. Effects of Metal Surfaces

The AlO_x and the 304-L SS metal plates both exhibited appreciable reactivity with MMH (Table 4). MMH was less reactive than hydrazine under these conditions (Figure 14). Reduced surface area runs were performed only

TABLE 4. OBSERVED MMH^a LOSS RATE CONSTANTS WITH METAL SURFACES IN AIR^b

Run (#)	Metal	Surface Area (m ²)	$k_{\text{obs}} \times 10^2$ (hr ⁻¹)
73	None	-	3.90
74	"	-	3.65
75	"	-	3.58
85	"	-	3.50
Average ^d =			$\frac{3.66 \pm 0.17}{3.66 \pm 0.17}$
69	AlO_x	23.8	12.0
78	"	23.8	14.6
79	"	23.8	15.0
Average ^d =			$\frac{13.9 \pm 0.9}{13.9 \pm 0.9}$
83	AlO_x	12.1	7.00
84	"	11.7	6.50
76	Aluminum	20.9	4.70
77	"	20.9	4.20
Average ^d =			$\frac{4.45 \pm 0.25}{4.45 \pm 0.25}$
80	304-L SS	20.9	12.9
81	"	20.9	13.9
Average ^d =			$\frac{13.4 \pm 0.5}{13.4 \pm 0.5}$
71	Zinc	20.9	6.44
70	"	20.9	6.34
Average ^d =			$\frac{6.39 \pm 0.05}{6.39 \pm 0.05}$

^a Initial MMH concentration 83 ppm v/v

^b 298 ± 2 K

^c These values are k_{bkg}

^d Errors are standard errors

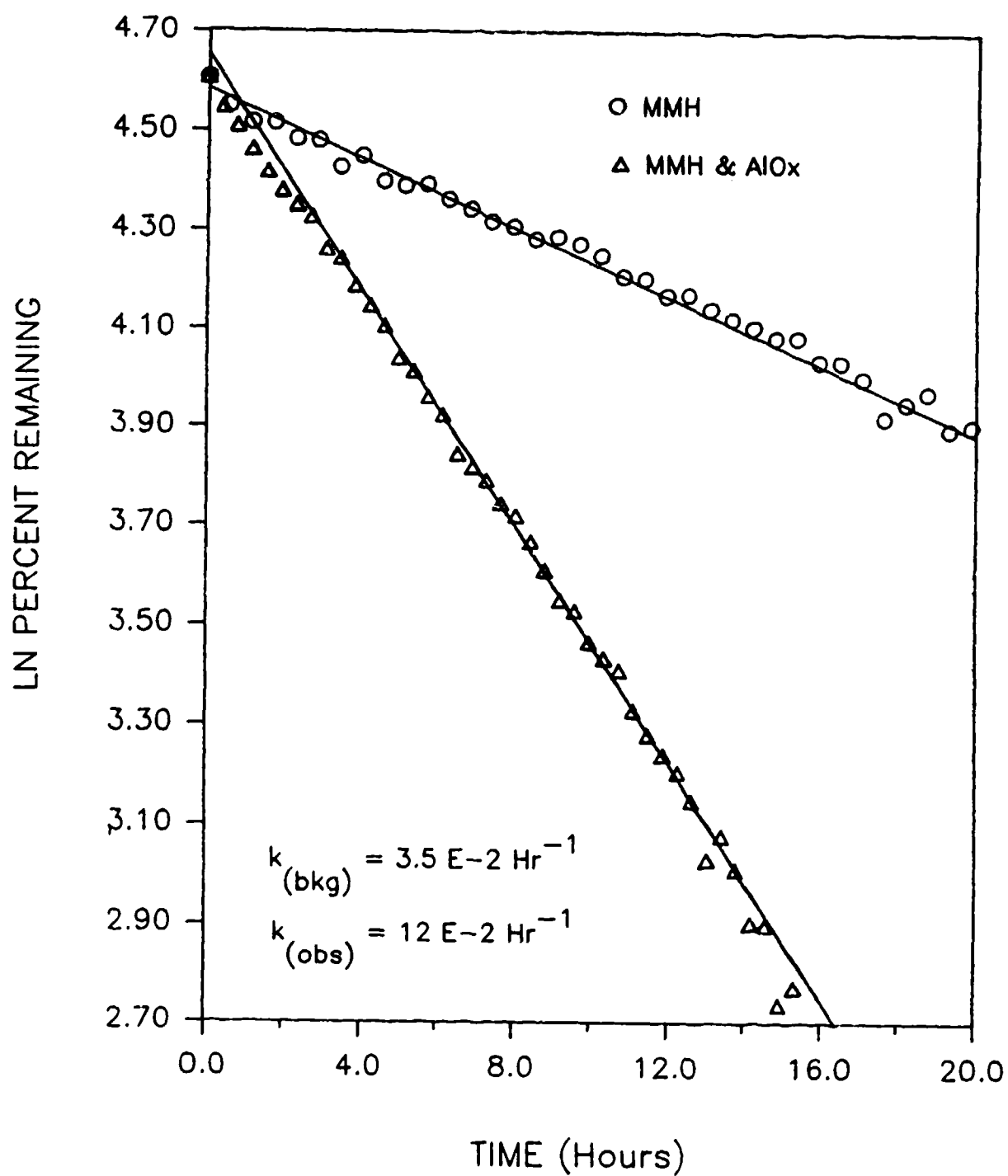


Figure 14. MMH Loss Rate in the Presence and Absence of 23.8 m² of AlOx

with AlO_x . Methanol (at 3 to 9 percent of the initial MMH concentration) and traces of methyldiazene were observed as products in the presence of metal plates; both were at slightly higher concentrations than in the background runs. The concentrations of the reaction products were too low to obtain appearance/disappearance rate constants. No other reaction products were detected. At maximum surface area of AlO_x (23.8 m^2), $k_{\text{obs}} = 1.39 \pm 0.09 \times 10^{-1} \text{ hr}^{-1}$, and for 20.9 m^2 of 304-L SS, $k_{\text{obs}} = 1.34 \pm 0.05 \times 10^{-1} \text{ hr}^{-1}$.

The zinc and aluminum plates exhibited an MMH reactivity less than twice that of the background. The methanol and methyldiazene products were not formed in significantly greater yields than in background runs.

4. UDMH Loss Processes in the Chamber

The slowest background loss rate was observed for UDMH disappearance with an average $k_{\text{bkg}} = 1.15 \pm 0.14 \times 10^{-2} \text{ hr}^{-1}$ ($t_{1/2} = 60.1$ hours). No reaction products were observed in air or in the presence of 23.8 m^2 of AlO_x surface in air. The average k_{obs} in the presence of the AlO_x was $2.3 \pm 0.4 \times 10^{-2} \text{ hr}^{-1}$. UDMH was not tested with any other surfaces (Table 5). Log plots of runs in the absence and presence of 23.8 m^2 of AlO_x plates are shown in Figure 15. The initial curvature in the log plots, which was observed with hydrazine, was also observed with UDMH. Those deviations from linearity, however, were not nearly as severe.

5. Aerozine-50 Loss Processes in the Chamber

Loss rates for Aerozine-50, a 50/50 mixture of hydrazine and UDMH, were obtained by simultaneously monitoring the UDMH area at 2900 to 2775 cm^{-1} and the hydrazine peak at 957 cm^{-1} . The usual hydrazine integrated area was not used due to interference from the UDMH absorbance bands.

A k_{bkg} of $2.5 \times 10^{-2} \text{ hr}^{-1}$ ($t_{1/2} = 28$ hours) was obtained for the hydrazine portion of the Aerozine-50 loss, which is 1.5-times greater than the

TABLE 5. OBSERVED UDMH AND AEROZINE-50 LOSS RATE CONSTANT IN THE PRESENCE AND ABSENCE OF AlO_x SURFACES IN AIR^a

Run (#)	Fuel	Metal ^b	$k_{obs} \times 10^2$ (hr ⁻¹)
64	UDMH	None	^c 1.11
65	"	"	^c 0.94
66	"	"	^c 1.41
Average ^d =			1.15 ± 0.14
67	UDMH	AlO_x	2.70
68	"	"	1.90
Average ^d =			2.30 ± 0.40
88	Aerozine-50	None	^c 2.47 (hydrazine) ^c 1.76 (UDMH)
90	Aerozine-50	AlO_x	--- (hydrazine) 4.04 (UDMH)

^a 298 ± 2 K

^b 23.8 m^2

^c These values are k_{bkg}

^d Errors are standard errors

value obtained for kinetic runs with hydrazine alone. The k_{bkg} of $1.8 \times 10^{-2} \text{ hr}^{-1}$ ($t_{\frac{1}{2}} = 39$ hours) for UDMH was also 1.5 times greater than the average k_{bkg} for UDMH when tested separately.

One test with Aerozine-50 was performed with 23.8 m^2 of AlO_x plates present in the chamber and only the UDMH decay rate was monitored. The k_{obs} in this experiment was $4.04 \times 10^{-2} \text{ hr}^{-1}$ ($t_{\frac{1}{2}} = 17$ hours), 2.5-times greater than the UDMH k_{bkg} .

D. DISCUSSION

1. Fluorocarbon-Film Interaction

In the absence of metallic surfaces, hydrazine vapor disappears from the FEP chamber with $t_{\frac{1}{2}} = 41$ hours. There are four crucial observations

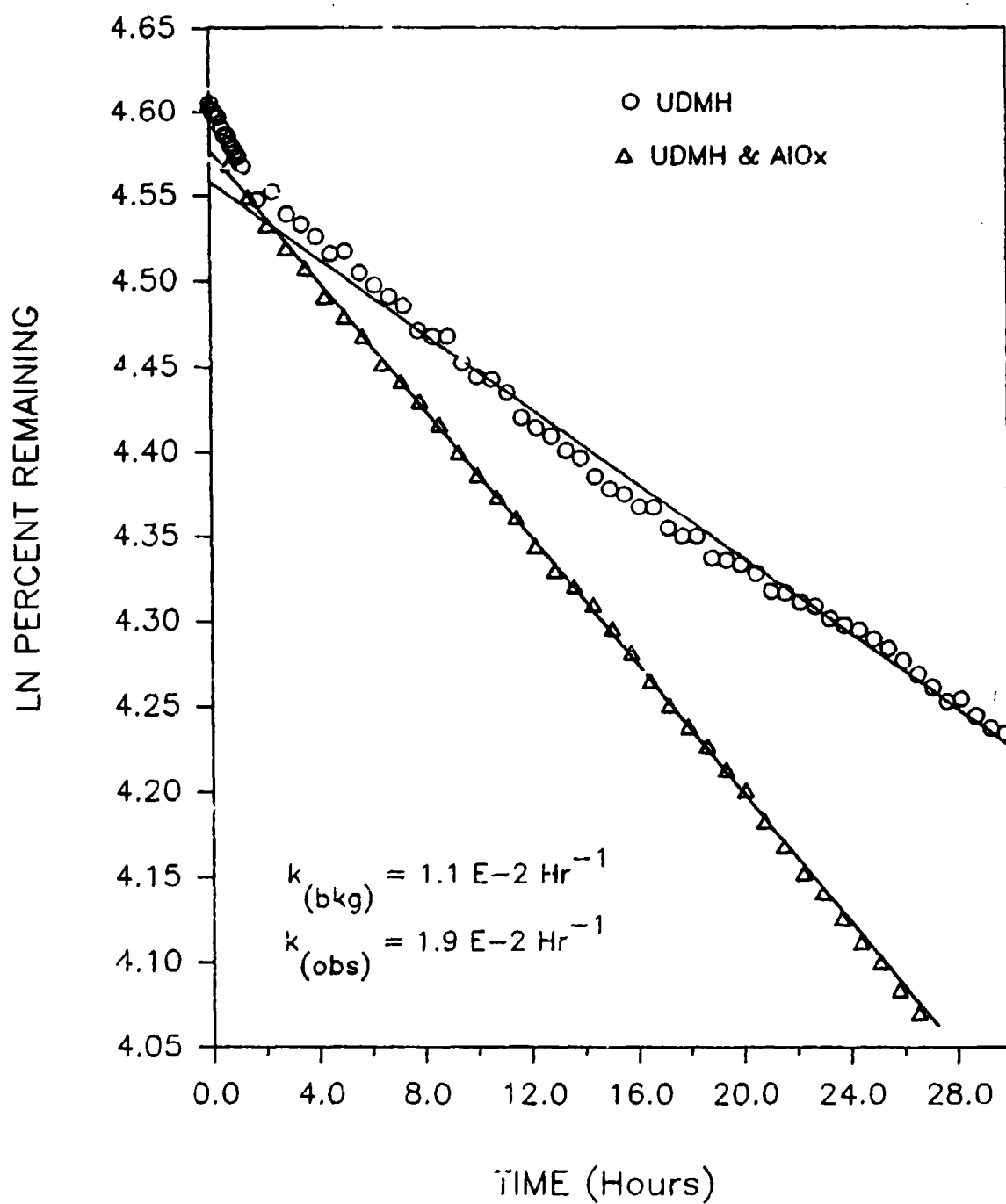


Figure 15. UDMH Loss Rate in the Presence and Absence of 23.8 m² of AlOx

concerning the mechanism of this disappearance. First, the k_{bkg} for substances as diverse as sulfur hexafluoride, methane, methanol and the fuel hydrazines varied by only a factor of nine (Reference 12). Second, the k_{bkg} were the same in nitrogen as in air, and no trace of reaction products were detected (except for MMH). Third, increasing the internal surface area of fluorocarbon-film without increasing the external area had no effect on the k_{bkg} . Finally, the addition of water vapor to a previously used chamber containing only pure air resulted in the reappearance of hydrazine vapor.

a. Loss Rates

Table 6 summarizes the k_{bkg} under standard conditions for the fuel hydrazines and several other compounds. Data from a 320-liter chamber, constructed of the same FEP and used at Tyndall AFB, are also included (References 11, 12).

The k_{bkg} for methane from the smaller chamber was greater than that from the larger chamber, but if a correction is made for the different s/v ratios, the k_{bkg} from the two chambers are nearly identical. The k_{bkg} for oxidatively inert aprotic materials from either chamber are approximately $5 \pm 1 \times 10^{-3} \text{ hr}^{-1}$ (corrected to an s/v ratio of 3.39 m^{-1}). Methanol, a protic, polar, and oxidatively inert substance, has a greater k_{bkg} than aprotic, nonpolar molecules, but is similar to that of the protic, polar fuel hydrazines. It appears that the k_{bkg} is not determined by molecular weight or oxidative reactivity, but rather by the protic nature of the molecule and the s/v ratio of the chamber. Because the hydrazine k_{bkg} are the same in air or nitrogen, and oxidation products are not generally detected, physical rather than chemical processes are probably responsible for the k_{bkg} of fuel hydrazines and other materials from the FEP chamber. Similar conclusions have been reported elsewhere (Reference 11, 17). Vapor transmission rate (VTR) data also support this conclusion; they show that FEP is about four to ten times more permeable to polar protic substances than to aprotic substances (Table 7).

TABLE 6. FIRST-ORDER LOSS RATE CONSTANTS
FROM FEP CHAMBERS^a

Compound	$k_{bkg} \times 10^2$ (hr ⁻¹)
TF-Freon	0.5
Methane	^b 0.43 0.6
Sulfur hexafluoride	^b 0.6
Methanol	1.6
Hydrazine	^b 1.7 2.2
MMH	3.7
UDMH	1.1

^a Ambient temperature, 50-75 ppm v/v
initial concentration

^b Data from the Tyndall chamber (s/v =
8.9 m⁻¹) corrected to an s/v ratio of
3.39 m⁻¹

b. Surface Adsorption/Permeation

Adsorption onto the FEP surface or absorption into the void volume of the film are two physical processes that, separately or in some combination, result in the loss of gas-phase material. The reversibility of this adsorption process is demonstrated by the reappearance of hydrazine when the chamber was flooded with humid gas. A more detailed description of permeation that accounts for the permanent loss of gas-phase material is as follows: after adsorption onto the surface, absorption into the void volume of the FEP can occur; the material is then transported through the film with subsequent desorption on the exterior of the chamber surface. This sequence of adsorption-absorption-desorption assumes that the FEP is initially not covered

TABLE 7. VAPOR TRANSMISSION RATES^a THROUGH FEP^b

Compound	VTR (g·m ⁻² day ⁻¹ atm ⁻¹)
Carbon tetrachloride	22
Hexane	29
Acetone	33
Ethanol	82
Water	99
Acetic acid	182

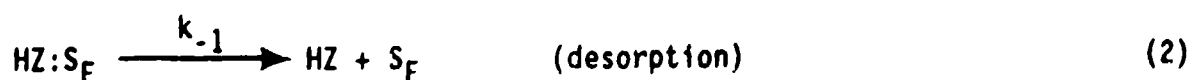
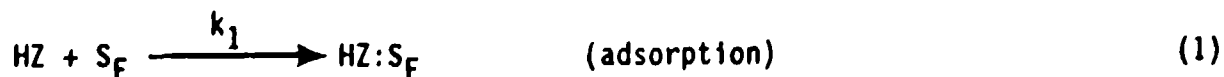
^a Standard test method (ASTM E-96-53 Mod.),
308 K (Reference 18)

^b 0.0025-cm (1-mil) thick

by adsorbate, and that the establishment of the sorption equilibrium (steady-state) will result in a kinetic effect at the start of the process.

c. Kinetic Analysis

The k_{bkg} considered so far have been determined from the linear portion of the exponential decay curves. The initial 15 to 25 percent of the loss curves show significant deviations from simple first-order decay. This initial curvature and biphasic feature is consistent with the establishment of a reversible surface adsorption process followed by irreversible permeation through the film (or absorption into the film), shown by Equations (1), (2), and (3):





The following kinetic schemes (Cases I and II) can be developed based on the above equations. In these schemes, the following are used:

- [HZ] = gas-phase concentration of hydrazine
- [S_F] = concentration of unoccupied FEP surface sites
- [HZ:S_F] = concentration of occupied FEP surface sites
- [-HZ] = concentration of hydrazine which has permeated out of the chamber
- k₁ = rate constant for hydrazine adsorption to unoccupied FEP surface sites
- k₋₁ = rate constant for hydrazine desorption from occupied FEP surface sites
- k₂ = rate constant for the irreversible permeation through the FEP

CASE I: Equilibrium adsorption rapidly established, sparse coverage, k₁ > k₂:

$$\text{loss rate} = k_2 [\text{HZ:S}_F] \quad (4)$$

At sparse coverage:

$$[\text{S}_F] = [\text{S}_F]_0 \quad (5)$$

where

[S_F]₀ = concentration of unoccupied FEP surface sites at time t=0

At equilibrium:

$$\frac{[\text{HZ:S}_F]}{[\text{HZ}] [\text{S}_F]} = K \quad (6)$$

where

$$K = \frac{k_1}{k_{-1}} \quad (7)$$

$$\text{loss rate} = k_2 K [\text{S}_F]_0 [\text{HZ}] \quad (8)$$

and:

$$k_2 K [S_F]_0 = k_{bkg} \quad (9)$$

then:

$$\text{loss rate} = k_{bkg} [HZ] \quad (10)$$

This case proves that the observed loss rate is a simple first-order decay, which is not consistent with the observed kinetics for hydrazine.

CASE II: Approach to steady state, adsorption equilibrium not established rapidly, sparse coverage, $k_1 \approx k_2$,

$$\frac{d[HZ:S_F]}{dt} = -k_2[HZ:S_F] - k_{-1} [HZ:S_F] + k_1 [HZ] [S_F] \quad (11)$$

If the initial value of $[HZ:S_F] = 0$ and the rate constants are assumed to have similar magnitudes, a true equilibrium is never established. During the initial stages of the reaction, as the surface sites are being filled, the net rate of disappearance from the gas phase is the greatest. As the concentration of surface sites begins to reach a steady state, the net loss rate slows due to desorption that replenishes some gas-phase material.

The exact solution to the differential equation (Equation (11)) is available but not readily amenable to use in experimental situations (Reference 19); therefore, a numerical fitting routine has been used to determine the microscopic rate constants. Initial estimates of the three rate constants were used to calculate a concentration versus time curve, and the sum of deviations from the experimental data were minimized iteratively. Table 8 contains a listing of the derived rate constants for several different conditions and compounds. The values of k_1 reported in Table 8 are the pseudo-first-order rate constants, $k_1 [S_F]_0$.

TABLE 8. DERIVED RATE CONSTANTS FOR ADSORPTION/PERMEATION OF FUEL HYDRAZINES ON FEP^a

Run (#)	Compound	Conditions	k_1	k_{-1}	k_2	k_{bkg}
			$(hr^{-1} \times 10^2)$			
44	Hydrazine	Dry Air	9.6	59	13.5	1.6
avg.	Hydrazine	Dry Air	9.7	62	15	1.7
94	Hydrazine	Dry Nitrogen	8.8	38	11	1.7
avg.	Hydrazine	Dry Air ^b	9.6	56	15	1.7
avg.	Hydrazine	Humid Air ^{b,c}	8.9	15	15	3.5
avg.	Aerozine-50	Dry Air (Hydrazine) (UDMH)	7.9	35	15	2.1
64	UDMH	Dry Air	2.8	19	13	1.1

^a Ambient temperature, 50-75 ppm v/v initial concentration

^b 24 m² of added FEP

^c 14,700 ppm v/v water vapor

Of these possible schemes, both hydrazine and UDMH loss-rate profiles are satisfactorily handled by the Case II (approach to steady state). The computer determination of the rate constants provides calculated hydrazine/time data, and a comparison of the calculated and observed data is shown in Figure 16. An estimate of the amount of hydrazine that is surface bound, $[HZ:S_F]$, is also calculated. In a typical run, $[HZ:S_F]$ starts at zero and reaches a maximum value of 15 percent of the initial hydrazine concentration after 20 percent of the reaction. Considering the simplicity of the model used here, the fit of the calculated and observed data is satisfactory. A more complete modeling of this kind of system is available (Reference 20).

Because the overall loss rate constants for hydrazine and its derivatives are similar, it is not surprising that the adsorption, desorption and permeation rate constants shown in Table 8 are similar. The effect of humidity is clarified by noting that, under humid conditions, the desorption

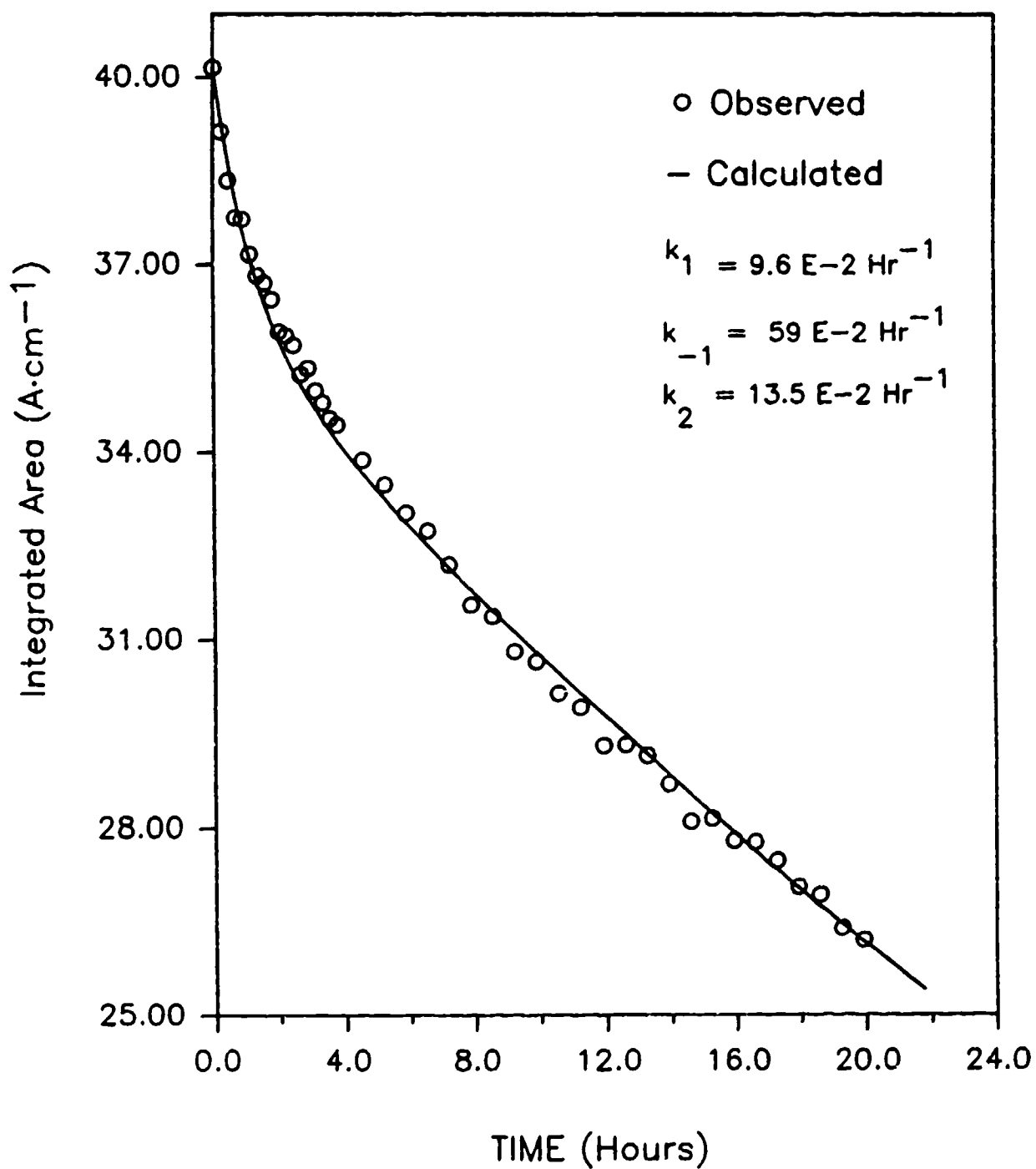


Figure 16. Theoretical Versus Actual Hydrazine Concentration as Integrated Area in Initial Nonlinear Portion of Hydrazine Loss Rate Curve

rate constant, k_{-1} , decreases significantly. Humidity effects can be explained by increased adsorption of water into (or onto) the FEP surface. For polar, protic molecules such as hydrazine, the increased hydrophilicity of the film would stabilize the surface bound species, $[HZ:S_F]$, and decrease the desorption rate. Hydrazine, which is known to form a stable hydrate, may be particularly susceptible to humidity effects.

The effect of surface modification may also explain the increased loss rates observed with Aerozine-50. Adsorption of the more polar hydrazine may increase the UDMH loss rates, and vice versa.

The loss rates for MMH are greater, and may more properly be described by Case I (a rapidly established adsorption equilibrium). Initial curvature is not seen in MMH experiments, and microscopic rate constants can not be dissected from the observed rates because $k_{bkg} = K \cdot k_2$.

2. Metallic Surface Interactions

After developing a reasonable picture of the processes involved in the loss of fuel hydrazines from an FEP chamber, a further step in determining the environmental fate of fuel hydrazines is a study of the interaction of fuel hydrazines with environmental surfaces. The surfaces of interest are those which might be found at fuel handling and use facilities. This was carried out by adding aluminum, 304-L SS, zinc, and titanium metal plates to the environmental chamber and observing the loss rates of the fuel hydrazines. In all cases, the loss rates in the presence of metal plates were greater than those observed in a background situation.

a. Loss Rates

In the simplest kinetic scheme, a step for the interaction of the metallic surface is added to the scheme outlined previously. Thus, Equations (1), (2), and (3), then:



where k_{met} represents the rate constants for interaction with the metallic surface, S_M . Kinetically, processes such as adsorption or reaction to non-hydrazine products are indistinguishable, and we use k_{met} as the sum of these processes. The overall loss rate, which is also the observed loss rate (k_{obs}) is:

$$\text{loss rate} = k_{\text{bkg}}[\text{HZ}] + k_{\text{met}}[\text{S}_M]^n[\text{HZ}] \quad (13)$$

where

n = order with respect to metal surface

thus

$$\text{loss rate} = k_{\text{obs}}[\text{HZ}] \quad (14)$$

where

$$k_{\text{obs}} = k_{\text{bkg}} + k_{\text{met}}[\text{S}_M]^n \quad (15)$$

If we define

$$k_m = k_{\text{met}}[\text{S}_M]^n \quad (16)$$

then the apparent surface interaction rate constants, k_m , for hydrazine, MMH, and UDMH are calculated by subtracting k_{bkg} from k_{obs} .

The highly reactive nature of the AlO_x plates allowed a study of the response of the k_m value with respect to surface area of added plates. For both hydrazine and MMH, k_m increases as the square of the surface area ($n = 2$, Equation (16)). This is demonstrated by a plot of $\log(k_m)$ against $\log(\text{area})$ for hydrazine and MMH with the AlO_x surface (Figure 17). The data are shown with lines of slope equal to two. The values of k_m and k_{met} calculated using $n = 2$ are shown in Table 9. The reactivity shown by titanium surfaces deserves additional study at higher surface areas.

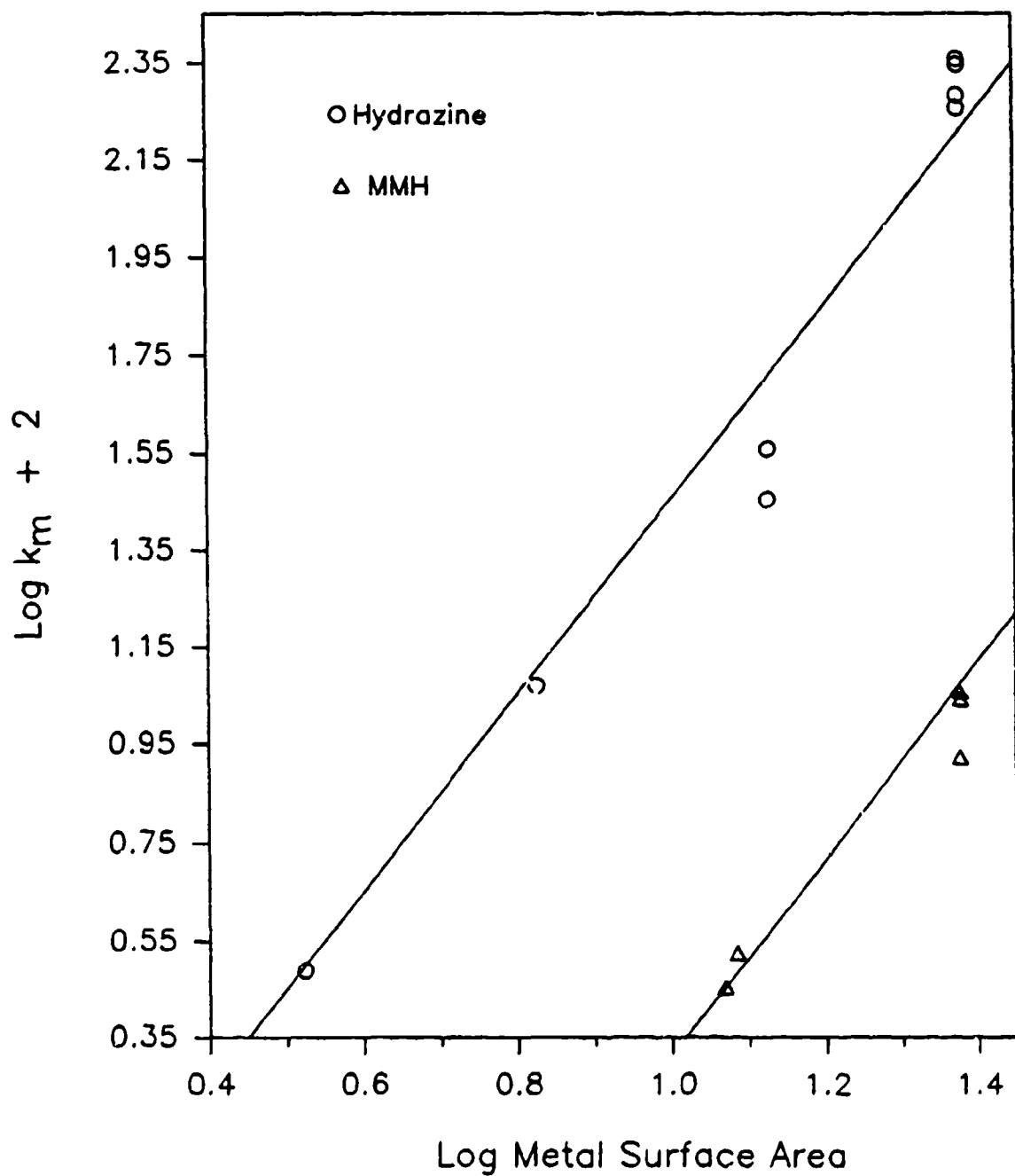


Figure 17. $\text{Log}(k_m)$ Versus $\text{Log}(\text{area})$ for Hydrazine and MMH; Lines Shown Have a Slope of 2

TABLE 9. RATE CONSTANTS FOR FUEL HYDRAZINES WITH METAL SURFACES IN AIR^a

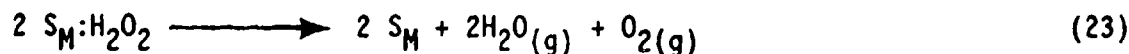
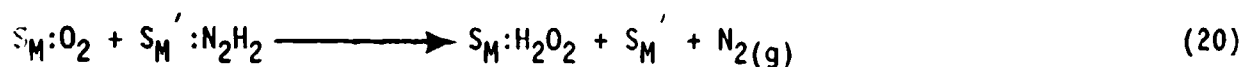
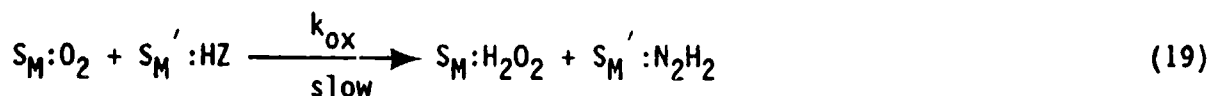
Metal	Surface Area (m ²)	$k_m \times 10^2$ (hr ⁻¹)	$k_{met} \times 10^5$ (hr ⁻¹ m ⁻⁴)
Hydrazine			
AlO _x	23.8	208	367
	13.4	32	178
	11.7	58	424
	6.7	12	267
	3.3	3.1	285
	Average ^b =		300 ± 40
Aluminum	23.8	1.7	3.0
304-L SS	20.9	1.9	4.3
Titanium	2.1	0.8	180
Zinc	19.2	3.1	8.4
	21.3	3.3	7.3
MMH			
AlO _x	23.8	10.2	18.0
	12.1	3.3	22.5
	11.7	2.8	20.4
Average ^b =		20.3 ± 1.3	
Aluminum	20.9	0.8	1.8
304-L SS	20.9	9.7	22.2
Zinc	20.9	2.7	6.2
UDMH			
AlO _x	23.8	1.1	1.9
A-50			
AlO _x	23.8	2.3 (UDMH) --- (HZ)	4 ---

^a 298 ± 2 K

^b Errors are standard errors

a. Kinetic Analysis

The observed rate expression is consistent with a kinetic scheme involving adsorption of hydrazine and oxygen onto different sites followed by an irreversible bimolecular oxidation reaction (Equations (17) - (23)).



For two different types of surface sites, S_M (an oxygen binding site) and S_M' (an H-bonding hydrazine site), the overall rate of the bimolecular surface oxidation reaction is:

$$\text{rate} = k_{ox} [S_M:O_2] [S_M':HZ] \quad (24)$$

$$\text{rate} = k_{ox} (\theta_O) SA_T (\theta_H) SA_T \quad (25)$$

where (θ_O) and (θ_H) are the fractions of the total surface area (SA_T) covered by oxygen and hydrazine, respectively.

Equation (26) shows the general Langmuir relationship:

$$\theta_G = \frac{K [G]}{1 + K [G]} \quad (26)$$

where

G = an adsorbing gas

Combining the general Langmuir relationship with Equation (25), gives:

$$\text{rate} = k_{ox} [SA_T]^2 \frac{K_O [O_2]}{1 + K_O [O_2]} \frac{K_H [HZ]}{1 + K_H [HZ]} \quad (27)$$

In an air atmosphere with 70 ppm v/v hydrazine, sparse surface coverage ($K_O [O_2] \ll 1$, $K_H [HZ] \ll 1$) and $[O_2]$ constant, the overall rate of the bimolecular surface oxidation reaction becomes:

$$\text{rate} = k_{ox} K_O [O_2] K_H [SA_T]^2 [HZ] \quad (28)$$

from Equation (16), then

$$k_{met} = k_{ox} K_H K_O [O_2] \quad (29)$$

The observed specific rate constant, k_{met} , is then equal to the microscopic rate constant for oxidation, k_{ox} , the Langmuir adsorption constants (K_H and K_O), and the oxygen pressure $[O_2]$. For different surfaces or different fuel hydrazines, the relative k_{met} values also include the relative adsorption constants.

Other possible rate-controlling steps that would show an observed rate with a second-order dependence on vacant surface area involve the following: dissociation of molecular oxygen to atomic oxygen; dual site adsorption of hydrazine; or the dissociation of hydrazine. Reactions of gaseous hydrazine with two atomic oxygens, and of the dissociated hydrazine with molecular oxygen, depend on the square of the occupied surface area. It is

unlikely that dissociated hydrazine ($-NH_2$) is involved in these room temperature reactions. This leaves rate controlling steps involving dissociated oxygen, or dual-site adsorption of hydrazine, as the only remaining viable alternatives to the proposed rate-controlling surface reaction (Equation (19)). Although the details of the mechanisms differ, the overall conclusions would be similar.

c. Relative Reactivities

The relative reactivities (normalized for surface area) of the fuel hydrazines toward AlO_x are:

$$\begin{array}{ccccccc} \text{hydrazine} & > & \text{MMH} & > & \text{Aerozone-50} & > & \text{UDMH} \\ 158 & & 11 & & 2 & & 1 \end{array}$$

Tests performed with other metal surfaces or with the less reactive fuels generally yielded a k_{obs} that was double the k_{bkg} . This could be a result of only adsorption onto the extra surface area ($20 - 23 \text{ m}^2$) that was added to the reaction chamber; therefore, a factor of two in the k_{obs} may not be an indication of surface reactivity.

Assuming that the environmentally important surface area of a metal plate is its measured geometric area, the relative environmental reactivities of these fuels toward exposed metal surfaces are:

For hydrazine:

$$\begin{array}{ccccccc} AlO_x \approx \text{Titanium} & >> & \text{Zinc} & > & \text{Aluminum, 304-L SS} \\ 100^x & & 60 & & 3 & & 1 \end{array}$$

For MMH:

$$\begin{array}{ccccccc} 304-L \text{ SS} \approx AlO_x & > & \text{Zinc} & > & \text{Aluminum} \\ 12 & & 11^x & & 3 & & 1 \end{array}$$

These rankings are based on the relative k_{met} values shown in Table 9 and include relative effects of the adsorption equilibria for hydrazine and oxygen.

The actual surface area of the aluminum hydroxide coating on the AlO_x plates is estimated to be 10 times greater than the geometric area, and it is not surprising to find that these plates are fairly reactive. Aluminum, with its normal smooth oxide coat, is catalytically unnotable; however, a thickened oxide coating of bayerite results in a catalytically active surface because of the extremely large surface area.

The titanium experiments were conducted with only a very small geometric area, and final conclusions about its reactivity await further work.

The real surprise in the relative reactivities of the metallic surfaces is the reactivity of a smooth 304-L SS surface toward MMH. Adsorption measurements made with the model compound methylamine show that stainless steel has a relative adsorption equilibrium constant six times greater than alumina (per m^2), and this may account for some of the apparent reactivity of the stainless steel (Reference 21).

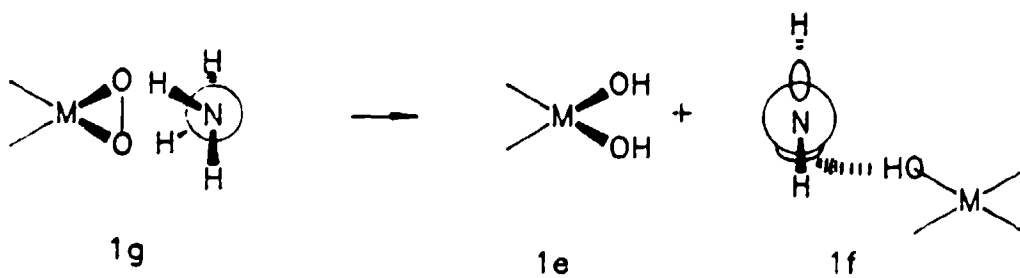
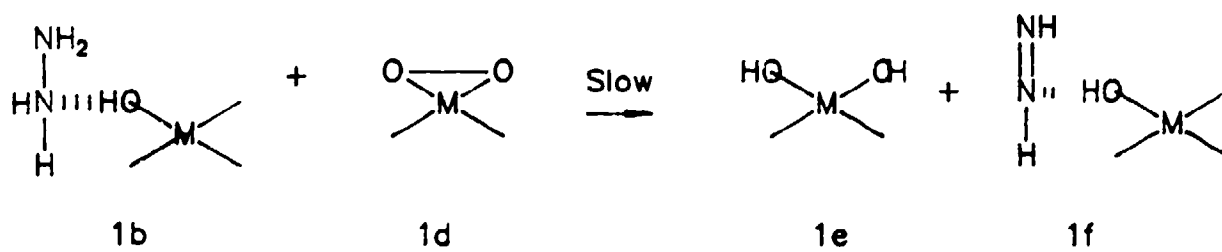
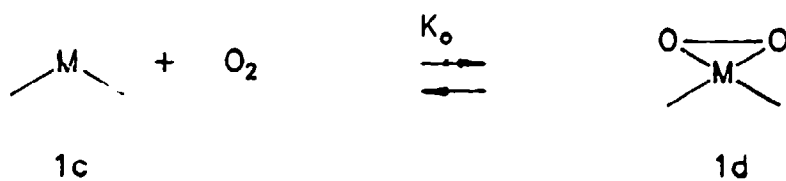
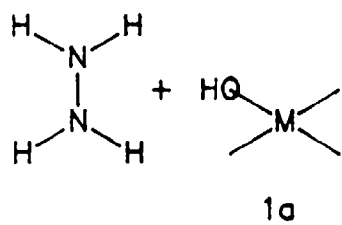
d. Mechanisms

(1) Hydrazine Oxidation. A mechanism that describes the air oxidation of hydrazine promoted by the AlO_x and other surfaces and the appearance of the intermediates, hydrogen peroxide and diazene, is shown in Scheme 1.

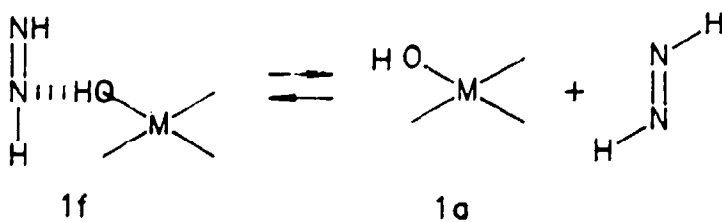
Hydrazine vapor is adsorbed onto the metal surface via hydrogen bonding (1b) at a site shown here as a hydrated metal oxide (1a). Oxygen is adsorbed molecularly (1d) at a different type of site (1c), shown as a metal atom. Chemisorption of oxygen with dissociation to atomic oxygen is also possible, and an alternate scheme can be written which leads to the same conclusions. The structure (1d) shows oxygen adsorbed in a peroxo-structure parallel to the surface (Reference 22).

An irreversible bimolecular oxidative dehydrogenation proceeding through a six-membered ring transition state (1g) yields a dihydroxy metal (dissociated hydrogen peroxide, 1e) and a diazene (1f). The diazene can

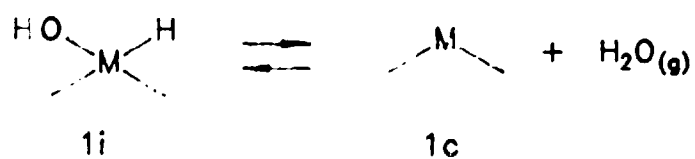
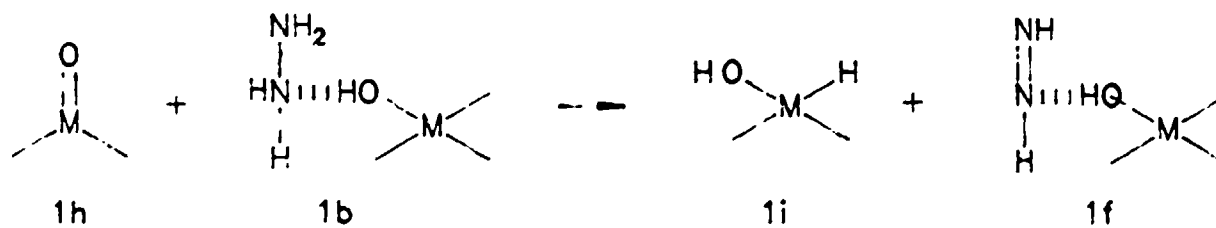
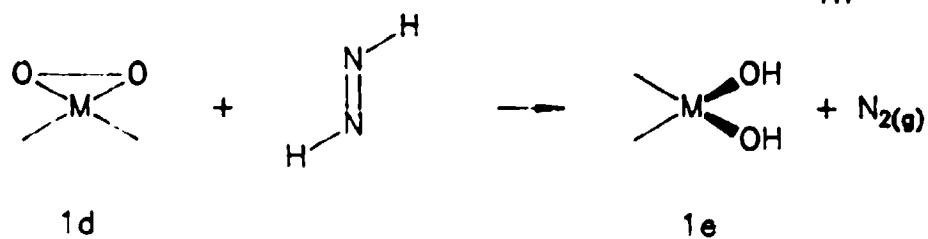
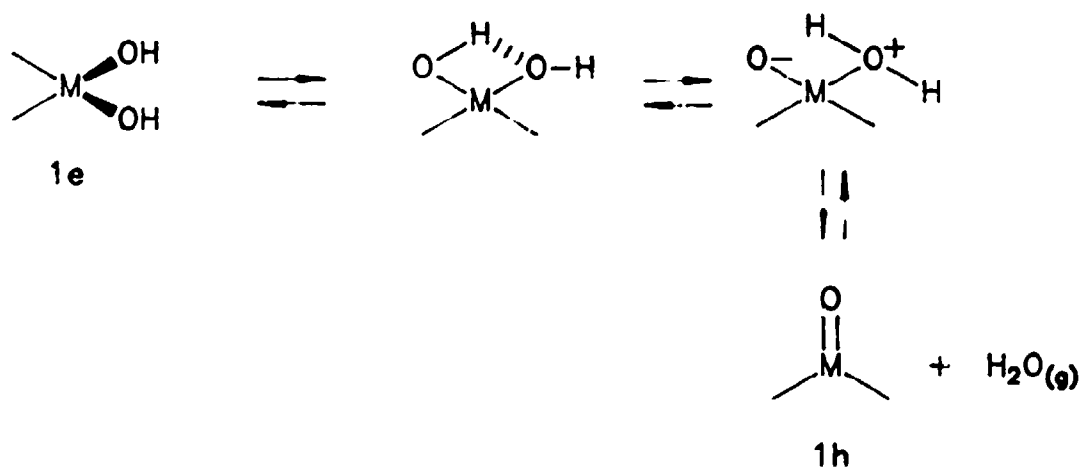
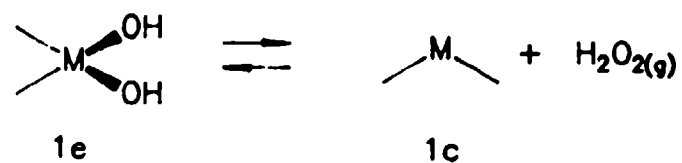
Scheme 1



Top View



Scheme 1 (concluded)



further react through the same type of transition state with adsorbed oxygen, to yield nitrogen and another dihydroxy metal site. Alternately, diazene, or even hydrazine, can react with chemisorbed hydrogen peroxide. Dihydroxy metal sites (1e) can undergo reductive elimination to yield the original oxygen binding site (1c) and hydrogen peroxide. Desorption of the hydrogen peroxide would then account for its appearance in the vapor phase. Re-adsorption of hydrogen peroxide and further oxidation of more hydrazine or diazene result in a catalytic cycle with respect to metal-atom sites. The ultimate products of hydrazine oxidation are nitrogen and water.

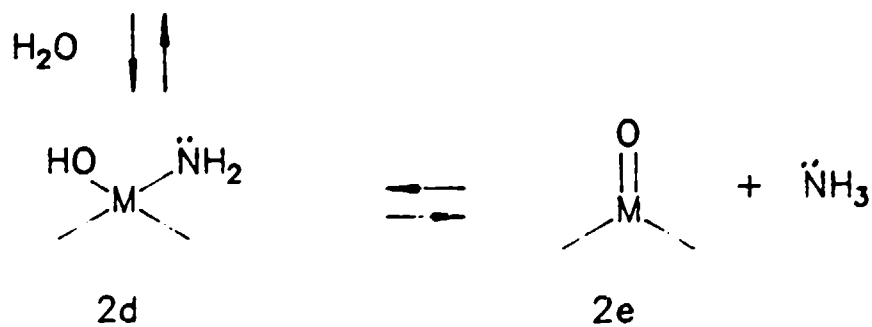
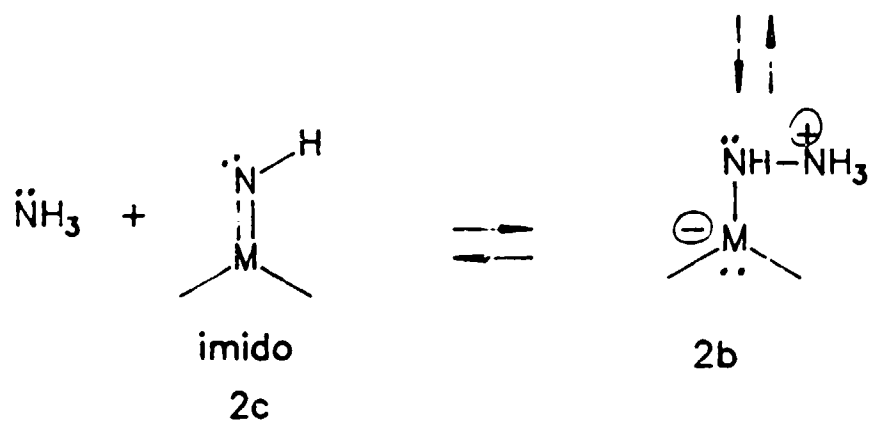
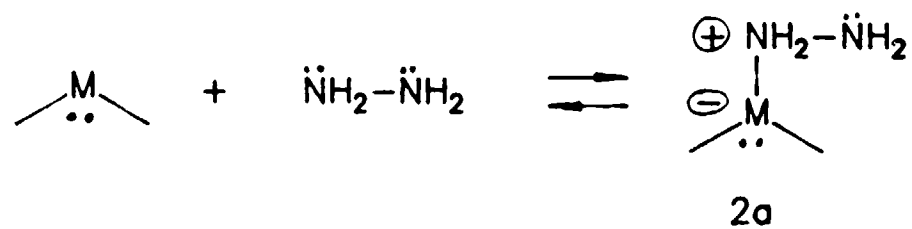
The same scheme applies to the oxidation of MMH, where the products of oxidation are water, methanol, and nitrogen. Traces of the intermediate methyldiazene were observed, but were at too low a level to quantify. In flow reactor studies at 330 K, methane was observed as a surface-catalyzed air-oxidation product of MMH and was believed to arise from the decomposition of the intermediate methyldiazene (see SECTION III). No methane was observed in chamber studies of MMH oxidation.

The unreactivity of UDMH may be due to the lack of adjacent hydrogens on N_1-N_2 , which prevents the initial oxidative dehydrogenation step. Small increases in the k_{obs} are probably only due to adsorption effects.

(2) Ammonia Formation. In these experiments, ammonia was noted as a trace product (< 5 percent) in hydrazine kinetic runs only when active metal surfaces were present. Other workers have detected its formation in background runs, but some exposed metal surfaces (mostly aluminum) were present in their chambers (Reference 2). This mechanistically significant reduction product deserves deeper consideration, in view of its importance in hydrazine decompositions in general and its role as a final product in nitrogen fixation.

A mechanism accounting for the overall reaction in which hydrazine and water react with a metal surface to yield ammonia and an oxidized metal surface is shown in Scheme 2. The initially formed Lewis acid adduct (2a)

Scheme 2



undergoes a proton transfer, and the resulting intermediate (2b) undergoes an ammonia elimination concomitant with formation of an imido structure (2c). Reaction of water with the imido function forms a surface-bound hydroxy amide (chemisorbed hydroxyl amine, 2d) analogous to adsorbed hydrogen peroxide. Reductive elimination from the hydroxy amide leads to ammonia and metal oxide. The putative intermediates shown in Scheme 2 are similar to those incorporated in general nitrogen fixation schemes (Reference 22).

E. CONCLUSIONS

Hydrazine, MMH, and UDMH vapors are lost from the FEP environmental chamber interior by adsorption onto and permeation through the FEP surface. Loss rates are governed by the polarity and the protic nature of the molecules rather than by molecular weight. Air-oxidation reactions do not appear to be important for loss processes in the absence of metal surfaces in a permeable chamber. Due to the significant loss by permeation, further studies of the homogeneous air-oxidation reactions of the fuel hydrazines should be conducted in nonpermeable inert reaction chambers.

The ultimate environmental fate of the fuel hydrazines may not be controlled by their homogeneous oxidation rates in "pure air." The strong surface area dependence and reactivity toward a model environmental surface, such as aluminum hydroxide, suggests that particulate - hydrazine reactions in the atmosphere may have a more important role than previously believed. Additionally, the factors by which reactive atmospheric constituents such as ozone or NO_x control the homogeneous decay rate need to be considered.

UDMH appears to be the least reactive fuel hydrazine in air or with model environmental surfaces. Further investigations are necessary to determine the mechanisms of its dispersal in the environment.

SECTION III

FLOW REACTOR STUDIES: PACKED MICROREACTOR

A. INTRODUCTION

Gas-phase kinetic studies, including work detailed in Section II, have clearly shown that the air oxidation reactions of the hydrazines have both a heterogeneous and homogeneous component in any real vessel (References 3 - 7). To assess the relative contributions of these components, it is necessary to examine each in the absence of the other. This section describes investigations that characterize the general reactivity patterns, kinetics, and products of the surface-promoted air-oxidation reactions of hydrazines.

The effects of surfaces on the air oxidation reactions of hydrazines can be examined directly by using the techniques of heterogeneous catalysis. In particular, a gas chromatography technique (originally developed by Hall and Emmett, Reference 23) using microreactors permits the simple, convenient, and quantitative study of the comparative efficiencies of a number of catalysts. More recent work has shown the generality and utility of the method (References 24 - 26).

The fixed-bed microreactor is characterized by the use of small quantities of catalyst (0.05 to 5 grams) packed into a tube and mounted in a GC. The catalysts were metal and metal oxide powders, and other possibly reactive materials. The GC provides a temperature controlled oven, a controlled flow of carrier gas, a means to introduce small amounts of reactant, a sensitive detector for determining product composition, and a means to trap the eluted products. The relatively large ratio of carrier gas to reactant ensures essentially isothermal conditions and eliminates external mass transfer resistance (Reference 27).

Operated in a pulsed mode with a reactive carrier gas such as air, the fixed-bed reactor is particularly suitable for the study of pseudo-first-order oxidation reactions (oxygen in large excess). The use of a nonreactive carrier gas, such as nitrogen, permits the measurement of the extent of adsorption

(References 28 and 29), the heat of adsorption (Reference 30), and any thermal decomposition of the reactant under reaction conditions (Reference 31).

Conversely, studies with unreactive model compounds or reactive compounds in inert carrier gases can provide information concerning the nature of the surface.

B. EXPERIMENTAL

1. Materials

The metal and oxide powders were commercially obtained. These powders were aluminum (Mallinkrodt, BET area $0.4526 \text{ m}^2/\text{g}$), Alundum® (Curtin, 100 - 200 mesh, BET area $0.1945 \text{ m}^2/\text{g}$), alumina (Woelm W200 acid, BET area $200 \text{ m}^2/\text{g}$), chromium (Alpha, 100 mesh, M2N, BET area $0.1376 \text{ m}^2/\text{g}$), copper(I) oxide (Baker), copper(II) oxide (Johnson Matthey puratronic grade), iron (Alpha, 200 mesh, M2N+, BET area $0.1096 \text{ m}^2/\text{g}$), iron(III) oxide (Fisher or Johnson Matthey puratronic grade), nickel (MC&B, 200 mesh, BET area $0.456 \text{ m}^2/\text{g}$), silica (Cabot, Cab-O-Sil® fumed, grade M-5), silica-alumina (Grace, grade 135-08-5X1950), silica gel (Davidson, 140 - 200 mesh, BET area $345 \text{ m}^2/\text{g}$), 316 SS (Materials Research Corporation, 100 mesh, BET area $0.0745 \text{ m}^2/\text{g}$), 304-L SS (Alpha, 100 mesh, Fe:Cr:Ni 70:19:11, BET area $0.1615 \text{ m}^2/\text{g}$), titanium (Alpha, 100 mesh, M3N, BET area $0.785 \text{ m}^2/\text{g}$), and zinc (Alpha, 200 mesh, M5N, BET area $0.0715 \text{ m}^2/\text{g}$). New Mexico desert sand, well-aged concrete, and cinder block were obtained locally, crushed, and sized to 120 mesh.

A sample of mixed iron oxides (Fe_xO_y) was prepared by exposing iron powder to distilled water and evaporating it at 383 K. The iron oxide powder was sized to 120 mesh and the BET surface area was determined to be $0.8746 \text{ m}^2/\text{g}$.

BET surface area determinations were performed by Micromeritics Instrument Corporation, Narcross, GA.

Hydrazine and MMH were propellant grades (Olin) analyzed according to MIL-D-26536-C and MIL-P-27404B, respectively. Typical analyses were >98.7

percent and less than 1.5 percent water. UDMH (Aldrich) and tetramethylhydrazine (TMH, Fluka) were reagent grade materials and used as received.

Methylamine (Airco), dimethylamine (Matheson), and trimethylamine (Matheson) were used as supplied. All other solvents were reagent grade and used as supplied. Ultrapure or puratronic grade materials are referred to as UP.

1,2-Dimethylhydrazine (SDMH; bp 349.6 K, 88 kPa) was prepared from dimethylhydrazine dihydrochloride (Aldrich) by distillation from saturated potassium hydroxide. The crude SDMH was dried over barium oxide overnight and then fractionally distilled from fresh barium oxide. Trimethylhydrazine (TMH; bp 326 K, 88 kPa) was prepared by lithium aluminum hydride reduction of methylene dimethylhydrazine according to the procedure of Class, Aston, and Oakwood (Reference 32).

2. Instrumentation

a. Gas Chromatograph

A Hewlett-Packard Model 7620A GC equipped with a flame ionization detector (FID) was used in the microreactor studies. The injection ports of the GC were lined with PTFE sleeves to minimize metal-fuel interaction. Breathing air (analyzed according to Federal Specification BBA103A Amendment 1 Grade C) or purified nitrogen was used as the carrier gas at a flow rate of 0.08 - 0.2 mL/s.

b. FTIR Spectrometer

A Nicolet MX-1 FTIR spectrometer equipped with a deuterated triglycine sulfate (DTGS) detector was used in quantitative gas analyses. Data collection was performed by the Nicolet FTIR with spectral analysis performed on a Nicolet 1200S data terminal. A 165-mL gas cell with a 10-cm pathlength was used.

3. Apparatus

The microreactors were constructed from 12.7-cm sections of 0.63-cm outside diameter PTFE tubing with an inside diameter of 0.25 cm. PTFE compression fittings (Swagelok) were used to mount the reactor tubes into the GC. The reactor tubes were capped with Zitex (Chemplast, Inc.) 90-X PTFE filter membranes wedged into the compression fittings to prevent the loss of powdered material. A smaller version for use with fine powders had a 0.63-cm PTFE union as the body of the tube to provide the reactor with a 0.63-cm bed length. The outlet of the reactor tubes was connected by a short length of 0.159-cm PTFE tubing to the flame ionization detector of the GC. The reactors held 1 to 3.5 grams of powder while the smaller version held approximately 0.15 to 0.35 grams of fine powder.

4. Procedures

a. Microreactor

A microreactor, filled with a weighed amount of powdered metal or oxide, was mounted in the GC and allowed to stabilize in a flow of air or nitrogen carrier gas at 328 ± 3 K oven temperature (injector temperature 373 K, flame ionization detector (FID) temperature 473 K) for 30 minutes. The carrier flow was adjusted to 0.16 - 0.2 mL/s. A series of constant volume injections, usually 0.25 μ L, was made until the integrated area of the eluted peak(s) were constant within ± 5 percent for a series of three injections.

b. Quantitative Product Analysis

In order to perform a quantitative product analysis, the eluents from the reactor tubes were trapped in the IR gas cell (instead of being directed to the FID detector) and the contents were analyzed by FTIR. Extinction coefficients applicable to the gas cell and spectrometer were determined by injecting known aliquots of reactants or products into an evacuated gas cell. The values for the extinction coefficients were found to be consistent with those reported by Tuazon et al. (Reference 6). Because of the low FID response of hydrazine, quantitative analysis of hydrazine was performed by trapping the

eluent in a 6-mm glass tube packed with 60 - 80 mesh firebrick coated with 0.1-molar sulfuric acid. The absorbed hydrazine was eluted into water and the aqueous solution analyzed by coulometric titration (Reference 33).

c. Analytical Frequencies and Extinction Coefficients

A listing of analytical frequencies and extinction coefficients used in the quantitative analysis of product mixtures by FTIR is presented in Table 10.

d. Adsorption Studies

The microreactor system was used to determine several physico-chemical parameters useful for surface characterization. Both the amount of adsorbate necessary to saturate the surface and the heats of adsorption were measured.

TABLE 10. INFRARED ANALYTICAL FREQUENCIES AND EXTINCTION COEFFICIENTS

Compound	Frequency (cm^{-1})	Extinction ^a Coefficient (base e) ($\text{atm}^{-1}\text{cm}^{-1}$)
MMH	889	7.7
UDMH	896	8.1
SDMH	864	5.0
CH ₃ OH	1033	17.6
CH ₄	3017	12.1
	1306	6.45
CH ₃ N ₂ H	845	^b (7.7)
NH ₃	967	19.1

^a Peak-to-baseline measurement of the Q-branch at 2 cm^{-1} resolution

^b Estimated to be the same as MMH

(1) Plateau Method for Strong Adsorption. To determine the amount of adsorbate necessary to saturate the surface of a powder sample, a series of small injections were made until the flame ionization detector (FID) response reached a plateau. The final total area was taken as the plateau value (I_p), and the amount of eluent(s) strongly adsorbed were calculated using Equation (30).

$$M = \frac{1000 \cdot D}{FW \cdot wt} \sum V_i \left(1 - \frac{I_i}{I_p} \right) \quad (30)$$

where

M = micromoles of samples adsorbed per gram of adsorbent
 D = density (g/mL) of the liquid hydrazine
 FW = formula weight (g/mol) of the hydrazine
 wt = weight of adsorbent (grams)
 V_i = volume of i-th injection (μ L)
 I_i = integrated response of peak(s) of the i-th injection
 I_p = plateau value of the integrated response

Equation (30) is valid only in the absence of a reaction. In the presence of a reaction, the M value is complicated by variable product response factors in the FID and by the formation of non-FID responsive products such as nitrogen, CO_2 , ammonia, or water.

(2) Reversible Adsorption. The retention time for a substance passing through a packed reactor is a function of the flow rate of the carrier gas, the interparticle volume, the system dead volume, and the equilibrium constant for interaction of the vapor with the solid packing. By measuring the retention of a noninteracting gas, such as methane, the interparticle and system dead volume can be subtracted. Thus, the net retention volume of a substance, V_n , is given by

$$V_n = F (t - t_0) \quad (31)$$

where

V_n = net retention volume
 F^n = flow rate of carrier gas
 t = retention time of interacting substance
 t_0 = retention time of noninteracting substance (usually methane)

The usual gas-solid equation

$$K_{sc} = \frac{V_n}{wt} \quad (32)$$

where

K_{sc} = gas-solid adsorption constant
 wt = weight of the solid

gives K_{sc} , a measure of the gas-solid interaction. The temperature dependence of K_{sc} gives the isotheric heat of adsorption.

(3) Heats of Adsorption. The temperature dependence of K_{sc} as measured in the gas-solid chromatographic technique was used to determine ΔH_{st} , the isosteric heat of adsorption (Reference 30). ΔH_{st} is, in effect, the heat adsorbed when one mole of adsorbate is adsorbed by an infinite amount of solid. The slope, $-\Delta H_{st}/R$, can be obtained by plotting $\ln(V_n/T)$ against $1/T$, where T is the absolute temperature. The retention volumes of methane, methanol, and UDMH as a function of temperature were determined for 316 SS in an air carrier.

C. RESULTS

1. Reactivity Screening

Reactivity of hydrazines was evidenced by more than one peak in the GC trace or unusually large hold-up of sample. Reactions were confirmed by trapping the eluent and determining eluent composition.

a. Hydrazine

Hydrazine was completely consumed when exposed to 316 and 304 SS, iron, Fe_xO_y , aluminum, Al_2O_3 , zinc, chromium, nickel, titanium, sand, concrete, and cinder block powders using air as the carrier gas. Experiments using unpacked reactor tubes showed an 89 percent recovery by IR and a 54 percent recovery by coulometry.

Using nitrogen as the carrier, appreciable amounts of hydrazine were eluted (Table 11). The recovery improved with each injection, apparently because the surface was passivated by hydrazine or its decomposition products.

The adsorption of hydrazine on the T-6 PTFE packing was estimated to be 2.6 micromoles/g.

b. MMH

Blank experiments using unpacked reactor tubes showed a 103 percent recovery by IR.

The reaction products of MMH with air, catalyzed by metal and oxide surfaces, are methane, methyldiazene (MD), methanol, and in some cases, traces of ammonia. The product distributions are shown in Table 12.

A comparison of the reactivity and products of MMH in air, nitrogen, and humidified air is shown in Table 13. Both MMH and its reaction products slowly saturated the surface of the catalyst. Methane was the first product to elute, followed by methyldiazene, MMH, and methanol. After several injections, the chromatograms became constant in shape and area. The retention volumes of the products decreased as the surface was reused, which resulted in increased overlap of the components.

TABLE 11. RECOVERY OF HYDRAZINE IN NITROGEN CARRIER^a

Surface	Injection No. (0.5 μ L)	Recovered Hydrazine (%)
Iron	1	62
Iron	2	83
Iron	3	84
Fe _x O _y	1	0.6
Fe _x O _y	2	0.5
304-L SS	1	25
304-L SS	2	59
304-L SS	3	45
Unpacked PTFE Reactor ^b	1	86
Unpacked PTFE Reactor ^b	2	109
Unpacked PTFE Reactor ^b	3	105
Unpacked PTFE Tube ^c	1	104
Unpacked PTFE Tube ^c	2	91
T-6 Packing ^d	1	84
T-6 Packing ^d	2	99
T-6 Packing ^d	3	91
T-6 Packing ^e	1	58
T-6 Packing ^e	2	97
T-6 Packing ^e	3	100

^a 328 \pm 3 K

^b 0.64 cm (0.25 in.) wide-bore, thin-wall tubing

^c 0.64 cm (0.25 in.) narrow-bore, thick-wall tubing

^d T-6 chromatography packing in narrow-bore tubing (1.25 grams)

^e T-6 chromatography packing in wide-bore tubing (2.4 grams)

c. Other Hydrazines

Blank experiments using unpacked reactor tubes with UDMH showed a 93 percent recovery by IR. The di-, tri-, and tetramethyl substituted

TABLE 12. MICROREACTOR PRODUCTS: MMH IN AIR^a

Surface	Products					Recovered Carbon (%)
	CH ₃ OH (%)	MD (%)	CH ₄ (%)	NH ₃ (%)	MMH (%)	
316 SS	2.6	21.3	0.9	---	50.5	75.3
304-L SS	7.8	16.5	0.6	3.4	39.5	67.5
Iron	8.5	16.5	17.0	1.1	9.6	53.0
Fe ₂ O ₃	18.9	---	29.0	---	---	48.1
Fe ₂ O ₃ (UP ^b)	6.6	---	---	---	70.0	76.6
Fe ₃ O ₄ (UP)	2.3	---	---	---	65.0	67.3
Fe _x O _y	37.2	---	40.4	---	---	77.6
Aluminum	5.7	21.3	---	2.1	19.1	48.0
Al ₂ O ₃	18.1	14.9	29.0	2.6	10.6	75.2
Zinc	1.1	16.5	---	---	69.0	86.6
Chromium	2.1	19.7	8.2	---	60.4	90.4
Nickel	7.4	15.4	14.9	---	7.4	45.1
Titanium	4.0	24.2	9.6	---	38.8	76.6
Cu ₂ O	3.2	17.5	18.6	---	41.0	80.3
CuO (UP)	---	---	---	---	99.0	99.0

^a 328 ± 3 K^b UP: Ultrapure

hydrazines are less reactive than hydrazine or MMH. UDMH and TMH showed slight reactivity only on Fe_xO_y. A trace amount of an unidentified oxidation product containing a methylene group (=CH₂) with an IR absorption at 3077 cm⁻¹ was formed. N-methyl or N,N-dimethylformaldehyde hydrazone is a possibility. Methanol or methane were not detected.

MMH showed slight reactivity on Fe_xO_y and titanium powder, and formed methanol and traces of an unidentified product, possibly dimethyldiazene.

2. Adsorption Studies

a. Plateau Method for Strong Adsorption

This technique was applied to the methylhydrazines, methylamine (MA), dimethylamine (DMA), and trimethylamine (TMA). The results are presented in Tables 14 and 15.

TABLE 13. COMPARISON OF MMH REACTIONS IN NITROGEN, AIR, AND HUMIDIFIED AIR^a

Surface	Carrier	Relative Product Yields				
		CH ₃ OH (%)	MD (%)	CH ₄ (%)	NH ₃ (%)	MMH (%)
316 SS	Air	3.4	28.2	1.1	---	67.1
	Nitrogen	0.5	trace	---	---	99.5
304-L SS	Air	11.5	24.3	0.9	---	58.2
	Nitrogen	2.6	trace	---	---	97.4
Iron	Air	16.0	31.1	32.1	2.1	18.1
	Nitrogen	1.6	---	---	---	98.4
Nickel	Air	16.4	34.1	33.0	2.2	16.4
	Humid Air	42.0	---	58.0	---	---
	Nitrogen	---	---	---	---	100.0
Fe _x O _y	Air	48.0	---	52.0	---	---
	Humid Air	41.0	---	59.0	---	---
	Nitrogen	5.0	8.0	58.0	---	29.0
Fe ₂ O ₃	Air	39.3	---	60.7	---	---
	Nitrogen	---	---	23.4	---	76.6
Fe ₃ O ₄	Air	3.4	---	---	---	96.5
	Nitrogen	1.0	---	---	---	99.0
Cu ₂ O	Air	4.0	21.8	23.2	---	51.0
	Nitrogen	1.8	---	---	---	98.2

^a 328 ± 3 K

The plateau method assumes that the adsorbate is strongly adsorbed (Reference 28). After a packed reactor tube reached the elution plateau, the continued flow of air for several hours slowly removed the strongly adsorbed material from the surface. When another series of injection was made, the FID quickly reached the I_p value. Because the measurements were taken over a period of 10 to 15 minutes, the errors caused by slow desorption were assumed to be small. These kinetic desorptive phenomena were not pursued further.

TABLE 14. STRONG ADSORPTION OF HYDRAZINES ON METAL AND OXIDE SURFACES IN AIR^a

Surface	BET Area m ² /g	Amount Adsorbed (Micromoles/m ²)			
		UDMH	SDMH	TMH	TTMH
316 SS	0.0745	8	7	1	3
304-L SS	0.1615	5	9	2	3
Iron	0.1096	1	0	0	0
Fe ₂ O ₃	0.8746	2	2	2	2
Aluminum	0.4526	2	3	0.5	1
Al ₂ O ₃	0.1945	3	1	0	1
Zinc	0.0715	6	7	0	5
Chromium	0.1376	4	4	2	1
Nickel	0.456	3	3	1	1
Titanium	0.785	1	1	0	0

^a 328 ± 2 K

The adsorption phenomena shown by the methylhydrazines and methylamines (Tables 14 and 15) were also shown by MMH; however, quantitative measures of MMH adsorption phenomena could not be performed.

b. Adsorption of Fuel Hydrazines on Sand, Concrete, and Cinder Block

No hydrazine was eluted from samples of New Mexico desert sand, well-aged concrete, and cinder block. MMH was completely eluted with all three sample materials.

c. Reversible Adsorption

The gas-solid equilibrium constants for the methylamines on metal and oxide surfaces are presented in Table 16. The results are reported in mL/m² to allow comparison among the solids with different surface areas.

TABLE 15. STRONG ADSORPTION OF METHYLAMINES ON METAL AND OXIDE SURFACES IN AIR^a

Surface	Amount Adsorbed (Micromoles/m ²)		
	MA	DMA	TMA
316 SS	2.9	1.8	1.2
304-L SS	6.4	3.2	1.5
Iron	1.9	1.1	0.3
Fe _x O _y	1.8	1.7	1.5
Aluminum	2.3	0.9	0.1
Al ₂ O ₃	3.1	5.1	0.6
Zinc	6.2	3.6	1.4
Chromium	4.3	3.6	1.8
Nickel	5.2	9.0	0.6
Titanium	0.4	0.3	0.09

^a 330 ± 2 K

TABLE 16. REVERSIBLE GAS-SOLID EQUILIBRIUM CONSTANTS IN AIR^a

Solid	K _{sc} (mL/m ²)		
	MA	DMA	TMA
316 SS	4.0	1.9	0.80
304-L SS	9.6	3.1	0.62
Iron	0.18	0.12	0.14
Fe _x O _y	2.3	0.14	---
Aluminum	5.2	3.3	1.9
Al ₂ O ₃	1.5	1.0	0.34
Zinc	1.4	2.8	0.50
Chromium	1.0	0.5	0.39
Nickel	0.72	0.53	---
Titanium	0.06	0.06	0.056

^a 330 ± 2 K

d. Heats of Adsorption

The K_{sc} values are reported in Table 17. The ΔH_{st} for methane is assumed to be zero. The derived heats for methanol and UDMH are -11 kJ/mol and -22 kJ/mol, respectively. The heats are consistent with a weak, physical adsorption rather than chemisorption as the surface interaction (Reference 30)

D. DISCUSSION

At 330 K in an air carrier, hydrazine and MMH were reactive to all the surfaces studied, but UDMH, SDMH, and TMH were only reactive to Fe_xO_y . The fully substituted TTMH and the methylamines were completely unreactive on all substrates.

TABLE 17. RETENTION VOLUMES OF METHANE, METHANOL, AND UDMH ON 316 SS IN AIR^a

Compound	Temp. (K)	V_r (mL)	V_r^b (mL)	$K_{sc} \times 10^2$ (mL/g)
Methane	331.7	5.31	0.000	0
	343.2	5.56	0.000	0
	358.3	5.62	0.000	0
	379.4	5.47	0.000	0
	392.2	5.24	0.000	0
Methanol	331.7	5.84	0.534	5.04
	343.2	6.05	0.490	4.62
	392.2	5.57	0.335	3.16
UDMH	331.7	6.67	1.36	12.8
	343.2	6.79	1.23	11.6
	358.3	6.62	1.00	9.43
	379.4	6.03	0.564	5.32
	392.2	5.75	0.506	4.77

^a Tubular reactor contained 10.6 grams of 316 SS; typical flow was approximately 0.08 mL/s of air.

^b Calculated using Equation (31)

1. Hydrazine

In air, hydrazine was completely consumed by contact with all the surfaces studied. In nitrogen, however, iron and PTFE powders gave 84 and 100 percent recoveries, while 304-L SS powder showed approximately 50 percent recovery, and Fe_xO_y showed no recovery. The reactivity of Fe_xO_y , a strong oxidizing agent, is expected, but the reactivity of 304-L SS is surprising.

The major reaction was the surface-promoted oxidation of hydrazine. The reactions of hydrazine with Fe_xO_y and Fe_2O_3 do not require oxygen but reactions with Fe_3O_4 and Cu_2O do. Presumably, the following reactions occur:



and



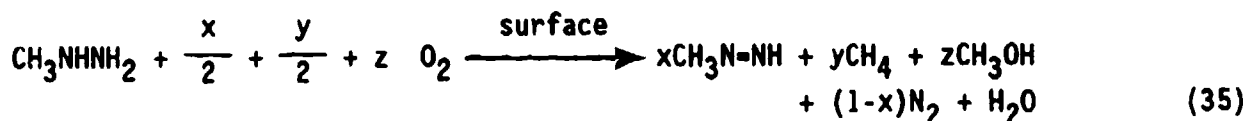
The oxidation of hydrazine to nitrogen and water requires a four-electron change. Because the iron products were not characterized, the reactions could be written with a variety of reduced iron species.

PTFE, after initial loading, appears unreactive in nitrogen. Thus, thermal decomposition of hydrazine at 330 K in nitrogen is negligible. In air, under the same conditions, oxidation is complete.

2. MMH

Similar to hydrazine, MMH is unreactive in nitrogen. As with hydrazine, both Fe_xO_y and Fe_2O_3 are reactive toward MMH in the absence of oxygen.

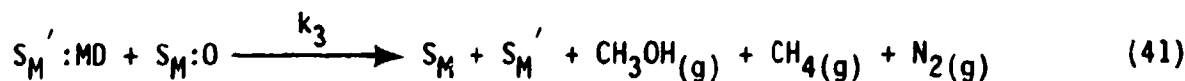
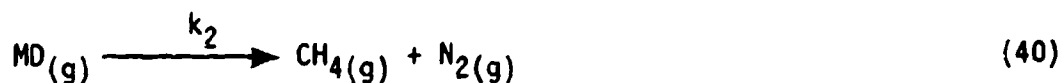
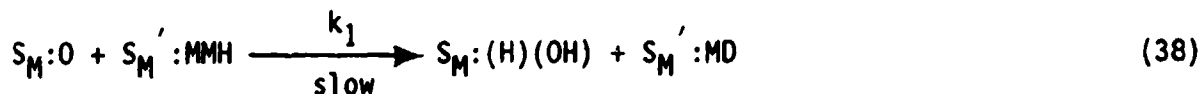
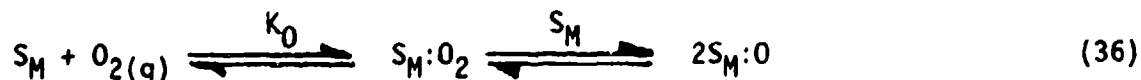
The products of MMH oxidation are methane, methanol, methyldiazene, and in several cases, traces of ammonia.



where x , y , and z are stoichiometric coefficients and $x + y + z = 1$.

The stoichiometry above does not account for the traces of ammonia detected in a few reactions. Any proposal for the MMH oxidation reaction mechanism must take into account that the reaction is surface-promoted or catalyzed and requires oxygen in most cases, and that methyldiazene is thermally unstable at these temperatures.

The following sequence of reactions is proposed:



where S_M' represents an active site for reversible binding of hydrazines; and S_M represents a surface site for oxygen binding.

Methyldiazene is thermally unstable and its decomposition reactions are expected to be fast; thus, the overall rate is controlled by k_1 . The rate of oxidation of MMH is then as follows:

$$\text{rate} = k_1 [S_M:O] [S_M':MMH] \quad (42)$$

Substituting:

$$\text{rate} = k_1 K_O [S_M] [O_{2(g)}] K_H [S_M'] [MMH_{(g)}] \quad (43)$$

The observed rate of disappearance of MMH is as follows:

$$-\frac{d[MMH_{(g)}]}{dt} = k_{\text{obs}} [MMH_{(g)}] \quad (44)$$

or

$$-\frac{d[MMH_{(g)}]}{[MMH_{(g)}]} = k_{\text{obs}} dt \quad (45)$$

The integrated form:

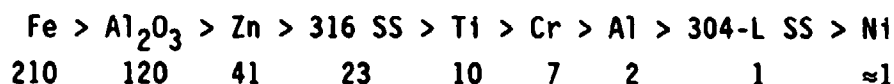
$$\ln \frac{[MMH_{(g)}]_t}{[MMH_{(g)}]_0} = -k_{\text{obs}} t_n \quad (46)$$

where $[MMH_{(g)}]_t + [MMH_{(g)}]_0$ is the fraction of MMH remaining after the contact time (t_n) and

$$k_{\text{obs}} = k_1 K_O K_H [S_M] [S_M'] [O_{2(g)}] \quad (47)$$

The contact time (t_n) is equal to $K_{sc} \cdot \text{wt}/\text{flow rate}$. The overall surface reactivity, represented by k_{obs} , can be calculated if K_{sc} is known. Because MMH reacts under conditions required to measure K_{sc} , the K_{sc} values for methylamine on the various surfaces have been used as models for MMH adsorption.

Table 18 summarizes the reactivity data along with the calculated k_{obs} values and relative reactivities. The reactivity order of surfaces for the oxidation of MMH in air is as follows:



The relative reactivities are similar regardless of whether the observed rate constants are normalized with respect to surface area, or, as in Table 18, to the square of the surface area.

Under the conditions of the microreactor experiments, the surfaces of the metal powders are expected to be fully oxide coated, and the catalytic ability must be due to the nature of the metal/metal oxide layer. Although titanium is a common material of construction in hydrazine fuel systems, the reactivity shown here is due to the ability of the Ti/TiO₂ surface film to bind MMH and oxygen, and then to catalyze the bimolecular oxidative dehydrogenation reaction.

An interesting comparison can be made with the reactivities shown by similar surfaces in the environmental chamber studies (SECTION II). For MMH the reactivities were:



The orders of reactivity for the two very different types of experiments are similar, suggesting that ordinary smooth aluminum surfaces, although covered by an oxide layer, are unreactive, while high surface-area aluminum oxides are inherently more reactive. Chemically pure zinc and zinc-coated steel show slightly increased reactivity over aluminum. This observation

TABLE 18. SURFACE REACTIVITIES FOR MMH OXIDATION IN AIR^a

Surface	Fraction ^b Remaining	t_n^c (s)	$k_{obs} \times 10^2$ (s ⁻¹)	$k' \times 10^{2d}$ (s ⁻¹ m ⁻⁴)	Relative Reactivity ^e
316 SS	0.670	5.89	6.80	113	23
304-L SS	0.613	32.0	1.53	4.93	<1.0>
Iron	0.186	0.575	293	1050	210
Aluminum	0.414	19.4	4.55	11.2	2.3
Al ₂ O ₃	0.146	3.05	63.1	591	120
Zinc	0.797	2.00	11.4	200	41
Chromium	0.668	3.48	11.6	35.4	7.1
Nickel	0.164	9.64	18.7	4.3	0.9
Titanium	0.506	0.593	115	47.0	9.6

^a 328 ± 3 K^b Normalized data from Table 12 for 1 μL^c Flow rate is 0.167 mL/s, K_{sc} from Table 15^d Normalized per square of surface area^e Relative k' values

is notable because of the importance of galvanized steel as a material of construction in hangars and other enclosures. The placement of 304-L SS is contradictory in the two sets of experiments, but the microreactor study results are self-consistent in that the activity of both 304-L SS (with its chromium-rich surface) and chromium are similar.

Equations (40) and (41) of the proposed mechanism suggest that the formation of methanol is solely related to surface reactivity, while the decomposition of methyldiazene to methane also occurs in the gas phase. The fraction of methanol formed (normalized for surface contact by accounting for K_{sc}) should be a measure of surface reactivity for methanol formation. Results of calculations based on product distributions are gathered in Table 19.

Other surfaces, such as Fe₂O₃ and Fe₃O₄, for which K_{sc} values are not available, also show high selectivity for methanol.

TABLE 19. METHANOL PRODUCT SELECTIVITY

Surface	Methanol Fraction ^a	Methanol Selectivity ^b	Relative Selectivity ^b
316 SS	0.105	0.026	<1.0>
304-L SS	0.313	0.033	1.3
Iron	0.204	1.12	43
Fe ₂ O ₃	0.479	1.80	10
Aluminum	0.211	0.092	3.5
Al ₂ O ₃	0.294	0.056	2.2
Zinc	0.063	0.042	1.6
Chromium	0.097	0.050	1.9
Nickel	0.197	0.197	7.6
Titanium	0.106	0.147	5.6

^a Yield of methanol divided by yield of total methyl products, Table 12.

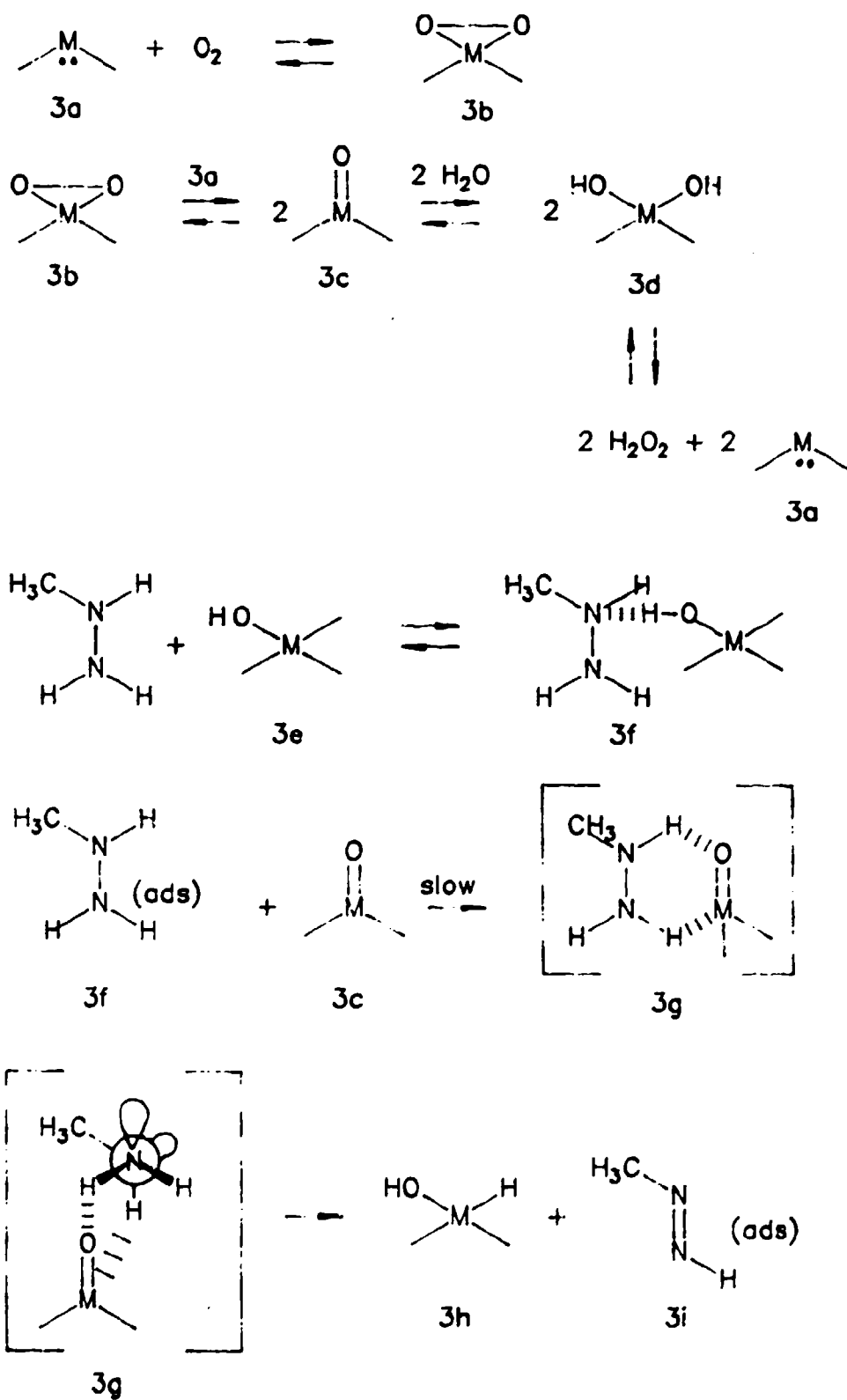
^b Methanol fraction divided by K_{sc} for methyl amine, Table 15.

Based upon the microreactor product and kinetic studies, the mechanism shown in Scheme 3 is proposed for the surface-catalyzed air oxidation of MMH. Although the scheme is representational, it provides a pictorial view of the overall reaction that accounts for the reactivity and selectivity observations, and allows for some predictions in this area.

In Scheme 3, the first step is the adsorption of oxygen at an active site. The surface oxide formed can be represented by a number of possible structures (3a, 3c) including a dihydroxy structure (3d), which is a hydrated form of (3c). Because the oxide site is uncharacterized, we have chosen to represent the active site as (3c) for simplicity and clarity. It should be emphasized that stoichiometrically and kinetically the three representations are equivalent. At ambient temperature, some of the dihydroxy form (3d) may dissociate to hydrogen peroxide and a metal-atom site, but at elevated temperatures no evidence of hydrogen peroxide is noted.

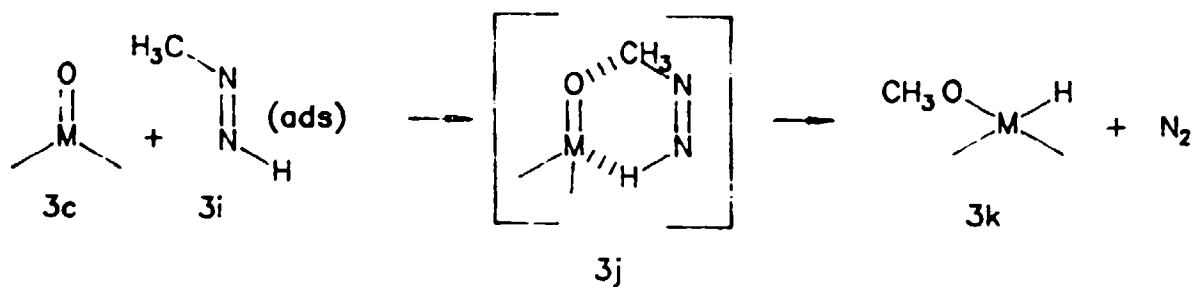
Rapid and reversible adsorption of MMH to form the hydrogen bonded structure (3f) is followed by a rate-limiting oxidative dehydrogenation through

Scheme 3

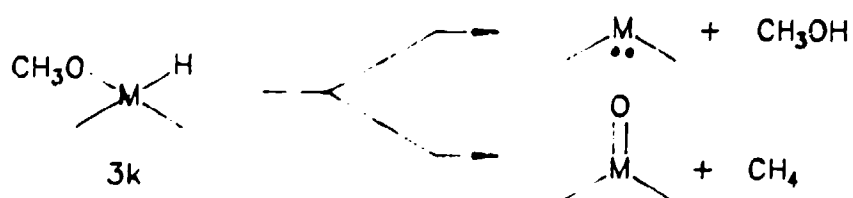
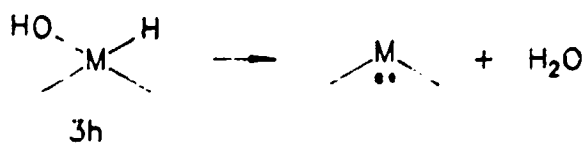
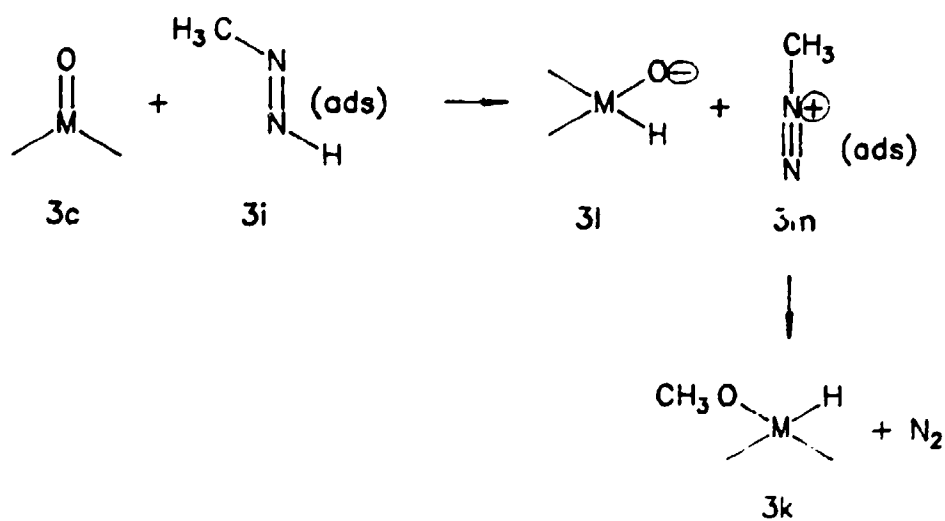


Scheme 3 (concluded)

concerted



step wise



transition state (3g) to methyldiazene (3i). The hydroxy-hydrido surface structure (3h) is a convenient formalism that shows the dehydrogenation (oxidation) of MMH and the hydrogenation (reduction) of the surface. The requirement for hydrogens on both nitrogens of the hydrazine may be the primary reason for the lack of reactivity of UDMH and the more-substituted hydrazines.

Reductive elimination of water from (3h) regenerates the active site. The methyldiazene may desorb and thermally decompose in the gas phase or undergo a similar sequence through (3j) to a methoxy-hydrido surface structure (3k). Partitioning of (3k) to methane and methanol via competitive reductive eliminations should be controlled by the relative stabilities of the surface oxide and surface atom. The observed methanol/methane selectivity ratios shown in Table 19 are in good agreement with this hypothesis. The metal oxide stabilities decrease in the order Ti, Zn, and Ni for the MO and MO₂ oxides, and Al, Cr, and Fe for the M₂O₃ series.

E. CONCLUSIONS

Microreactor studies have proven to be a convenient and valuable tool in the adsorption and surface-promoted reactions of the hydrazines. These studies have provided quantitative rate and product data for the surface-promoted air oxidation reactions and have allowed the development of hypotheses concerning the hydrazine/surface interaction. These studies have also estimated the effects of structure on reactivity and provided insight into the nature of the surface intermediates involved in this chemistry.

Factors that control the rates and selectivity of the various surfaces in the microreactor are understandable in terms a proposed mechanism for the surface-promoted oxidation that is equivalent to that suggested earlier based on environmental chamber studies.

UDMH, SDMH, and the more substituted hydrazines proved unreactive on all surfaces in air at 330 K. Because of its importance as a propellant, further work with UDMH is recommended.

SECTION IV

FLOW REACTOR STUDIES: LAMINAR FLOW REACTOR

A. INTRODUCTION

Development of a basic understanding of the chemical processes in the earth's atmosphere depends on the gathering of accurate rate and mechanistic data for the gas-phase reactions of both natural and man-made constituents (References 14 and 34). A wide variety of experimental techniques for the study of gas-phase reactions have been described and applied to atmospheric problems (References 14 and 35). Flow reactors (References 36 and 37), flash photolysis and pulse radiolysis instruments, (References 38 and 39) and environmental chambers (SECTION II, and Reference 14) have all been used to further our understanding of atmospheric chemistry. The increased recognition of possible inaccuracies due to unassessed interferences from heterogeneous reaction components in earlier gas-phase studies has prompted the development of techniques to minimize wall effects.

Flow reactors used for gas-phase kinetics studies generally operate under laminar flow conditions at pressures on the order of 100 Pa (References 40). Because the rate constants of many reactions depend on total pressure (References 14, 36 and 37), rate data taken at low pressures may be misleading if used to estimate the rates of processes at or near atmospheric pressure. Additionally, while the reactants are well-mixed by molecular diffusion at low pressures, diffusion to (and reaction on) the walls of the reactor under these conditions is often a significant and not easily corrected source of experimental error (References 41 - 43).

This report details the development and use of a new type of flow reactor designed to circumvent some of the limitations of the low-pressure flow systems. The Laminar Flow Reactor (LFR) is designed to study bimolecular gas-phase reactions at atmospheric pressure in order to provide experimental conditions representative of the troposphere. The flow, reactant introduction, and reaction monitoring systems have been designed to reduce or eliminate wall reactions.

1. Overview of the Laminar Flow Reactor Concept

Drawings of the Laminar Flow Reactor are shown in Figures 18 and 19. A diffuser is located behind flow-straightening screens to eliminate turbulence and provide a flat, uniform, laminar flow of an inert carrier-gas containing the first reactant, which is referred to as the uniform field reactant. This reactant is usually supplied in stoichiometric excess.

A second reactant is mixed with a separate inert carrier gas stream and is introduced to the laminar flow by an array of small-diameter porous tubes. These tubes are perpendicular to the laminar flow, and the reactant/carrier gas mixture is forced out of the tubes by a small positive pressure. The second reactant is introduced into the central portion of the reactor cell and does not contact the walls.

The reactants are mixed by the confluence of the carrier streams and microscale turbulence caused by the introduction array. Because molecular diffusion is one of the slowest mass transfer processes at ambient pressures, the second reactant remains localized in the central portion of the uniform flow field and is confined away from the apparatus walls. This diffusional confinement allows for the observation of the reactants, intermediates, and products downstream of the delivery array before wall contact occurs, by means of a folded-path White Cell and FTIR system.

In the experiments described below, excess ozone was used as the uniform field reactant, and a vaporized liquid hydrazine or alkene was used as the second reactant. The method, however, is generally applicable to any two vapor-phase reactants.

2. General Flow Reactor Theory

The flow/diffusion/reaction process for dilute reactants in an inert carrier-gas (References 44 - 47) can be described by the following:

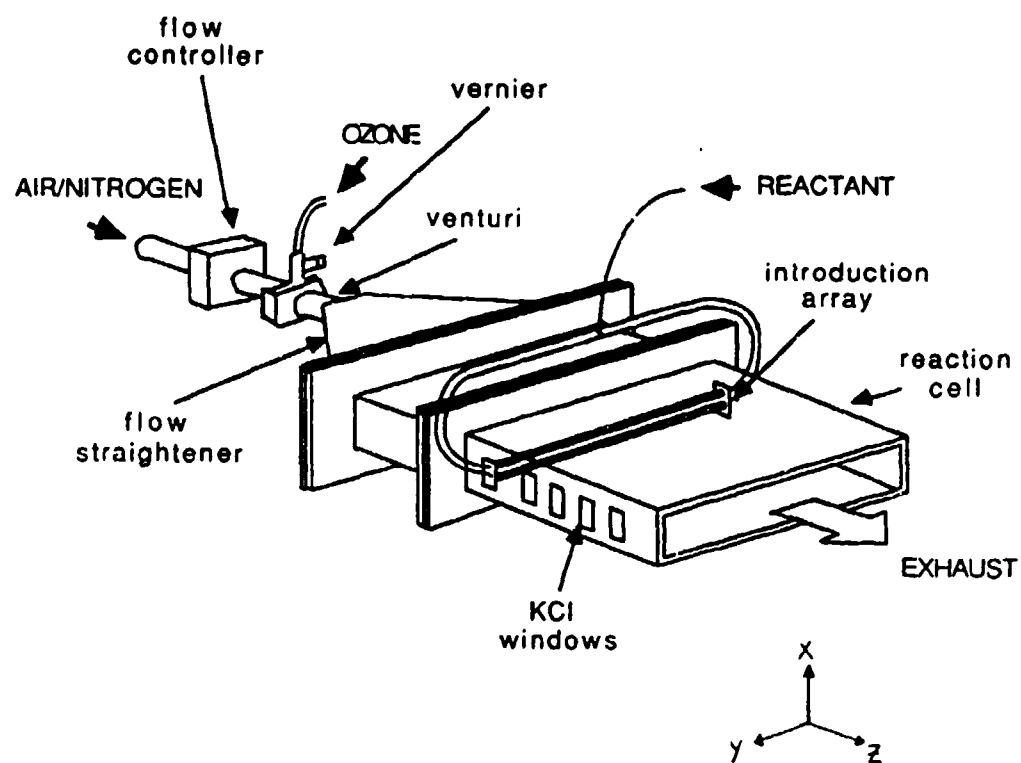


Figure 18. Laminar Flow Reactor

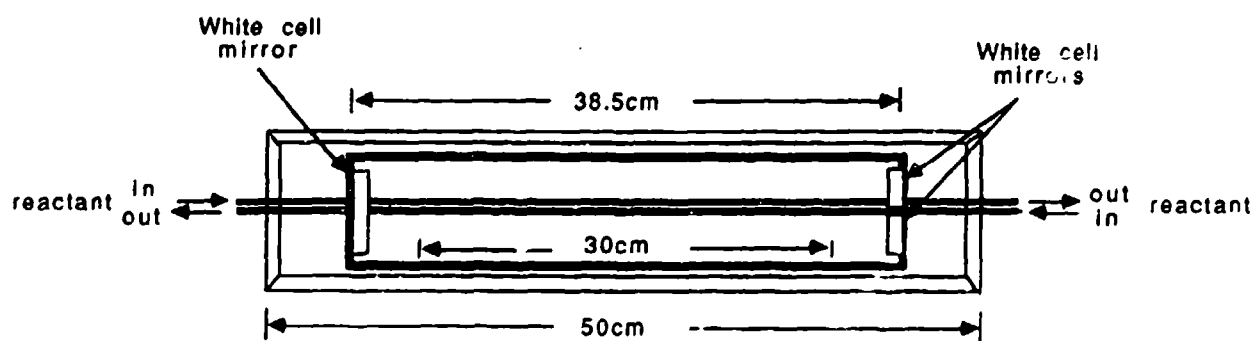


Figure 19. Head-on View of the Laminar Flow Reaction Cell

$$\frac{\partial C_a}{\partial t} + v \cdot \nabla C_a = D_{ab} \nabla^2 C_a - [\sum_i k_i C_i] C_a \quad (48)$$

where

- C_a = concentration of a species, a, as a function of the spatial coordinates and time
- v = velocity of the flowing gas stream in the reactor reference frame
- ∇ = grad operator
- D_{ab} = diffusion coefficient for the species a in the carrier gas
- ∇^2 = Laplacian operator
- k_i = rate constant for the reaction between a and i
- C_i = concentration of a species i that reacts with species a

The physical significance of each term in Equation (48) is as follows. $\partial C_a / \partial t$ is the rate of change of C_a at some fixed point in the reactor (at steady state $\partial C_a / \partial t = 0$). The change in C_a with position resulting from carrier-gas flow (forced convection) is given by $v \cdot \nabla C_a$. $D_{ab} \nabla^2 C_a$ is the change in C_a with position resulting from molecular diffusion. Finally, $[\sum_i k_i C_i] C_a$ is the change of C_a with position resulting from chemical reaction. The solution function $C_a(x, y, z, t)$ for a particular reactor configuration allows rate constants to be obtained from experimental data.

In the following general solution to Equation (48) under steady state conditions, Cartesian coordinates are used and pseudo-first-order reaction conditions are assumed. Laminar flow is assumed with a constant flow-velocity (i.e., the velocity vector is constant across most of the reactor cross-section). Laminar flow with a constant velocity vector can be achieved if: (1) the entry length (the distance required to fully develop the laminar-flow velocity profile) is much greater than the total length of the reactor, and (2) the Reynolds number is below that for turbulent transition in a rectangular conduit. An important simplifying assumption is that diffusion along the z-axis is negligible compared to convective transport. With these assumptions, Equation (48) becomes Equation (49):

$$v \frac{\partial C_a}{\partial z} = D_{ab} \left(\frac{\partial^2 C_a}{\partial x^2} + \frac{\partial^2 C_a}{\partial y^2} \right) - [\sum_i k_i C_i] C_a \quad (49)$$

Solution of Equation (49) is facilitated by substituting the trial function $C_a = C_a' \cdot \exp(-\sum_i k_i C_i / v)$ (where $C_a' = C_a$ uncorrected for reaction, References 44 and 48), which yields Equation (50), a pure flow/diffusion problem. Formally, Equation (50) is identical to a large class of transient diffusion problems for which solutions exist when $C_a'(x,y,z)$ is an analytic function at some value of $z = z_0$ and when one or more other constraining (boundary) conditions are given (References 48 and 49).

$$v \frac{\partial C_a'}{\partial z} = D_{ab} \left(\frac{\partial^2 C_a'}{\partial x^2} + \frac{\partial^2 C_a'}{\partial y^2} \right) \quad (50)$$

Fortunately C_a' does not need to be determined explicitly. Equation (50) can be solved by separating variables (Reference 42) to produce a solution of the form $C_a'(x,y,z) = X(x)Y(y)Z(z)$. The complete solution is of the form

$$C_a(x,y,z) = X(x)Y(y)Z(z) \cdot \exp(-\sum_i k_i C_i / v) z \quad (51)$$

If C_i is varied systematically, plots of $\ln(C_a(x,y,z,C_i)/C_a(x,y,z,C_i=0))$ against C_i return k_i/v as the slope. The C_a' terms cancel identically.

If a spectrometer cell is used to measure C_a , the situation is more complex. In this case, the measured quantity is the average value of C_a in the spectrometer cell, $C_{a,avg}$, and is given by

$$C_{a,avg} = \frac{1}{V_c} \int_{V_c} C_a(x, y, z) dV_c \quad (52)$$

where

V_c = cell volume

In Equation (52), the $X(x)$ and $Y(y)$ components of C_a' cancel identically, but a more explicit expression for $Z(z)$ is required. In general, $Z(z)$ is of the form $Z(z) = B \exp(-p^2 z)$ (Reference 48) where p^2 and B are constants to be determined by application of the boundary and initial conditions. The expression for $C_{a \text{ avg}}$ can now be integrated for the case of a single reactant, C_i , to give:

$$\frac{C_{a \text{ avg}}(C_i)}{C_{a \text{ avg}}(C_i = 0)} = \frac{A(C_i)}{A(C_i = 0)} \quad (53)$$

$$= \frac{p^2}{p^2 + \frac{k_i C_i}{v}} \left[\frac{e^{\left(\frac{-k_i C_i z_1}{v}\right)} - e^{\left(\frac{-k_i C_i z_2}{v}\right)}}{e^{-p^2 z_1} - e^{-p^2 z_2}} \right] \quad (54)$$

Rate constants can be obtained by plotting $(C_{a \text{ avg}}(C_i)/C_{a \text{ avg}}(C_i=0)) = (A(C_i)/A(C_i=0))$ where A is the absorbance signal. The separation constant B cancels identically, and both the rate constants, k_i , and the remaining separation constant, p , can be determined by graphic or nonlinear modeling methods.

In the special case that the diffusonally confined reaction zone is smaller than the size of the spectrometer cell, diffusional or eddy transport of the minor reactant, species a , along the x and y coordinates cannot be detected by measuring $C_{a \text{ avg}}$ up to the limits of the spectrometer cell. For reaction zones larger than the spectrometer cell and smaller than the internal wall dimensions, $C_{a \text{ avg}}$ will gradually decrease due to diffusive spreading. If the reaction zone is equal to the internal dimensions of the reactor, $C_{a \text{ avg}}$ will remain constant in the absence of reaction.

If all the kinetic processes are first-order, and the LFR is operated in the regime of a diffusonally confined reaction zone larger than spectrometer cell but smaller than the wall dimensions, then the change of $C_{a \text{ avg}}$ along the z -coordinate can be related to the sum of the reaction rates and diffusional spreading rates. The latter can be determined independently by omitting the reactant, C_i , and determining $C_{a \text{ avg}}(z)$. The transformation of $C_{a \text{ avg}}(z)$ to

$C_{avg}(t)$ for either process is easily accomplished because the linear velocity, v , is known.

B. EXPERIMENTAL

1. Materials

Hydrazine and MMH were propellant grades (Olin) analyzed according to MIL-P-26536-D and MIL-P-27404B respectively. Ozone was produced by a Welsbach Laboratory Ozonator model T-816. 2,3-Dimethyl-2-butene (TME, 99 percent) was purchased from Wiley Organics Co. and used as received.

2. Instrumentation

Changes in reactant concentrations within the reaction cell were monitored by absorbance changes with an FTIR spectrometer in conjunction with a White Cell optical system.

a. FTIR Spectrometer

A Mattson Sirius 100 FTIR spectrometer equipped with a remote HgCdTe detector operated at 77 K was used. The HgCdTe detector was mounted on an adjustable aluminum base plate external to the FTIR, but within a purgeable air space. Data collection and processing were performed using a Pixel 80 supermicrocomputer using the UNIX operating system and Mattson-supplied programs. Kinetic data were collected over the mid-infrared region (4000 to 700 cm^{-1}) at 4 cm^{-1} resolution. Product spectra were collected at 1 cm^{-1} resolution.

b. Multiple-path Optics

A White cell optical system (Infrared Analysis, Inc.) of 10.64-meter pathlength was used. The overall pathlength of the optical system was determined to be a multiple of the base length (38.5 cm) by counting the number of dots on the nesting mirror made by a coincidental helium-neon (HeNe) laser

beam (Reference 8). The laser beam could be made coincident by interposing a removable mirror into the spectrometer's internal optics. The IR beam could be visualized by means of a photoluminescent screen (Quantex Mod.Q-42-R) and had a diameter of 2 cm at the entrance of the White Cell.

c. Analytical Frequencies and Extinction Coefficients

Single absorption peaks and extinction coefficients measured at 4 cm^{-1} resolution were used for concentration determinations. The extinction coefficients and frequencies used were: hydrazine $\epsilon_{(e)} = 5.87 \text{ atm}^{-1}\text{cm}^{-1}$ at 958 cm^{-1} ; MMH $\epsilon_{(e)} = 4.69 \text{ atm}^{-1}\text{cm}^{-1}$ at 888 cm^{-1} ; and ozone $\epsilon_{(e)} = 7.31 \text{ atm}^{-1}\text{cm}^{-1}$ at 1058 cm^{-1} . The extinction coefficients at 4 cm^{-1} resolution were 13 - 40 percent lower than those at 1 cm^{-1} as reported in SECTION II. The extinction coefficients of ozone at both 1 cm^{-1} and 4 cm^{-1} resolutions were determined experimentally by establishing a series of ozone concentrations in the carrier flow through the LFR and measuring the IR and UV absorbances. A sample of the carrier/ozone stream was vacuum aspirated through a Knauer UV photometer with a 1-cm capillary flow-through cell operated at 254-nm. The UV extinction coefficient was taken to be 308 $\text{atm}^{-1}\text{cm}^{-1}$ (Reference 50). The extinction coefficient of the 1058 cm^{-1} band of ozone at 1 cm^{-1} resolution was found to be 10.0 $\text{atm}^{-1}\text{cm}^{-1}$. McAfee, Stephens, Fitz and Pitts report 9.7 $\text{atm}^{-1}\text{cm}^{-1}$ (Reference 51).

The conversion of absorbance values by Beer's Law results in gas pressures in the units of atmospheres. For convenience, concentration units are reported in ppm units where ppm refers to the partial pressure in $\text{atm} \cdot 10^{-6}$. Changes to concentrations in $\text{molecules} \cdot \text{cm}^{-3}$ were made using the Ideal Gas Law.

d. Gas Chromatograph

A Hewlett-Packard Model 7620A GC equipped with a flame ionization detector was used in the diffusion coefficient studies. The injection ports of the GC were lined with PTFE sleeves to minimize metal/hydrazine interactions. An open, 13.8-meter PTFE tube was mounted in the gas chromatograph in place of a chromatographic column. The internal diameter of the tube

(0.242 cm) was determined from the weight of water contained in the tube and the length of the tube. Breathing air (analyzed according to Federal Specification BBA103A Amendment 1 Grade C) was used as the carrier gas.

3. Apparatus

a. Laminar Flow Reactor

The Laminar Flow Reactor was composed of a mass-flow-controlling system, flow straightener, reaction cell, and reactant delivery systems as shown in Figures 18 and 19. The mass-flow-controlling system was supplied by Kurz Instruments, Inc., and consisted of a 505 Series flow meter, a 710 Series controller, and a 730 Series valve. This system allowed for flow control of the matrix gas (nitrogen or air) up to 308 L/min. Kurz also supplied the flow diffuser and straightener. A perforated screen was inserted near the end of the flow diffuser, followed by a 10-cm expansion section that eliminated any remaining turbulence and established a laminar flow in the reaction cell. The reaction cell was a rectangular duct constructed of 6 mm poly(methyl methacrylate) sheets. Potassium chloride windows (60 × 40 mm) were embedded in one wall of the reaction cell to allow for entrance and exit of an IR beam. A 2-meter flexible exhaust duct, constructed of polyethylene film, was attached to the end of the reactor cell and lead to an exhaust hood to allow for the safe removal of effluents. The entire system was placed on a moveable table (relative to a stationary IR beam from the FTIR spectrometer). The temperature of the air/nitrogen stream was measured with a right angle thermocouple (Nanmac Corporation) placed at the end of the reaction cell. Hydrazines and other reactants were introduced into the reaction cell by passing nitrogen (1 - 4 mL/s) through a vaporizer, which consisted of a fritted-glass gas dispersion bubbler containing 1 mL of liquid reactant (Figure 20). The vaporized reactant in the carrier nitrogen flow was split into two streams leading to opposite ends of the introduction array, which consisted of two parallel 30-cm lengths of microporous PTFE tubing (Gore-Tex TA001, 1-mm inside diameter, 1.6-mm outside diameter, 2-micron pores) centered in the junction of the flow straightener and the reaction cell. The two strands of microporous tubing were separated by 6 mm. After passing through the microporous tubes, the two streams were rejoined and vented

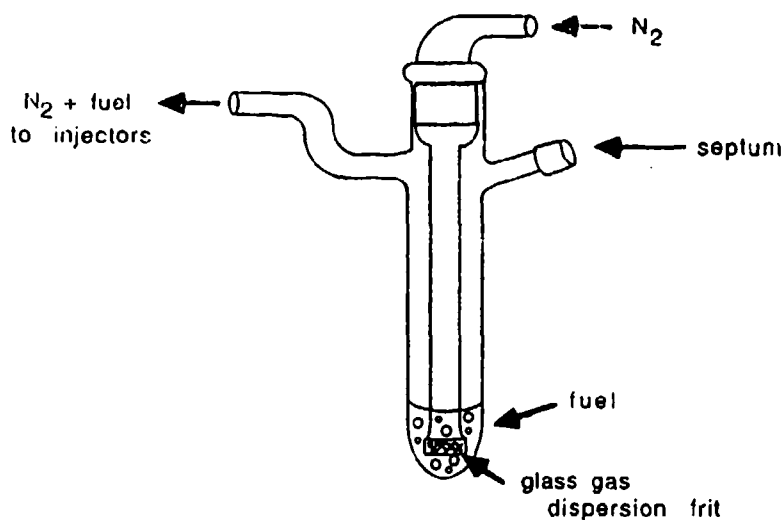


Figure 20. Vaporizer (Fritted-Glass Gas Dispersion Bubbler)

to a hood. The concentration of the vaporized liquid reactant could be controlled by varying the flow of nitrogen through the vaporizer with an Omega FMA 115 mass flow controller and, if necessary, immersing the vaporizer in a warm water bath.

Ozone was produced by passing oxygen through an ozone generator at a flow of 4 L/min. The ozone generator produced a 1.5 percent-by-weight mixture of ozone in oxygen as calculated from operational specifications listed in the Welsbach Ozone Systems manual. Ozone was introduced into the main carrier stream prior to entering the diffuser, and its concentration was controlled by a Fox venturi/Republic metering valve. The input connection size for the venturi was 0.64 cm, which constricted to an inner diameter of 0.32 cm. The outlet connection was 1.27 cm. At the closed position of the metering valve, all the ozone flow was bypassed to a hood and no ozone entered the reaction cell. As the metering valve was opened, the venturi effect caused ozone to enter the main carrier stream. Micrometer settings on the metering valve allowed ozone concentrations to be conveniently repeated or varied.

All materials in contact with ozone or reactant vapors were stainless steel, PTFE, or FEP.

b. Gas Purification System

Air and nitrogen used in the Laminar Flow Reactor was purified by a Balston Model 75-20 air filter. The air filter removed all particulate materials and dried the air to a dew point of 233 K (127 ppm water, v/v). Nitrogen gas was liquid nitrogen boil-off and had less than 25 ppm water and less than 5 ppm oxygen. The temperature of the air or nitrogen stream was controlled by passing the gas through a copper coil submerged in a temperature controlled water/antifreeze bath.

4. Procedures

a. General Procedure for Laminar Flow Kinetics

In a typical experiment, the nitrogen or air laminar flow stream (140 - 308 L/min) was established and the temperature of the reaction cell was allowed to equilibrate. Ozone generation was allowed to stabilize with the entire ozone flow bypassing the reactor. Single beam reference spectra were collected and stored for use in computing absorbance spectra for concentration measurements. A sample of liquid reactant was syringed into the vaporizer, and a flow of nitrogen through the vaporizer was established. The concentration of vaporized reactant in the reactor cell was allowed to stabilize (generally 2 - 5 minutes), and prereaction (background) spectra were collected. The metering valve was opened to allow ozone to enter the reaction cell and reaction spectra were collected.

b. Test Methods

Two procedures were used to monitor the disappearance of reactants and the appearance of products in the reaction cell.

(1) Variable-Position Fixed-Ozone Kinetic Method. The first (and most common) procedure was to determine the average concentration ($C_{a,avg}$) of the reactant at different positions along the z-axis of the reaction cell at a constant excess ozone concentration. Using peak height, 8 - 10 reaction spectra were analyzed per experiment. The reaction time at which each spectrum was obtained was calculated from the flow rate of the air/nitrogen stream and the distance from the introduction array. The array position was taken as $z = 0$, $t = 0$. Mass flow rates from the Kurz 505 flow meter were corrected to the carrier gas temperature and ambient pressure (84 kPa). The concentration/time data were calculated from the FTIR absorbance spectra/extinction coefficients of the reactants and ozone, and the linear flow rate/z-position.

(2) Fixed-Position Variable-Ozone Kinetic Method. The second (or alternate) procedure involved determining the $C_{a,avg}$ at a fixed z-position ($z = 20$ cm) downstream from the introduction array and varying the ozone concentration from 0 to 300 ppm (v/v) by means of the vernier metering valve. The concentration/concentration data were analyzed graphically based on the use of Equation (53).

c. Diffusion Coefficients

The chromatographic peak broadening technique of Grushka and Maynard was used to determine diffusion coefficients (References 52 and 53). The procedure requires an open-ended tube of diameter, d , and length, L , where $L \gg d$. The diffusion coefficient of the solute is measured in the predetermined carrier gas by injecting a narrow plug into an open tube. The plug of solute broadens while transversing the tube, and the amount of broadening is measured using a suitable detector. The height of a theoretical plate, H , can be measured directly from the peak width at half height using Equation (55):

$$H = \frac{L \cdot W_b^2}{5.54 t_r^2} \quad (55)$$

where

L = column length
W_{1/2} = peak width at half height
t_r = retention time (using units of length)

The diffusion coefficient, D₁₂ can be determined by using

$$D_{12} = \frac{L}{4t_r} H \pm H^2 \left(\frac{d^2}{3} \right)^{\frac{1}{2}} \quad (56)$$

where

d = tube diameter

Submicroliter quantities of hydrazines or other standards were injected into the GC using a syringe (injector temp 423 K, flow 0.13 - 0.17 mL/s); the peak characteristics were determined for a minimum of three replicates. Injection volumes were such that peak broadening was independent of sample size.

C. RESULTS

1. Flow and Diffusion Characteristics of the Laminar Flow Reactor

The Laminar Flow Reactor was designed to provide a uniform, constant, laminar flow of carrier-gas (i.e., a flow field described by a single velocity vector, v) by applying well-known principles of fluid dynamics (References 54 - 57). Turbulence in the reaction cell is prevented by the use of an expansion section downstream of the flow straightening screen. The development of a parabolic velocity profile is prevented by operating at Reynolds numbers such that the entry length is much greater than the physical length of the reaction cell (Reference 58).

a. Flow Performance Data for the Laminar Flow Reactor

The velocity field in the flow reactor was measured at Reynolds numbers of 1380 and 2100 with a hot wire anemometer. The average value and variance for 48 different sampling positions uniformly distributed within the kinetic flow section were obtained. The flowing gas was nitrogen at 84 kPa. The average velocity at a Reynolds number of 1380 was 13 cm/s with a variance of ± 0 ; the average velocity at a Reynolds number of 2100 was 20 cm/s with a variance of ± 1 . No evidence of turbulence was obtained, and the variance in the velocity at the higher Reynolds number was small enough to permit accurate chemical kinetic measurements. Velocity variances on the order of 10 percent have no adverse effects on the measurement of diffusion constants to 2 percent accuracy (References 55 and 56). Under the conditions of kinetics measurements, the LFR was operated with linear velocities of 6.2 to 13.7 cm/s, corresponding to Reynolds numbers of 650 - 1425.

b. Characterization of the Microporous Tubing

The flow loss characteristics of the PTFE microporous tubing used to introduce the second reactant into the laminar flow field were studied by determining the net flow loss as a function of input flow and tubing length. Both nitrogen and methane were studied as the flowing gases, Table 20.

The flow loss can be described by the following empirical relationship:

$$F/F_0 = \exp(-Gl/P) \quad (57)$$

where

F = outlet flow rate in mL/s
F₀ = inlet flow rate in mL/s
G = loss constant in cm⁻¹ kPa
l = length in cm
P = pressure in kPa

TABLE 20. MICROPOROUS TUBING FLOW LOSS RATES^a

Flow (mL/s)		Inlet Pressure (kPa)	Length (cm)	G (cm ⁻¹ kPa)
Inlet	Outlet			
0.442	0.073	150	36.5	7.4
2.50	0.382	150	36.5	7.7
0.866	0.30	223	36.5	6.6
^b 0.328	0.066	150	36.5	6.6
0.833	0.32	250	30.0	8.0
1.25	0.68	250	20.0	7.6
0.833	0.60	250	10.0	8.2
			Average =	7.4

^a Nitrogen, 294 K^b Methane, 294 K

c. Diffusional Characterization with Methane

Initial characterization of the combined flow, introduction array, and optical system in the absence of reaction was performed with methane as a model IR-active inert gas. Methane was introduced from a double-strand array at an inlet flow of 0.5 mL/s. The absorbance of the 3017 cm⁻¹ peak of methane was monitored as a function of position along the z-axis (converted to time) and linear velocity of the carrier gas. The results are depicted in Figure 21 and clearly illustrate the three regimes of overlap of the diffusionally confined zone and spectrometer cell. At the highest carrier flows and linear velocity, the confined zone is expanding along both the x- and y-axes, and the absorbance reaches a maximum when the height of the confined zone matches that of the spectrometer cell (4 cm). Expansion in the y-direction is presumably of the same order of magnitude, and at the maximum absorbance z-position the total y-length is still less than the base-path length of the spectrometer cell. Continued expansion results in smooth decay of the absorbance as the confined zone expands and overlap with the spectrometer cell decreases. Finally, at the longest times (lowest carrier flows), the confined zone has expanded to the inside dimensions of the reactor and no further change in absorbance takes place.

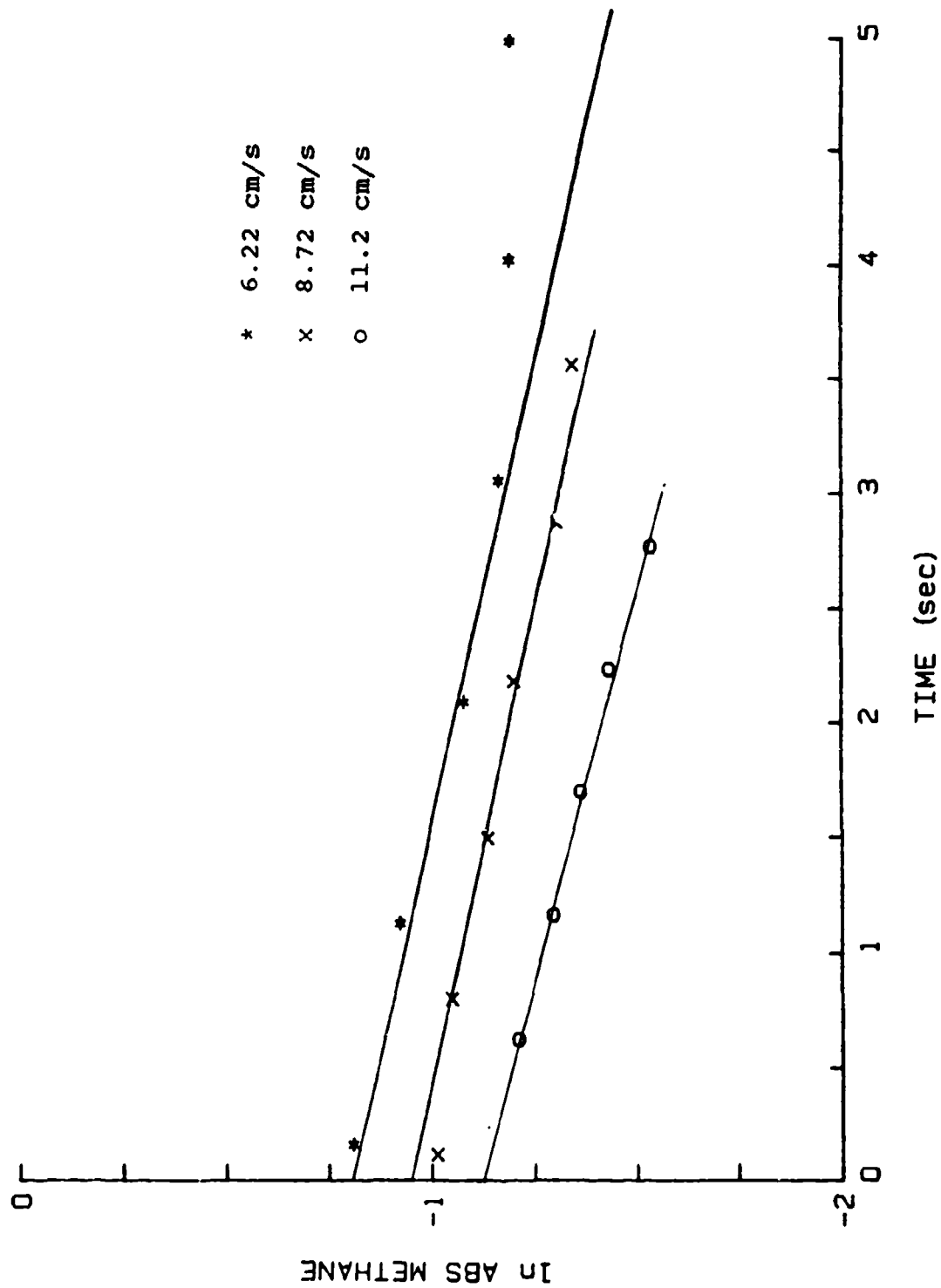


Figure 21. $\ln(\text{absorbance})$ Versus Time for Methane Diffusion Characterization

At higher introduction rates of methane (> 1 mL/s), the initial expansion is not apparent, and the absorbance/time relationship is a linear exponential decay until reaching the size of the reaction cell.

The operational window that guarantees minimal wall contact in the LFR appeared to involve array introduction rates greater than 1 mL/s and reaction times less than 5 - 7.5 s.

d. Diffusional Characterization with the Hydrazines

The reactant concentration/time relationships for experiments conducted in the absence of ozone are termed background or diffusion-only rates. These rates are characterized by the apparent first-order rate constant (k_{bkg}) and are related to the expansion of the diffusionally confined zone of reactant into the laminar flow. Background rates were measured for each kinetic experiment.

(1) Hydrazine. Operating the LFR within the general limitations defined by the methane diffusion experiments (introduction rates of hydrazine/carrier gas flows greater than 1 mL/s, laminar flow velocities such that total residence time in the LFR remained under 7.5 s, and Reynolds numbers less than 1500), FTIR spectra were recorded at 8 - 10 z-positions downstream of the introduction array and converted to concentrations. The average concentration of hydrazine vapor in the spectrometer cell (C_{avg}) was found to decrease exponentially with increasing z-coordinate. Because there is no reaction in the nitrogen flow, the decrease in concentration must be related to diffusional expansion. The concentration/time relationship was treated as a first-order decay, and the decay constant (k_{bkg} , Table 21) was obtained from the slope of $\log(\text{concentration})/\text{time}$ plot.

The observed value of k_{bkg} was slightly larger in a laminar flow of air as compared to nitrogen (nitrogen was used as the vaporizer carrier in both cases). During experiments with a laminar flow of air, which contained the ambient concentration of carbon dioxide (300 ppm v/v) and a trace of water

TABLE 21. BACKGROUND HYDRAZINE LOSS RATE
CONSTANTS IN NITROGEN

File (#)	Temp (K)	$k_{bkg} \times 10^2$ (s ⁻¹)
H120A	289	2.6
H120B	289	<u>5.5</u>
Average =		4.05 ± 1.45
H118	299	4.8
H118A	300	<u>4.7</u>
Average =		4.75 ± 0.05
H124A	307	10.0
H124B	306	<u>8.7</u>
Average =		9.35 ± 0.65
H123	312	21.0
H123A	312	<u>17.0</u>
Average =		19.0 ± 2.0
^a H214	299	9.9
^a H214A	299	<u>6.7</u>
Average =		8.3 ± 1.6

^a Measured in air

vapor (125 ppm v/v), a clear, viscous liquid was deposited on the microporous tubing and eventually blocked the flow of hydrazine. When a sample of the viscous liquid was dissolved in dilute hydrochloric acid, a colorless gas was released as evidenced by effervescence of the solution. Ion chromatography of the aqueous acid solution showed only the presence of hydrazine. It was postulated that the material was an adduct of hydrazine and carbon dioxide such as carbazic acid, H_2NNHCO_2H , and that the larger k_{bkg} for hydrazine in air was due to both diffusion and the reaction of hydrazine with carbon dioxide. Because of this interference, it was necessary to rebuild the introduction array after every few experiments in air. No build-up of viscous liquid was noted when nitrogen was used as the laminar flow gas.

(2) MMH. MMH was found to behave similarly to hydrazine. The values of k_{bkg} at several temperatures are shown in Table 22. The value of diffusion-only rate for MMH was about 40 percent of the value for hydrazine at 300 K. MMH was not studied in an air laminar flow.

e. Diffusion Coefficients of Hydrazines in Air

Theoretical models of the reaction kinetics for the decomposition of hydrazines in a laminar flow reactor or environmental models are enhanced by a knowledge of the diffusion coefficients for the reactants and products. Using the open-tube gas chromatographic method outlined by Grushka and Maynard (References 52 and 53), the gas-phase diffusion coefficients (D_{ab}) of the methylhydrazines, ethanol (EtOH), and methane (CH_4) were measured at a series of temperatures. The diffusion coefficients over the range of 336-390 K

TABLE 22. BACKGROUND MMH LOSS RATE
CONSTANTS IN NITROGEN

File (#)	Temp (K)	$k_{bkg} \times 10^2$ (s ⁻¹)
M16A	285	3.5
M16B	285	3.7
Average = 3.6 ± 0.1		
M19	287	3.5
M19A	286	5.6
Average = 4.55 ± 1.05		
M110A	292	3.7
M110B	292	2.9
Average = 3.3 ± 0.4		
M14A	299	11.0
M15A	299	13.0
Average = 12.0 ± 1.0		
M117	313	14.0
M117A	313	11.0
Average = 12.5 ± 1.5		

are presented in Table 23. The literature values for ethanol are available at several temperatures and compare well with the measured values (Reference 59).

The temperature dependence of diffusion constants can be expressed by Equation (58):

$$D_{ab} = D_0 \exp(-E/RT) \quad (58)$$

where E is an apparent diffusional activation barrier and D_0 is a pre-exponential term. Linear least squares analyses of the temperature dependence of the diffusion coefficients in Table 23 give the results shown in Table 24.

2. Kinetic Behavior of the Ozonization Reaction

The complex concentration/time relationships shown in the reaction of ozone with the hydrazines were analyzed by two procedures: (1) the method of initial rates, used for the hydrazine/ozone reaction, and (2) an approximate

TABLE 23. DIFFUSION COEFFICIENTS IN AIR^a

Compound	Temperature			
	336 K	354 K	373 K	390 K
MMH	0.2158	0.2664	0.3010	
UDMH	0.1147	0.1274 (353 K)	0.1442	0.1650
SDMH		0.1828	0.1897	0.2133
TMH		0.1087 (353 K)	0.1382	0.1616
TTMH ^b		0.0985 (352 K)	0.1183	0.1294
MDMH ^b		0.1698 (352 K)	0.1889	0.2188
EtOH ^c	0.1515 (342 K)	0.1816 (352 K)	0.1930	0.2242
CH ₄	0.2146	0.2496	0.2611	

^a Measured in cm²/s

^b Methylenedimethylhydrazine

^c $D = 0.136$ (300.5 K); $D = 0.148$ (314 K). Reference 59 reports 0.135 (298 K) and 0.154 (340 K).

TABLE 24. TEMPERATURE DEPENDENCE OF
DIFFUSION COEFFICIENTS

Compound	E^a (J/mol)	D_0^a (cm ² /s)	D_{ab} (298 K) (cm ² /s)
MMH	9387	6.303	0.143
UDMH	7239	1.515	0.082
SDMH	481	0.924	0.132
TMH	12313	7.239	0.050
TTMH	8274	1.6767	0.059
MDMH ^b	7491	2.172	0.106
EtOH	5105	1.023	^c 0.130
CH ₄	5546	1.589	0.169

^a Diffusional barrier and pre-exponential terms for use in Equation (58)

^b Methylenedimethylhydrazine

^c (Reference 59) reports 0.135 at 298 K

a. Hydrazine

solution to the MMH/ozone kinetic system based on the theory of delayed-branching chain kinetics. The two analyses were not mutually exclusive and represent different facets of the same reaction sequence.

When ozone was added to the laminar flow field through the venturi/metering valve, the hydrazine concentration dropped appreciably as the hydrazine/ozone mixture traversed the reaction cell. The log(concentration)/time profile is linear over most of the range, but does show some acceleration (downward curvature) at long reaction times (Figure 22). Extrapolation of the reaction curve to $t = 0$ gives an intercept for the initial concentration of hydrazine that is slightly lower than expected based on the diffusion-only line extrapolated to $t = 0$. This observation is discussed later.

The initial portion of the reaction appears to be a first-order decay, as shown by the linearity of the log plot during the first half of the reaction (Figure 22). If the major factors responsible for the loss of

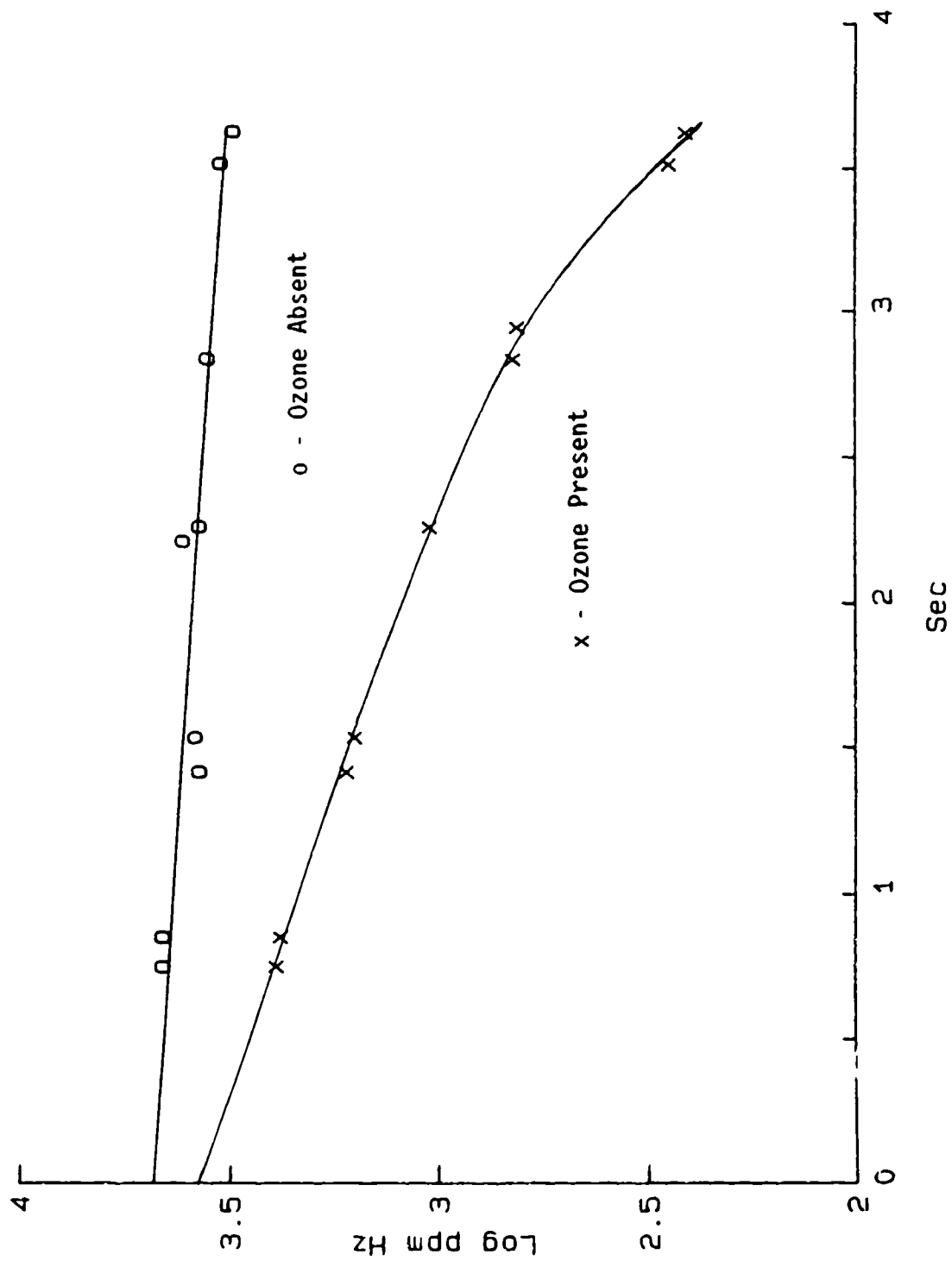


Figure 22. Hydrazine Loss Rate in the Presence and Absence of Ozone

hydrazine during the initial part of the reaction are diffusional expansion and the reaction with ozone, the initial rate is:

$$-\frac{d[\text{HZ}]}{dt} = (k_{\text{bkg}} + k_i[\text{Oz}]^n) [\text{HZ}] \quad (59)$$

where

[HZ] = concentration of hydrazine
[Oz] = concentration of ozone
 k_i = rate constant for ozonization reaction
 n = order in ozone

If the concentration of ozone is approximately constant, then the observed initial rate is first-order and:

$$k_{\text{obs}} = k_{\text{bkg}} + k_i[\text{Oz}]^n \quad (60)$$

Because k_{bkg} is determined independently and the ozone concentration is measured, k_i can be determined. The results shown in Table 25 are consistent with the reaction being first-order in ozone, $n = 1$. Further support for the first-order dependence on ozone is derived from the alternate kinetic procedure described below.

The stoichiometry was determined by comparing the change in hydrazine concentration to the change in ozone concentration during two different intervals of the reaction. The ozone/hydrazine stoichiometric ratio was found to be 1:1 during the nonaccelerating stages of the reaction; during the accelerating stage, however, the consumption of hydrazine increased to two to three times that of ozone.

The reaction rate was studied over the range of ozone concentrations of 55 to 100 ppm. With initial hydrazine concentrations of approximately 40 ppm, the resulting initial ozone/hydrazine ratio varied from 1.4 to 2.5.

TABLE 25. HYDRAZINE LOSS RATE CONSTANTS
WITH OZONE IN NITROGEN

File (#)	Temp (K)	$k_i \times 10^{17}$ ($\text{cm}^3 \text{molecule}^{-1} \text{s}^{-1}$)
H120A	289	3.33
H120B	289	<u>1.29</u>
Average =		3.31 ± 1.02
H125	296	7.37
H125A	296	<u>6.97</u>
Average =		7.17 ± 0.2
H118	299	14.6
H118A	300	<u>16.2</u>
Average =		15.4 ± 0.8
H124A	307	23.6
H124B	306	<u>18.5</u>
Average =		21.1 ± 2.55
H123	312	12.1
H123A	312	<u>17.2</u>
Average =		14.7 ± 2.55
^a H214	299	20.6
^a H214A	299	<u>20.0</u>
Average =		20.3 ± 0.3

^a Measured in air

The reaction of hydrazine with ozone in air proceeded 1.25-times faster than in nitrogen. The oxygen content of the nitrogen flow gas is estimated at 6500 ppm (v/v), or about 65-times the ozone concentration (1.5 percent ozone in oxygen), while the oxygen content in air is 210,000 ppm (v/v). Because the introduction array was plugged by the reaction of hydrazine with CO_2 in air, this minor rate effect was not considered sufficient cause for further investigation of air as a laminar flow gas.

(1) Temperature Effect. The reaction of hydrazine and ozone was studied at temperatures from 289 K to 312 K. The temperature of the laminar flow gas was measured by a low mass thermocouple placed at the exit of the

reaction cell. To maintain a similar range of absorbance changes, both the ozone concentration and laminar flow rates were varied. Figure 23 shows rate plots at various temperatures with the ozone concentration normalized.

An Arrhenius plot of the rate constants is shown in Figure 24. The activation energy (E_a) was found to be 47 ± 13 kJ/mol, and the $\log(10)$ -A-value was found to be 16 ± 2 cm³mol⁻¹s⁻¹.

(2) Alternate Kinetic Procedure. The rate constant for the hydrazine/ozone reaction was also determined by using the alternate kinetic procedure in which the z-position was constant and the ozone concentration was varied. The $\log(\text{hydrazine concentration})/\text{ozone concentration}$ plot is shown in Figure 25. Two runs were analyzed by Equation (56) and gave a rate constant for the hydrazine/ozone reaction of $9.4 \pm 0.2 \times 10^{-17}$ cm³molecule⁻¹s⁻¹ at 299 K. This procedure assumes that the reaction is first-order in ozone, and the linearity of Figure 25 confirms the order in ozone.

b. MMH

The kinetics of the MMH/ozone reaction shows even more clearly the accelerating rate phenomenon exhibited by hydrazine. The MMH reaction appears to be proceeding in at least two clearly defined stages: a slow initial decay, followed by a more rapid reaction as the MMH loss rate accelerates (Figure 26).

The MMH ozonization rate was studied over the range of ozone concentrations of 5 to 220 ppm. With initial MMH concentrations of approximately 50 ppm, the resulting initial ozone/hydrazine ratio varied from 0.1 to 4.4. During the initial nonaccelerating stage, the average stoichiometry was one MMH per ozone, but as the reaction accelerated, the stoichiometry increased to approximately seven MMH per ozone.

The accelerating rate characteristics in the reaction of MMH with ozone required a kinetic analysis for which an explicit solution was not

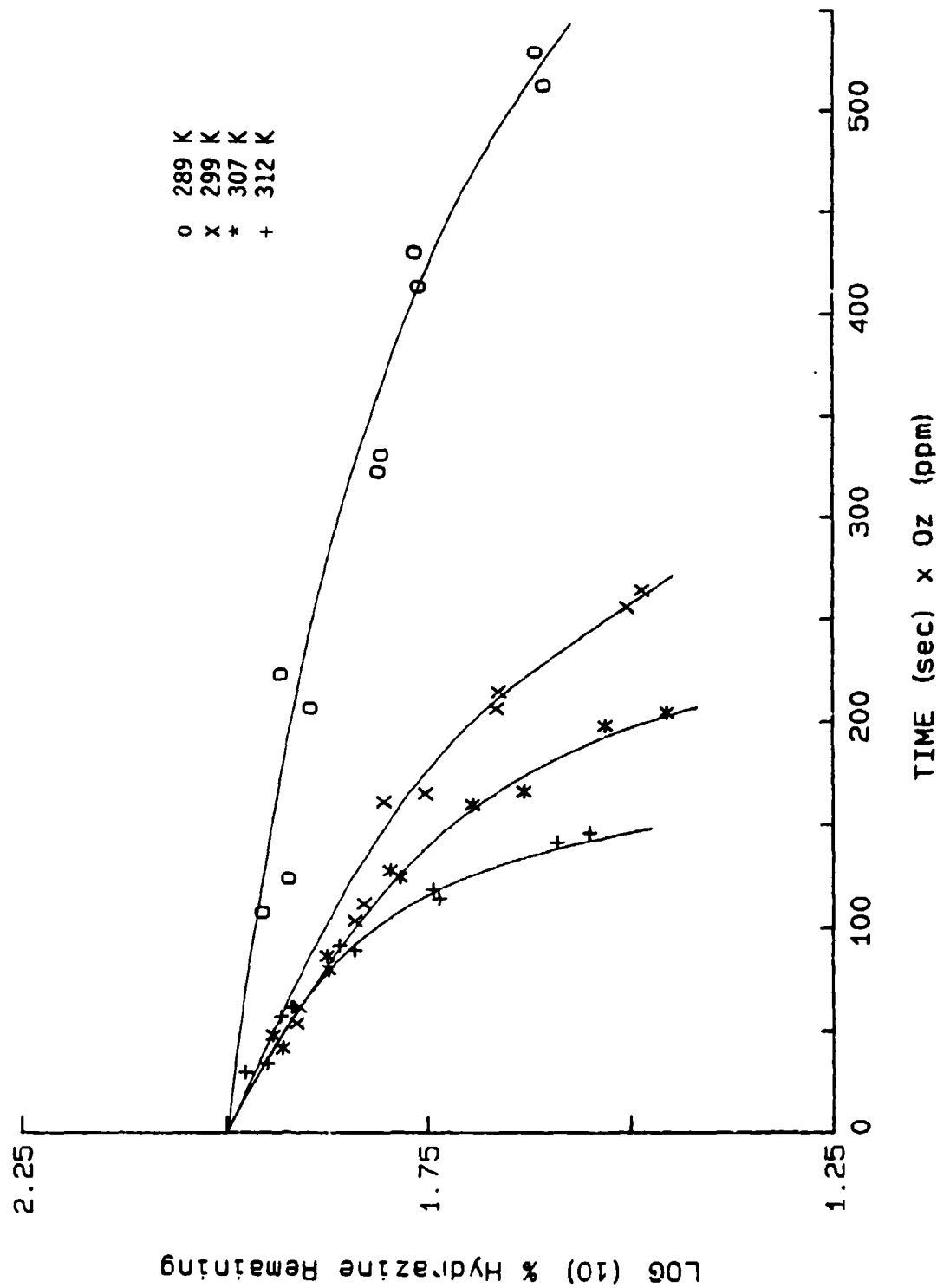


Figure 23. Effect of Temperature on the Hydrazine Loss Rate in Ozone

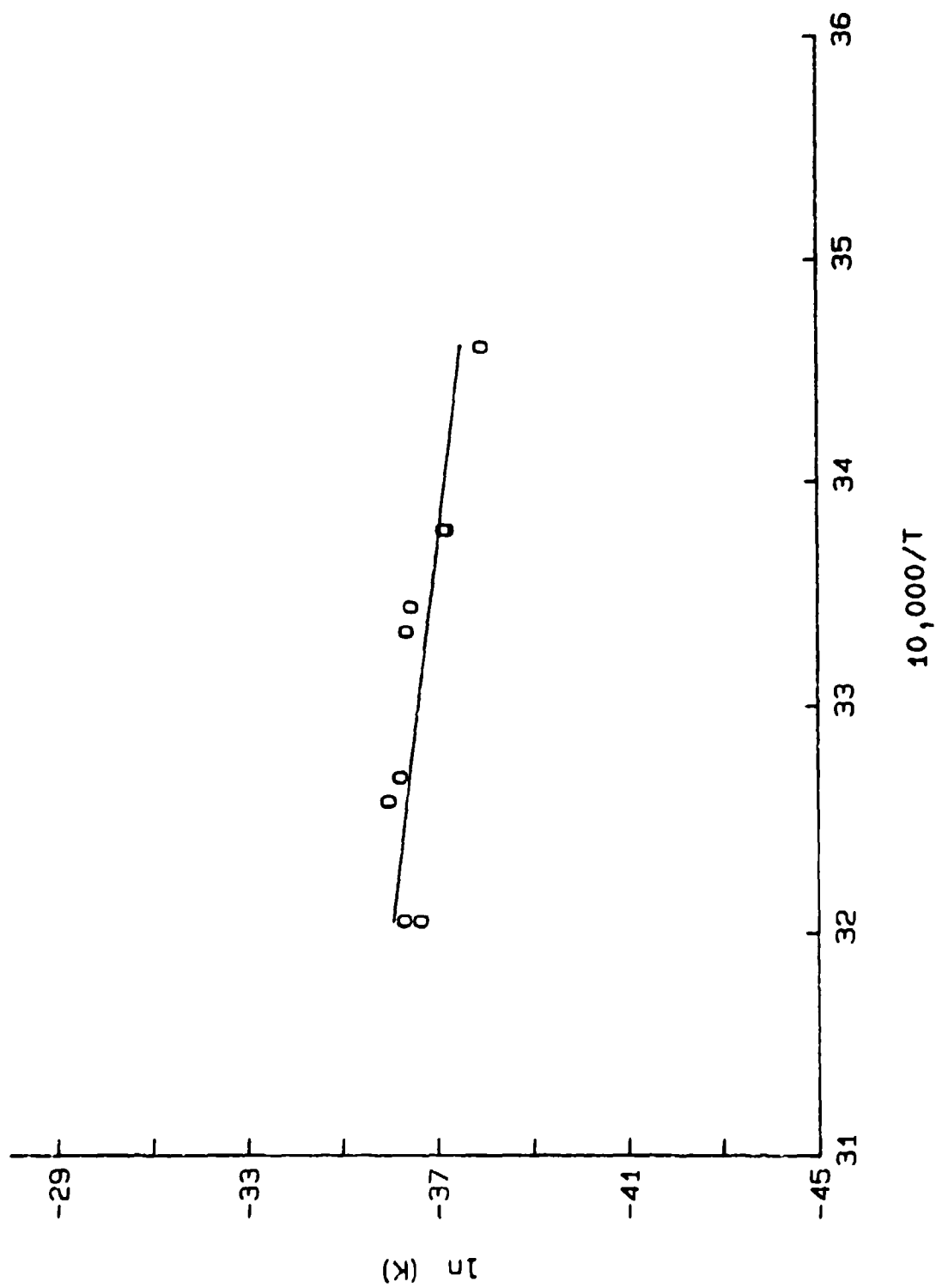


Figure 24. Arrhenius Plot for the Reaction of Hydrazine and Ozone

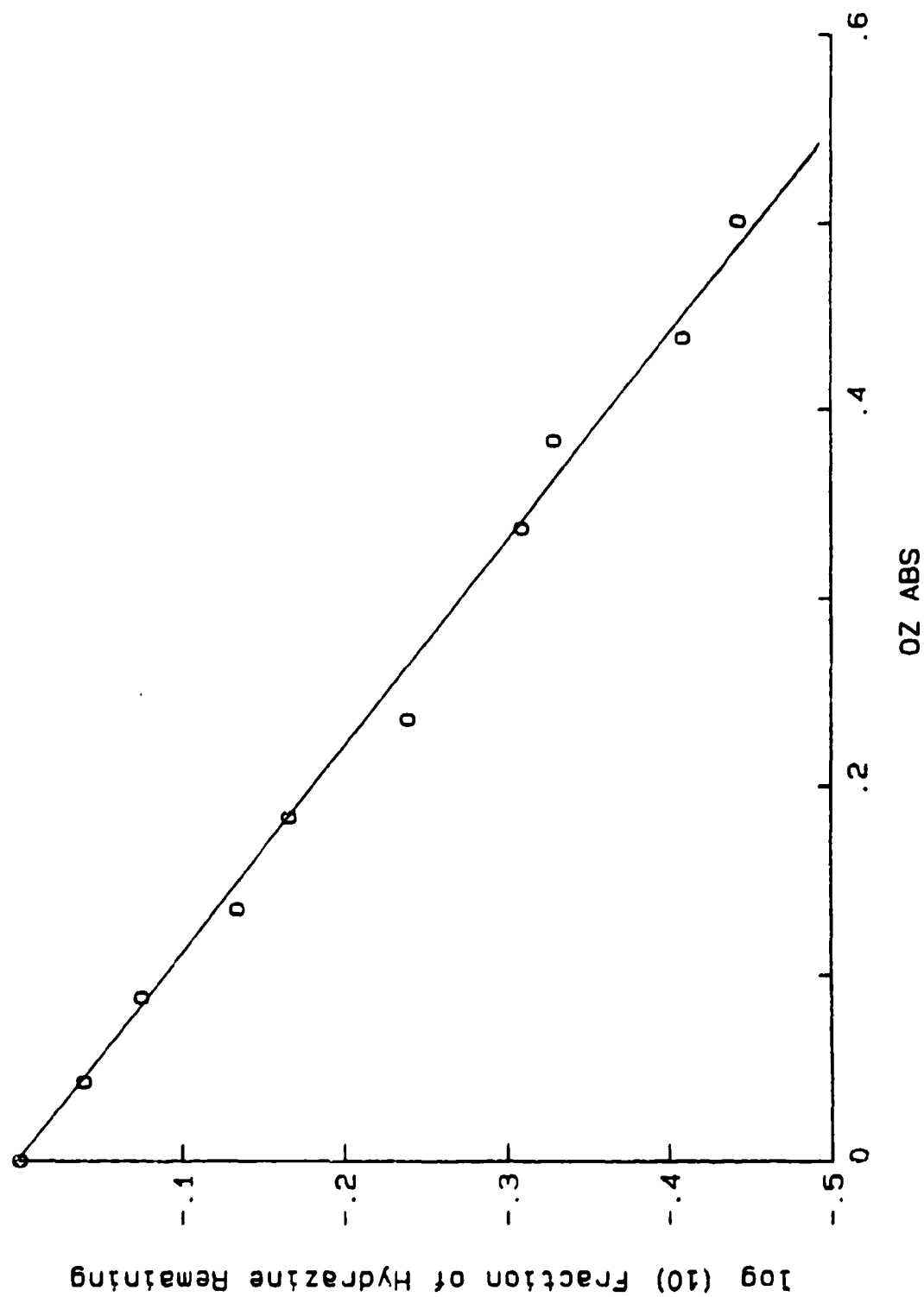


Figure 25. Hydrazine Loss Rate in Ozone Using the Alternate Kinetic Procedure

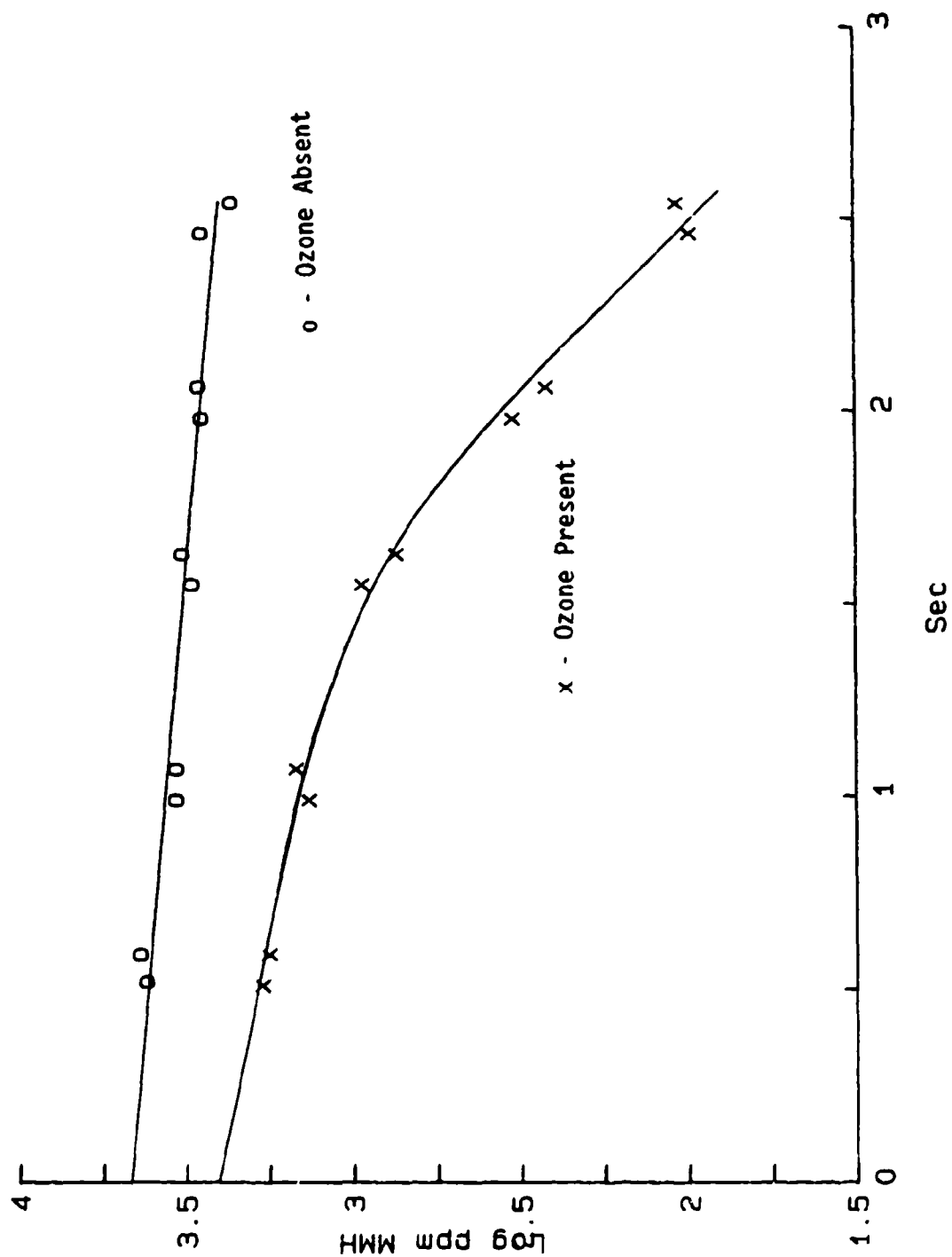


Figure 26. MMH Loss Rate in the Presence and Absence of Ozone

available. The oxidation of MMH with ozone and oxygen is similar to many slow combustion reactions that involve delayed-branching kinetics (References 60 and 61). An analogous analysis technique was developed that provided the rate parameters I and B, from which rate constants assigned to the MMH/ozone reaction (k_i) and methyldiazene/ozone reaction (k_b) could be extracted. The conceptual and mathematical aspects are developed in the following Discussion section. Table 26 shows the results of this analysis.

(1) Temperature Effect. The MMH ozonization reaction was studied over the temperature range 285 K to 313 K. Figure 27 displays the effect of temperature on the overall rates. For clarity, the ozone concentrations are normalized.

Arrhenius plots of the rate constants are shown in Figure 28. The activation energy for the initiation rate constant (k_i) was found to be

TABLE 26. MMH LOSS-RATE CONSTANTS WITH OZONE IN NITROGEN

File (#)	Temp (K)	$k_i \times 10^{17}$ ($\text{cm}^3 \text{molecule}^{-1} \text{s}^{-1}$)	$k_b \times 10^{16}$ ($\text{cm}^3 \text{molecule}^{-1} \text{s}^{-1}$)
M16A	285	4.35	0.74
M16B	285	<u>1.42</u>	<u>3.0</u>
		Average = 2.89 ± 1.47	1.87 ± 1.13
M110A	292	0.87	3.98
M110B	292	<u>1.08</u>	<u>3.58</u>
		Average = 0.98 ± 0.11	3.78 ± 0.2
M14A	299	9.05	2.36
M15A	299	<u>8.35</u>	<u>2.55</u>
		Average = 8.70 ± 0.35	2.46 ± 0.1
M117	313	8.03	16.7
M117A	313	<u>7.68</u>	<u>16.7</u>
		Average = 7.86 ± 0.18	16.7 ± 0.0

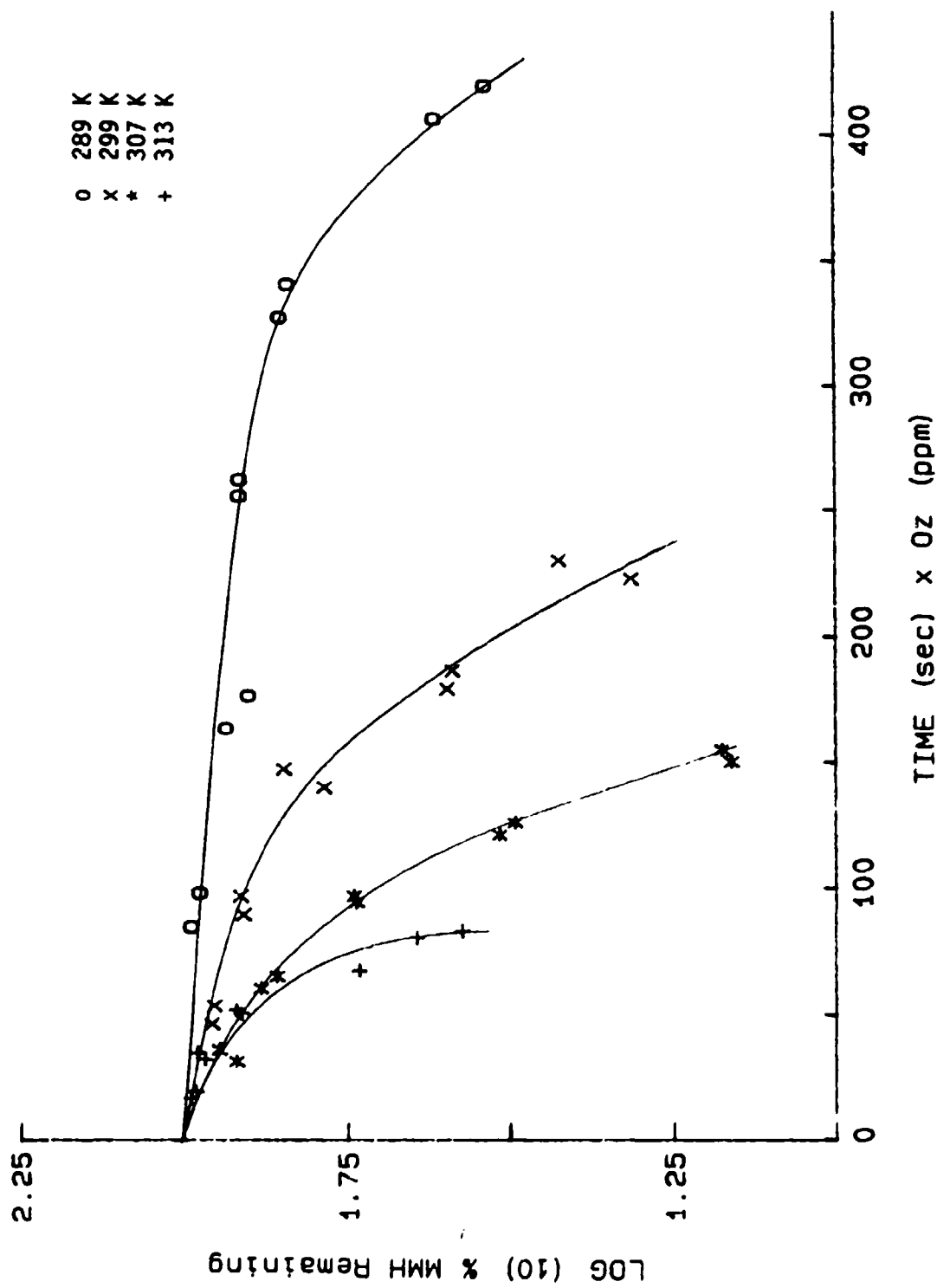


Figure 27. Effect of Temperature on the MMH Loss Rate Profile in Ozone

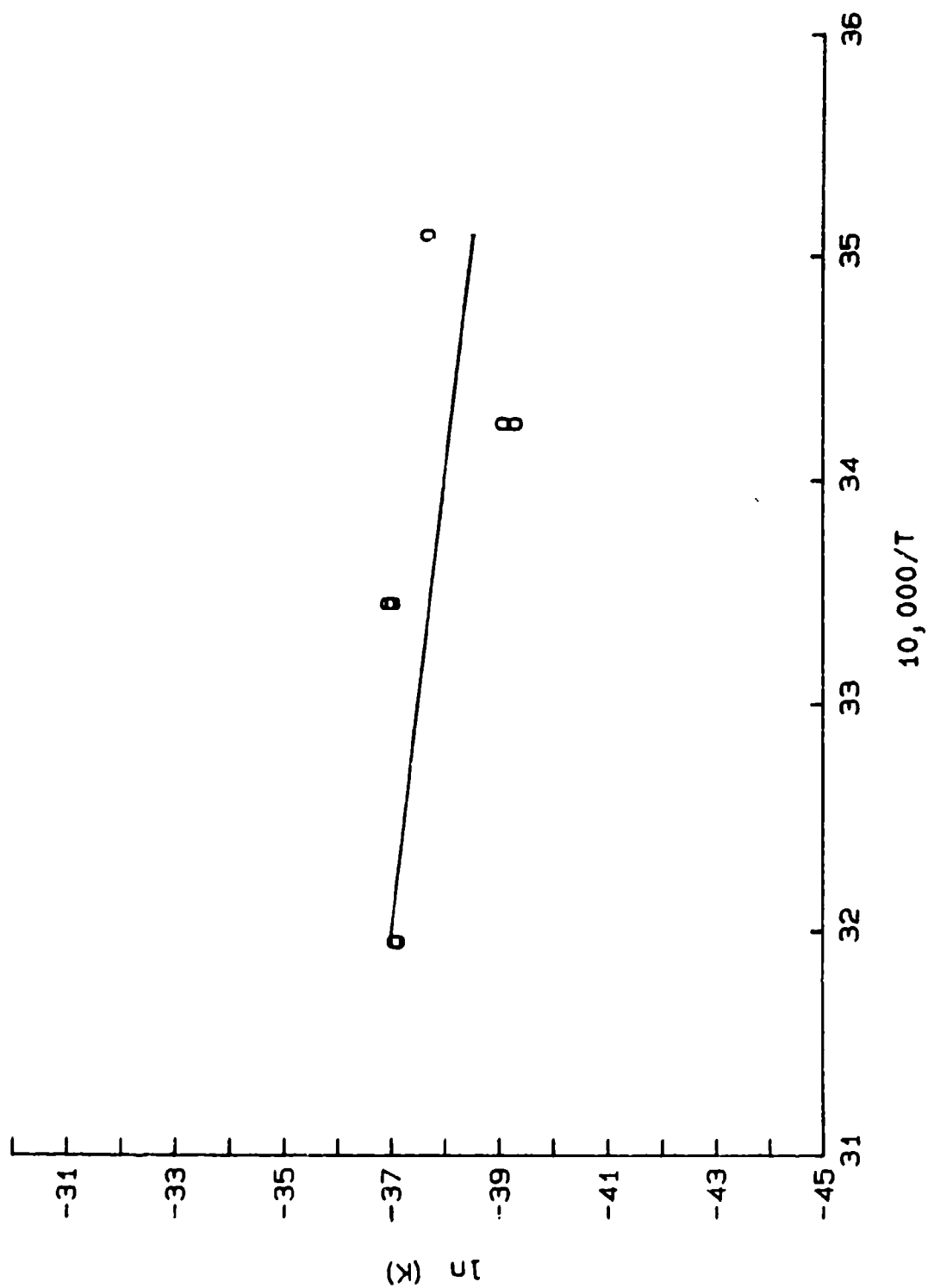


Figure 28. Arrhenius Plot for the Initiation Reaction of NH_3 and Ozone

40.9 ± 24 kJ/mol with a $\log(10)$ pre-exponential value of 14.5 ± 4 $\text{cm}^3\text{molecule}^{-1}\text{s}^{-1}$. For the branching rate constant (k_b), the corresponding values are 48.2 ± 14.4 kJ/mol and 16.9 ± 2.5 $\text{cm}^3\text{molecule}^{-1}\text{s}^{-1}$ (Figure 29).

(2) Alternate Kinetic Procedure. The fixed-position variable-ozone kinetic procedure shows the same MMH loss rate features (Figure 30). The obvious non-first-order behavior of the reaction precludes the use of Equation (56) for a detailed kinetic analysis; however, the similar profiles obtained by the two kinetic procedures are notable. The fixed-position variable-ozone procedure does provide some added detail at very short reaction times that cannot be accessed by the variable-position procedure. The intercept value of MMH concentration determined by extrapolation of the rate profile to zero time in a variable-position fixed-ozone experiment was appreciably smaller than that estimated by extrapolation of a diffusion-only line. The same phenomenon can be seen in Figure 30 where an apparent sharp drop in MMH concentration occurs at the lowest ozone concentrations. In the analysis of a zero-order or first-order reaction (hydrazine/ozone), the time that is taken as $t = 0$ is irrelevant. For any other order rate law, zero time must coincide with the actual start of the reaction. The apparent initial rapid drop in reactant concentration is most probably due to a late assignment of zero reaction time due to a underestimate of the z -position. The true origin must be somewhat upstream ($z < 0$) of the geometrical position of the introduction array ($z = 0$, $t = 0$). The concept of a "virtual" origin in flow reactors has been noted and discussed by other workers (References 54 and 62).

c. TME

To validate the laminar flow reactor as a kinetic tool, ozonolysis of the alkene 2,3-dimethyl-2-butene (TME) was studied. The rate law (first-order in TME and ozone), rate constant, and products for the reaction of TME with ozone have been independently determined (Reference 63).

The diffusion-only loss rate of TME was found to be below the FTIR/LFR detection limits. With the introduction of ozone into the reaction

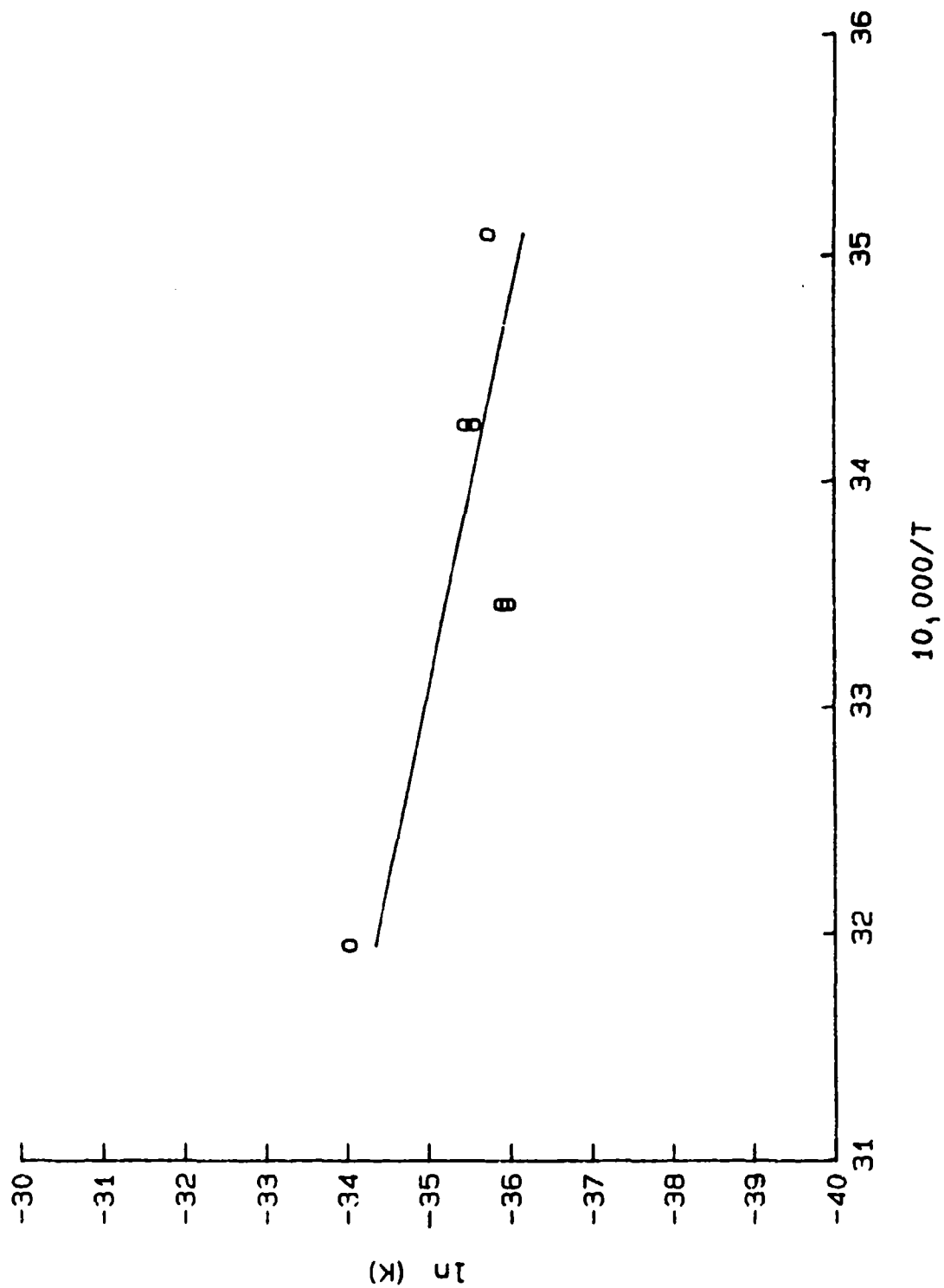


Figure 29. Arrhenius Plot for the Branching Reaction of H_2 and Ozone

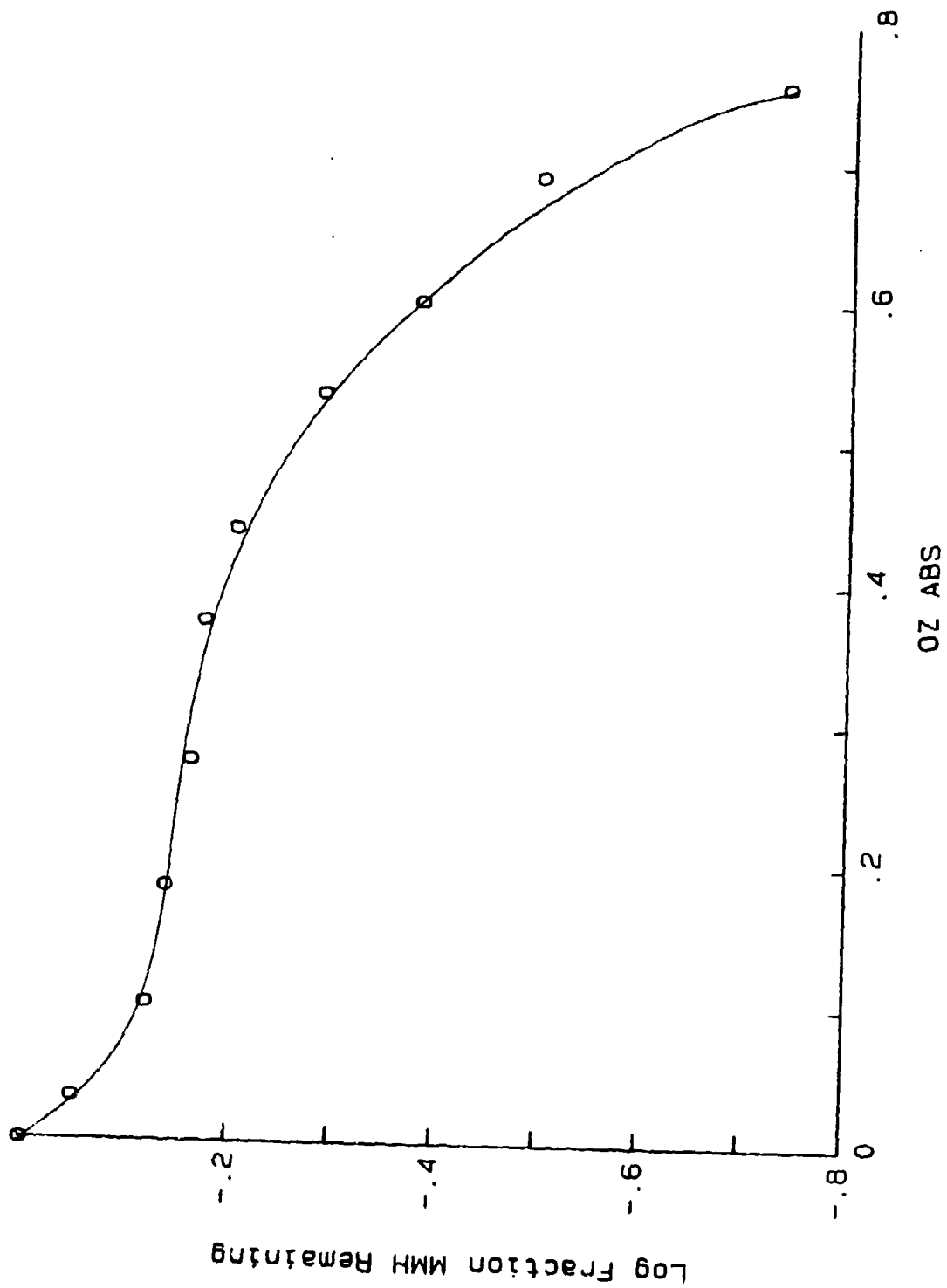


Figure 30. MMH Rate Loss Profile in Ozone
Using the Alternate Kinetic
Procedure

cell containing TME, a new IR absorption at 1745 cm^{-1} corresponding to the carbonyl stretching frequency of acetone was detected. At longer reaction times (variable-position method), the absorbance due to acetone reached a constant value (100 percent reaction). The amount of acetone formed was independent of ozone concentration as long as the ozone was present in excess. The pseudo-first-order rate constant for the appearance of acetone was calculated from the slope of the least squares line obtained by plotting the $\log(\text{fraction reaction})$ versus time. Division of the observed pseudo-first-order rate constant by the ozone concentration gives the second-order rate constant for acetone appearance. The LFR experimental value for the rate constant of the reaction of TME with ozone was found to be $1.06 \pm 0.05 \times 10^{-15}\text{ cm}^3\text{molecule}^{-1}\text{s}^{-1}$ at 297 K, while Huie and Herron report $1.05 \times 10^{-15}\text{ cm}^3\text{molecule}^{-1}\text{s}^{-1}$ at 298 K (Reference 63).

3. Products of the Ozonization Reaction

a. Hydrazine

The products of the ozonization of hydrazine were characterized their FTIR spectra at 1 cm^{-1} resolution. The spectra of the products were obtained by subtracting the spectra of hydrazine and ozone from that of a reaction mixture. The products observed in the difference spectrum were hydrogen peroxide, water, and diazene (Figures 31 and 32). Diazene (N_2H_2) was identified by IR absorptions at 1276, 1295, and 1314 cm^{-1} . The products were the same in a laminar flow of air or nitrogen (Reference 6).

b. MMH

The products of the reaction of MMH and ozone were characterized by FTIR difference spectra at 1 cm^{-1} resolution. The products observed included formaldehyde, methyldiazene, diazomethane, methanol, hydrogen peroxide, water, and possibly CO_2 (Figure 33 and 34). Methyl hydroperoxide was not observed as reported by Tuazon et al. (Reference 6). The concentration of methyldiazene, as measured by its absorbance at 845 cm^{-1} , was highest at early stages of the reaction and decreased at longer reaction times.

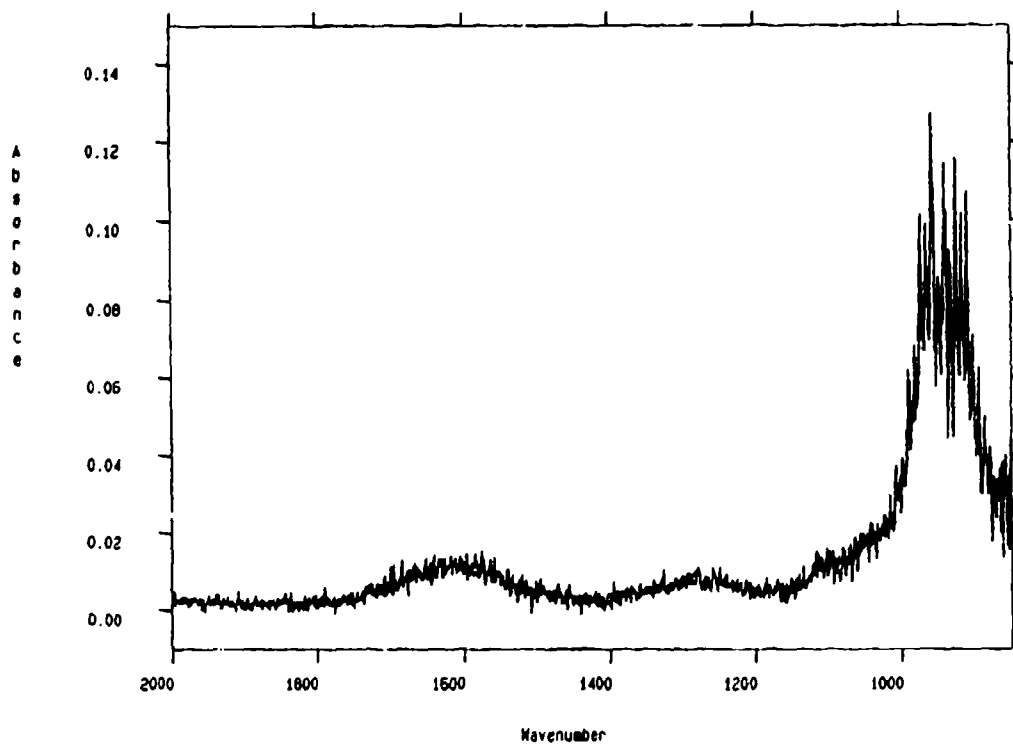
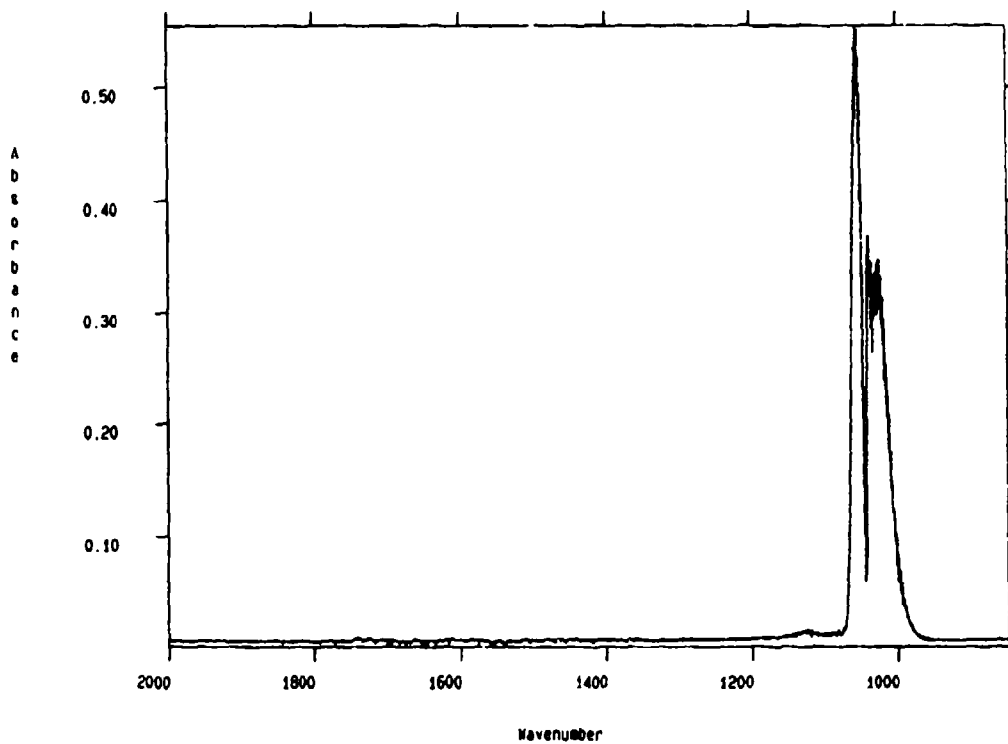


Figure 31. Gas-Phase IR Spectra of (a) Ozone and (b) Hydrazine Showing Comparative Band Positions

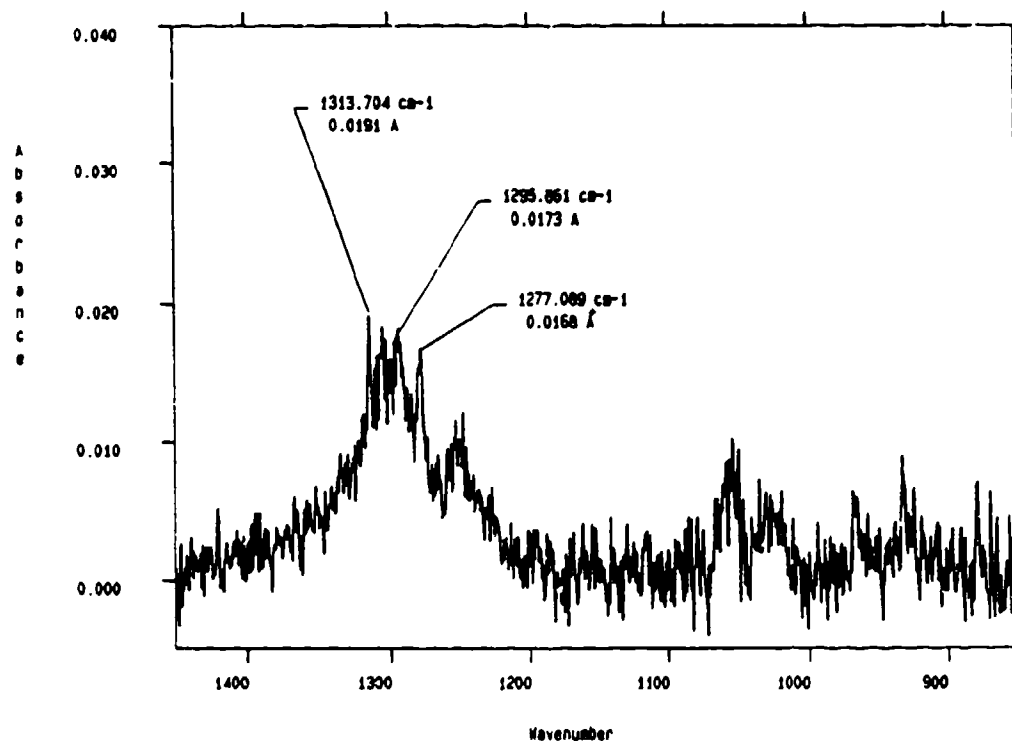
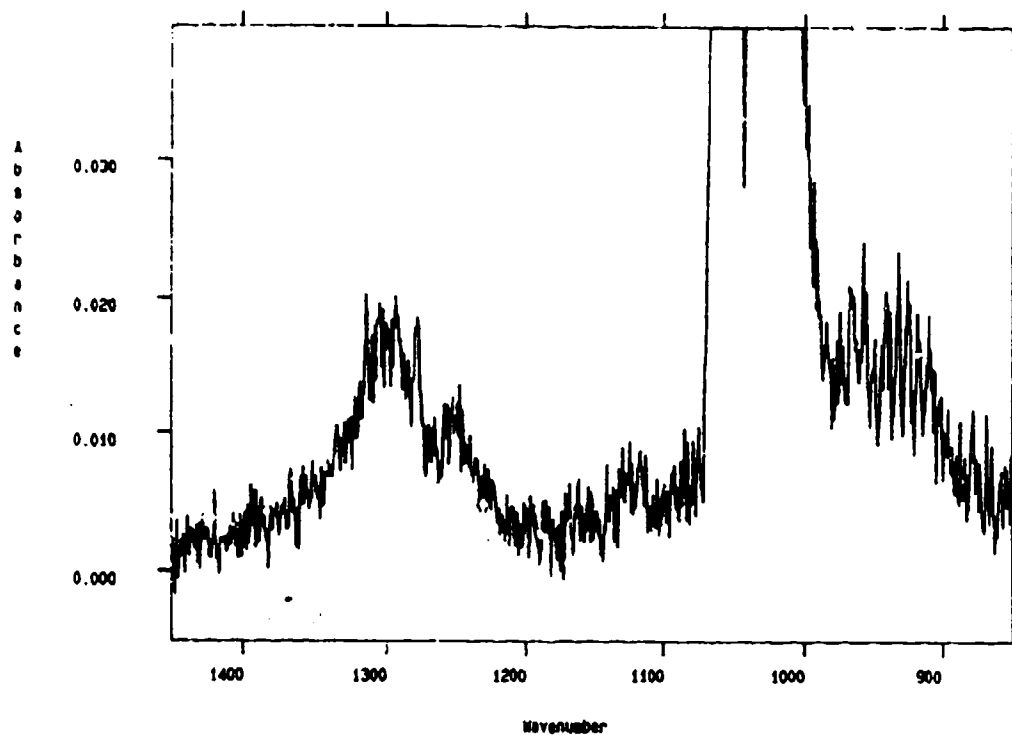


Figure 32. Gas-Phase IR Spectra of Hydrazine/
Ozone:(a) Reaction Mixture;
(b) Products, Including Hydrogen
Peroxide and Diazene

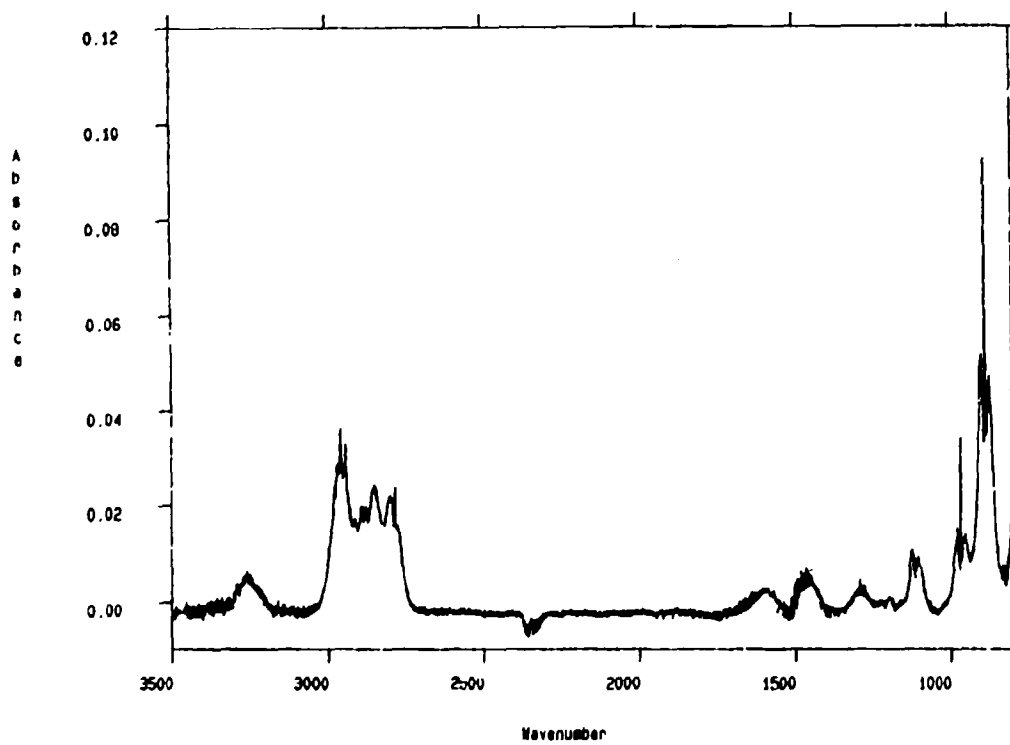
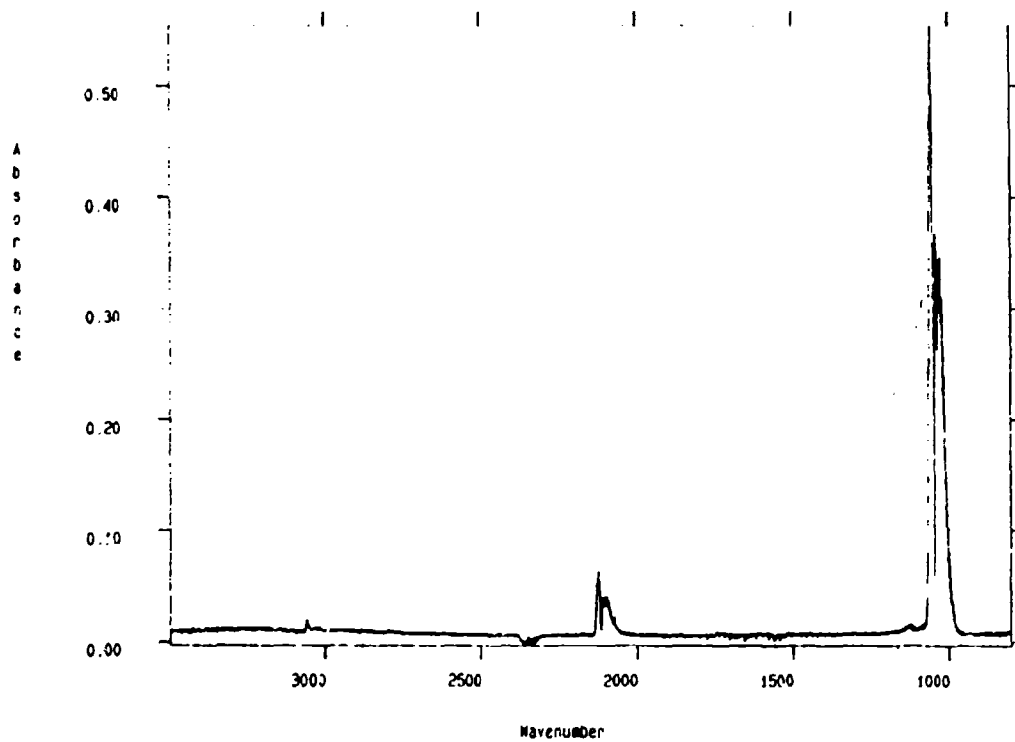


Figure 33. Gas-Phase IR Spectra of
(a) Ozone and (b) MMH Showing
Comparative Band Positions

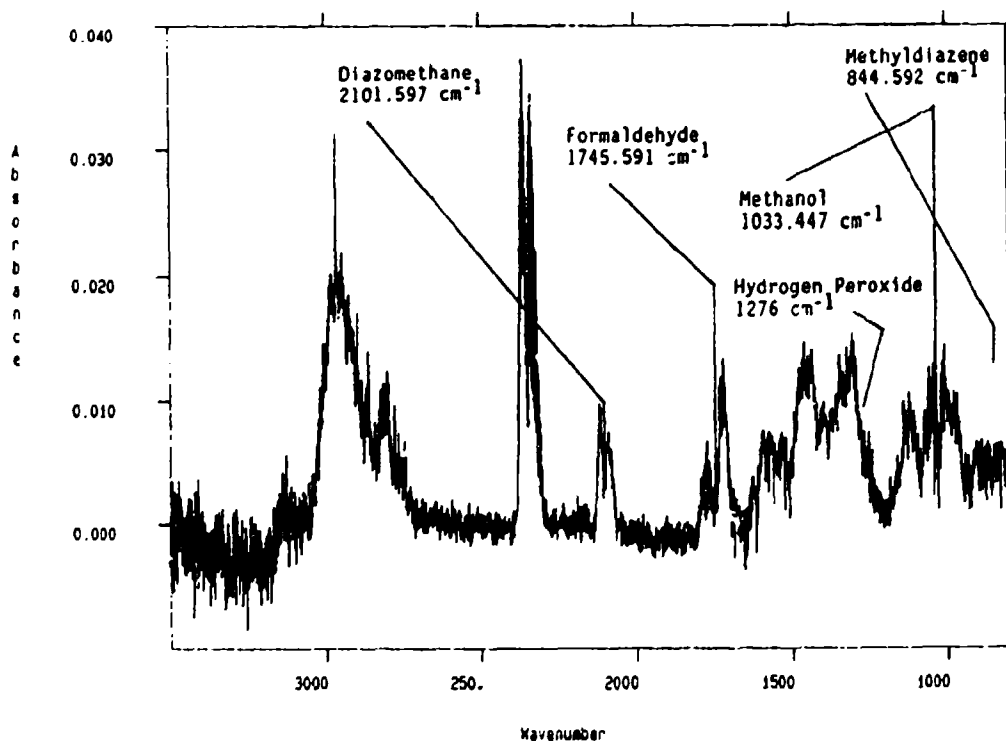
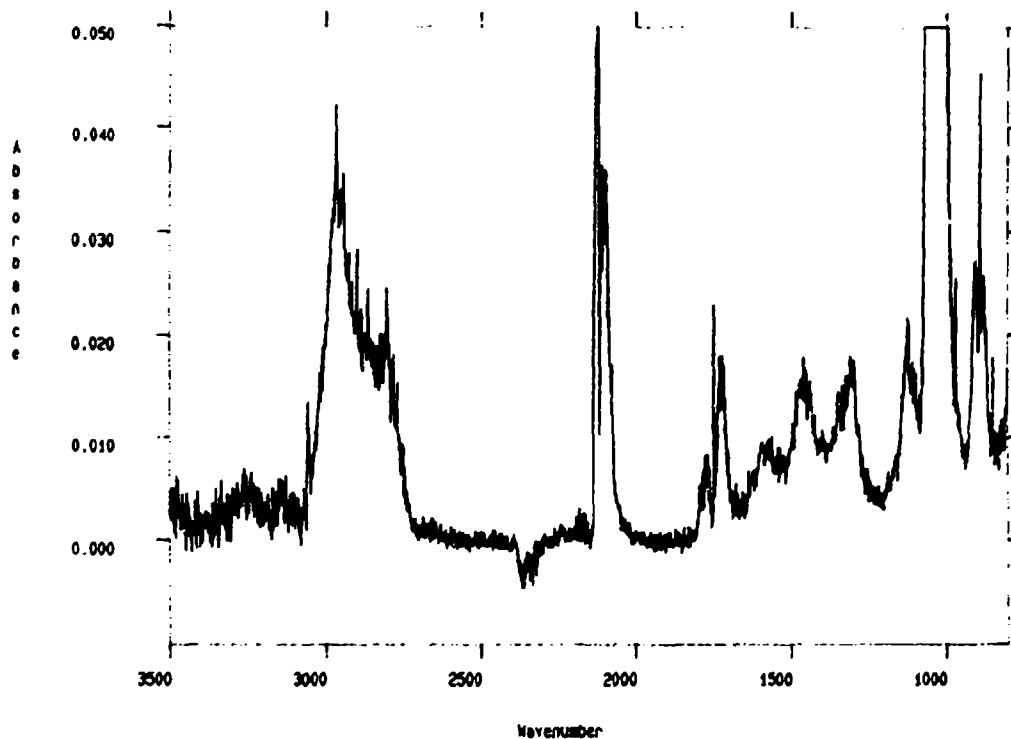


Figure 34. Gas-Phase IR Spectra of MMH/Ozone:
 (a) Reaction Mixture; (b) Products,
 Including Methyl diazene, Methanol,
 Hydrogen Peroxide, Formaldehyde, and
 Diazomethane

c. TME

The major product of the reaction of TME with ozone in nitrogen or air was identified as acetone by its FTIR spectrum, (Figures 35 and 36).

D. DISCUSSION

1. The Laminar Flow Reactor

The goal of the laminar flow reactor (LFR) experiments was to develop a technique for the study of gas-phase reactions at ambient temperatures and pressures with a minimum of wall effects. A key feature of the LFR concept is an introduction array that allows mixing of a reactant vapor with a uniform field reactant within a limited reaction zone. The laminar flow of inert matrix gas and uniform field reactant then confines the reaction zone away from the container walls, while the progress of the reaction is monitored by a noninvasive analytical technique.

The verification of laminar flow was easily accomplished by fluid dynamics measurements. Details of the reaction zone plume were inferred from permeation loss rates from the microporous tubing, and from observation of the reaction zone with an inert gas such as methane, or with the hydrazines in the absence of a second reactant.

a. Reactant Profile

The loss rate from the introduction array tubing was determined as a function of the length of the introduction array tubing. The loss rate was found to exponentially decay as the introduced gas passed down the length of tubing (Table 20). With two countercurrent strands, the reactant profile in the yz-plane is given by:

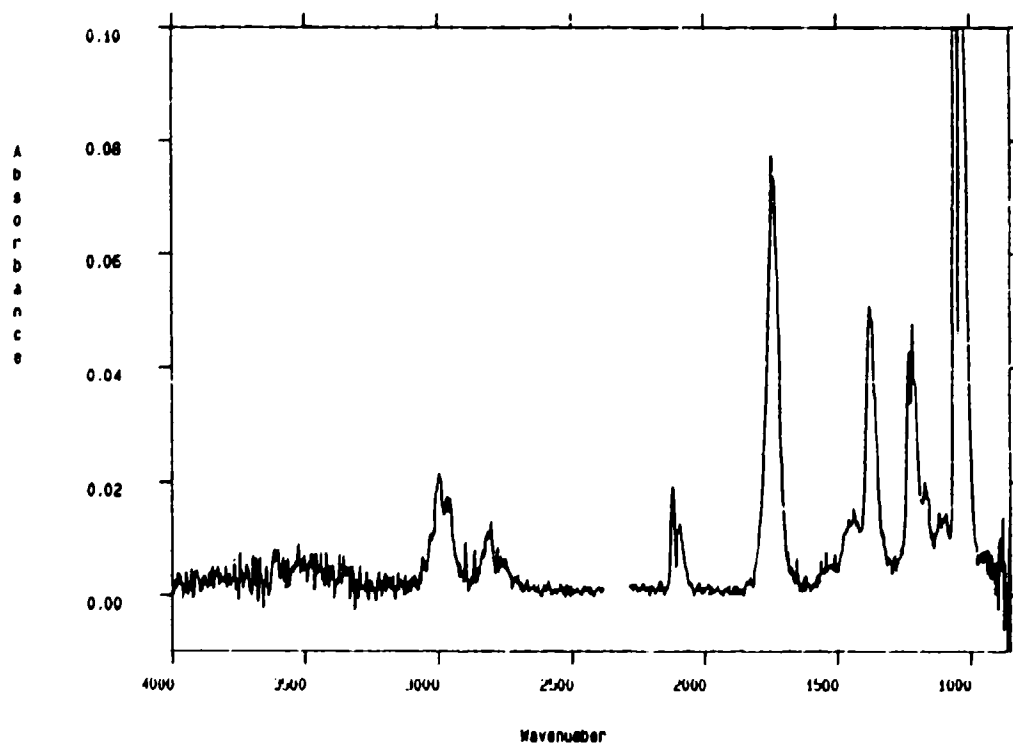
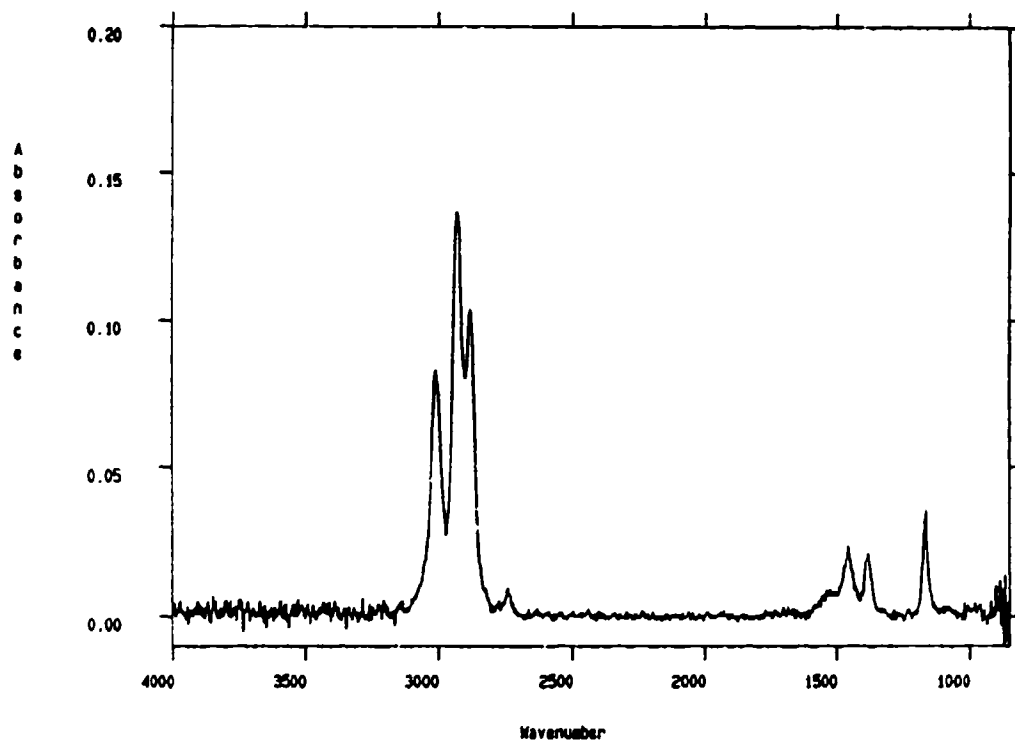


Figure 35. Gas-Phase IR Spectra of (a) TME and (b) TME/Ozone Reaction Mixture

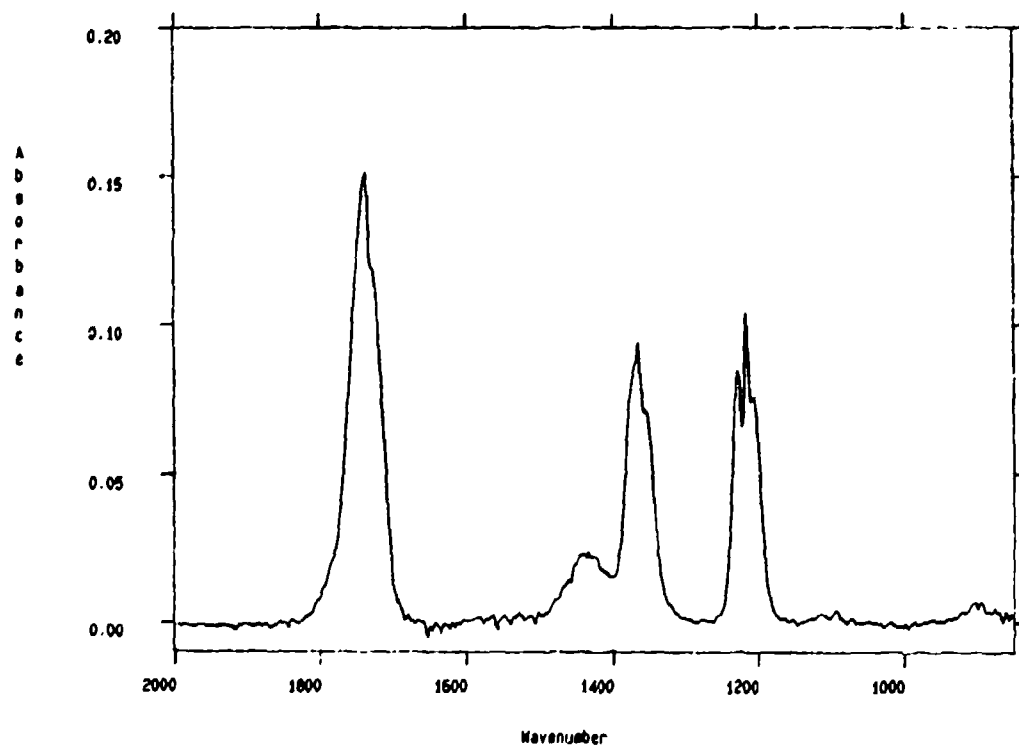
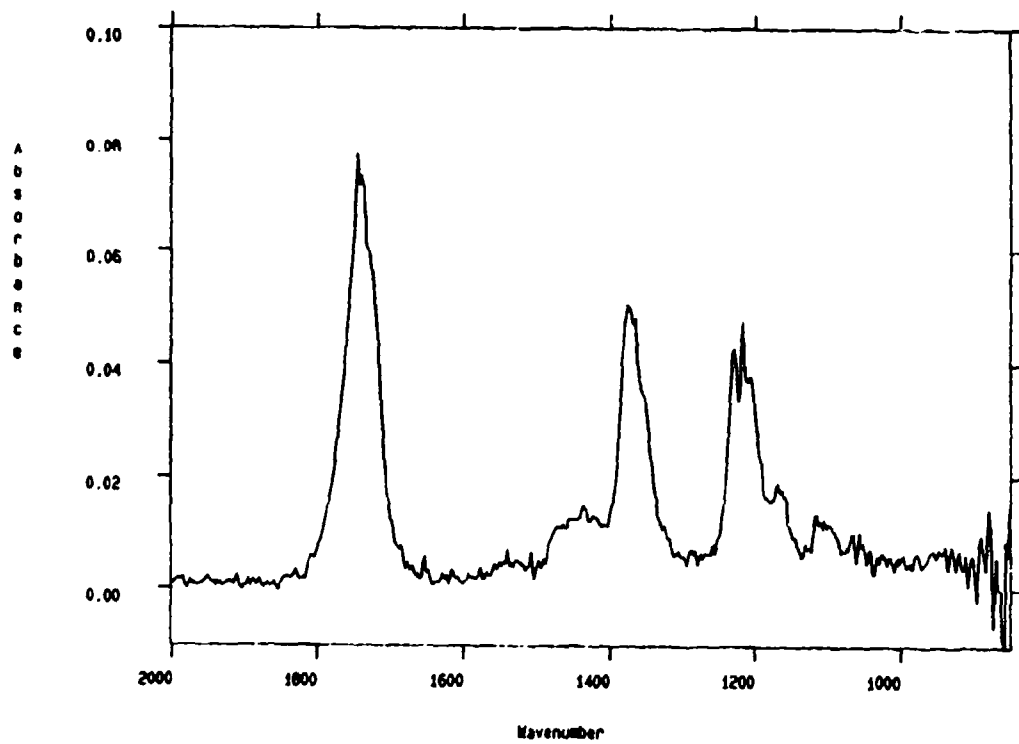


Figure 36. Gas-Phase IR Spectra of (a) TME/Ozone Reaction Product, and (b) Acetone Reference Spectrum

$$C(y) = \frac{1}{2} [1 - \exp(-Gy)] + (1 - \exp[-G(H-y)]) \quad (61)$$

where

C = concentration at y in the yz-plane
 G = loss constant from Table 20
 H = length of microporous tubing strand

The initial reactant profile under typical LFR conditions of vaporizing gas pressure of 250 kPa and two lengths of tubing each 30-cm long is shown in Figure 37. The profile is expected to flatten as it progresses down the reaction cell as a result of diffusion away from the higher concentration zones at the ends of the array. Equation (61) shows that the use of more than two strands in the array would not smooth the profile any further. It is conjectured that initially the plume is radially symmetrical with an overall radius determined by the input flow rate. The input flow rates of vaporizing gas for hydrazine were 200 - 250 mL/min, while those of MMH were 75 - 100 mL/min, suggesting a larger initial reaction zone for hydrazine. As a result of a larger initial reaction zone, concentration gradients would be smaller, and gradient-driven diffusion effects, such as reaction zone expansion, should also be smaller for hydrazine.

The observed values of k_{bkg} for hydrazine are 40 percent of those for MMH, in agreement with the input flow rate ratio and not in agreement with the relative diffusion coefficients (Table 24).

b. Wall Effects

The initially formed reaction zone is smaller than the internal dimensions of the LFR (Figure 18). If the progress of the reaction is followed only up to a time that reasonably precludes expansion of the confined zone to the walls of the LFR, then it is reasonable to assume that wall effects are negligible. Determination of the variables that affect wall contact times was made using methane. For an initially small reaction zone, it was possible to measure the expansion of the reaction zone up to the size of the spectrometer

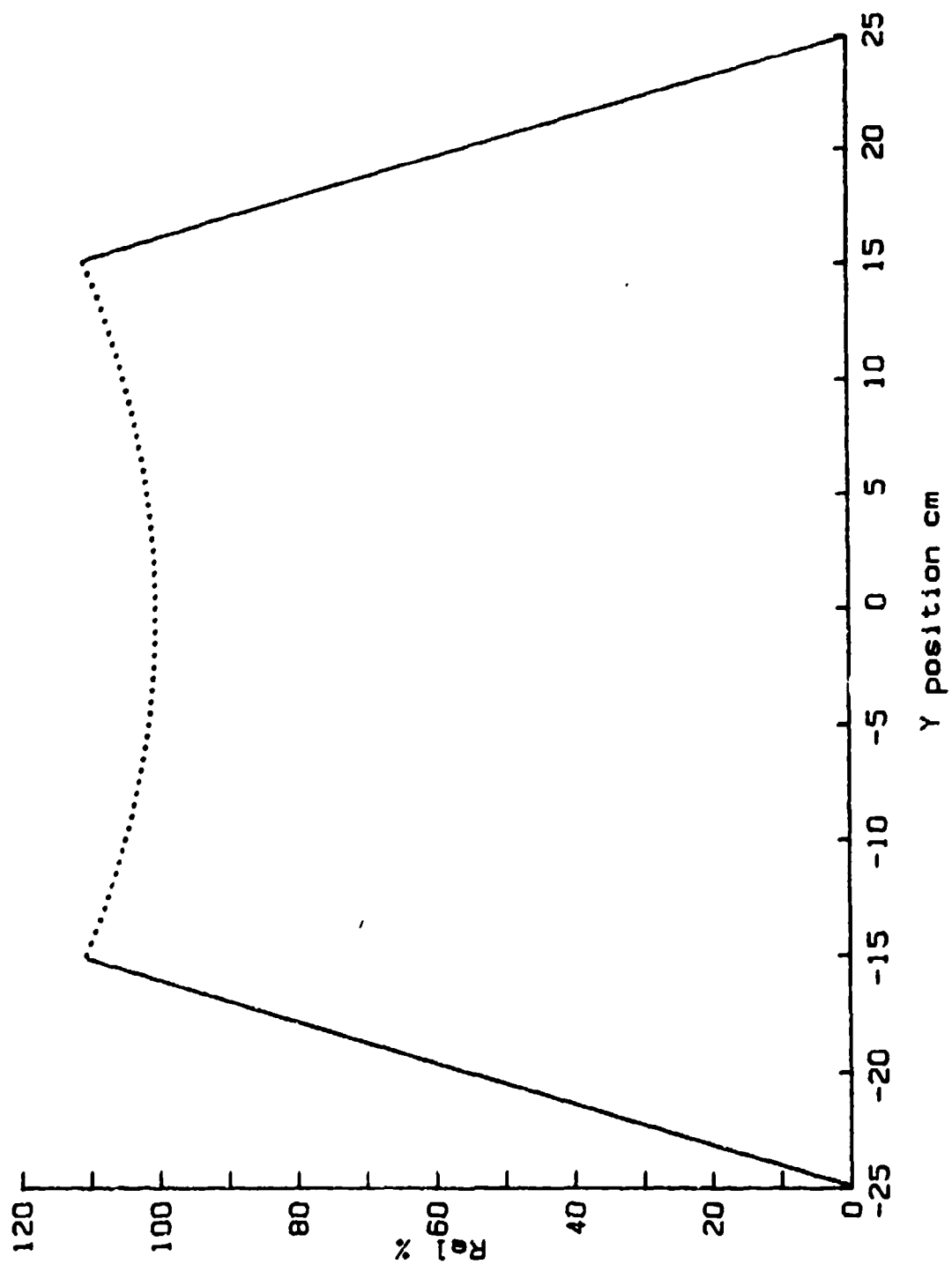


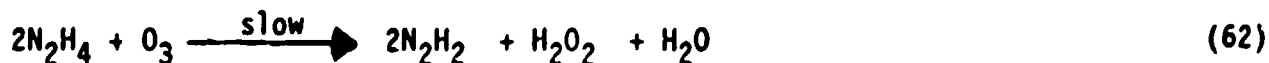
Figure 37. Initial Reactant Profile Under Typical LFR Conditions

cell and beyond that to the dimensions of the reactor cell itself. By operating at conditions that created a larger initial reaction zone, the expansion to spectrometer cell size was bypassed. Because the reaction was monitored at times shorter than the wall contact time, it was assumed that wall effects were minimal.

2. Kinetics and Mechanism of the Ozonization Reaction

a. Hydrazine/Ozone Reaction

During the first half of the reaction, the rate law for the reaction of hydrazine with ozone was determined to be first-order in both hydrazine and ozone. The stoichiometry of the reaction in the initial stages was found to be 1:1. The concurrence of the rate law and stoichiometry suggests the following reaction:



The overall reaction is more complicated, however, as indicated by the behavior at longer reaction times: the rate accelerates, and more than one hydrazine is consumed per ozone reacted. These observations suggest that a chain reaction mechanism may be operative, which becomes apparent at longer reaction times. Scheme 4 shows a detailed set of chain reactions consistent with the products and initial-rate observations. In Scheme 4, the reaction between hydrazine and ozone comprises the initiation reaction. At the beginning of the reaction, the kinetic chain length is short; as the concentrations of reactive intermediates build, however, branching reactions provide exponentially increasing concentrations of the chain carrying radicals, HO and HO₂. The propagation steps consume hydrazine and diazene, but not chain carriers. Thus, as the reaction proceeds, the ratio of hydrazine/ozone consumed increases.

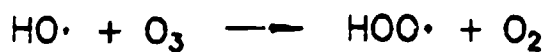
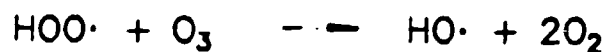
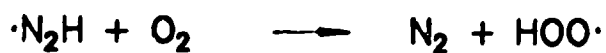
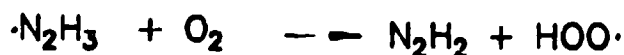
The rate constant for the hydrazine/ozone reaction determined by the variable position procedure was found to be $1.75 \times 10^{-16} \text{ cm}^3 \text{ molecule}^{-1} \text{ s}^{-1}$

Scheme 4

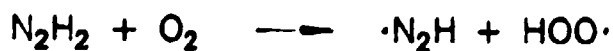
Initiation



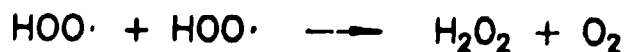
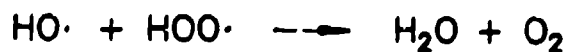
Propagation



Branching Chain



Termination



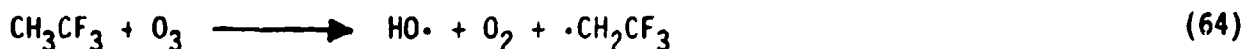
(299.5 K), in excellent agreement with the value reported by Pitts and Tuazon of $1 \times 10^{-16} \text{ cm}^3 \text{ molecule}^{-1} \text{ s}^{-1}$ (298 K) (Reference 64). The fixed position procedure gave a slightly lower value of $9.4 \times 10^{-17} \text{ cm}^3 \text{ molecule}^{-1} \text{ s}^{-1}$ (298 K), but was still in good general agreement.

The Arrhenius activation energy of 47 kJ/mole is consistent with the endothermicity of the initial H-abstraction step in Scheme 4. Depending on the assumed value for the N-H bond strength (355 - 368 kJ/mol), the initiation step is endothermic by 40 - 50 kJ/mol. The pre-exponential value [$\log(10) A = 16 \pm 2 \text{ cm}^3 \text{ mol}^{-1} \text{ s}^{-1}$], however, is fairly high, even considering the positive entropic effect of forming three molecules as products.

The HCl-catalyzed destruction of ozone has a log-A value of 14.4, similar to the values for hydrazine and MMH (Reference 65):



The reactions of ozone with other H-atom sources such as CH_3CF_3 show more normal log A-values in the range of 11 - 11.5 (Reference 66):

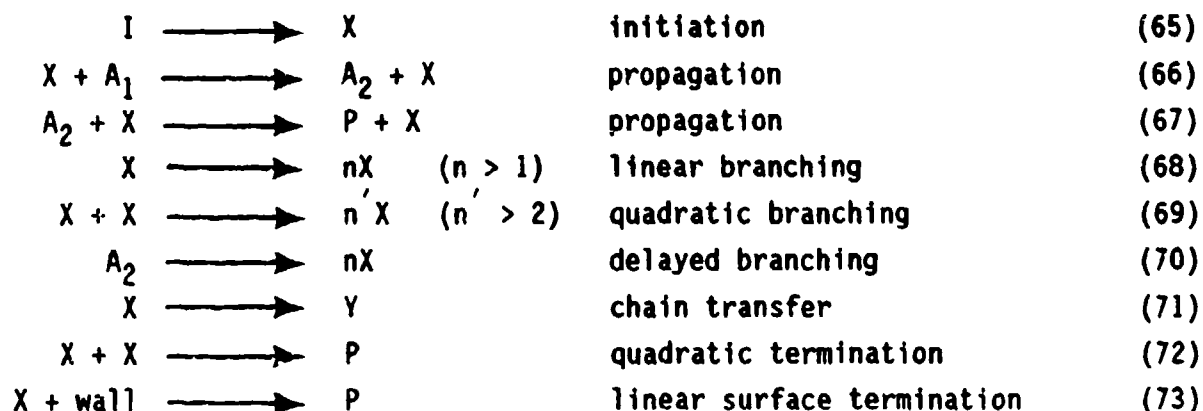


b. MMH/Ozone Reaction

The accelerating rate of the reaction of MMH or hydrazine with ozone suggests that the mechanism may involve an autocatalytic effect in which one of the products of the reaction catalyzes its own formation. This effect is more obvious in the reaction of MMH with ozone, and is discussed in detail here.

(1) Seymenov Theory of Delayed Branching Chain Reactions.

Free-radical chain reactions consist of sets of elementary reactions denoted as initiation, propagation, branching, chain transfer, and termination sequences (References 67 and 68). For the general case, the mechanism can be written as follows:



where

I = initiating agent
 X, Y = reactive radical centers
 A_1 = initial reactant
 A_2 = intermediate product
 P = final inert product

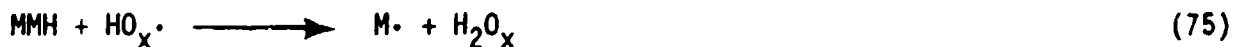
The initiation sequence provides a source of chain-carrying radicals (X), while the termination sequences destroy the chain carriers. The propagation sequence is responsible for product formation and does not change the concentration of chain carriers. Chain transfer reactions, such as Equation (71), also do not affect the overall concentration of reacting radicals or the overall rate of reaction if the new chain carrier Y is of the same reactivity as X . Branching is a reaction sequence, subsequent to initiation, that increases the chain-carrier concentration.

For the reaction of MMH with ozone, the corresponding reactions are as follows:

Initiation:



Propagation:





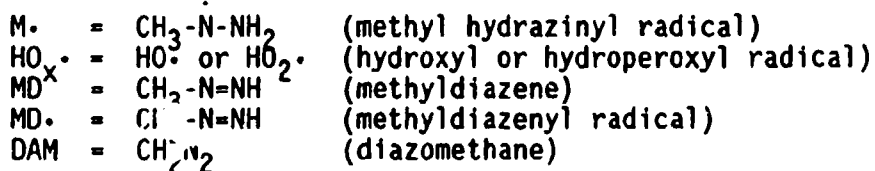
Delayed Branching:



Termination:



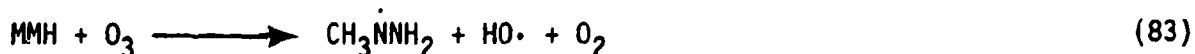
where



The increase in the concentration of chain carriers due to Equations (79) and (80) causes an increase in the rate of propagation and an auto-catalytic increase in the "active center" (methyldiazene) responsible for the branching. The end result is an overall rate acceleration. If the "active center" is not present at the start of the reaction, the process is called delayed branching (References 67 and 68). A detailed listing of possible reactions is given in Scheme 5.

(2) Approximate Solution for Delayed Branching Kinetics.

Explicit analytical solutions to the differential equations for the reactions containing quadratic terms are not available. Based on concepts developed by Bardwell and Hinshelwood (Reference 69) and Wu-Shu and Bardwell (Reference 70), the following approximate model can be developed. For the initiation reaction, Equation (83):

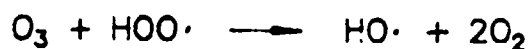
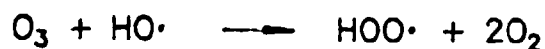
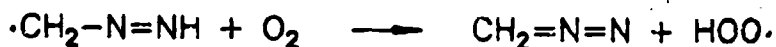
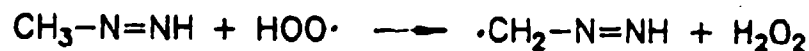
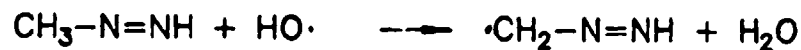
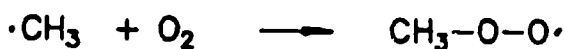
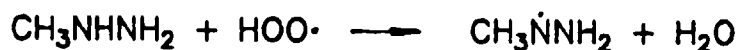
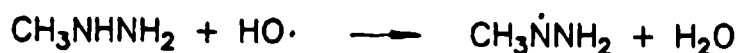


Scheme 5

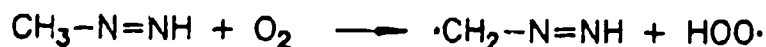
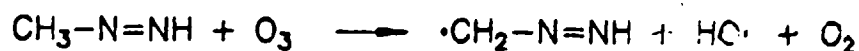
Initiation



Propagation



Branching Chain



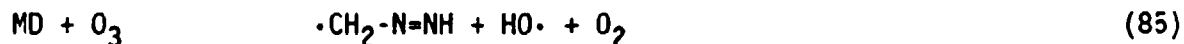
Termination



the rate of initiation, R_i , is

$$\begin{aligned} R_i &= k_i [\text{MMH}] [\text{O}_3] \\ &= k_i' [\text{MMH}] \end{aligned} \quad (84)$$

with k_i' as a pseudo-first-order rate constant ($[\text{O}_3]$ is constant). For the branching reaction,



the rate of delayed branching is

$$\begin{aligned} R_b &= k_b [\text{MD}] [\text{O}_3] \\ &= k_b' [\text{MD}] \end{aligned} \quad (86)$$

Each branching step is accompanied by the formation of two chain carriers, each of which acts to replace an MD. Thus, the rate of change of the branching molecule, MD, is

$$\begin{aligned} \frac{d[\text{MD}]}{dt} &= R_i + 2 k_b' [\text{MD}] - k_b' [\text{MD}] \\ &= R_i + k_b' [\text{MD}] \end{aligned} \quad (87)$$

In integral form ($[\text{MD}] = 0$ at $t = 0$),

$$[\text{MD}] = \frac{R_i}{k_b'} (\exp(k_b' t) - 1) \quad (88)$$

Ignoring quadratic and wall termination reactions, the rate of change of $[\text{HO}_x]$ (the sum of $[\text{HO}]$ and $[\text{HO}_2]$) is

$$\frac{d[\text{HO}_x]}{dt} = 2 R_i + 2 k_b' [\text{MD}] \quad (89)$$

Substituting for [MD],

$$\frac{d[HO_x]}{dt} = 2 R_i \exp(k_b' t) \quad (90)$$

Equation (90) shows that the concentration of chain carrying radicals increases exponentially with time. In integral form ($[HO_x] = 0$ at $t = 0$),

$$[HO_x] = 2 \frac{R_i}{k_b'} (\exp(k_b' t) - 1) \quad (91)$$

Substituting $B = k_b'$ and $I = 2 R_i$,

$$[HO_x] = \frac{I}{B} (\exp(Bt) - 1) \quad (92)$$

While Equations (87) - (92) describe the changes in concentrations for the intermediate methyldiazene and the very reactive oxyradicals, the LFR experiment measures the disappearance of the reactant MMH. The reaction responsible for the majority of MMH consumption is a propagating reaction (Equation (76)). Assuming that every chain carrying radical (HO_x) consumes one MMH, then the integral of $[HO_x]$ from $t = 0$ to t gives the amount of MMH consumed in the time period 0 to t :

$$\int_0^t [HO_x] dt = \frac{I}{B^2} (\exp(Bt) - Bt - 1) \quad (93)$$

$$[MMH]_0 - [MMH]_t = \frac{It}{B^2} (\exp(Bt) - Bt - 1) \quad (94)$$

The LFR reaction data for the MMH ozone reaction was analyzed by a Simplex fitting technique (Reference 71), which provided the best values of I and B , Table 20. Figure 38 shows experimental data and the theoretical line based on Equation (94). Division of the I parameter by the

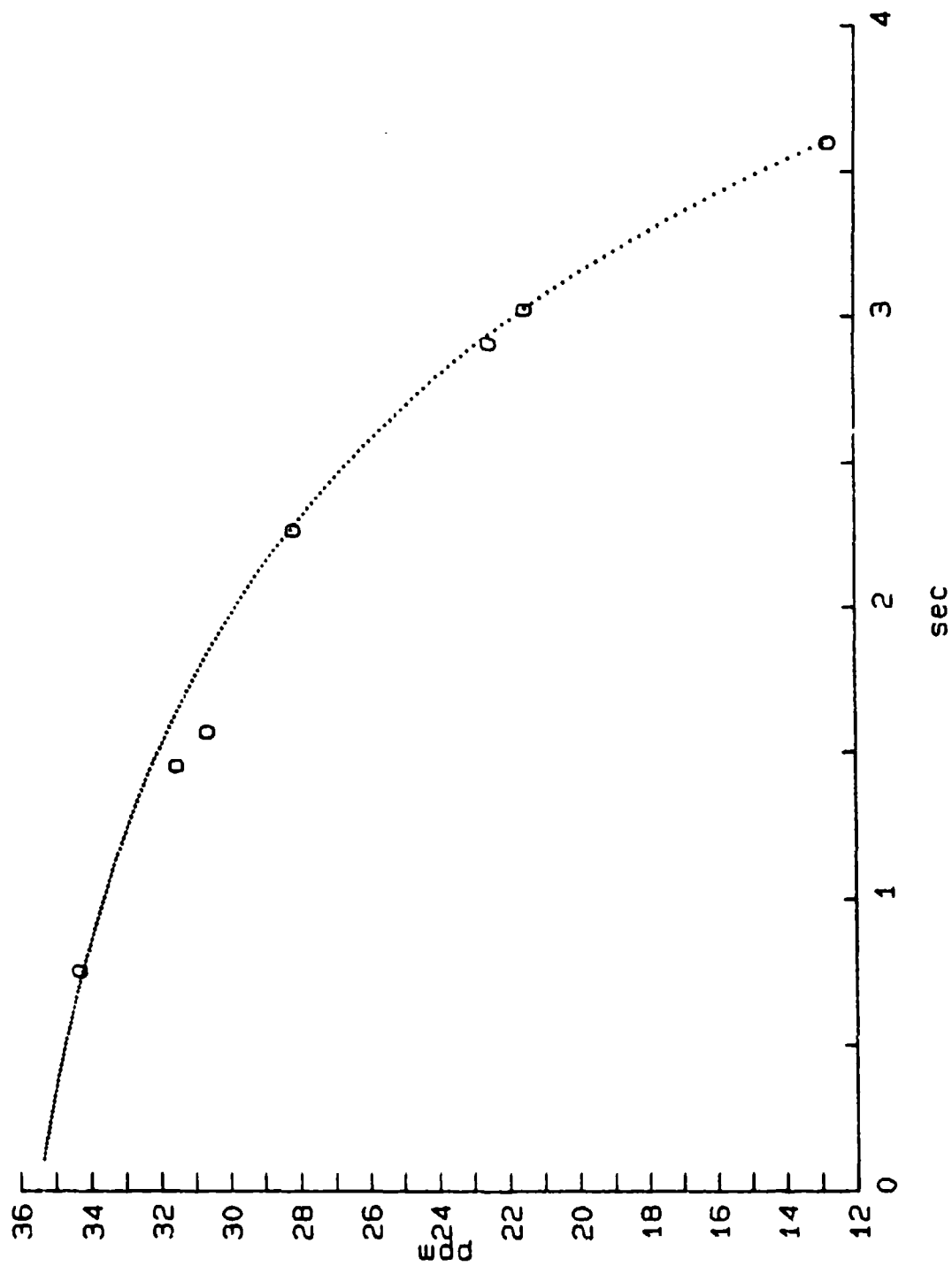


Figure 38. Superimposed Experimental and Theoretical Data for the Reaction of MMH and Ozone Based on Equation (94)

initial ozone and MMH concentrations gives the rate constant k_1 , which is identified as the elementary reaction rate constant for the MMH/ozone reaction. In the development above, B was identified as the pseudo-first-order rate constant $k_b [O_3]$ in the reaction responsible for delayed branching (Equation (85)). Other intermediate products, such as formaldehyde or diazomethane, might be involved as branching centers and are lumped with methyldiazene.

The rate constant for the MMH/ozone reaction determined by the variable position procedure and fitting to Equation (94) was found to be $8.7 \pm 0.35 \times 10^{-17} \text{ cm}^3 \text{ molecule}^{-1} \text{ s}^{-1}$ (299 K), in poor agreement with the value reported by Pitts and Tuazon of greater than $1 \times 10^{-15} \text{ cm}^3 \text{ molecule}^{-1} \text{ s}^{-1}$ (298 K) (Reference 64). The Pitts and Tuazon value was estimated by measuring the overall rate of reaction in a large environmental chamber. Only the initial and long reaction time concentration values were measured and some problems with mixing were noted. Because of the accelerating rate of the reaction, a two-point determination of the rate constant grossly overestimates the initiating rate constant.

Equation (74) is endothermic ($\Delta H = 40 - 50 \text{ kJ/mol}$) and the Arrhenius activation energy was found to be 41 kJ/mole. The pre-exponential value, $\log(10) A = 15 \pm 4 \text{ (cm}^3 \text{ mol}^{-1} \text{ s}^{-1})$, is again high but similar to the value determined for hydrazine.

The derived k_b value of $24.6 \pm 0.1 \times 10^{-17} \text{ cm}^3 \text{ molecule}^{-1} \text{ s}^{-1}$ at 299 K is several times greater than the k_1 value. This greater reactivity is reasonable considering that diazenes in general are more reactive than hydrazines.

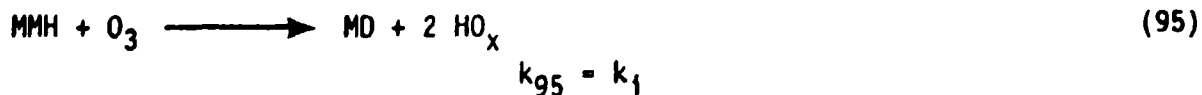
Although Equation (94) was derived for the MMH/ozone reaction, no assumptions were made that would invalidate its use for the reaction of hydrazine and ozone. In the hydrazine case, diazene takes the role as the delayed branching agent. Evidence of branching or accelerating rate is only found at very long intervals in the hydrazine/ozone reaction, indicating that k_b for diazene may be appreciably smaller than for methyldiazene.

One surprising aspect of the reactions of hydrazine and MMH with ozone is the detection of diazene and methyldiazene as relatively stable intermediates in this reaction. Their persistence in the presence of a large excess of ozone is not in accord with previous implications of their reactivity (Reference 72).

(3) Probability Simulation of Branched-Chain Kinetics. The probability simulation or Monte Carlo method can be used to simulate the results of a series of random events that may occur independently, consecutively, concurrently, or repetitively. The result of a Monte Carlo simulation is the frequency of "successful" events compared to the total number of random events considered. Because the rate of a reaction is also a measure of the frequency of "successful" events, the method has been applied to a number of kinetic systems (References 73 and 74).

The procedure consists of selecting a set of elementary reactions and normalizing the concentrations and rate constants so that the product of a rate constant and its associated concentration terms represents a probability of reaction. This probability is then compared to a computer-generated random number, and if the probability of reaction is greater than the random number, the trial is successful and the concentrations of the species involved in the reaction are adjusted. For a set of reactions, each individual reaction is tested in a random fashion. This method is ideal for fast digital-computers, and was implemented on a 80286-based machine.

For the set of key reactions shown in Equations (95) - (99), the rate constants for all but Equation (97) have been determined previously or by the approximate treatment above. The value for k_{97} was estimated as $1 \times 10^{-10} \text{ cm}^3 \text{ molecules}^{-1} \text{ s}^{-1}$ based on the value of k_{96} .



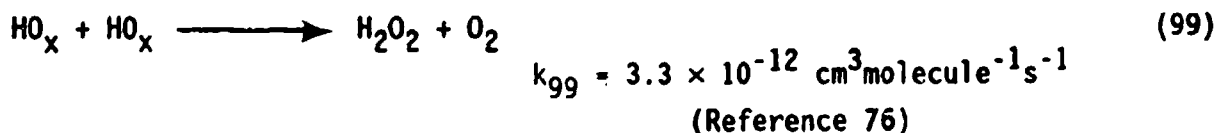
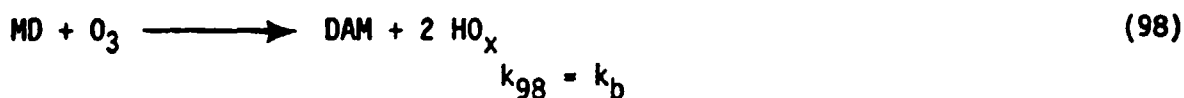
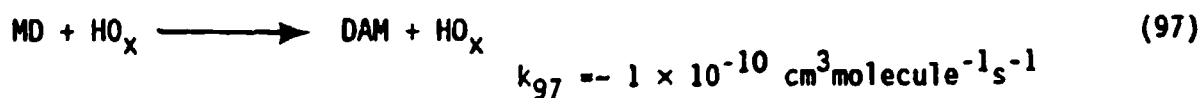
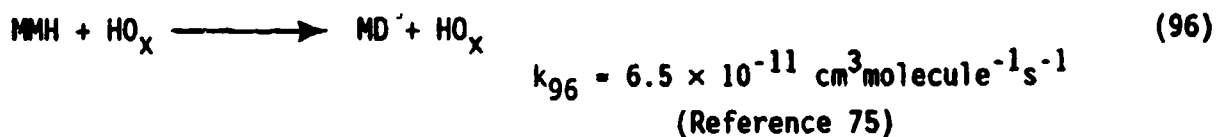


Figure 39 shows the results of a Monte Carlo simulation with 2×10^6 total trials. The Monte Carlo modeled results are in good agreement with the experimental data, but differ slightly from those calculated from Equation (94). The treatment that lead to Equation (94) completely ignored the termination reaction (Equation (99)), and as a result, the initial rate is faster than in the Monte Carlo simulation.

(4) Atmospheric Oxidation Reactions of Hydrazines. Environmental chamber and laminar flow reactor experiments indicate that ozone is a major contributor to the homogeneous oxidation reactions of hydrazine and MMH. The autoxidation rate with oxygen is too slow to measure, but the reaction with ozone occurs with a moderately fast rate at ambient temperatures. Based on the LFR results, estimates can be made of the half-lives of hydrazine and MMH in the atmosphere.

Because half-lives for second-order reactions are concentration-dependent, the variations in concentration of ozone with respect to season, altitude, latitude, time of day, and air quality must be considered. For example, the ozone concentration in the troposphere is greatest in late winter and early spring, is greater in the northern hemisphere, and peaks at

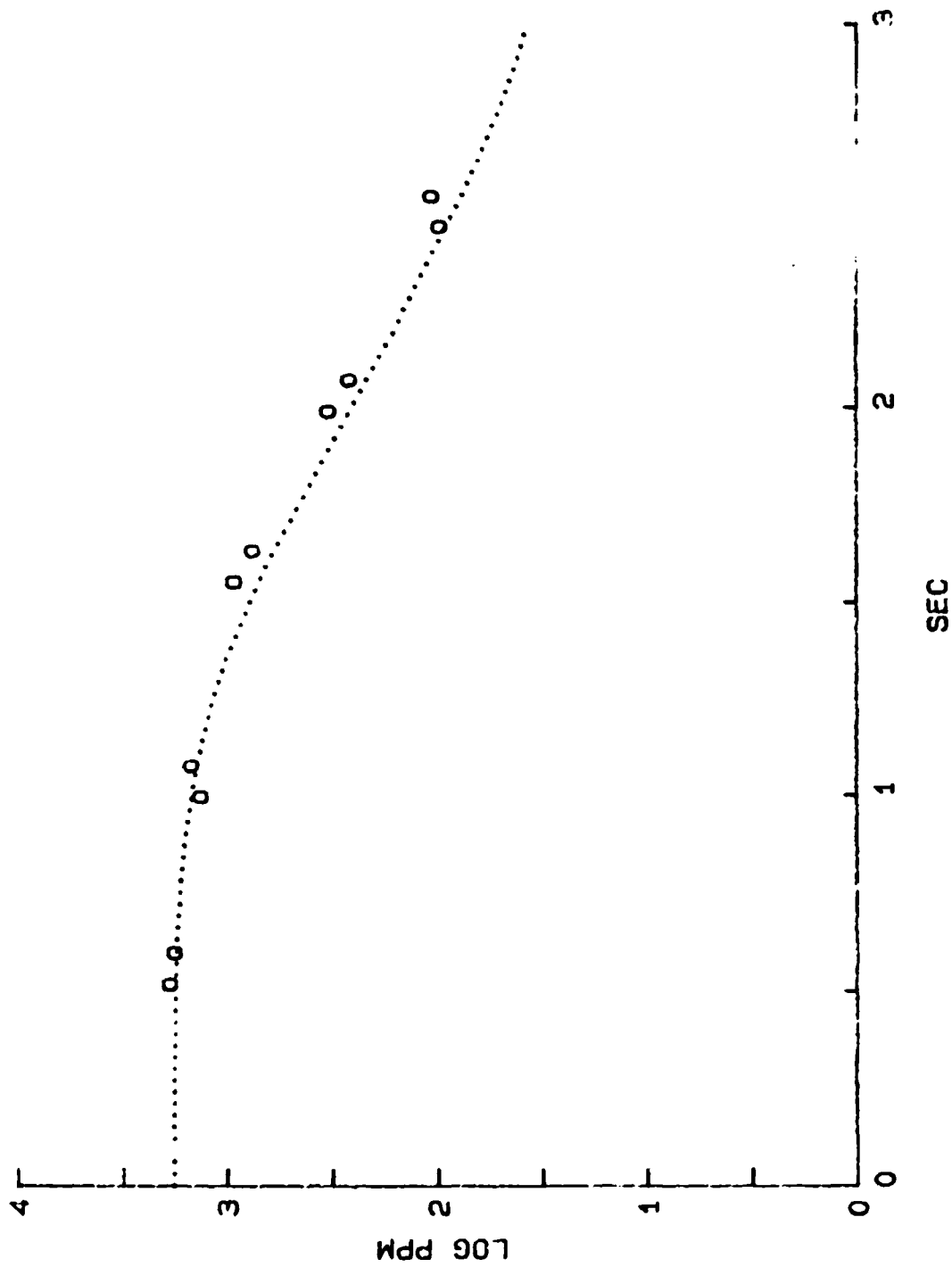


Figure 39. Superimposed Experimental Data and Monte Carlo Simulation Results

approximately 20 kilometers above the earth's surface (Reference 14). The ozone concentration also varies from as little as 0.02 ppm v/v in rural areas to as much as 0.5 ppm in heavily polluted urban atmospheres (Reference 14).

With the above considerations in mind, the half-lives for hydrazine and MMH were estimated, based on a second-order reaction with ozone. These calculations assumed that the ozone concentration was constant and much greater than the concentration of the hydrazine.

In a moderately polluted atmosphere (0.15 ppm ozone), the half-life of hydrazine is estimated to be approximately 1.5 hours at 285 K and 15 minutes at 310 K. In a rural area, however, where the ozone concentration is 0.05 ppm, the half-life increases to 4 hours at 285 K and 1 hour at 310 K.

Under the high dilution conditions assumed for these calculations, the establishment of a branched chain reaction with a long kinetic chain length is not expected. The elementary bimolecular reaction of MMH and ozone is best represented by the initiation rate constant, k_i ; its value was used to determine the half-life of MMH in the atmosphere. Analogous to the hydrazine case, if MMH were released into a moderately polluted atmosphere, it is calculated to have a half-life of approximately 3 hours at 285 K and 45 minutes at 310 K. In a rural area, the half-life is expected to increase to 9 hours at 285 K and 2.5 hours at 310 K.

The half-lives reported here for the persistence of hydrazines in the atmosphere are based on the reaction of hydrazine with ozone. They do not take into account the reactions of hydrazine with carbon dioxide, hydroxyl radicals, or any other reactive species in the atmosphere, nor are any heterogeneous or photochemical reactions considered. The actual half-lives will be shorter than the calculated values to the extent that these additional reactions are important. Harris et al. reported the half-lives of hydrazine and MMH to be approximately 3 hours due to the reaction with hydroxyl radicals (Reference 75). This calculation was based on an average hydroxyl radical concentration of approximately one million radicals per cubic centimeter.

Several of the products formed upon the reaction of hydrazine or MMH with ozone in the atmosphere are likely to be at least as toxic as the reactants themselves. These products include diazene from hydrazine, and diazomethane, methyldiazene, and formaldehyde from MMH. As illustrated in Schemes 4 and 5, further reaction of the nitrogenous compounds ultimately yields nitrogen. Formaldehyde is further oxidized photolytically, or by the sequential reaction with hydroxyl radicals and oxygen to yield carbon monoxide and hydroperoxyl radicals (Reference 14).

In a daytime atmosphere, hydroxyl and hydroperoxyl radicals formed from the ozonization of the hydrazines can cause a cycle of reactions that involve: the oxidation of nitric oxide to nitrogen dioxide; the photolysis of nitrogen dioxide to nitric oxide and oxygen atoms; and the combination of oxygen atoms with dioxygen to form ozone. The net result is an increase in ozone.

(5) Suggestions for Further Work. The work detailed above suggests that the LFR technique is a important tool for the study of chemical reactivities. Full exploitation of the technique by the atmospheric chemist will require further developments in the following areas:

- Characterization of the laminar flow profile, perhaps with a laser velocimeter technique
- Visualization of the reactant profile near the introduction array, using a technique such as thermography
- Mathematical theory of introduction array profiles, including the role of diffusion coefficients
- Evaluation of other reactant monitoring techniques, such as VIS-UV spectrophotometry or luminescence
- Exploration of the range of ozonization rates, including the reactions of ozone with NO or NO₂
- Addition of a photon flux array for the study of photochemical reactions
- Mechanistic studies of other amino compounds to provide a basis for understanding the reactivities of MMH and hydrazine

- Additional evaluation of the fixed-position procedure
- Theory and simulation of branching chain reactions

E. CONCLUSIONS

The Laminar Flow Reactor has proven to be useful for the study of the kinetics and mechanisms of bimolecular gas-phase reactions at atmospheric pressure. The concept, method, and design of the LFR are validated by its use in accurately reproducing the rate constant and product for a known ozonization reaction.

The LFR can be used to elucidate the nature of complex reactions (such as those of ozone with hydrazines) and to provide quantitative insights into the mechanism of the reaction that are not available by other techniques.

While there is no direct evidence that the LFR eliminates surface effects, indirect evidence reasonably suggests that wall contact of the reactants is minimal.

This method, coupled with a suitably sensitive detection system, is capable of measuring second-order rate constants in the range of 10^{-15} to 10^{-18} $\text{cm}^3 \text{molecule}^{-1} \text{s}^{-1}$ at 298 K and atmospheric pressure.

The rates and mechanisms measured by the LFR technique for the reaction of hydrazine and MMH with ozone have provided a quantitative assessment of the maximum lifetimes of these molecules in the atmosphere. Coupled with the results of the surface-catalyzed oxidation studies, an overall picture of the environmental fate of hydrazines in the atmosphere is developing.

SECTION V

SURFACE SPECTROSCOPIC STUDIES

A. INTRODUCTION

The air-oxidation reactions of hydrazine and MMH are strongly dependent on the state of the hydrazine. The homogeneous oxidation rates of gaseous hydrazines with oxygen are too slow to accurately measure. Even in low surface-to-volume ratio environmental containers made of inert fluorocarbon films, physical interactions such as adsorption of the hydrazine onto the walls of the chamber dominate over chemical oxidation. Surface-bound hydrazine is much more readily oxidized, as shown by both chamber and packed flow-reactor studies. The efficiency of this surface-catalyzed oxidation depends on the initial adsorption of the hydrazines onto the active surface.

1. Objective

This section describes studies of the hydrazine/surface interaction using diffuse reflectance infrared Fourier transform (DRIFT) spectroscopy. The DRIFT spectroscopic technique has been applied to model environmental surfaces such as silica and alumina with adsorbed hydrazines to determine the mode of surface interaction and the effects of adsorption on the structure of the adsorbate.

2. Background

Radiation reflected from the surface of a finely powdered sample consists of two components. The first is due to specular reflectance, which is reflected at an angle related to the angle of incidence. The second component is the result of radiation that has penetrated 3 - 5 mm into the sample and has undergone multiple scattering at the surfaces of the particles. A small fraction of this radiation is scattered out of the sample and emitted as diffuse reflectance. This diffused radiation has penetrated the surfaces of the sample particles and carries information concerning the nature of the particle surface, including any adsorbed species.

The sensitivity improvements in infrared spectroscopy due to the Fourier transform technique has enabled diffuse reflectance studies of surfaces to become practical. By comparing the DRIFT spectra of surfaces with and without adsorbed molecules, the vibrational spectrum of the adsorbed species becomes available.

B. EXPERIMENTAL

1. Materials

The oxide powders were commercially obtained. These powders were alumina (Woelm W200 acid, BET area $200 \text{ m}^2/\text{g}$), copper(I) oxide (Baker), iron(III) oxide (Johnson Matthey puratronic grade), silica (Cabot, Cab-O-Sil® fumed, grade M-5), and silica-alumina (Grace, grade 135-08-5X1950).

Hydrazine and MMH were propellant grades (Olin) analyzed according to MIL-P-26536-C and MIL-P-27404B, respectively. Typical analyses were >98.7 percent and less than 1.5 percent water. UDMH (Aldrich) was reagent grade material and used as received. Methylamine (Airco) was used as supplied. All other solvents were reagent grade and used as supplied.

A sample of mixed iron oxides (Fe_xO_y) was prepared by exposing iron powder to distilled water and evaporating at 383 K. The iron oxide powder was sized to 120 mesh and the BET surface area was determined to be $0.8746 \text{ m}^2/\text{g}$.

2. Instrumentation

A Mattson Sirius 100 FTIR spectrometer fitted with a HgCdTe detector was used to house the Harrick diffuse reflectance cell. Data collection and analysis were performed by a Pixel 80 microcomputer using Mattson-supplied programs.

Diffuse reflectance studies were performed in a Harrick high-vacuum chamber diffuse reflectance apparatus (HVC-DRA) mounted in the Mattson FTIR. The diffuse reflectance cell was attached to a vacuum manifold. The HVC-DRA was

fitted with potassium bromide (KBr) windows, thermocouple sensor, and heaters, and was capable of operating at temperatures up to 573 K. Normally, 32 or 64 interferograms were added together and processed using triangular apodization. A ratio of the single beam spectra of the clean surface (background) and surface with adsorbed vapors (sample) was obtained, and the resulting transmittance spectrum converted to an absorbance spectrum. The instrumental resolution was specified as 4 cm^{-1} .

3. Procedures

The HVC-DRA was charged with a solid sample, evacuated to 100 Pa, and heated to 380 K for 1 hour to remove weakly adsorbed water and other gases. The HVC-DRA was cooled to ambient temperature and the appropriate vapor was introduced into the HVC-DRA. Deuterated Cab-O-Sil® was prepared by repeated exposure to deuterium oxide (D_2O) vapor followed by evacuation (three times, 1 kPa and 5 minutes, 298 K) to give a predominantly hydrogen-deuterium exchanged surface.

Adsorbed molecules can be detected on the surface of solids by diffuse reflectance techniques. The HVC-DRA was used to record DRIFT spectra in controlled atmospheres and at nonambient temperatures. Solid samples of deuterated Cab-O-Sil®, copper(I) oxide, silica-alumina, mixed iron oxides, alumina, and iron(III) oxide were exposed to hydrazine, pyridine, MMH, and UDMH. Methanol and methylamine (MA) were also studied on several surfaces for calibration purposes.

C. RESULTS

1. Silica Surfaces

Cab-O-Sil® (nondeuterated) is a finely divided fumed-silica surface that is characterized by the presence of free Si-OH groups (3734 cm^{-1} sharp), adjacent groups SiO-H...O-HSi (3672 cm^{-1} , broad), and hydrogen-bonded water ($3540\text{--}3400\text{ cm}^{-1}$, broad) (Reference 77). Evacuation and heating (vacuum baking)

causes the lower frequency bands to decrease in intensity and the free Si-OH band to increase.

Repeated exposure to D₂O vapor causes the (nondeuterated) Cab-O-Sil® surface to be predominantly hydrogen-deuterium exchanged. New bands for the free and adjacent Si-O-D groups appear at 2764 cm⁻¹ and 2700 cm⁻¹. The reflectance spectrum of a vacuum-baked and deuterated Cab-O-Sil® sample is shown in Figure 40. Free surface O-H and O-D groups are indicated by the sharp features at 3734 cm⁻¹ and 2764 cm⁻¹, respectively. The shoulders on the low frequency side are caused by adjacent Si-OH or Si-OD groups that are interacting by hydrogen bonding. The O-H region shows a negative absorbance, because the same sample (before deuteration) was used to produce the background interferogram. The H-D frequency ratio is 1.35.

a. Hydrazine

Exposure of deuterated Cab-O-Sil® to 250 Pa of hydrazine vapor produced the spectrum shown in Figure 41. The O-H and O-D regions both show negative absorbance. The O-H and O-D bands have been broadened by hydrogen bonding with adsorbed hydrazine, resulting in a broad envelope of absorbances between 3700 cm⁻¹ and 2000 cm⁻¹. In the liquid state, hydrazine displays vibrations at 3200 cm⁻¹ and 3338 cm⁻¹ (Reference 78). In the adsorbed state, a band at 3200 cm⁻¹ is clearly visible superimposed on the broad hydrogen bonding envelope; the 3338 cm⁻¹ liquid state band appears as a shoulder near the 3326 cm⁻¹ peak. There is no evidence of a gas-phase contribution to the spectrum.

Two important spectral features of Figure 41 are the strong bands at 1613 cm⁻¹ and 1474 cm⁻¹. Hydrazine vapor has corresponding lines at 1628 cm⁻¹ and 1493 cm⁻¹. The 1613 cm⁻¹ and 1474 cm⁻¹ bands are probably due to -NH₂ deformation vibrations of surface hydrogen-bonded hydrazine. The deformation frequency shifts of 15 to 19 cm⁻¹ are in the same direction, and of comparable magnitude, to that shown by ammonia adsorbed to a silica surface (References 79 and 80).

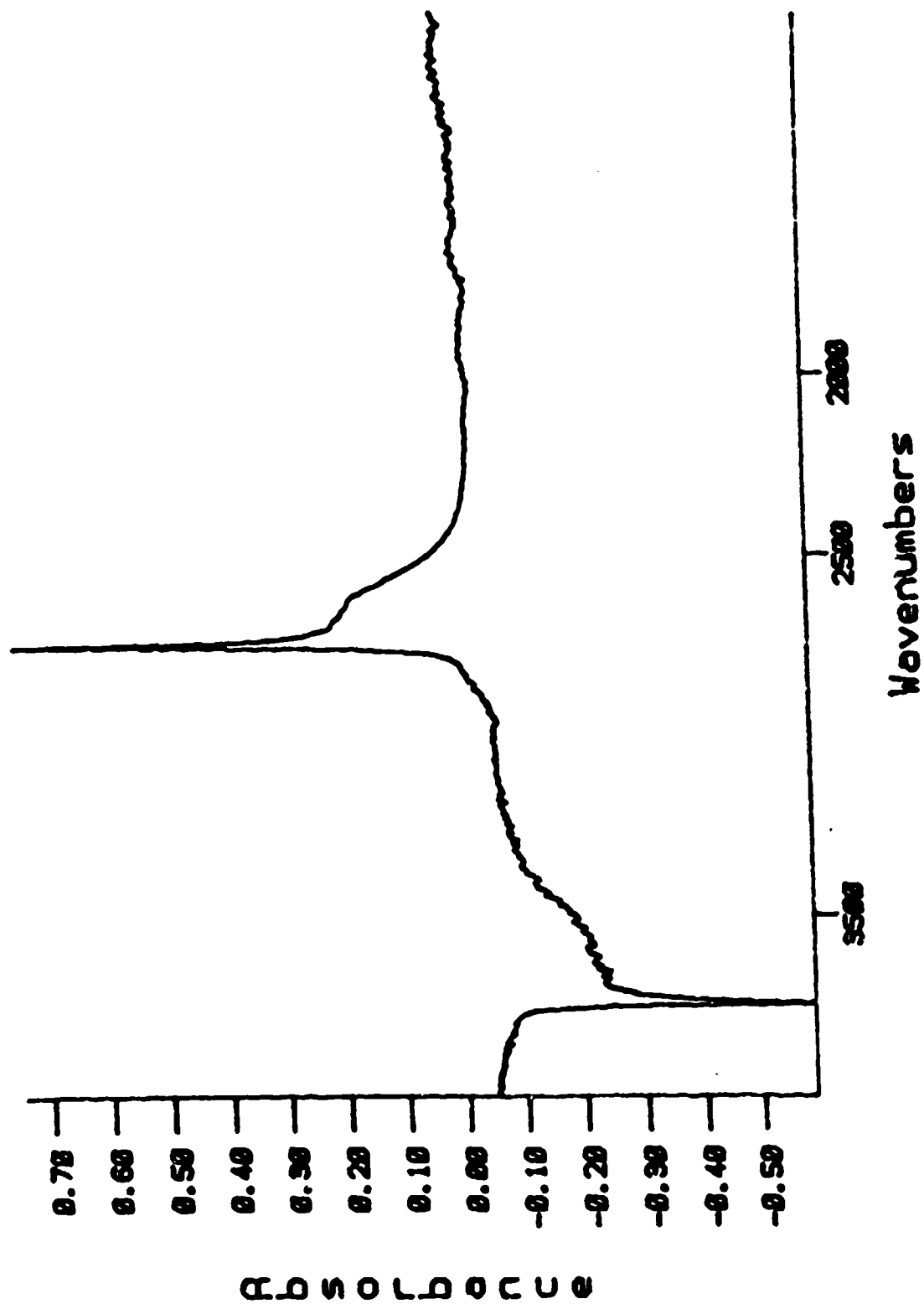


Figure 40. Diffuse Reflectance Spectrum of Deuterated Cab-O-Sil® (Nondeuterated Reference Spectrum)

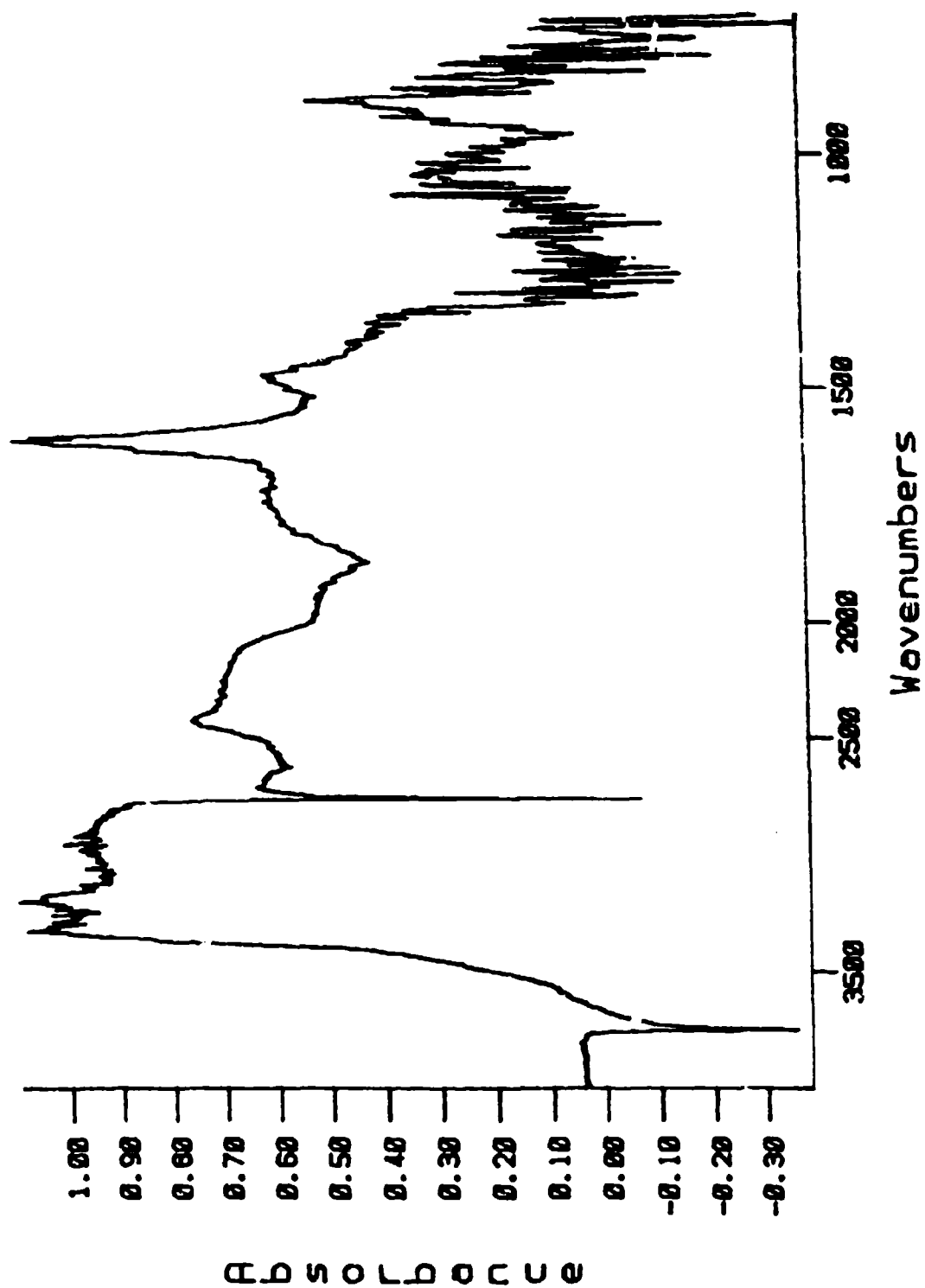


Figure 41. Diffuse Reflectance Spectrum of
Hydrazine Absorbed onto Deuterated
Cab-O-Sil

The HVC-DRA containing the deuterated silica-hydrazine sample was then evacuated for 25 minutes at ambient temperatures, and the spectrum shown in Figure 42 was obtained. Comparing Figure 42 with Figure 41 shows that isotope exchange has occurred, as evidenced by the shift from negative to positive absorbance of the free O-H peak at 3734 cm^{-1} . A significant reduction in the intensity of the broad absorbance band between 3700 cm^{-1} and 3000 cm^{-1} was also observed, and the bands indicative of liquid-like hydrazine disappeared. The reappearance of H on the surface and the loss of hydrazine shows that both the H-D exchange and the adsorption processes are readily reversible at room temperature.

b. Pyridine

Pyridine is a useful probe to determine the nature of the surface-adsorbate interaction for amino compounds. Deuterated Cab-O-Sil® was exposed to pyridine vapor in the HVC-DRA. The spectrum of the adsorbed pyridine indicated that both free and adjacent O-D groups were lost. The in-plane ring deformation modes of pyridine, which appeared at 1445 , 1579 , and 1595 cm^{-1} , were indicative of an hydrogen-bonded pyridine (1445 cm^{-1}). This contrasts with Lewis-coordinated ($1447 - 1460\text{ cm}^{-1}$) or Bronsted-protonated (1540 cm^{-1}) species reported elsewhere (Reference 81). The free and adjacent O-D groups were replaced by pyridine-hydrogen bonded groups.

c. MMH

MMH also exchanges and hydrogen bonds to the deuterated Cab-O-Sil® surface. Free Si-OH and adjacent Si-OH functions were observed to increase at 3750 , 3710 , 3626 , and 3531 cm^{-1} . The larger number of identifiable O-H stretches may be due to Si-OH groups in different sites, i.e., with O-H or N-H nearest neighbors. Of particular interest are the C-H stretching and methyl group deformation frequencies of MMH (Reference 82). The C-H regions of adsorbed and liquid phase MMH (Figures 43 and 44, respectively) show an overall similarity, but significant shifts are easily seen. The fundamental bands at 2990 , 2967 , and 2804 cm^{-1} for adsorbed MMH are at higher energy than in the

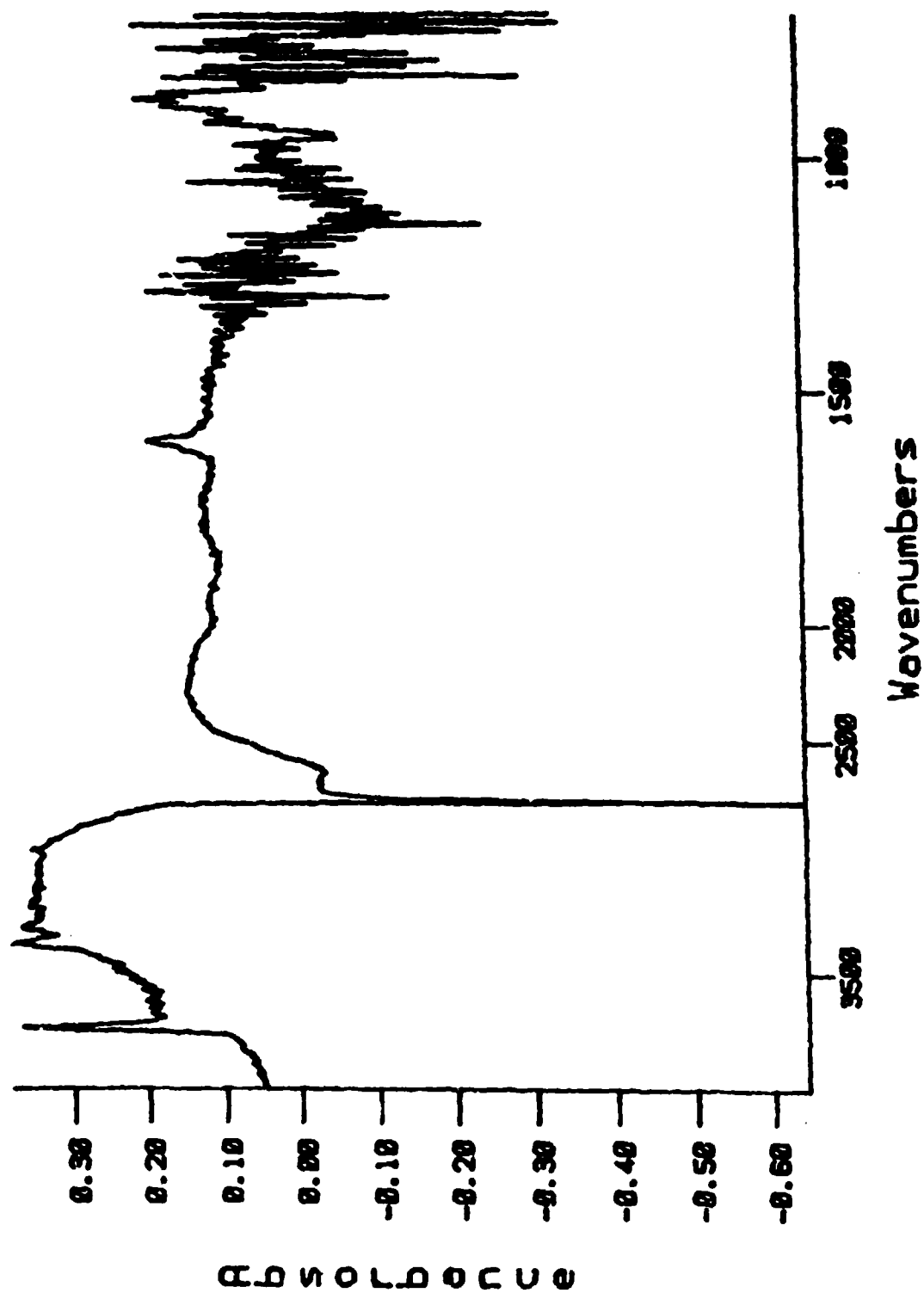


Figure 42. Diffuse Reflectance Spectrum of Hydrazine Adsorbed on Deuterated Cab-O-Sil® After Evacuation (Deuterated Cab-O-Sil® Reference)

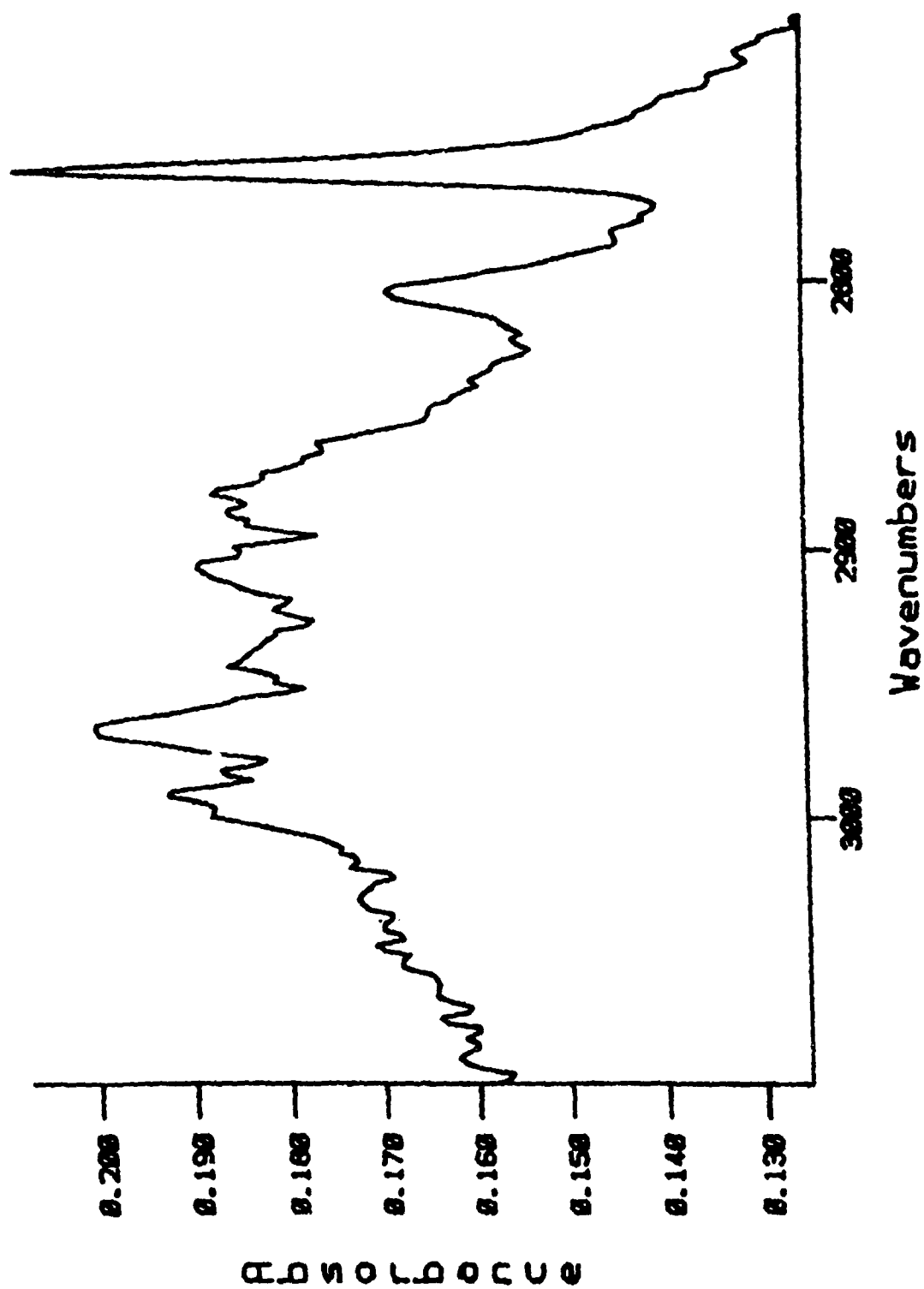


Figure 43. Diffuse Reflectance Spectrum of MMH
Adsorbed on Deuterated Cab-O-Sil®
(Deuterated Cab-O-Sil® Reference)

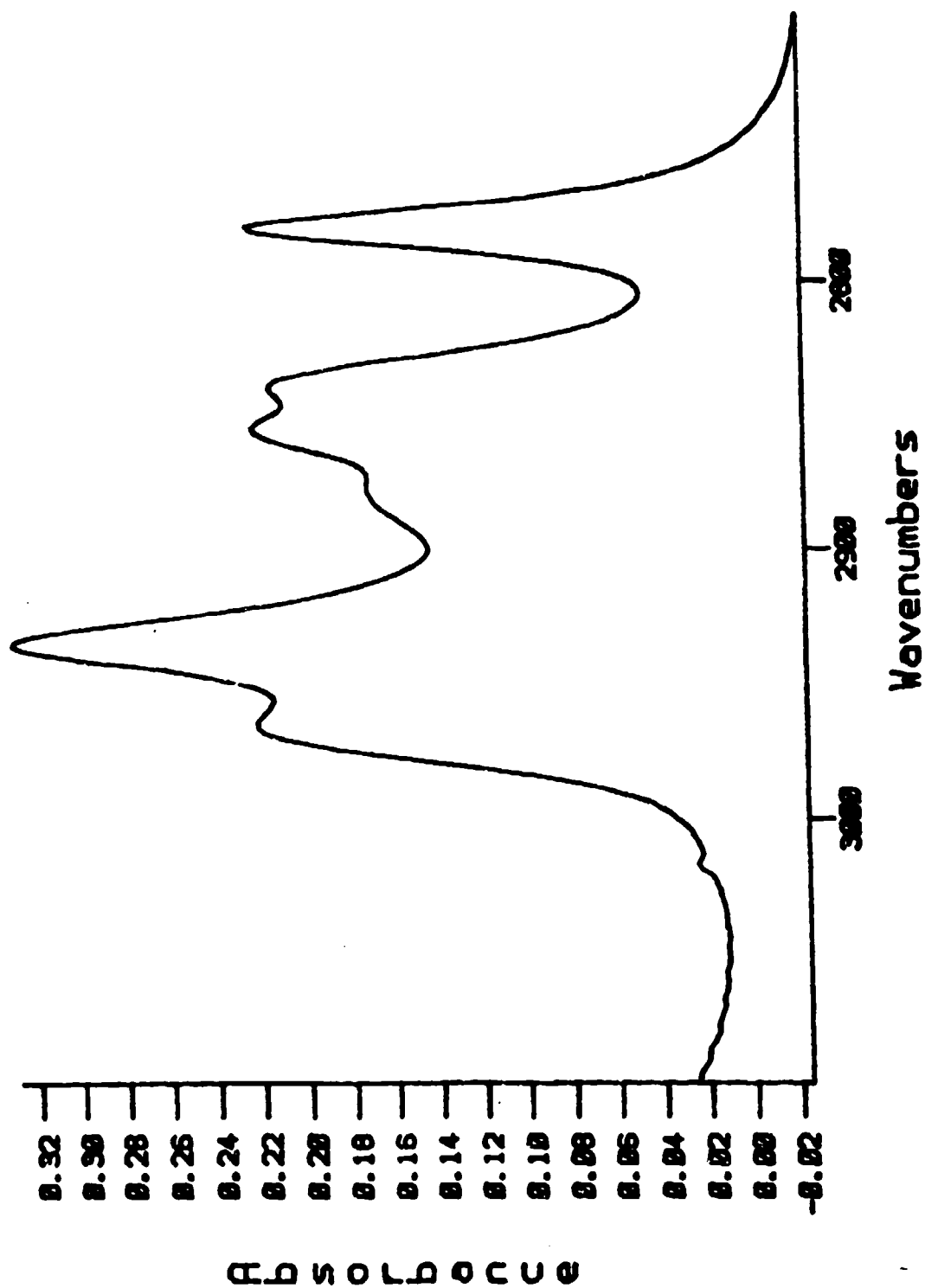


Figure 44. Carbon-Hydrogen Stretching Region of PMH (Thick Film)

liquid or gas-phase spectrum of MMH (Reference 83). These shifts are listed in Table 27.

The abnormally low frequency C-H fundamental at 2780 cm^{-1} (liquid MMH) has been attributed to interaction of the C-H bond with the pair of nonbonding electrons on the adjacent nitrogen (References 84 and 85). Hydrogen bonding or other Lewis acid interactions with the lone pair should alter this effect and result in a shift to a higher frequency. This fundamental was found at 2804 cm^{-1} in adsorbed MMH. The methyl deformation bands in the $1350 - 1450\text{ cm}^{-1}$ region are known to shift to higher frequencies with increasing electronegativity of the attached atom (Reference 86), and were shifted $4 - 16\text{ cm}^{-1}$ to higher frequencies in adsorbed MMH. The combination band observed at 2907 cm^{-1} is the sum of two shifted deformation modes, and the shift was the largest adsorbed surface versus liquid band shift observed (Table 27).

TABLE 27. METHYL GROUP FREQUENCIES OF MMH ADSORBED ON DEUTERATED CAB-O-SIL®

Mode	Adsorbed (cm^{-1})	Liquid (cm^{-1})	Shift ^a (cm^{-1})	Gas ^b (cm^{-1})
Asymmetrical stretch	2990	2966	+24	2969
Asymmetrical stretch	2967	2935	+32	2949
Combined deformation	2943	2877	+34	---
Combined deformation	2907	2855	+52	2851
Combined deformation	2879	2840	+39	---
Symmetrical stretch	2804	2780	+24	2875
Deformation	1476	1472	+4	1464
Deformation	1454	1438	+16	---
Deformation	1421	1411	+10	---

^a Shift with respect to liquid phase

^b Reference 82

d. UDMH

UDMH adsorbed on deuterated Cab-O-Sil® also showed H-D exchange, and the methyl-group frequency shifts were nearly the same as those shown by MMH (Table 28).

2. Other Surfaces

a. Silica-Alumina and Alumina

Both silica-alumina and alumina substrates cause similar shifts when hydrazines, methylamine, or methanol are adsorbed on their surfaces (Table 29).

b. Iron(III) Oxide, Mixed Iron Oxides, and Copper(I) Oxide

The DRIFT spectrum of iron(III) oxide exposed to MMH or UDMH vapors in the HVC-DRA showed adsorption of the hydrazine and shifts of the methyl-group frequencies (Table 30). A copper(I) oxide sample showed the same phenomena, but methyl-group shifts could not be measured because of low intensity signals.

When exposed to either MMH or UDMH, both copper(I) and iron(III) oxides formed as yet unidentified surface species with adsorptions at $2100 - 2130 \text{ cm}^{-1}$ and $2190 - 2230 \text{ cm}^{-1}$. At room temperature, the 2115 cm^{-1} band increased steadily with exposure time, and methane was observed in the gas phase.

The DRIFT spectrum of copper(I) oxide with MMH vapor shows gas-phase MMH bands present between 1000 and 700 cm^{-1} (Figure 45). The 2115 cm^{-1} absorption is already visible after 2 minutes at 295 K. Negative absorbances in the spectrum indicate that MMH displaced some unidentified adsorbed species. The spectrum of the exposed copper(I) oxide was taken 2 minutes after beginning the removal of the MMH vapor began (Figure 46). The figure shows the absence of gas-phase MMH, and that the relative intensities of the C-H and N-H

TABLE 28. METHYL GROUP FREQUENCIES OF UDMH ADSORBED ON DEUTERATED CAB-O-SIL®

Mode	Adsorbed (cm ⁻¹)	Liquid ^a (cm ⁻¹)	Shift ^b (cm ⁻¹)	UDMH-KBr ^c (cm ⁻¹)
Asymmetrical stretch	2996	2976	+20	3259 (283 K)
Asymmetrical stretch	2967	2947	+20	3143 (196 K)
Combined deformation	2933	2889	+44	---
Combined deformation	2872	2848	+24	3015
Symmetrical stretch	2836	2811	+25	2970 (159 K)
Symmetrical stretch	2792	2766	+26	2918 (147 K)
Deformation	1469	1463	+6	---
Deformation	1461	1450	+11	---

^a Reference 87

^b Shift with respect to liquid phase

^c Solid on KBr plate

TABLE 29. SUMMARY OF OBSERVED FREQUENCY SHIFTS^a FOR METHYL ADSORBATES

Adsorbate	Silica	Silica-Alumina	Alumina
MMH	+24	+22	+22
UDMH	+26	+26	+15
MeOH	+26	+12	-11
MeNH ₂	(+7) ^b	---	---

^a For the low-frequency symmetrical C-H stretch, in wave numbers relative to liquid state

^b With respect to gas phase

stretching bands are reversed (the negative gas-phase water bands near 3600 cm⁻¹ and 1600 cm⁻¹ are the result of a poor instrument purge during collection of the background interferogram). Continuous evacuation of the HVC-DRA for 1 hour

TABLE 30. METHYL GROUP FREQUENCIES OF MMH AND UDMH ADSORBED ON IRON(III) OXIDES

Adsorbed (cm^{-1})	Liquid (cm^{-1})	Shift (cm^{-1})
<u>MMH</u>		
2991	2996	+25
2965	2935	+30
2930	2877	+53
2881	2855	+26
2859	2840	+19
2805	2780	+25
<u>UDMH</u>		
2988	2976	+12
2961	2947	+14
2925	2889	+36
2870	2848	+22
2828	2811	+17
2785	2766	+19

followed by heating to 343 K for 30 minutes gave the spectrum shown in Figure 47. Both N-H and C-H stretching vibrations are still visible, and the presence of methane gas inside the cell is revealed by its characteristic 3017 cm^{-1} band. The 2115 cm^{-1} feature is still evident, as is the curious growth and loss of bands in the CO_2 region near 2350 cm^{-1} . Exposure of iron(III) oxide to UDMH vapor followed by vacuum baking at 560 K for 72 hours gave a spectrum showing the 2115 cm^{-1} band strongly and distinctly.

The reactive surface of the mixed iron oxides was studied in a similar manner. A program of evacuation and heating showed that the surface lost water readily up to 515 K and stabilized after 2 hours. Cooling to 323 K and admitting MMH as a gas at 30 - 60 Pa showed the typical pattern of four MMH bands at 1118, 968, 889, and 789 cm^{-1} with slightly altered band shapes. After 10 minutes, the samples showed the nearly complete absence of MMH and the appearance of characteristic bands due to methane (1305 cm^{-1}) and methanol (1032 cm^{-1}). These results are in agreement with earlier studies of the MMH/air

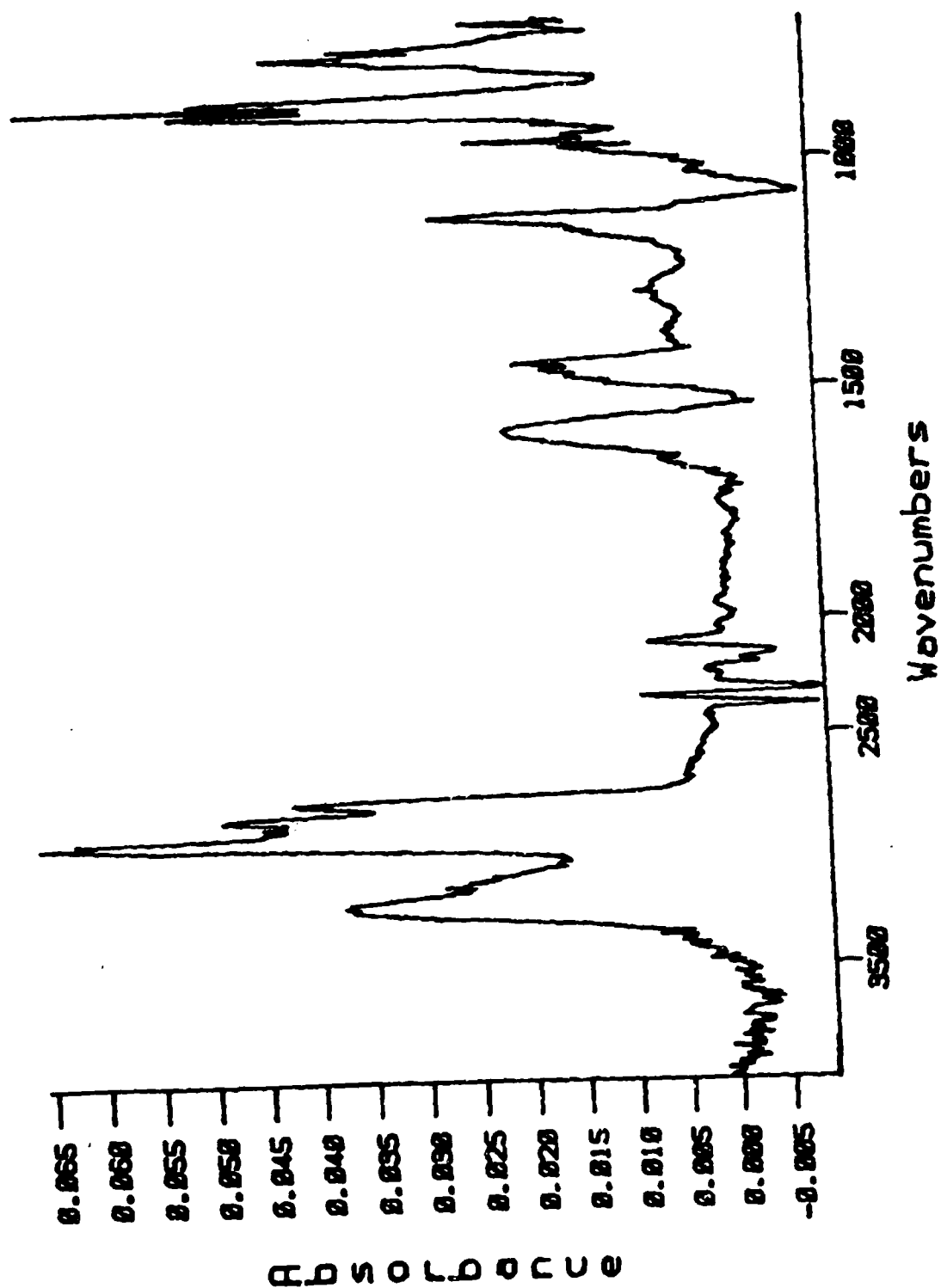


Figure 45. Diffuse Reflectance Spectrum of NiO Adsorbed on Copper(I) Oxide After 2-Minute Exposure (Copper(I) Oxide Reference)

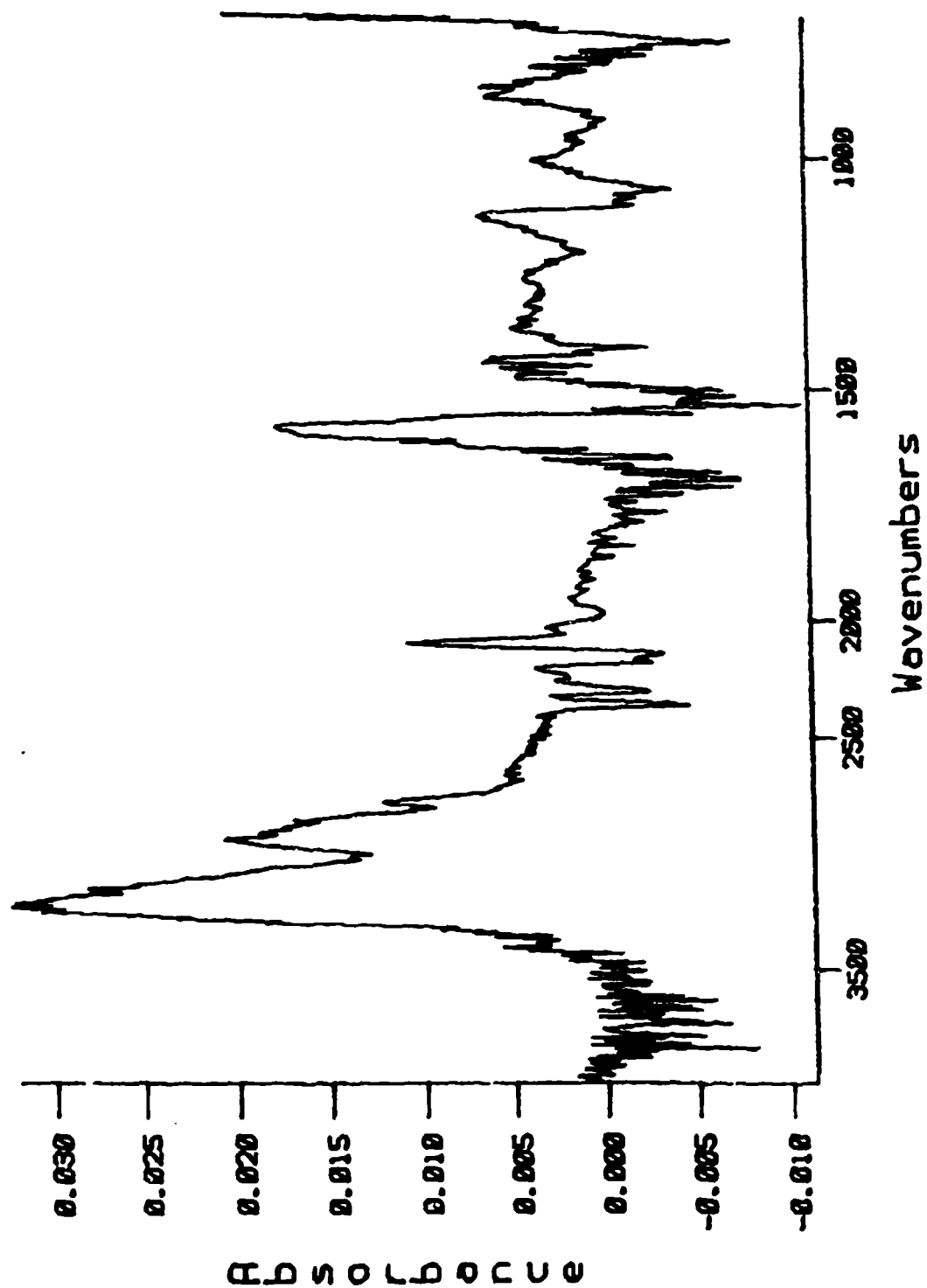


Figure 46. Diffuse Reflectance Spectrum of
NiO Adsorbed on Copper(I) Oxide,
2 Minutes After Evacuation
(Copper(I) Oxide Reference)

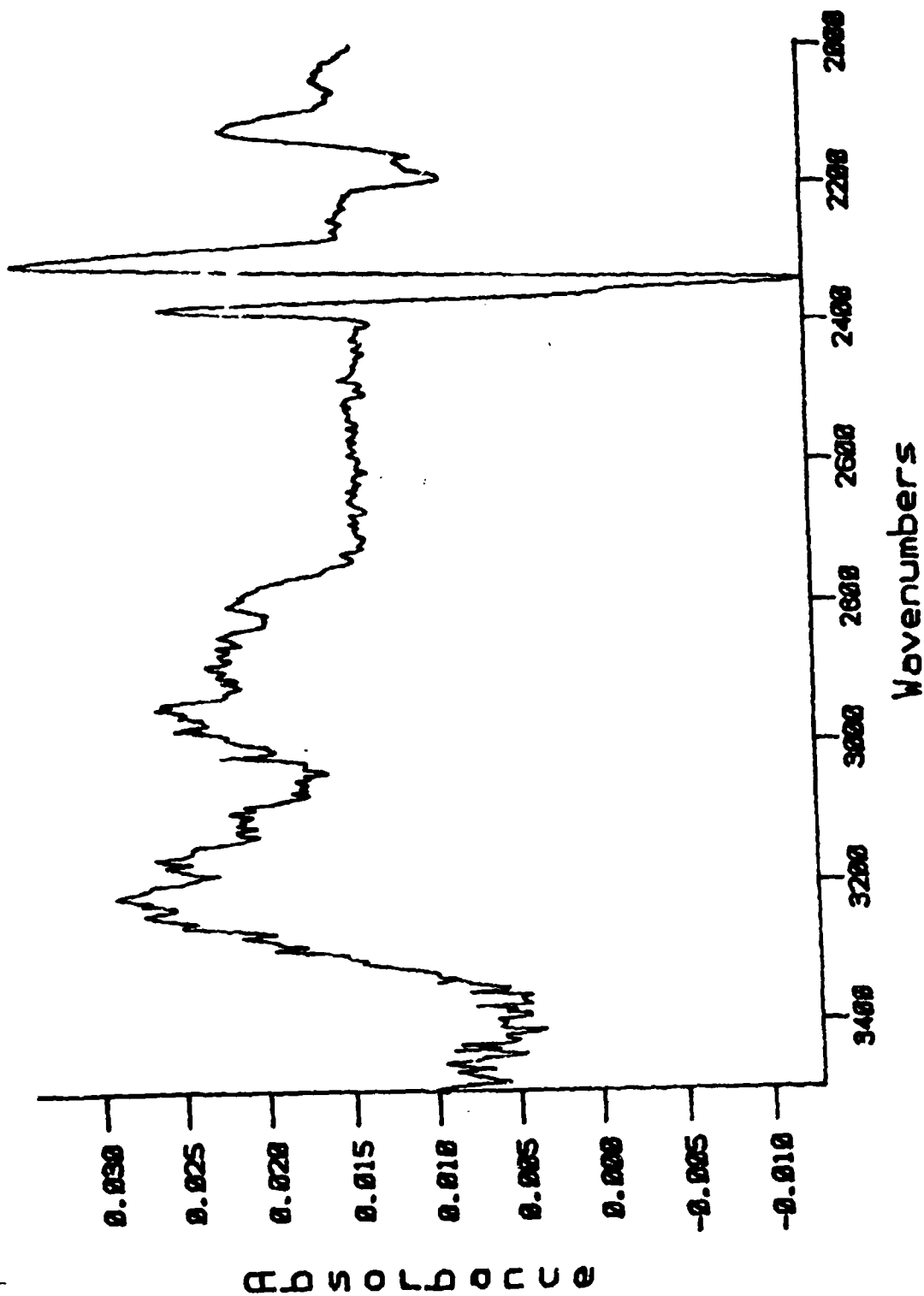


Figure 47. Diffuse Reflectance Spectrum of Copper(I) Oxide Surface After Exposure to NH_3 and Heating to 343 K for 30 Minutes (Copper(I) Oxide Reference)

oxidations in packed microreactors (SECTION III). After 20 minutes, the gaseous products were removed and the spectrum was that of the initial surface.

The presence of surface products on iron(II) and copper(I) oxides was investigated further by examining the DRIFT spectra of the solids that had been exposed to MMH or UDMH in a packed microreactor (SECTION III). Adsorptions at $2190 - 2226 \text{ cm}^{-1}$ and at $2110 - 2120 \text{ cm}^{-1}$ were detected on both the iron(III) and copper(I) oxide surfaces when exposed to either MMH or UDMH. New bands were also identified from the reaction of MMH with air on copper(I) oxide at $3030, 2945, 2713, \text{ and } 2645 \text{ cm}^{-1}$. Ultra-pure iron(III) and copper(I) oxide samples showed the presence of adsorbed or trapped CO_2 at $2300 - 2400 \text{ cm}^{-1}$, which is the same frequency as gaseous CO_2 . The adsorbed or trapped CO_2 was not removed by heating and evacuation. Some mineral species that possess 5A cavities can trap CO_2 and show CO_2 bands that are nearly identical to gas-phase CO_2 bands, and the CO_2 cannot be removed by evacuation (Reference 88). Electron spectroscopy for chemical analysis (ESCA) spectra of the iron(III) and copper(I) oxides used in these studies, however, showed no trace of CO_2 .

D. DISCUSSION

The use of deuterated Cab-O-Sil® as a mechanistic tool for the infrared spectroscopic study of adsorptive interactions with hydrogen-bonding adsorbates, such as the hydrazines, has several distinct advantages. Because the -OH spectral region is cleared by deuteration and few functional groups have vibrational bands near the -OD group ($2800 - 2400 \text{ cm}^{-1}$), both frequency and intensity changes are readily observed. The finely divided form of deuterated Cab-O-Sil® makes it ideal for diffuse reflectance studies.

DRIFT studies of the adsorption of hydrazine, MMH, UDMH, and the model compounds, methylamine and methanol, on the environmentally important silica and alumina surfaces show some striking commonalities. These polar molecules are all rapidly adsorbed/desorbed at room temperature. The adsorption process is accompanied by H/D-exchange if the silica surface is deuterated. The overall spectral properties of the surface-bound species are similar to those of the liquid or vapor, indicating that the surface interaction is primarily physical.

Chemisorption is involved only in the case of methanol and alumina. Finally, bound N-methyl and O-methyl groups show similar small shifts to higher energies for stretching, combination, and deformation modes in the physisorbed state.

A structure for the H-bonded MMH surface species consistent with the results is shown in Figure 48. The choice of N-1 as the acceptor atom for the unsymmetrical hydrazines is suggested by the similar methyl-group frequency shifts shown by MMH, UDMH, and methylamine. Because N-1 of UDMH cannot act as a N-H donor and is also the more basic nitrogen, the most favorable cyclic structure would involve N-1 as an acceptor and N-2 as a N-H donor. A similar structure for water, bound to surface silanol groups, has been proposed (Reference 77).

The unsymmetrical C-H stretching frequency of methanol is decreased by 11 cm^{-1} on adsorption onto alumina. Adsorption onto silica or silica-alumina, however, caused shifts to higher frequency, $+26\text{ cm}^{-1}$ and $+12\text{ cm}^{-1}$, respectively.

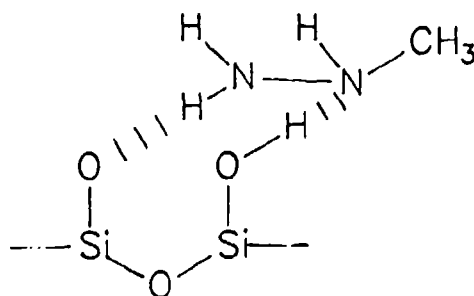


Figure 48. Illustration Showing MMH Adsorbed to Silica Surface

This is an important observation because Greenler has shown that methanol chemisorbs onto alumina with formation of surface-methoxy species such as Al-OCH_3 (Reference 89).

Structure-reactivity relationships have often been developed by using changes in molecular vibrational frequencies as probes of structure. Bellamy has reviewed a number of such studies (Reference 86). Electronegativity has been used to rationalize trends in such relationships, but the Pauling scale lacks the resolution for satisfactory correlation. Sanderson has recently developed a precise and internally consistent scale of electronegativities (Reference 90). Correlation of Sanderson electronegativities with the symmetrical methyl deformation frequencies of $\text{CH}_3\text{-Y}$ compounds shows linearity by Periodic row and monotonic change within Groups (Figure 49).

Using the linear relationship for the First Row elements,

$$E = 0.015 (\nu, \text{cm}^{-1}) - 18.122 \quad (100)$$

where

E = Sanderson electronegativity
 ν = Frequency of the symmetrical methyl deformation frequency in wavenumbers of the mono- $\text{CH}_3\text{-Y}$ compound

the electronegativity of the -NHNH_2 group is estimated to be 3.01 in the liquid state. The $+10 \text{ cm}^{-1}$ shift observed with adsorption onto deuterated Cab-O-Sil® corresponds to an increase in electronegativity to 3.16. This increase is related to the altered dipole-dipole interactions that occur when the electron density on nitrogen decreases as the lone pair becomes involved in H-bonding. Because all the methyl-group frequencies are shifted to the same degree, the band at 2780 cm^{-1} cannot be uniquely related to the nitrogen lone pair. The resultant partial positive charge and the associated 10 cm^{-1} increase can be compared to the 45 cm^{-1} shift shown by methylamine upon protonation. The methyl group deformation frequency in crystalline UDMH hydrobromide could not be confidently assigned; however, the symmetrical C-H stretch showed a shift of 147

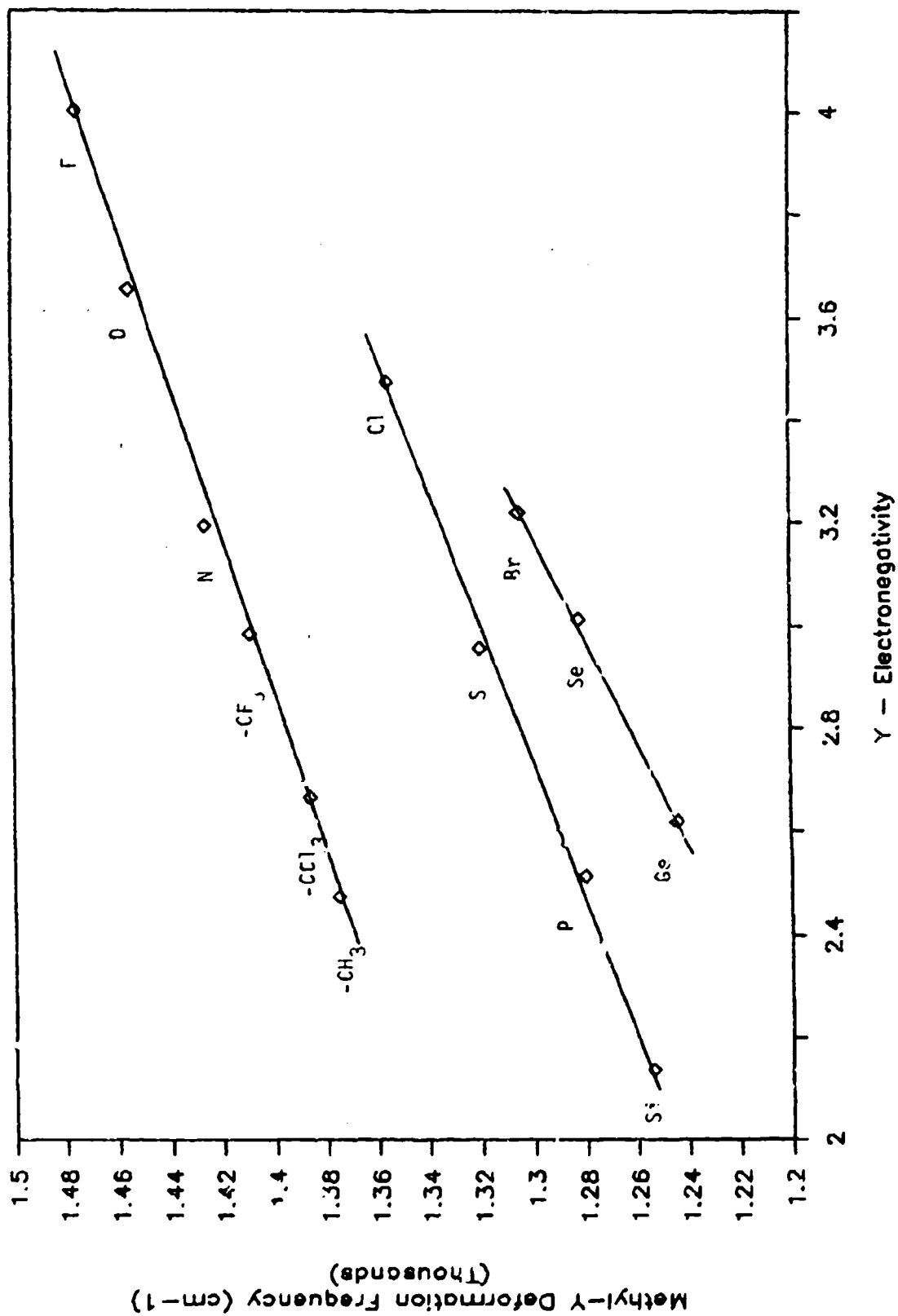


Figure 49. Correlation of Sanderson Electronegativities with Methyl Deformation Frequencies

cm^{-1} relative to the liquid. Adsorption onto deuterated Cab-O-Sil® causes a 20 cm^{-1} increase in the UDMH stretch.

E. CONCLUSIONS

Adsorption of hydrazine, MMH, and UDMH onto the hydroxylated surfaces of silica, alumina and silica-alumina is the result of reversible physisorption. The primary interaction is through H-bonding, and H/D-exchange occurs if the surface is deuterated. The adsorbed hydrazines have a structure similar to that in the liquid as evidenced by similar, but slightly shifted, vibrational frequencies. Analysis of these shifts shows that a 5 percent increase in the apparent Sanderson electronegativity of the hydrazinyl nitrogen occurs on adsorption, consistent with the dipole-dipole interactions of H-bonding. The adsorption of methanol onto alumina occurs by a different mechanism from the adsorption of methanol or MMH onto silica, and these mechanisms can be distinguished by the DRIFT technique.

SECTION VI

CONCLUSIONS

The current understanding of the environmental fates of the propellant hydrazines in the atmosphere is based on an evaluation of the relative importance of the heterogeneous and homogeneous reactions with atmospheric constituents. Although oxygen is the major reactive component of air, its homogeneous rate of reaction with the hydrazines is so slow that the ultimate fate of the hydrazines is dictated by ozone, particulate matter, and other minor atmospheric constituents.

The half-lives of hydrazine and MMH in a moderately polluted daytime atmosphere containing ozone, hydrocarbons, and nitrogen oxides is less than two hours, due to their reactions with ozone or hydroxyl radicals. Although their environmental persistence is quite short, mechanistic studies suggest that their environmental impact may be amplified by a cascade effect on the hydroxyl/hydroperoxyl radical concentration, resulting in increased ozone concentrations in an already polluted atmosphere.

A balancing factor is the efficiency of the adsorption or surface-catalyzed air oxidation processes (or both) that may take place on hydrophilic airborne particulate matter. These surface interactions generally do not result in the desorption of reactive intermediates and represent an innocuous pathway for the removal of atmospheric hydrazine or MMH.

So much less is known about the atmospheric chemistry of UDMH that further studies of its gas phase and heterogeneous reactions are critically required.

The characteristics of the individual reaction sequences that control the concentrations of gas-phase hydrazines are now fairly well understood. However, our understanding of the interdependence of these sequences with the complex suite of reactions already present in our polluted atmosphere is only minimal, and the ultimate consequences of the addition of hydrazines to the atmosphere need to be fully assessed.

REFERENCES

1. Lenga, R.E., Editor, The Sigma-Aldrich Library of Chemical Safety Data, Edition I, Sigma-Aldrich Corporation, Milwaukee, Wisconsin, 1985.
2. Hannum, J.A.E., Hazards of Chemical Rockets and Propellants: Volume III. Liquid Propellants, CPIA Publication 394, Chemical Propulsion Information Agency, The Johns Hopkins University, Applied Physics Laboratory, Laurel, Maryland, September 1984.
3. Stone, D.A., The Autoxidation of Hydrazine Vapor, CEEDO-TR-78-17, Civil and Environmental Engineering Office, Tyndall AFB, Florida, January 1978.
4. Stone, D.A., The Autoxidation of Monomethylhydrazine Vapor, ESL-TR-79-10, Engineering and Services Laboratory, Tyndall AFB, Florida, January 1979.
5. Stone, D.A., The Autoxidation of Unsymmetrical Dimethylhydrazine and 50% Unsymmetrical Dimethylhydrazine-50% Hydrazine Mixtures, ESL-TR-80-21, Engineering and Services Laboratory, Tyndall AFB, Florida, April 1980.
6. Tuazon, E.C., Carter, W.P.L., Brown, R.A., Winer, A.M., and Pitts, J.N., Atmospheric Reaction Mechanisms of Amine Fuels, ESL-TR-82-17, Engineering and Services Laboratory, Tyndall AFB, Florida, March 1982.
7. Moody, K.N., "The Vapor Phase Oxidation of Hydrazine," Ph.D. Thesis, The University of Leeds, England, 1985.
8. White, J.L., "Long Optical Paths at Large Aperture," Journal of the Optical Society of America, Vol 32, 1942, p. 285.
9. Wefers, K. and Misra, C., Oxides and Hydroxides of Aluminum, pp. 48-50, Alcoa Laboratories, Aluminum Company of America, Alcoa Center, Pennsylvania, 1987.

REFERENCES
(CONTINUED)

10. Alwitt, R.S., "The Aluminum-Water System," Oxides and Oxide Films, Vol 4, edited by J.W. Diggle and A.K. Vijh, Marcel Dekker Inc., New York, New York, 1976.
11. Stone, D.A. and Wiseman, F.L., Hydrazine Loss Processes In a Teflon® Film Reaction Chamber: Laboratory Results and Kinetic Models, ESL-TR-87-68, Engineering and Services Laboratory, Tyndall AFB, Florida, March 1988.
12. Stone, D.A., "Hydrazine Decay in a Teflon® Film Reaction Chamber," Proceedings of the Third Conference on the Environmental Chemistry of Hydrazine Fuels, Panama City, Florida, September 1987, p. 66.
13. Tuazon, E.C., Carter, W.P., Winer, A.M., and Pitts, J.N. Jr., "Reactions of Hydrazines with Ozone Under Simulated Atmospheric Conditions," Environmental Science and Technology, Vol 12, 1978, p. 954.
14. Finlayson-Pitts, B.J. and Pitts, J.N. Jr., Atmospheric Chemistry, pp. 555-559, Wiley-Interscience, New York, New York, 1986.
15. Murcray, D.G. and Goldman, A., Handbook of High Resolution Laboratory Spectra of Atmospheric Interest, pp. 250-257, CRC Press, Boca Raton, Florida, 1981.
16. Ackerman, M.N., Burdge, J.J., and Craig, N.C., "Infrared Spectra and Vibrational Assignments of Trans-CH₃N-NH, CH₃N-ND, CD₃N-NH, and CD₃N-ND," J. Chem. Phys., Vol 58, 1973, pp. 203-215.
17. Stone, D.A., Wiseman, F.L., Kilduff, J.E., Koontz, S.L., and Davis, D.D., "The Disappearance of Fuel Hydrazine Vapors in Fluorocarbon-Film Environmental Chambers -- Experimental Observations and Kinetic Modeling," Environmental Science and Technology, Vol 23, March 1989, pp. 328-333.

REFERENCES
(CONTINUED)

18. Du Pont, Teflon® Film Product Information, E.I. du Pont de Nemours & Co. (Inc.), Wilmington, Delaware.
19. Capellos, C. and Bielski, B.H.J., Kinetic Systems, Wiley-Interscience, John Wiley & Sons, Inc., New York, New York, 1972.
20. Wiseman, F.L., "Modeling the Decay of Hydrazine in Teflon® Film Reaction Chambers," Proceedings of the Third Conference on the Environmental Chemistry of Hydrazine Fuels, Panama City, Florida, September 1987, p. 76.
21. Kilduff, J.E., Davis, D.D., and Koontz, S.L., "Surface Catalyzed Air Oxidation Reactions of Hydrazines: Tubular Reactor Studies," Proceedings of the Third Conference on the Environmental Chemistry of Hydrazine Fuels, Panama City, Florida, September 1987, p. 128.
22. Gland, J.L., Sexton, B.A., and Fisher, G.B., "Oxygen Interactions with the Platinum(III) Surface," Surface Science, Vol 95, No 587, 1980.
23. Hall, W.K. and Emmett, P.H., "An Improved Microcatalytic Technique," J. Am. Chem. Soc., Vol 79, 1957, p. 2091.
24. Mather, D.S., Chambey, H.D., and Shina, A., "Advances in the Application of Gas Chromatography to the Study of Heterogenous Catalysis," J. Chrom., Vol 99, 1974, pp. 281-289.
25. Djordjevic, N.M. and Lamb, R.J., "Effects of Dilution of Poly (ethyl-vinylbenzene-divinylbenzene) Adsorbent on the Adsorption of Aliphatic, Alicyclic, and Aromatic Hydrocarbon Adsorbates from Effective Zero to Finite Surface Coverage," Anal. Chem., Vol 60, 1988, pp. 124-130.

REFERENCES
(CONTINUED)

26. Volf, J., Koubek, J., and Pasik, J., "A Contribution to the Measurement of Adsorption Isotherms by the Pulse Chromatograph Technique," J. Chrom., Vol 81, 1973, p. 9.
27. Doraiswamy, L.K. and Sharma, M.M., Heterogeneous Reactions: Analysis, Examples and Reactor Design, Vol 1, p. 184, John Wiley and Sons, New York, New York 1984.
28. Rocca, F.F., de Mourges, L., and Trambouze, Y., "Chromatographic Measurement of Hydrogen Adsorption on Supported Metallic Catalysts," J. Gas Chrom., Vol 6, 1968, p. 161.
29. Gruber, H.L., "An Adsorption Flow Method for Specific Metal Surface Area Determination," Anal. Chem., Vol 34., 1962, p. 1828.
30. Habgood, H.W. and Hanlon, J.F., "A Gas Chromatographic Study of the Adsorptive Properties of a Series of Activated Charcoals," Can. J. Chem., Vol 37, 1959, p. 843.
31. Bassett, D.W. and Habgood, H.W., "A Gas Chromatographic Study of the Catalytic Isomerization of Cyclopropane," J. Am. Chem. Soc., Vol 64, 1960, pp. 769-773.
32. Class, J.B., Aston, J.G., and Oakwood, T.S., "Trimethylhydrazine and Tetramethylhydrazine," J. Am. Chem. Soc., Vol 75, 1953, p. 2937.
33. Olson, E.C., "The Coulometric Determination of Hydrazine and Substituted Hydrazines," Anal. Chem., Vol 32, 1960, pp. 1545-1547.
34. Chamberlain, J.W., Theory of Planetary Atmospheres, Academic Press, New York, New York, 1978.

REFERENCES
(CONTINUED)

35. Pearson, R.G. and Moore, J.W., Kinetics and Mechanism, John Wiley and Sons, New York, New York, 1981.
36. Poirier, R.V. and Carr, R.W., "The Use of Tubular Flow Reactors for Kinetic Studies Over Extended Pressure Ranges," J. Phys. Chem., Vol 75, No 10, 1971, p. 1593.
37. Keyser, L.F., "High Pressure Flow Kinetics. A Study of the OH + HCl Reaction From 2 to 100 Torr," J. Phys. Chem., Vol 88, 1984, pp. 4750.
38. Gutman, D., Saunders, N., and Butler, J.E., "Kinetics of the Reactions of Methoxy and Ethoxy Radicals with Oxygen," J. Phys. Chem., Vol 86, 1982, p. 66.
39. Jonah, C.D., Mulac, W.A., and Zeglinski, P., "Rate Constants for the Reaction of OH + CO, OD + CO, and OH + Methane as a Function of Temperature," J. Phys. Chem., Vol 88, 1984, p. 4100.
40. Howard, C.J., "Kinetic Measurements Using Flow Tubes," J. Phys. Chem., Vol 83, 1979, p. 3.
41. Clyne, M.A.A. and Nip, W.P., "Kinetics of Fluorine Atom Reactions Using Resonance Absorption Spectrometry in the Far Vacuum Ultraviolet. Reactions F + HCl, CH₄, CHCl₃, CHCl₂F, and CHClF₂," Int. J. Chem. Kinet., Vol 10, 1978, p. 397.
42. Anderson, J.G., Margitan, J.G., and Kaufman, F., "Gas Phase Recombination of OH with NO and NO₂," J. Chem. Phys., Vol 60, 1974, p. 3310.
43. Debley, P.E., "Hydrogen Maser with Deformable Storage Bulb," Review of Scientific Instrumentation, Vol 41, 1970, p. 1290.

REFERENCES
(CONTINUED)

44. Ogren, P.J., "Analytical Results for First-Order Kinetics in Flow Tube Reactors with Wall Reactions," J. Phys. Chem., Vol 79, 1975, p. 1749.
45. Brown, R.L., "Tubular Flow Reactors with First-Order Kinetics," Journal of Research at National Bureau of Standards (US), Vol 83, 1978, p. 1.
46. Bolden, R.C., Hemsworth, R.S., Shaw, M.J., and Twiddy, N.D., "Measurements of Thermal-Energy Ion-Neutral Reaction Rate Coefficients for Rare-Gas Ions," Journal of Physics B: Atomic and Molecular Physics, Vol 3, 1970, p. 45.
47. Farragher, A.L., "Ion-Molecule Reaction Rate Studies in a Flowing Afterglow System," J. Chem. Soc., Trans. Faraday Soc., Vol 66, 1970, p. 1411.
48. Crank, J., The Mathematics of Diffusion, 2nd Ed., Oxford University Press, Oxford, England, 1975.
49. Kreyszig, E., Advanced Engineering Mathematics, Chap. 10, John Wiley and Sons, 1972.
50. Simons, J.W., Paur, R.J., Webster, H.A., and Bair, E.J., "Ozone Ultraviolet Photolysis," J. Chem. Phys., Vol 59, 1973, p. 1203.
51. McAfee, J.M., Stephens, E.R., Fitz, D.R., and Pitts, J.N. Jr., "Infrared Absorptivity of the 9.6 Micron Ozone Band as a Function of Spectral Resolution and Abundance," J. Quant. Spectrosc. Radiat. Transfer, Vol 16, 1976, p. 829.
52. Grushka, E. and Maynard, V.R., "Molecular Structure Effect on the Diffusion of Heptane Isomers," J. Phys. Chem., Vol 78, 1974, p. 1428.

REFERENCES
(CONTINUED)

53. Grushka, E. and Maynard, V.R., "Measurements of Diffusion Coefficients of Octane Isomers by the Chromatographic Broadening Method," J. Phys. Chem., Vol 77, 1973, p. 1437.
54. Walker R.E. and Westenberg, A.A., "Molecular Diffusion Studies in Gases at High Temperature. I. The 'Point Source' Technique," J. Chem. Phys., Vol 29, 1958, p. 1139-1146.
55. Walker, R.E. and Westenberg, A.A., "Molecular Diffusion Studies in Gases at High Temperature. II. Interpretation of Results on the He-N₂ and CO₂-N₂ Systems," J. Chem. Phys., Vol 29, No 5, 1958, p. 1147.
56. Walker, R.E. and Westenberg, A.A., "Measurements of Multicomponent Diffusion Coefficients for the CO₂-He-N₂ System Using the Point Source Technique," J. Chem. Phys., Vol 32, No 5, 1960, p. 1314.
57. Walker, R.E. and Westenberg, A.A., "Molecular Diffusion Studies in Gases at High Temperature. III. Results and Interpretation of the He-A System," J. Chem. Phys., Vol 31, No 2, 1959, p. 519.
58. Bird, B.R., Stewart, W.E., and Lightfoot, E.N., Transport Phenomena, pp. 173-174, John Wiley and Sons, New York, New York, 1960.
59. Mason, E.A. and Monchick, L.J., "Transport Properties of Polar-Gas Mixtures," J. Chem. Phys., Vol 36, 1962, p. 2746.
60. Hucknall, D.H., Chemistry of Hydrocarbon Combustion, Chapman and Hall, London and New York, 1985.
61. Minkoff G.J. and Tipper, C.F.H., Chemistry of Combustion Reactions, pp. 100-136, Butterworths, London, 1962.

REFERENCES
(CONTINUED)

62. Hoyerman, K.H., "Interactions of Chemical Reactions, Transport Processes, and Flow," Physical Chemistry An Advanced Treatise, Vol VIB, W. Jost, Editor, J. Wiley & Sons, New York, New York, 1975, pp. 931-1006.
63. Huie, R.E. and Herron, J.T., "Temperature Dependence of the Rate Constants for Reactions of Ozone with Some Olefins," I. J. Chem. Kinetics, Symposium No 1, 1975, published as a Supplement to Vol VII, pp. 165-181.
64. Pitts, J.N. and Tuazon, E.C., "Reaction of Hydrazines with Ozone Under Simulated Atmospheric Conditions," Environmental Science and Technology, Vol 15, 1981, p. 823.
65. Park, C., "Reaction Rates for $O_3 + HCl \rightarrow O + O_2 + HCl$, $Cl + O_3 \rightarrow ClO + O_2$, and $HCl + O \rightarrow OH + Cl$ at Elevated Temperatures," J. Phys. Chem., Vol 81, 1977, p. 499.
66. Dilleuth, F.J., Lalancette, B.D., and Skidmore, D.R., "Reaction of Ozone with 1,1-Difluoroethane and 1,1,1-Trifluoroethane," Journal Phys. Chem., Vol 80, 1976, p. 571.
67. Semenov, N.N., Chemical Kinetics and Chain Reactions, pp. 41-79, Oxford, England, 1935.
68. Semenov, N.N., Some Problems in Chemical Kinetics and Reactivity, Vol 2, Translated by M. Boudart, pp. 217-284, Princeton University Press, 1959.
69. Bardwell, J. and Hinshelwood, C., "The Cool Flame of Methyl Ethyl Ketone," Proceedings of the Royal Society Series A, Vol 205, 1951, p. 375.
70. Wu Shu, N.C., and Bardwell, J., "Temperature Coefficients in Hydrocarbon Oxidation," Can. J. Chem., Vol 33, 1955, p. 1415.

REFERENCES
(CONTINUED)

71. Jurs, P.C., Computer Software Applications in Chemistry, pp. 125-140, J. Wiley and Sons, New York, 1986.
72. Back, R.A., "The Preparation, Properties, and Reactions of Diimide," Reviews of Chemical Intermediates, Vol 5, 1984, pp. 293-323.
73. Johnson, K.J., Numerical Methods in Chemistry, pp. 392-400, Marcel Dekker, New York, 1980.
74. Dixon, D.A. and Schafer, R.H., "Computer Simulation of Kinetics by the Monte Carlo Technique," J. Chem. Ed., Vol 50, 1973, pp. 648-650.
75. Harris, G.W., Atkinson, R., and Pitts, J.N. Jr., "Kinetics of the Reactions of the OH Radical with Hydrazine and Methylhydrazine," J. Phys. Chem., Vol 83, 1979, pp. 2557-2559.
76. Kaufman, M. and Sherwell, J., "Kinetics of Gaseous Hydroperoxyl Radical Reactions," Prog. Reaction Kinetics, Vol 12, 1983, pp. 1-53.
77. Hair, M.L., Infrared Spectroscopy in Surface Chemistry, Marcel Dekker, New York, 1967.
78. Durig, J.R., Bursh, S.F., and Mercer, E.E., "Vibrational Spectrum of Hydrazine-d₄ and Raman Study of Hydrogen Bonding in Hydrazine," J. Chem. Phys., Vol 44, 1966, p. 4238.
79. Peri, J.B., "Infrared Study of OH and NH₂ Groups on the Surface of a Dry Silica Aerogel," J. Phys. Chem., Vol 70, 1966, p. 2937.
80. Tanabe, K., Solid Acids and Bases, Academic Press, New York, 1970.

REFERENCES
(CONTINUED)

81. Parry, E.P., "An Infrared Study of Pyridine Adsorbed on Acidic Solids. Characterization of Surface Acidity," J. Catal., Vol 2, 1963, p. 371.
82. Durig, J.R., Harris, W.C., and Wertz, D.W., "Infrared and Raman Spectra of Substituted Hydrazines. I. Methylhydrazine," J. Chem. Phys., Vol 50, 1969, p. 1449.
83. Chatt, J., Duncanson, L.A., and Venazi, L.M., "Directing Effects in Inorganic Substitution Reactions. Part II. An Infrared Spectroscopic Investigation of the Inductive Effects of a Variety of Unchanged Ligands in Complex Compounds of Platinum(II)," J. Chem. Soc., 1955, p. 4461.
84. McKean, D., "Nonequivalent CH Bonds in CH₃ Compounds from CD₂H Infrared Studies," Chem. Comm., 1971, p. 1373.
85. Bellamy, L.J., The Infrared Spectra of Complex Molecules, Chapman and Hall, London, 1975.
86. Bellamy, L.J. and Williams, T., "Infrared Spectra and Polar Effects. Part III. Internal Spectral Relationships," J. Chem. Soc., 1956, p. 2753.
87. Durig, J.R. and Harris, W.C., "Infrared and Raman Spectra of Substituted Hydrazines. II. Unsymmetrical Dimethyl Hydrazine," J. Chem. Phys., Vol 51, 1969, p. 4457.
88. Farmer, B.C., The Infrared Spectra of Minerals, The Mineralogical Society, London, 1975.
89. Greenler, R.G., "Infrared Study of the Adsorption of Methanol and Ethanol on Aluminum Oxide," J. Chem. Phys., Vol 37, 1962, p. 2094.

REFERENCES
(CONCLUDED)

90. Sanderson, R.L., "Electronegativity and Bond Energy," J. Am. Chem. Soc., Vol 105, 1983, p. 2259.

APPENDIX A TEST DATA FOR SECTION II

EARLY HYDRAZINE BLANK RUNS WITH NO FAN ON DURING RUN

I.A. = 1000 - 880 cm⁻¹, except Run 7, 8, 9, I.A. = 1000 - 900 cm⁻¹
(500-μl H₂ injected, except Run 1 & 8, 250-μl; Run 2, 245-μl)

RUN #	NAME	k ₁ hr ⁻¹	k ₁ hr ⁻¹	k ₂ hr ⁻¹	k _{obs} hr ⁻¹	t 1/2 hr	INITIAL AREA ABS·cm ⁻¹ m ²	EXP. TEMP °C	WATER	ATM	BIG. Run	Time	COMMENTS
1	HZ0718	0.156	0.153	0.157	0.064	10.8	16.8	1	21.5	Low	Air-CO ₂	1.780 22.4	First Run (CH ₄ = 0.00267)
2	HZ0721	0.111	0.16	0.102	0.0304	22.8	18.3	1	21.0	Med	Air-CO ₂	2.069 24.5	Humid outside (CH ₄ = 0.00638)
7	HZ0730	0.067	0.158	0.175	0.0312	22.2	25.0	1	23.4	Low	Air	1.722 22.5	Dry, final temp 21.8 °C
8	HZ0731	0.052	0.138	0.184	0.0295	23.5	23.6	2	nr	2.1 mL	Old Air	nr 18.6	Continuation of test 7 (previous)
9	HZ0801	0.052	0.155	0.22	0.0276	25.1	25.7	1	22.7	Med	Air	1.332 25.0	Final temp 24 °C
10	HZ0805	0.066	0.156	0.144	0.0272	25.5	34.1	1	21.7	Med	Air-CO ₂	1.247 20.3	Mirror pathlength changed
11	HZ0807	0.053	0.16	0.162	0.0254	27.3	34.4	1	23.5	Med	Air-CO ₂	1.196 18.3	Final 21.9 °C, GN ₂ purge
12	HZ0808	0.042	0.196	0.118	0.0143	48.5	35.8	1	nr	Low	Air	1.251 68.4	Very, very dry
14	HZ0812	0.064	0.338	0.192	0.0205	33.8	24.9	1	23.3	5 mL	Air	nr 17.2	Pathlength changing
15	HZ0902	(not used)			0.0520	13.3	3.8	1	22.7	20 mL	Air	3.172 17.8	Only 1st rate, short path
16	HZ0903	(not used)					3.9	2				3.269	Not used; pathlength change
17	HZ0904	0.043	0.288	0.175	0.0150	46.2	34.0	1	22.2	Low	Air	1.339 18.3	Dry, final temp 20.0 °C
18	HZ0905				0.0210	33.0	34.6	1	21.5	30 mL	Air	1.407 70	Weekend, power fail; nonlinear part
19	HZ0909	0.063	0.156	0.154	0.0273	25.4	33.4	1	nr	30 mL	Air-CO ₂	1.193 24.0	After H ₂ O, HZ appeared <2 ppm
20	HZ0911	0.061	0.36	0.155	0.0160	43.3	35.5	1	22.6	Med	Air	1.260 23.1	Temp ± 3 °C
27	HZ0924	-	-	-	0.0216	32.1	33.6	1	20.1	Low	Air	1.286 17.2	Mystery bump, run not used in avg
28	HZ0926				0.0207	33.5	36.7	1	nr	Low	Air	1.233 25.3	Purged 24 hr. been cold
Average													Runs 2, 7, 8, 9, 10, 11, 12, 17, 20, 27, 28
Std. Dev.													*Based on k _{obs} value, not avg. of half lives
Average													Runs 9, 14, 18, 19
Std. Dev.													*Based on k _{obs} value, not avg. of half lives

EARLY HYDRAZINE BLANKS IN GHZ WITH NO FAN DURING RUN

I.A. = 1000 - 880 cm⁻¹

(500-μL HZ injected except Run 3, 250-μL; Run 4.5, 180-μL)

RUN	NAME	k1 hr ⁻¹	k-1 hr ⁻¹	k2 hr ⁻¹	k _{obs} hr ⁻¹	t 1/2 hr	INITIAL AREA ABS·cm ⁻¹ m ²	EXP. TEMP °C	WATER	ATM	BIG.	Run Time	COMMENTS	
3	HZ0722	0.058	0.39	0.147	1.45E-02	47.8	18.7	-	nr	Low	GH ₂	2.017 17.2	CH ₄ = 0.00135	
4	HZ0724	0.057	0.328	0.126	1.36E-02	51.0	34.8	-	1	21.0	Low	GH ₂	1.758 23.4	1 ft3/min purge, leaks in (CH ₄ = 0.00485)
4.5	HZ0724.5	-	-	-	1.31E-02	52.9	35.1	-	2	22.0	-	01d GH ₂	nr 16	HZ to previous, no purge (CH ₄ = 0.00624)
21	HZ0915	0.059	0.57	0.115	8.42E-03	82.3	40.8	-	1	21.4	Med	GH ₂	1.189 25.6	Tent purged weekend, Power failure
22	HZ0916	0.031	0.422	0.208	1.13E-02	61.3	39.1	-	2	22.4	Low	GH ₂	1.170 18.8	Were 8 dots on bottom mirror
23	HZ0917	0.037	0.519	0.172	1.02E-02	68.0	41.6	-	3	22.4	Low	GH ₂	1.260 18.8	Less CO ₂ each day of GH ₂ test
24	HZ0918	0.041	0.451	0.176	1.11E-02	62.4	40.2	-	4	22.3	30 mL	GH ₂	nr 19.3	1.3 A°cm ⁻¹ HZ after H ₂ O injected
25	HZ0919	0.053	0.459	0.208	1.58E-02	43.9	38.9	-	5	22.4	30 mL	GH ₂	1.31 22.1	Injected H ₂ O caused HZ appearance
26	HZ0922	0.062	0.45	0.162	1.52E-02	45.6	28.6	-	6	21.3	60 mL	GH ₂	0.933 20.3	BIG. maybe taken after H ₂ O injected

Average 0.048 0.446 0.154 1.19E-02 58.5 Average Values Dry
Std. Dev. 0.012 0.088 0.033 2.22E-03 " Standard Deviation
Runs 3, 4, 4.5, 21, 22, 23
*Based on k_{obs} value, not avg. of half lives

Average 0.052 0.453 0.182 1.40E-02 49.4 Average Values Wet
Std. Dev. 0.009 0.004 0.019 2.09E-03 " Standard Deviation
Runs 24, 25, 26
*Based on k_{obs} value, not avg. of half lives

BLANK RUNS IN AIR WITH SLOW SPEED FAN

I.A. = 1000 - 880 cm⁻¹
(500-μL Hz injection)

Standard Rate in Air = 0.0172 hr⁻¹

RUN #	NAME	k1 hr ⁻¹	k-1 hr ⁻¹	k2 hr ⁻¹	k _{obs} hr ⁻¹	t 1/2 Hr.	INITIAL AREA ABS·cm ⁻¹ m ²	EXP. TEMP °C	WATER	ATM	816. Run Time	COMMENTS
30	HZ1112	-	-	-	2.33E-02	29.7	37.4	- 1	27.3	Low	Old-Air 1.363	20.8 Room air, fan on last 5 hours, no change
31	HZ1113	0.10	0.70	0.16	1.67E-02	41.5	39.2	- 2	23.6	Low	Air 1.3	16.5 Air purge slow fan
44	HZ1217	0.10	0.58	0.11	1.59E-02	43.6	40.2	-	25.6	Low	Air 1.102	yes Air purge
48	HZ0102	0.10	0.70	0.20	1.95E-02	35.5	39.0	- 1	24	Low	NR	yes Air purge, rate faster
49	HZ0105	0.095	0.70	0.15	1.44E-02	48.1	39.7	- 2a	27.5	Low	Air 1.204	yes Air purge, hot injector
86	HZ0526	0.088	0.4	0.147	1.95E-02	35.5	40.6	-	22.5	Med	Air 0.799	23.1 Pecheck background rate, humid

Average	0.097	0.616	0.153	1.72E-02	40.3	Average Values Dry	Runs 31, 44, 48, 49, 86
Std. Dev.	0.005	0.118	0.029	2.02E-03	*	Standard Deviation	*Based on k _{obs} value, not avg. of half lives

BLANK RUNS WITH GM₂ AND SLOW SPEED FAN

I.A. = 1000 - 880 cm⁻¹
 Standard Rate in GM₂ = 0.01655 hr⁻¹
 (500-μL H₂ injection)

RUN	NAME	k1 hr ⁻¹	k-1 hr ⁻¹	k2 hr ⁻¹	k _{obs} hr ⁻¹	t 1/2 hr	INITIAL AREA ABS·cm ⁻¹ m ²	EXP. #	TEMP °C	WATER	ATM	BIG.	Run	COMMENTS	
Ø													Time		
94	HZ0629	0.088	0.38	0.114	1.69E-02	41.0	34.6	-	x1	21.3	Low	GM ₂	1.264	173	Long term #1
95	HZ706				1.67E-02	42.9	37.7	-	x2	23	Med	Old GM ₂	1.155	167	Long term #2
96	HZ713				1.48E-02	46.8	39	-	x3	na	Med	Old GM ₂		167	Long term #3
97	HZ724				1.36E-02	51.0	39.3	-	1	21.7	Low	GM ₂	0.977	31.4	50% RH outside, Dry inside
99	HZ817				3.43E-02	20.2	43.3	-	1	21.7	Low	GM ₂ +CO ₂	NA	22.3	1000 ppm CO ₂ in GM ₂
100	HZ820				2.13E-02	32.5	22.5	-	1	na	Low	GM ₂	NA	26	Faster than expected
101	HZ827				2.90E-02	23.9	29.6	-	1	21.4	60 mL	GM ₂ +CO ₂	0.763	27.9	After CO ₂ & H ₂ O BIG. was 0.548
<hr/>															
Average					1.65E-02	41.9	Average Values Dry Runs 94, 95, 96, 97, 100								
Standard Deviation					2.63E-03	*	Standard Deviation *Based on k _{obs} value, not avg. of half lives								
Dry + CO ₂					3.43E-02	20.2	Dry chamber plus 1000 ppm CO ₂								
Wet + CO ₂					2.90E-02	23.9	Injected 60 mL H ₂ O and 1000 ppm CO ₂								

HYDRAZINE AND FEP FILM ADDED TO CHAMBER

I.A. = 1000 - 880 cm⁻¹

(500-μL H₂ Injection)

RUN	NAME	k1 hr ⁻¹	k-1 hr ⁻¹	k2 hr ⁻¹	k _{obs} hr ⁻¹	t 1/2 hr	INITIAL AREA ABS·cm ⁻¹ m ²	EXP. TEMP θ °C	WATER	ATM	BIG. Run	COMMENTS	
θ		hr ⁻¹	hr ⁻¹	hr ⁻¹	hr ⁻¹	hr	ABS·cm ⁻¹ m ²	θ °C			Time		
50	HZ0113	0.102	0.48	0.136	0.0191	36.3	38.2 23.97	1	25.5	Low	Air	1.315 28.4	Power failure after 9 hr
51	HZ0115	0.071	0.36	0.126	0.061	43.1	39.3 23.97	2	24.3	Low	Air	1.239 24.2	A 20 hr purge between tests
52	HZ0116	0.095	0.70	0.15	0.0142	48.8	46.4 23.97	3	21	Low	Old Air	NR 28.2	Room Temp dropped to 7 °C during night
53	HZ0119	0.074	0.54	0.146	0.014	49.5	40.0 23.97	4	21.0	Low	Air	1.02 20.0	A 6 hr flush at 10 ft3/min
54	HZ0121	0.097	0.63	0.117	0.0132	52.5	41.1 23.97	5	nr	Low	GM ₂	1.153 23.6	Overnight GM ₂ purge
58	HZ0202	0.14	0.70	0.18	0.0236	29.4	39.0 23.97	9	28.5	Low	Air	1.313 20.2	Blowout 5 days after H ₂ O test
<hr/>													
Average		0.096	0.556	0.148	0.0174	39.8	Average Values (Runs 50-53, & 58)						
Std. Dev.		0.025	0.131	0.018	0.0036	*	Standard Deviation						
<hr/>													
Average		0.057	0.575	0.151	0.017	40.8	Average Values (Runs 51-53, & 58)						
Std. Dev.		0.028	0.140	0.019	0.00391	*	Standard Deviation						
<hr/>													
Average		0.080	0.533	0.141	0.0148	46.9	Average Values (Runs 51-53)						
Std. Dev.		0.011	0.139	0.010	0.000946	*	Standard Deviation						

*Based on k_{obs} value, not avg. of half lives

EEP FILM ADDED TO CHAMBER + 60 mL H₂O

I.A. = 1000 - 880 cm⁻¹
(500-μL Hz injected except Run 52, 305-μL)

RUN NAME	k1 hr ⁻¹	k-1 hr ⁻¹	k2 hr ⁻¹	k _{obs} hr ⁻¹	t 1/2 hr	INITIAL AREA ABS·cm ⁻¹ m ²	EXP. TEMP °C	WATER	ATM	BIG. Run Time	COMMENTS
55 HZ0123	0.1	0.1	0.07	0.0334	20.8	34.4	23.97	6	21.6	60 mL	Air 1.306 27.6 60mL H ₂ O = 14730 ppm, Wet BI = 0.918
56 HZ0126	0.078	0.195	0.22	0.0359	19.3	30.8	23.97	7	28.4	60 mL	Air 1.103 23.3 BIG. after H ₂ O = 0.860
57 HZ0129	(not used)			0.0282	24.6	37.4	23.97	8	25	60 mL	Air 1.015 28.9 Run not used, detector bumped

Average 0.089 0.148 0.145 0.0347 20.0 Average Values (Runs 55 & 56)

Std. Dev. 0.011 0.047 0.075 0.00125 * Standard Deviation

*Based on k_{obs} value, not avg. of half lives

STAINLESS STEEL (20.48 m²) WITH HYDRAZINE IN AIR AND HIGH SPEED FAN OFF/ON

I.A. = 1000 - 880 cm⁻¹
(500-μL Hz injected)

RUN NAME	k1 hr ⁻¹	k-1 hr ⁻¹	k2 hr ⁻¹	k _{obs} hr ⁻¹	k CAT hr ⁻¹	t 1/2 hr	k cat/A2 hr ⁻¹ m ⁻⁴	INITIAL AREA ABS·cm ⁻¹ m ²	EXP. TEMP °C	WATER	ATM	BIG. Run Time	COMMENTS
29 HZ0930 (on)	-	-	-	6.16E-02	0.044	11.3	1.06E-04	38.1	20.48	1	20.2	Low Air 1.366 24.9	Fan on 1st 7 hr, except during data collect
HZ0930 (off)	-	-	-	2.83E-02	0.011	24.5	2.65E-05						

ALUMINUM HYDROXIDE (23.8 m) PLATES (THIN) WITH HYDRAZINE IN AIR
 Dilute Area Low (1400 - 1250 cm⁻¹), Area High (3200 - 3050 cm⁻¹)
 I.A. = 1000 - 880 cm⁻¹
 (500-μL H₂ injected)

RUN NAME	k1 hr ⁻¹	k-1 hr ⁻¹	k2 hr ⁻¹	k _{obs} hr ⁻¹	k CAT hr ⁻¹	t 1/2 hr	k cat/A2 hr ⁻¹ m ⁻⁴	INITIAL AREA ABS-cm ⁻¹ m ²	EXP. TEMP °C	WATER	ATM	BIG. Run Time	COMMENTS
32 HZ1117A	-	-	-	4.750	4.733	0.1	8.33E-03	7.6 23.83	1 26.2	Low	Air	nr 1.7	Time 0: 38.5 A*cm ⁻¹ by extrapolation
33 HZ1117B	-	-	-	1.830	1.813	0.4	3.19E-03	18.1 23.83	2 28.2	Low	Air	1.339 2.5	Too fast for curved portion
34 HZ1117C	-	-	-	2.300	2.283	0.3	4.02E-03	17.2 23.83	3 26.5	-	Old Air	1.217 2.1	Final temp = 28.2 °C, HNNH rates
35 HZ1119	-	-	-	2.240	2.223	0.3	3.91E-03	20.6 23.83	4 28.3	Low	Air	1.272 1.6	Final temp 25.6 °C, 24 hr pretest purge
45 HZ1223	-	-	-	1.940	1.923	0.4	3.39E-03	28.1 23.83	1 25.5	Low	Air	1.135	No HNNH
89 HZ0609	-	-	-	0.763	0.746	0.9	1.31E-03	34.7 23.83	1b 22.3	Med	Air	0.750 2.3	MY VALUE, Humid, fan faster, HNNH graphs
91 HZ0612	-	-	-	0.466	0.449	1.5	7.90E-04	37.2 23.83	3b nr	Med	Air	0.741 17.2	Infinity Corr = -3.5 added to Int. Areas
Average				2.041	2.024	0.3	3.56E-03	All Runs					
Standard Deviation				1.29	1.29	*	2.27E-03	Standard Deviation					
Average				2.304	2.287	0.3	4.03E-03	All Runs except # 91					
Standard Deviation				1.21	1.21	*	2.12E-03	Standard Deviation					
*Average				1.815	1.797	0.4	3.17E-03	All Runs except # 32 & 91					
Standard Deviation				0.55	0.55	*	9.77E-04	Standard Deviation					

*Based on k_{obs} value, not avg. of half lives

ENCROUSTED ALUMINUM (23.8 m) PLATES (THIN) WITH HYDRAZINE IN GN2

I.A. = 1000 - 880 cm⁻¹

(500-μL H₂ injected)

RUN #	NAME	k1 hr ⁻¹	k-1 hr ⁻¹	k2 hr ⁻¹	k _{obs} hr ⁻¹	k CAT hr ⁻¹	t 1/2 hr	k cat/A2 hr ⁻¹ m ⁻⁴	INITIAL AREA ABS·cm ⁻¹ m ²	EXP. TEMP °C	WATER	ATM	BIG.	Run Time	COMMENTS		
36	HZ1121A	-	-	-	0.745	0.728	0.9	1.28E-03	36	23.83	1	25.8	Low	GN ₂	1.356	4.4	5th exp HZ; no HNNH seen; straight line
37	HZ1121B	-	-	-	0.992	0.975	0.7	1.72E-03	36.4	23.83	2	28.4	Med	Old GN ₂	NA	2.4	HNNH Observed
46	HZ1229	-	-	-	0.416	0.399	1.7	7.03E-04	39.2	23.83	1	26.5	Low	GN	NR	4.8	HNNH observed
92	HZ0618	-	-	-	0.173	0.156	4.0	2.75E-04	44.7	23.83	4b	23.4	Low	GN ₂	0.538	15.4	Plates 4th exp., 1 with UOHH

Average 0.581 0.565 1.2 9.95E-04 All Runs

Standard Deviation 0.31 0.31 * 5.50E-04 Standard Deviation

Average 0.718 0.701 1.0 1.23E-03 All Runs Except 92

Standard Deviation 0.24 0.24 * 4.15E-04 Standard Deviation

*Based on k_{obs} value, not avg. of half lives

HYDRAZINE + VARIABLE AREA ENCRUSTED ALUMINUM PLATES

I.A. = 1000 - 880 cm⁻¹
(500-μL Hz injected)

RUN #	NAME	k1 hr ⁻¹	k-1 hr ⁻¹	k2 hr ⁻¹	k _{obs} hr ⁻¹	k CAT hr ⁻¹	t 1/2 hr	k cat/A2 hr ⁻¹ m ⁻⁴	INITIAL AREA	EXP. TEMP °C	WATER	ATM	BIG. Run	COMMENTS		
									ABS·cm ⁻¹ m ²							
39	HZ1205	0.22	0.816	0.26	4.80E-02	0.031	14.4	1.29	39.6	3.34	1	25.4	Low	nr	21.3	Used 8 plates
40	HZ1209	0.21	0.33	0.66	1.34E-01	0.117	5.2	0.116	37.2	6.69	1	23.8	Low	nr	6.0	A 20 hr pretest purge, 16 plates
41	HZ1211	-	-	-	3.77E-01	0.360	1.8	0.0103	37.6	13.37	1	nr	Low	nr	7.8	Ar tank may have leaked into tent
43	HZ1216	-	-	-	3.00E-01	0.283	2.3	0.012	36.9	13.37	1	26.1	Low	nr	1.118	Tent purged 5.5 hr
60	HZ0213	-	-	-	6.00E-01	0.583	1.2	0.00844	23.1	11.70	1	nr	60 mL	nr	1.206	Used 28 plates

Average Half-life for k 2.4 0.288 All Runs
Standard Deviation * 0.505 Standard Deviation

Average 0.339 0.32 2.07 0.0116 Runs 41 and 43
Standard Deviation 0.0385 0.0385 * 0.00132

103

HYDRAZINE + CLEAN ALUMINUM

I.A. = 1000 - 880 cm⁻¹
(500-μL Hz injected)

RUN	NAME	k ₁ hr ⁻¹	k ₋₁ hr ⁻¹	k ₂ hr ⁻¹	k _{obs} hr ⁻¹	k CAT hr ⁻¹	t 1/2 hr	k cat/A2 hr ⁻¹ m ⁻⁴	INITIAL AREA ABS·cm ⁻¹ m ²	EXP. TEMP °C	WATER	ATM	BIG. Run	COMMENTS		
62	HZ0226	0.17	0.437	0.156	0.0360	0.0188	19.3	4.30E-05	38.0	20.90	1	26.0	Low	nr	1.150	Thick A1, 50 plates
63	HZ0302	0.14	0.495	0.189	0.0315	0.0143	22.0	3.27E-05	38.4	20.90	2	28.7	Low	nr	1.208	Mirrors realigned

Average 0.155 0.466 0.173 0.0338 0.0166 20.5 3.79E-05 Average Value For Runs 62 & 63
Std. Dev. 0.015 0.029 0.016 0.00225 0.00225 * 5.15E-06 Standard Deviation

*Based on k_{obs} value, not avg. of half lives

HYDRAZINE + STAINLESS STEEL PLATES (20.9 m²)

I.A. = 1000 - 880 cm⁻¹

(500-μl Hz injected)

RUN NAME	k1 hr ⁻¹	k-1 hr ⁻¹	k2 hr ⁻¹	k _{obs} hr ⁻¹	k CAT hr ⁻¹	t 1/2 hr	k cat/A2 hr ⁻¹ m ⁻⁴	INITIAL AREA ABS·cm ⁻¹ m ²	EXP. TEMP °C	WATER	ATM	BIG. Run Time	COMMENTS
38 HZ1126	0.125	0.33	0.17	0.0358	0.0186	19.4	4.26E-05	38.1 20.90	1	26.0	Low	Air 1.360 17.8	After 2 days trace NH3; 0.12 A

HYDRAZINE + TITANIUM PLATE (2.11 m²)

I.A. = 1000 - 880 cm⁻¹

(500-μl Hz injected)

RUN NAME	k1 hr ⁻¹	k-1 hr ⁻¹	k2 hr ⁻¹	k _{obs} hr ⁻¹	k CAT hr ⁻¹	t 1/2 hr	k cat/A2 hr ⁻¹ m ⁻⁴	INITIAL AREA ABS·cm ⁻¹ m ²	EXP. TEMP °C	WATER	ATM	BIG. Run Time	COMMENTS
61 HZ0219	0.13	0.38	0.116	0.025	0.0078	27.7	0.00175	38.8 2.11	1	23.0	Low	Air nr 28.3	Need more Ti

HYDRAZINE AND GALVANIZED STEEL (ZINC) PLATES

I.A. = 1000 - 880 cm⁻¹ (500-μL H₂ injected)
 (Surface Area = Run 42 m², 19.23 m²; Run 47, 10.45; Run 87 21.32 m²)

RUN	NAME	k1 hr ⁻¹	k-1 hr ⁻¹	k2 hr ⁻¹	k _{obs} hr ⁻¹	k hr ⁻¹	CAT hr	t 1/2 hr	k cat/A2 hr ⁻¹ m ⁻⁴	INITIAL AREA ABS·cm ⁻¹ m ²	EXP. TEMP °C	WATER	ATM	BIG.	Run	Time	COMMENTS
42	HZ1215	0.24	1.3	0.38	0.0477	0.031	14.5	8.25E-05	37.8	19.23	1	26	Low	Air	1.135	12.6	No NH ₃ , trace H ₂ NH
47	HZ1230	(not used)		1.2	0.075	0.058	9.2	5.29E-04	39.2	10.45	1	nr	Low	Air	nr	16.5	Not used, fast decay: power failure
87	HZ0528				0.0498	0.0326	13.9	7.17E-05	35.5	21.32	1	22.5	Low	Air	0.765	17.8	Repeat to verify

Average cat/A2 = 7.71E-05 Average Value For Runs 42 & 87
 Standard Deviation 5.38E-06 Standard Deviation

*Based on k_{obs} value, not avg. of half lives Run 47 not used

AEROZINE-50 TEST IN EMPTY CHAMBER

H₂ by Peak Height UDMH I.A. = 2900 - 2775 cm⁻¹
 (1000-μL Aerozine-50 injected)

RUN	NAME	k1 hr ⁻¹	k-1 hr ⁻¹	k2 hr ⁻¹	k _{obs} hr ⁻¹	t 1/2 hr	k cat/A2 hr ⁻¹ m ⁻⁴	INITIAL AREA ABS·cm ⁻¹ m ²	EXP. TEMP °C	WATER	ATM	BIG.	Run	Time	COMMENTS
88	AR0603	0.092	0.2835	0.13	0.0247	28.1	Hydrazine	-	1	22.0	Med	Air	0.753	36.6	PEAK picked HZ 957 cm ⁻¹ , humid
"	"	0.067	0.43	0.171	0.0176	39.4	UDMH	46.6	"	"	"	"	"	"	Rates > alone, interference for area

Ratio of A-50 UDMH loss/normal UDMH loss

AEROZINE-50 TESTS WITH ALUMINUM HYDROXIDE PLATES (Area = 23.83 m²)

I.A. = 2900 - 2775 cm⁻¹
(1000-μL AEROZINE-50 injected)

RUN NAME	k1 hr ⁻¹	k2 hr ⁻¹	k _{obs} hr ⁻¹	k CAT hr ⁻¹	t 1/2 hr	k cat/A2 hr ⁻¹ m ⁻⁴	INITIAL AREA ABS-cm ⁻¹ m ²	EXP. TEMP # °C	WATER #	ATM #	BIG. #	Run Time	COMMENTS
----------	------------------------	------------------------	--------------------------------------	---------------------------	-------------	--	---	-------------------	------------	----------	-----------	-------------	----------

90 AR0610 - - - 0.0404 0.0228 17.2 5.08E-05 48.6 23.83 2 22.4 Med Air 0.834 17.4 N2H2 area 1300-1260 cm⁻¹ determined

Ratio of A-50 + metal k obs/k obs A-50 empty chamber

MMH IN EMPTY TENT

I.A. = 800 - 700 cm⁻¹

(1000-μL MMH injected each run)

RUN NAME	k1 hr ⁻¹	k2 hr ⁻¹	k _{obs} hr ⁻¹	t 1/2 hr	INITIAL AREA ABS-cm ⁻¹ m ²	EXP. TEMP # °C	WATER #	ATM #	BIG. #	Run Time	COMMENTS
----------	------------------------	------------------------	--------------------------------------	-------------	---	-------------------	------------	----------	-----------	-------------	----------

72 MH0416 - - - 0.042 16.5 27.8 - 1 31.2 Low Air 1.272 22.5 Stopper on tent was loose
73 MH0421 - - - 0.039 17.8 30.4 - 2 24.0 Low Air 1.176 25.1 PC hung mid test, 1070-1025 Met IA 5.05
74 MH0422 - - - 0.0365 19.0 30.7 - 3 23.7 Med Air 0.942 6.1 Power Failure 0.55 this one
75 MH0423 - - - 0.0358 19.4 31.6 - 4 26.3 Low Air 1.008 23.3 Noisy data, hot!
85 MH0520 - - - 0.035 19.8 34.2 - - 20.7 Med Air 0.799 21.6 Very Humid weather, Trace Met=MMH

Average 0.0366 19.0 Average Values (Runs 73-75 & 85)

Standard Deviation 0.0015 * Run 72 not used in averages

*Based on k_{obs} value, not avg. of half lives

MMH + ALUMINUM (Area = 20.90 m²)

I.A. = 800 - 700 cm⁻¹

(1000-μL MMH injected)

RUN #	NAME	k1 hr ⁻¹	k-1 hr ⁻¹	k2 hr ⁻¹	k _{obs} hr ⁻¹	k CAT hr ⁻¹	t 1/2 hr	k cat/A2 hr ⁻¹ m ⁻⁴	INITIAL AREA A55·cm ⁻¹ m ²	EXP. TEMP θ °C	WATER	ATM	BIG. Run	Time	COMMENTS
76	MMH0428	-	-	-	0.047	0.0104	14.7	2.39E-05	29.8 20.90	1	25.5	Low	Air 1.134	31.3	Final 20.9 °C, 200 scans, 2.5 A°cm ⁻¹
77	MMH0501	-	-	-	0.042	0.00542	16.5	1.24E-05	32.8 20.90	2	21.8	Low	GN ₂ 1.013	26.4	Previous exposed UDMH, 1065-1025 = 1.8

Average

0.0445 0.00793 15.6 1.81E-05 Average Values Runs 76 & 77

Standard Deviation

0.0025 0.0025 * 5.72E-06 Standard Deviation

*Based on k_{obs} value, not avg. of half lives

MMH AND GALVANIZED STEEL (Area = 20.90 m²)

I.A. = 800 - 700 cm⁻¹

(1000-μL MMH injected)

RUN #	NAME	k1 hr ⁻¹	k-1 hr ⁻¹	k2 hr ⁻¹	k _{obs} hr ⁻¹	k CAT hr ⁻¹	t 1/2 hr	k cat/A2 hr ⁻¹ m ⁻⁴	INITIAL AREA A55·cm ⁻¹ m ²	EXP. TEMP θ °C	WATER	ATM	BIG. Run	Time	COMMENTS
71	MMH0414	-	-	-	0.0644	0.028	10.8	6.37E-05	28.4 20.90	2	29.6	Low	Air 1.327	21.9	Hot 29.6 °C! MeOH product, 9.61 A°cm ⁻¹
70	MMH0413	-	-	-	0.0634	0.027	10.9	6.14E-05	28.5 20.90	1	28.7	Low	Air 1.320	19.2	1075-975 area = 8.48, Peak height = 0.244

Average

0.0639 0.0273 10.8 6.26E-05 Average Values Runs 76 & 77

Standard Deviation

0.0005 0.0005 * 1.14E-06 Standard Deviation

*Based on k_{obs} value, not avg. of half lives

MMH AND ENCRUSTED ALUMINUM (Area = 23.83 m² for Runs 69, 78, & 79)

I.A. = 800 - 700 cm⁻¹ (Area = 11.70 m² for Runs 82 and 83)

(1000-μL MMH injected except for Run 78, 1200-μL) (Area = 12.12 m² for Run 84)

RUN #	NAME	k1 hr ⁻¹	k-1 hr ⁻¹	k2 hr ⁻¹	k _{obs} hr ⁻¹	k CAT hr ⁻¹	t 1/2 hr	k cat/A2 hr ⁻¹ m ⁻⁴	INITIAL AREA AB5·cm ⁻¹ m ²	EXP. TEMP θ °C	WATER	ATH	BIG. Run	Time	COMMENTS	
69	MMH0403	-	-	-	0.12	0.083	5.8	1.47E-04	28.0	23.83	*	27.3	Low	nr	21.4	Previous exposure to UDMH, no curvature
78	MMH0505	-	-	-	0.146	0.109	4.7	1.93E-04	38.2	23.83	1	20.7	Low	nr	15	End 25.4 °C, Low BIG., 1065-1025 = 1.1 A°cm ⁻¹
79	MMH0507	-	-	-	0.15	0.113	4.6	2.00E-04	34.0	23.83	2	21.4	Low	nr	15.7	Infinity correction used, Met 2.5
82	MMH0513	-	-	-	0.116	0.079	6.0	5.80E-04	32.0	11.70	1	26.7	Low	nr	2.5	Few data points, computer jammed
83	MMH0514	-	-	-	0.065	0.028	10.7	2.08E-04	33.4	11.70	2	nr	Low	nr	20.6	Peak height at 888 cm ⁻¹ = 1.677 A
84	MMH0518	-	-	-	0.07	0.033	9.9	2.28E-04	32.1	12.12	1	21.4	Low	nr	22.5	Plates added & 2 day blowout, 888 peak 1.78

Average 1.95E-04 All Runs Except 82

Standard Deviation * 2.67E-05 Standard Deviation

Average 23.8 m² Al runs 0.139 0.1.02 5.0 1.80E-04 Runs 69, 78, 79

Standard Deviation 0.0349 0.0349 * 2.34E-05 Standard Deviation

*Based on k_{obs} value, not avg. of half lives ** Single Runs above

MMH AND STAINLESS STEEL (Area = 20.9 m²)

I.A. = 600 - 700 cm⁻¹

(1000-μL MMH injected)

RUN #	NAME	k1 hr ⁻¹	k-1 hr ⁻¹	k2 hr ⁻¹	k _{obs} hr ⁻¹	k CAT hr ⁻¹	t 1/2 hr	k Cat/A2 hr ⁻¹ m ⁻⁴	INITIAL AREA ABS·cm ⁻¹ m ²	EXP. TEMP θ °C	WATER	ATM	BIG.	Run Time	COMMENTS
80	MMH509	-	-	-	0.129	0.0924	5.4	2.12E-04	34.1	20.9	1	21.0	Low	Air 0.882 17.6	Tent purge for 18 hr, 2.87 Met, 1065-1025
81	MMH511	-	-	-	0.139	0.102	5.0	2.34E-04	32.5	20.9	2	22.3	Low	Air 0.844 17.9	Data interrupt after 5 hr., 2.43 A°Cm ⁻¹

Average 0.134 0.0974 5.2 2.23E-04 Runs 80, 81

Standard Deviation 0.005 0.005 0.2 1.14E-05 Standard Deviation

*Based on k_{obs} value, not avg. of half lives ** Single Runs above

UDMH IN EMPTY TENT

I.A. = 955 - 865 cm⁻¹

RUN #	NAME	k1 hr ⁻¹	k-1 hr ⁻¹	k2 hr ⁻¹	k _{obs} hr ⁻¹	t 1/2 hr	INITIAL AREA ABS·cm ⁻¹ m ²	EXP. TEMP θ °C	WATER	ATM	BIG.	Run Time	COMMENTS
64	UD0306 (1700-μL UDMH injected)				0.0111	62.4	68.3	-	1	29.5	Low	Air 0.985 64.5	Weekend run
65	UD0309 (500-μL UDMH injected)				0.094	73.7	51.3	-	1	nr	-	Old Air nr 22.4	Same air, new bkg. area adj.
66	UD0311 (1000-μL UDMH injected)				0.0141	49.2	43.2	-	1	28.0	Med	Air 0.850 40.4	Damp day, curvature

Average 0.0115 60.1 Average Value For Runs 64, 65, and 66

Standard Deviation 0.00194 - Standard Deviation

*Based on k_{obs} value, not avg. of half lives Run 47 not used

UDMH AND ENCRUSTED ALUMINUM

I.A. = 955 - 865 cm⁻¹

RUN NAME	k1 hr ⁻¹	k-1 hr ⁻¹	k2 hr ⁻¹	k _{obs} hr ⁻¹	k CAT hr ⁻¹	t 1/2 hr	k cat/A2 hr ⁻¹ m ⁻⁴	INITIAL AREA ABS·cm ⁻¹ m ²	EXP. TEMP θ °C	WATER	ATM	BIG. Run	Time	COMMENTS
67 UD0319 (1000-μL UDMH injected)				0.027	0.0155	25.7	2.72E-05	35.6	23.83	1	Air	1.300	17.7	Air in 16 hr before run start, curvature
68 UD0320 (1500-μL UDMH injected)				0.019	0.00747	36.5	1.31E-05	51.1	23.83	2	Air	1.239	69.5	Weekend, curvature
Average				0.023	0.0115	30.1	2.02E-05	Average Values (Runs 67 & 68)						
Standard Deviation				0.004	0.004		7.04E-06							

OTHER MONOHYDRAZINE GASES

RUN NAME	k1 hr ⁻¹	k-1 hr ⁻¹	k2 hr ⁻¹	k _{obs} hr ⁻¹	INITIAL AREA ABS·cm ⁻¹ m ²	EXP. TEMP θ °C	WATER	ATM	BIG. Run	Time	COMMENTS
5a MF0728a TF freon leak rate				0.00497	14.9	1	NA	Low	GN ₂	16.1	3 compounds measured
MF0728b Methanol leak rate				0.0127	2.27						
MF0728c CO ₂ leak rate (IN)				1.16	0.02						
6 ME0729a Methanol Leak rate				0.0175	53.9	1	NA	Low	Air		
ME0729b				0.0207	61.6						
98 MA730 Methanol Leak Rate				0.013	15.9	1	NA	Low	NA		MeOH leak rate, recorded little data
13 MA0811a Methyl Amine / CO ₂				0.035		1		Low	Air	1.388	15.1
				0.12							

DEFINITIONS FOR APPENDIX A

I.A. = Integrated Area: The area under a peak integrated as absorbance versus wavelength.

HZ = Hydrazine

MH = Monomethylhydrazine

UO = UDMH

MF = Trifluoro-trichloro freon (TF freon)

ME = Methanol

MA = Methyl amine

Standard Deviation: Computed here is the standard deviation of the population (n); normally, the standard deviation of the sample is used (n-1). This is not the error listed in the report.

HZBLANKG2 = s169 = average rate HZ decay in blank test in GM₂

HZblankrate = s144 = average rate HZ decay in blank tent

MHblankrate = J277 = average rate MH decay in blank tent

UOblankrate = J354 = average rate UO decay in blank tent

APPENDIX B TEST DATA FOR SECTION IV

File (#)	Vaporization		Reaction		$k_i \times 10^{17}$ ($\text{cm}^3 \cdot \text{molecule}^{-1} \cdot \text{s}^{-1}$)	$k_s \times 10^{16}$ ($\text{cm}^3 \cdot \text{molecule}^{-1} \cdot \text{s}^{-1}$)				
	Flow (Std. ft^3/min)	Flow (mL/min)	Temp (K)	Intercept (ppm)			$i(\text{O}_2)$ (ppm)	k_{bkg} (sec^{-1})		
M16A	7	75	284.8	34	105.3	0.035	8	0.2	4.35	0.74
M16B	7	75	284.8	37	110	0.037	2.98	0.85	1.42	3
M110A	7	75	291.5	35	112.8	0.037	1.72	1.13	0.87	3.98
M110B	7	75	291.7	35.5	117.7	0.029	2.24	1.06	1.08	3.58
M14A	10	90	299.1	49	90.4	0.11	19.7	0.46	9.05	2.36
M15A	10	90	299	49	90.8	0.13	18.2	0.57	8.35	2.55
M117	11	100	313.2	43	37.9	0.14	6.13	1.48	8.03	16.7
M117A	11	100	312.9	39	36.9	0.11	5.48	1.53	7.68	16.7

File (#)	Vaporization		Reaction		$k_1 \times 10^2$ (sec ⁻¹)	k_{bkg} (sec ⁻¹)	$k_2 \times 10^2$ (ppm ⁻¹ sec ⁻¹)	$k \times 10^{17}$ (cm ³ molecule ⁻¹ sec ⁻¹)
	Flow (Std. ft ³ /min)	Flow (mL/min)	Temp (K)	Intercept (ppm)				
H120A	5	210	288.8	31	100.7	0.026	2.88	3.33
H120B	5	210	289.4	33	100.6	0.055	7.2	1.29
H125	5		295.6	38	88.5	0.072	7.67	7.37
H125A	5		295.8	40	88.3	0.072	7.8	6.97
H118	7	200	299.3	34	73	0.048	5.19	14.6
H118A	7	200	299.8	37	72.6	0.047	5.2	16.2
H124A	10	250	306.75	34	82.6	0.087	9.08	23.6
H124B	10	250	306.4	34	80.9	0.1	11.6	18.5
H123	10	250	311.6	40	60	0.21	26	12.1
H123A	10	250	312.2	40	61	0.17	24.1	17.2
H214	7	250	299	39	80.7	0.093	10.6	20.6
H214A	7	250	299.1	34	78.9	0.067	7.59	20
T27A	11	35	297	56				111
T28	11	35	298	65				101

M15A		M168		M110A		M110B	
TIME (sec)	[mmH] (atm $\times 10^{-6}$)	TIME (sec)	[mmH] (atm $\times 10^{-6}$)	TIME (sec)	[mmH] (atm $\times 10^{-6}$)	TIME (sec)	[mmH] (atm $\times 10^{-6}$)
0.77	30.8	0.77	35.3	0.76	34.7	0.75	34.3
1.49	28.2	0.85	34.2	0.87	33.7	1.45	31.5
1.61	24.6	2.32	29.3	1.45	30.7	1.57	30.6
2.32	24.8	2.38	29.7	2.27	29.2	2.32	29.5
2.44	21.2	2.97	24.3	2.32	29.1	2.9	22.5
2.97	20.1	3.09	24.2	2.9	25.3	3.02	21.5
3.09	20.5	3.69	17.2	3.02	24.6	3.6	12.7
3.69	13.8	3.5	12.5	3.6	14.6		
3.8	14.8						

M14A		M15A		M117		M117A	
TIME (sec)	[mmH] (atm $\times 10^{-6}$)	TIME (sec)	[mmH] (atm $\times 10^{-6}$)	TIME (sec)	[mmH] (atm $\times 10^{-6}$)	TIME (sec)	[mmH] (atm $\times 10^{-6}$)
0.51	42.7	0.52	44	0.45	41.1	0.45	39.1
0.59	41.8	0.59	43.7	0.52	40.3	0.52	37
0.99	36.8	0.99	39.3	0.86	39.1	0.86	35.6
1.07	38.7	1.07	39.7	0.93	40.1	1.34	30.8
1.55	31.4	1.55	29.6	1.34	34.4	1.38	30.3
1.62	28.6	1.63	34.1	1.37	35	1.72	24.2
1.98	20	1.98	19.1	1.79	22.7	2.14	14.7
2.06	18.2	2.06	18.7	2.13	18.5	2.2	13
2.46	11.8	2.46	10	2.2	15.8		
2.54	12.3	2.54	12.9				